Molecule to Supramolecule: Effect of assembly on the molecular properties of H-bonded chiral assembly of coordination complexes with amino acid derivatives

A
Thesis Submitted
In Partial Fulfillment of the Requirement
for the Degree of

DOCTOR OF PHILOSOPHY

By

Mrigendra Dubey

Department of Chemistry
Indian Institute of Technology Guwahati
Guwahati-781039
February-2011

Dedicated to my Parents

..... Mrigendra

INDIAN INSTITUTE OF TECHNOLOGY GUWAHATI

Department of Chemistry

STATEMENT

I hereby declare that the matter embodied in this thesis is the result of investigations carried out by me in the Department of Chemistry, Indian Institute of Technology Guwahati, India under the supervision of Professor Manabendra Ray, Professor, Department of Chemistry, Indian Institute of Technology Guwahati, India.

In keeping with the general practice of reporting observations, due acknowledgements have been made wherever the work described is based on the findings of other investigations.

February, 2011

I. I. T. Guwahati Mrigendra Dubey

Prof. Manabendra Ray
Professor
Indian Institute of Technology Guwahati
Department of Chemistry
Tel. 91 361 258 2310
Fax.91 361 258 2349

CERTIFICATE

This is to certify that Mr. Mrigendra Dubey has been working under my supervision since July 2006. I am forwarding his thesis, entitled, "**Molecule to Supramolecule: Effect of assembly on the molecular properties of H-bonded chiral assembly of coordination complexes with amino acid derivatives"** being submitted for the degree of Doctorate of Philosophy of this Institute. I certify that he has fulfilled all the requirements according to the rules of this Institute, and that the investigations embodied in this thesis have not been submitted elsewhere for a degree.

February- 2011
I. I. T. Guwahati

Prof. Manabendra Ray
Supervisor

Acknowledgements

At the very outset I take opportunity to express my deep sense of profound gratitude and indebtedness towards my learned mentor **Professor Manabendra Ray**, *Department of Chemistry, IIT Guwahati for his erudite inspiration, noble guidance, tireless efforts, perpetual encouragements and moral supports at each and every step of my research work, which enable me to complete my thesis work. This thesis grew out of a series of dialogues with my supervisor. Through his Socratic questioning, he brought me closer to reality, I had initially perceived, eventually enabling me to grasp its rich complexity. He has been convincing me to take these ideas and turn them into a thesis. He helped me to recognize what was important, and made many contributions to this work. I am fortunate enough to have his teaching about how to cultivate scientific thoughts.*

I would like to acknowledge my sincere gratitude to all my doctoral committee members, Dr. Gopal Das, Professor Bhisma K. Patel and Dr. V. Manivannan for their insightful advices and valuable suggestions.

I express my sincere appreciation to Professor R. N. Mukherjee, I.I.T. Kanpur for his valuable suggestions. His Ph.D. student Suman Barman helped in recording the some instrumental measurements at I.I.T. Kanpur.

I wish to express my heartiest thanks to Prof. J. B. Baruah, Department of Chemistry, I.I.T. Guwahati for valuable suggestions as well as providing me Uv-vis spectrophotometer.

I am grateful to Professor Arun Chattopadhyay, Head, Department of Chemistry, IIT Guwahati for providing good research environment.

I also express my sincere thanks to all faculty members, Department of Chemistry, IIT Guwahati for their help and encouragement.

I am thankful to the Institute, Indian Institute of Technology Guwahati for providing me with the state of the art infrastructure and facilities for advanced research.

I am grateful to all non-teaching staffs of the Department for their technical support.

I would like to thank DST under FIST program for providing single crystal XRD instrument facility and B. Das for mounting the crystal.

My sincere thanks to Chandan Borgohain, K. Senapati and Mr. Kh. Kesho Singh of Central Instruments facility, IIT Guwahati for their help in all the characterizations (SEM, TEM, NMR, ESI-Ms, and EPR) required during my research work.

I express my deep sense of gratitude to Professor L. D. S. Yadav and Professor J. P. Shrivastva (Allahabad University) for being the first persons who taught me how to work in the lab and helped me in many ways.

I would like to thank my former and present group members Dr. Rik Rani Koner, Dr. Subash Sahoo, S. H. Faizi, C. M. Rajesh and Chandani for their timely help, support and for the wonderful time we shared during this period.

I am thankful to all research scholars and M.Sc students, Department of Chemistry, IIT Guwahati for their help.

I extend my sincerest special thanks to Sahoo bhaiya, Shikha and Satish Singh and I also take this opportunity to thank Siva da, C. M. Reddy, Bimlesh, Pankaj, Apoorva, Rupam, Avijeet da, Sandeep, Atul for their constant help, motivation, enthusiastic company and all the wonderful time we spent in various events.

I wish to show my gratitude to Prof. P. Banarjee (IACS) and Dr. D. K. Dixit, Manish, Imran (CDRI, Lucknow) and Guahati University for analytical facilities.

The financial support from Council of Scientific and Industrial Research (CSIR) and Department of Science and Technology, New Delhi (DST) duly acknowledged.

I wish to express my sincere gratitude to my sisters (Gudiya didi and Deenu) and brother (Manish) for their constant unfailing support.

At last but not least, I want to express my sincere thanks to all of my family members, especially my Papa (Shri- Jagadish Dubey) and Mummi (Smt. Kanti Devi) for their constant encouragements and moral supports during my research work. They are the main soul and inspiration for each and every step that I achieve in my life.

Mrigendra Dubey

Abstract

Metal complexes of amino acid derived reduced Schiff base ligands generated several interesting architectures including chiral capsule, channels and cavity owing to their flexibility, H-bonding ability, and inherent chirality.[1,2] In this thesis, we have explored the chemistry of L-leucine derivative (Figure **1**), and characterized a set of spontaneously formed crown ether analogue multinuclear assemblies, binding both cation and anion of a binary salt in the solid state. Considerable amount of work has been reported[2] on the use of metal complexes as a crown ether/cryptand analogue,[3] as well as anion receptor,[4] but few molecular assemblies having both alkali metal ion and an anion binding site exist.[5] Systematically changing the other part such as amino acid, metal Ni(II) or Cu(II) and alkali metal ions as well as counter anions, we have explored effects on multinuclear formation. Consequently, we have synthesized different type of monomers as well as their conversion towards multinuclear assembly in presence of alkali metal salts. Because of flexible nature of assembly towards Ni(II) and Cu(II) we got accomplishment in synthesis and characterization of mixed metal assembly which is challenging in the field of coordination chemistry. On changing alkali metal ion Na^+/K^+ to Cs^+ monomer forms coordination polymer instead of multinuclear assembly. Apart from the coordination chemistry of leucine derivative, we have explored its gel formation properties by attaching hydrophobic pyrene moiety. To know the better understanding of gel formation, we have explored coordination chemistry of those gelators with Cu(II) and Zn(II) metal ions. Consequently, the complexes form void space within the lattice, and we were successfully inserted molecular iodine within the void space.

---

[1] (a) Sreenivasulu, B.; Vittal, J. J. *Angew. Chem., Int. Ed*. **2004**, *43*, 5769. (b) Ganguly, R.; Sreenivasulu, B.; Vittal, J. J. *Coord. Chem. Review* **2008**, *252*, 1027.

[2] (a) Alam, M. A.; Nethaji, M.; Ray, M. *Angew. Chem., Int. Ed*. **2003**, *42*, 1940. (b) Alam, M. A.; Nethaji, M.; Ray, M. *Inorg. Chem.* **2005**, *44*, 1302. (c) Alam, M. A.; Koner, R. R.; Das, A.; Nethaji, M.; Ray, M. *Cryst. Growth. Des.* **2007**, *7*, 1818. (d) Sahoo, S. C.; Ray, M. *Dalton Trans.* **2009**, 3230.

[3] (a) Gibney, B. R.; Wang, H.; Kampf, J. W.; V. L. Pecoraro. *Inorg. Chem.* **1996**, *35*, 6184. (b) Saalfrank, R. W.; Maid, H.; Mooren, N.; Hampel, F. *Angew. Chem., Int. Ed*. **2002**, *41*, 304. (c) Mezei, G.; Zaleski, C. M.; Pecoraro, V. L. *Chem. Rev*. **2007**, *107*, 4933.

[4] (a) Chen, X. M.; Aubin, S. M. J.; Wu, Y. L.; Yang, Y. S.; Mak, T. C. W.; Hendrickson, D. N. *J. Am. Chem. Soc*. **1995**, *117*, 9600. (b) Mizuno, T.; Wei, W. H.; Eller, L. R.; Sessler, J. L. *J. Am. Chem. Soc.* **2002**, *124*, 1134.

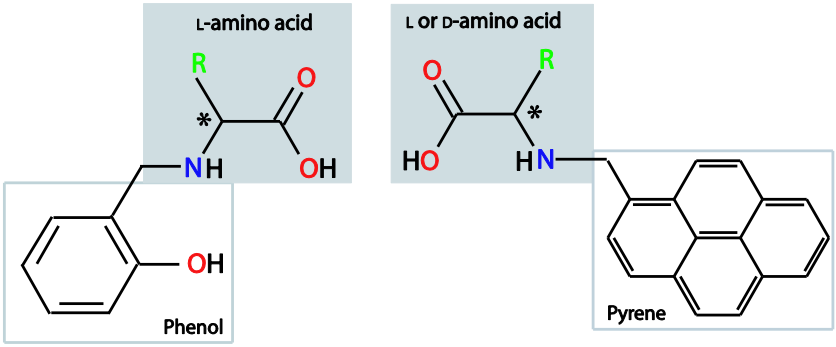

Figure 1. The amino acid derived ligands used.

The thesis has been divided in to seven chapters. Brief synopsis of each chapter has been provided below.

Chapter 1. This chapter summarizes the literature on the various types of self-assemblies based on hydrogen-bonded, Resorcin[4]arene-derivative, multi-dentate heterocyclic ligand, pH dependent or cation directed assemblies and finally assemblies with amino acid derivative ligands that defines the objective of the thesis.

Chapter 2. In this chapter, L-leucine derived ligand ($H_2L^{L\text{-}leu}$), KOH, and Ni(II)/Cu(II) salt in 2:2:1 ratio self-assembled into a rather large (~13 Å) supramolecular assembly with the formula $[K\{M(HL^{L\text{-}leu})_2\}_3]^+$ as shown in figure **2** and **3**. Structural characterization showed three $[M(HL^{L\text{-}leu})_2]$ units encapsulate K^+ similar to organic crown ethers/cryptand (Figure **3**). Substituting K^+ with Na^+ in the above reaction resulted in a set of structurally identical assemblies with the general formula $[M'\{M(HL^{L\text{-}leu})_2\}_3]^+$, where M' is either K^+ or Na^+ and M is either Ni(II) or Cu(II). The six H–bonds between phenolic oxygen and carboxylate oxygen from the neighboring $[M^{II}(HL^{L\text{-}leu})_2]$ units (Figure **3**) play the key role in stabilization of the assembly. Electrospray Ionization (ESI)–mass spectra of the assemblies in MeOH showed the retention of assemblies in solution. Uv–visible spectroscopic studies showed retention of assembly in N, N-dimethylformamide (DMF) which is stable even after the addition of 5 equiv of [18] crown–6. The assemblies show various degrees of dissociation to $[M(HL^{L\text{-}leu})_2]$ and M', in stronger H–bonding solvent like methanol. The dissociation can be reversed upon addition of excess KNO_3/$NaNO_3$ salt. Interestingly, visible spectra of potassium and sodium containing assemblies show that minor structural changes caused by replacing K^+ with Na^+ is sufficient to shift the d–d transition of Ni(II) by ~70 nm, thereby providing an indirect way of distinguishing K^+ and Na^+, none of which have spectroscopic signature in the visible range.

Overall, the structural characterization of the assemblies showed that six of L-leucine derived tridentate ligands, three Ni(II) ions and one K^+ or Na^+ self assemble into a rather large (~1 nm) sized assembly having binding site for one alkali metal ion and three sites for oxo anion (Figure **3**).

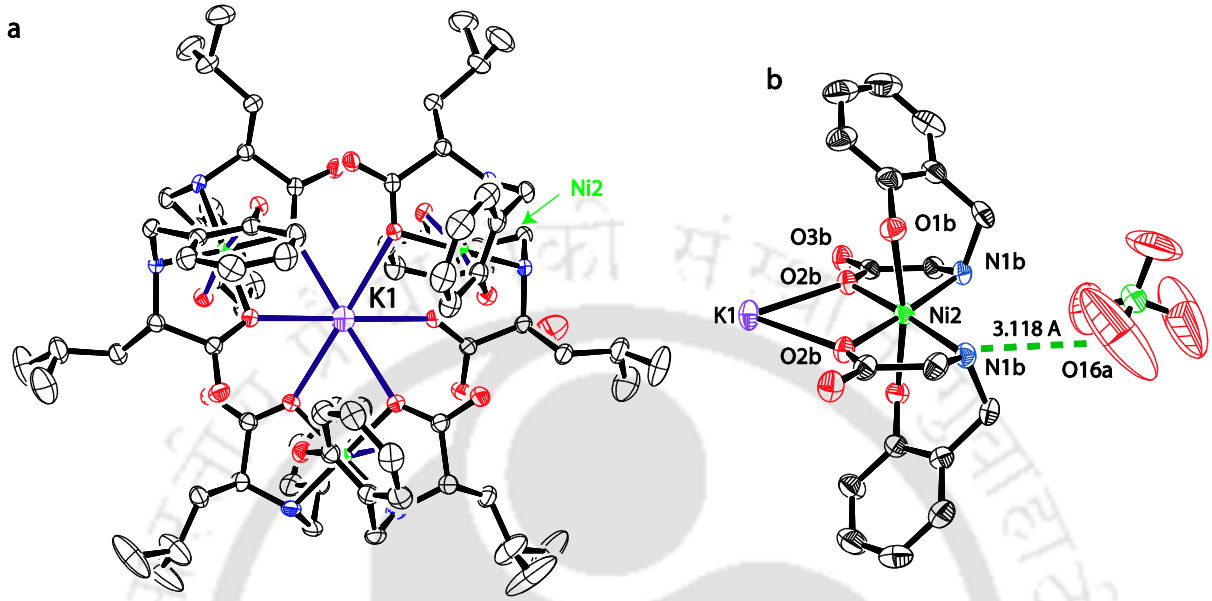

Figure 2. *(a) ORTEP diagram of K^+ encapsulated, Ni (II) containing assembly and (b) Coordination around one Ni(II) unit showing the cation and anion binding sites.*

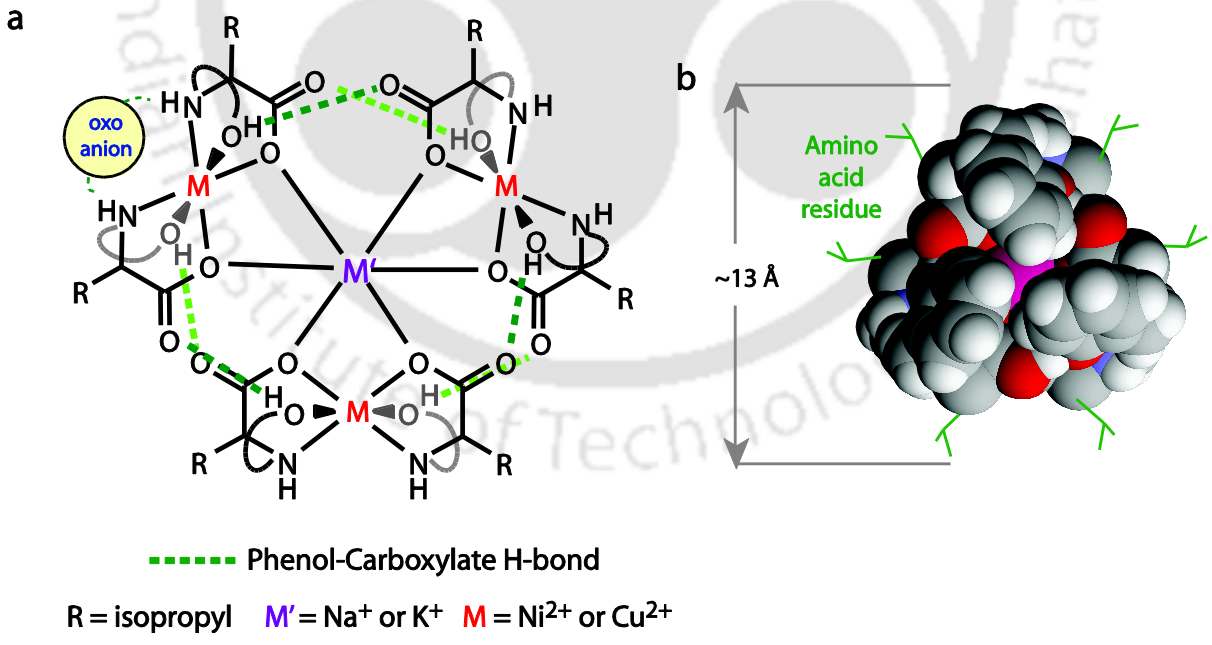

Figure 3. *(a) Sketch model of the assembly showing cation as well as anion binding sites and position of the six hydrogen bonds and (b) Space filling model of the assembly with isopropyl groups shown as sticks.*

Chapter 3. To prove the role of six hydrogen bonds in stabilizing assembly as well as supramolecular effect, we have synthesized and characterized different types of monomer using $H_2L^{L\text{-leu}}$ and $H_2L^{L\text{-tyr}}$ (figure **4**), by step wise axial ligand substitution and their transformation towards multinuclear assembly in presence of alkali metal based binary salts. Monomer to multinuclear transformation was confirmed from FTIR, ESI-Mass, visible spectra and X-ray crystallography. Notable, in this transformation is the *trans* orientation of the in-plane ligands in monomer to the *cis* orientation in the multinuclear assembly which is the vital for binding the alkali metal ion (Figure **5**).

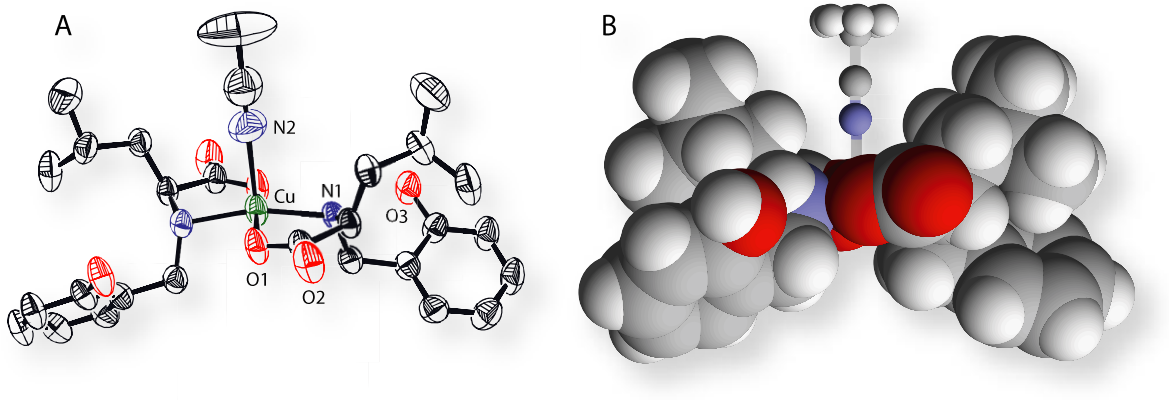

Figure 4. *(A) ORTEP diagram of monomer with thermal ellipsoids set to 30% probability level, and (B) A space filling model of C2 symmetric cavity in monomer.*

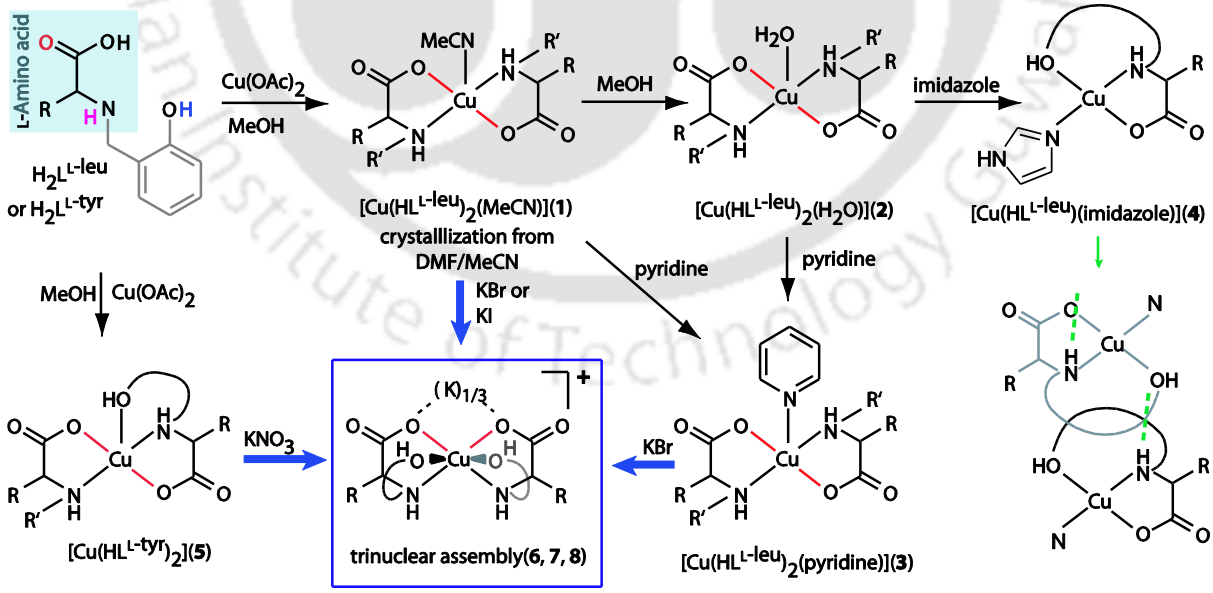

Figure 5. *Step wise synthesis of the monomers and monomer (trans) to assembly transformation (cis).*

This result substantiate that carboxylate groups necessary for alkali metal binding were not predisposed in the Cu(II) monomers but was a result of alkali metal ion influenced reorientation (Figure **5**). Further, square pyramidal monomer converted into octahedral after phenol coordination in multinuclear assembly, which was uncoordinated in monomer. On addition of alkali metal salt to monomer, a sharp change in d–d transition appears at lower energy (diff. 25 nm) in DMF. This occurrence supports the monomer to multinuclear conversion.

Chapter 4. In this chapter, we have explored the effect of amino acid substitution such as L-leucine to L-methionine and L-tyrosine on multinuclear assembly via direct synthesis, as well as the effect of larger size alkali metal cation such as Cs^+ and anion on monomer to assembly conversion. The CsCl plays the role towards coordination polymer formation instead of multinuclear assembly conversion (Figure **6**). The CsCl containing coordination polymer is readily converted into multinuclear assembly in presence of K^+/Na^+ salt. Besides formation of CsCl containing coordination polymer, monomer self-assembles into multinuclear assembly in presence of $CsNO_3$. Sequential conversions conclude that K^+ containing assembly most stable among all the assemblies (Figure **7**). These results emphasize the role of cation and anion in formation of assembly.

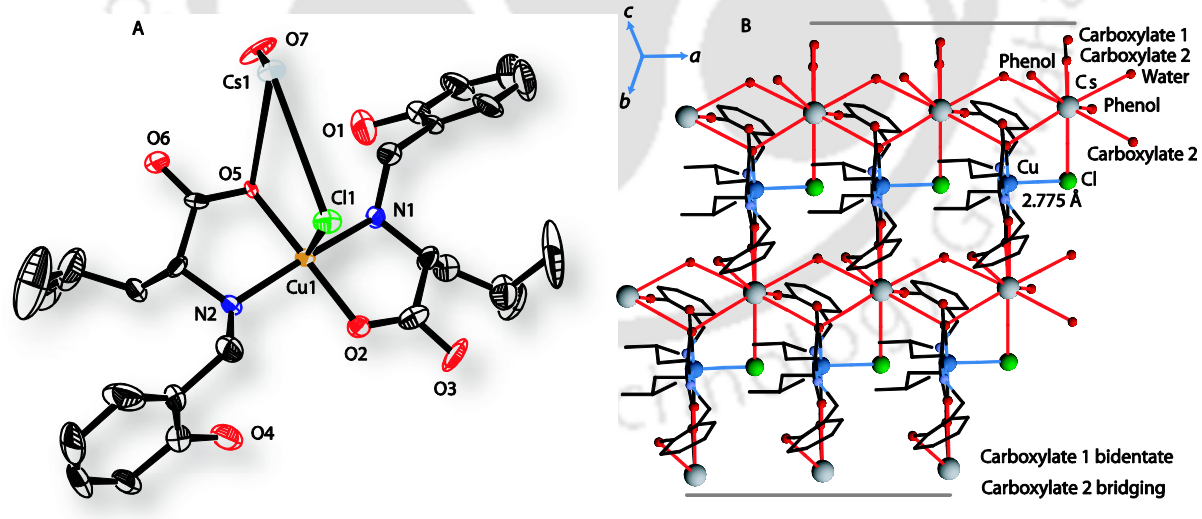

Figure 6. *(A) ORTEP diagram of Cs^+ containing coordination polymer (asymmetric unit) and (B) Lattice and coordination around Cs^+.*

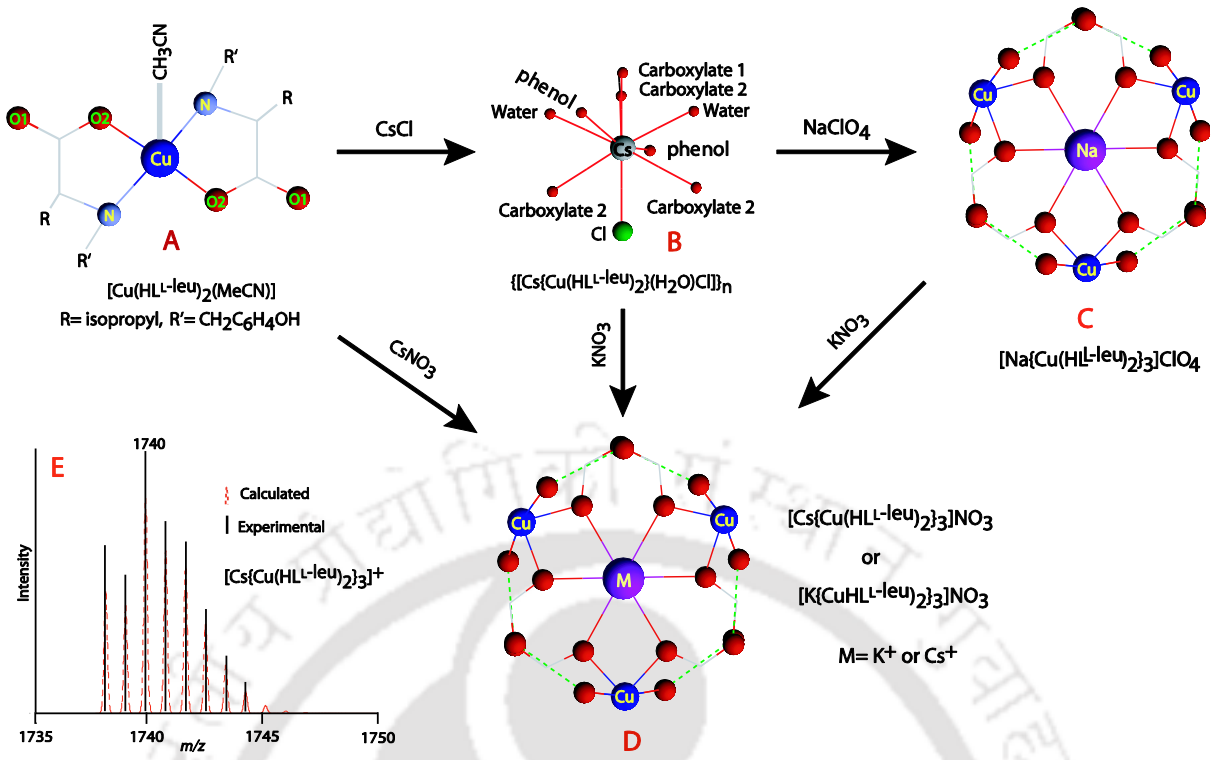

Figure 7. *A pictorial representation of coordination around alkali metal ion and sequential conversions of the assemblies where (A) Monomer [Cu(HL$^{L\text{-}leu}$)$_2$(CH$_3$CN)], (B) Assembly {[Cs{Cu(HL$^{L\text{-}leu}$)$_2$}H$_2$O]Cl}n, (C) Multinuclear assembly [Na{Cu(HL$^{L\text{-}leu}$)$_2$}$_3$]ClO$_4$, (D) Multinuclear assembly [K{Cu(HL$^{L\text{-}leu}$)$_2$}$_3$]NO$_3$ or [Cs{Cu(HL$^{L\text{-}leu}$)$_2$}$_3$]NO$_3$ and (E) ESI-Mass isotopic abundance pattern of the assembly [Cs{Cu(HL$^{L\text{-}leu}$)$_2$}$_3$]NO$_3$ red dotted(simulated) black(experimental) in MeOH.*

Chapter 5. In the previous chapters, we have explored Ni(II) and Cu(II) containing independent trinuclear assembly as well as different types of monomers and their conversion to multinuclear assembly. Behind these, our objective was to understand the effect of metal and ligand by varying of amino acid or metal Ni(II) to Cu(II), on formation of assembly. Consequently, we concluded that all the assemblies are isostructural without much significant change. Further, we got the clue to synthesize hetero-metallic assembly. In this chapter, we have synthesized and characterized a mixed metal trinuclear self-assembly [K(Ni$_2$Cu{(HL$^{L\text{-}leu}$)$_2$}$_3$)]ClO$_4$ of Ni(II) and Cu(II) in the 2:1 ratio using L-leucine derived ligand with metal: ligand ratio 1:2. As characterization of a mixed transition metal assembly is challenging in the field of coordination chemistry. Providentially, the assembly is well withstand in solid as well as in solution (Figure **8**). Mixed metal assembly was characterized by X-ray, ESI-mass spectroscopy, absorption spectroscopy and EPR spectroscopy. To know the correct proportion of Ni(II) and Cu(II), we performed the atomic absorption spectroscopic (AAS) analysis of isolated crystals as well as X-ray fluorescence (XRF) and energy dispersive X-ray (EDX) analysis of solid crystals. Atomic absorption spectroscopic analysis data supports

Ni(II) is to Cu(II) ratio is 2:1 in the mixed metal assembly. Though, insignificant discrepancy of values was found from batch to batch of samples, may be because of substitution of Ni(II) to Cu(II) or Cu(II) to Ni(II) within crystal. However, it is within error limit.

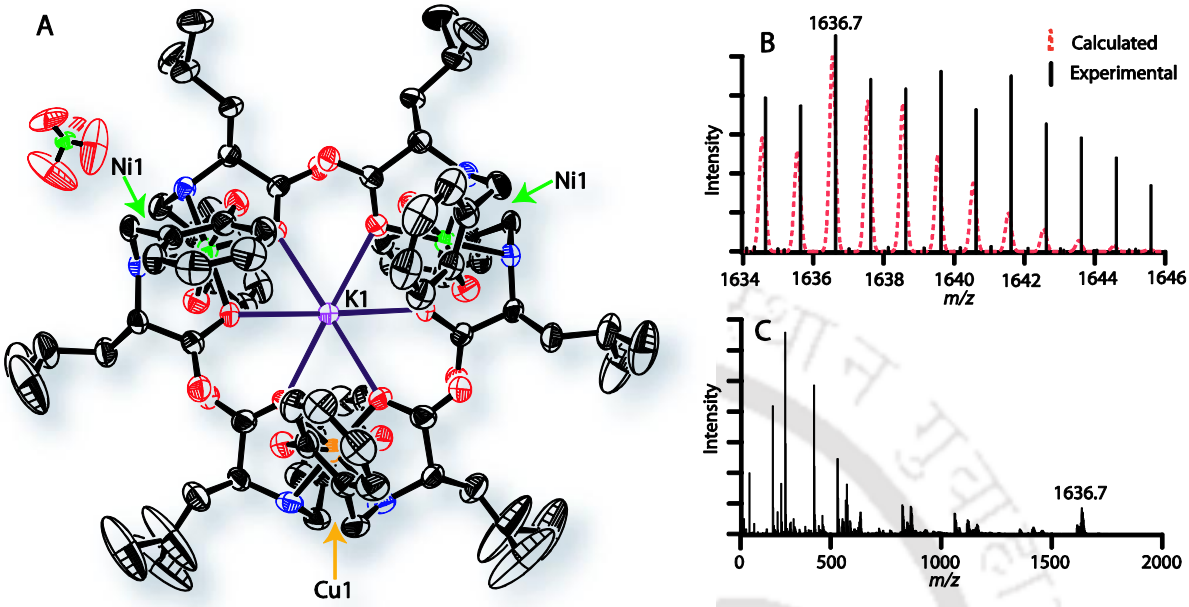

Figure 8. (A) *ORTEP diagram of mixed metal assembly with thermal ellipsoids set to 30% probability level and hydrogen atoms are omitted for clarity, (B) Isotopic abundance pattern calculated (red dotted) and experimental (black) and (B) ESI–MS spectrum for mixed metal assembly.*

Chapter 6. To know the role of phenol on multinuclear assembly formation, we have attached pyrene with leucine instead of phenol. Before exploring metal coordination of pyrene derived leucine, we have characterized a set of hydrogel in presence of LiOH as well as organogel, and elucidate the probable mechanism for self-assembly by using fluorescence spectroscopy. Absence of typical three monomer emissions for pyrene between 365–430 nm (observed in dilute solution) and observation of excimer emission at 480 nm exclusively for the gels suggest that extensive aggregation of pyrene units. Critical aggregation concentrations (CAC) calculated from the fluorescent spectra of the gradually diluted gels were found to be 0.007–0.009% w/v. Scanning electron microscopic (SEM) and Transmission electron microscopic (TEM) images of dried gels showed layered plate like structures for hydrogels while organogels showed exclusive formation of fiber (200nm – 1 μm) as shown in figure **9**. Explanation of these observations and presence of LiOH was elucidated with the additional information from powder diffraction on xerogels.

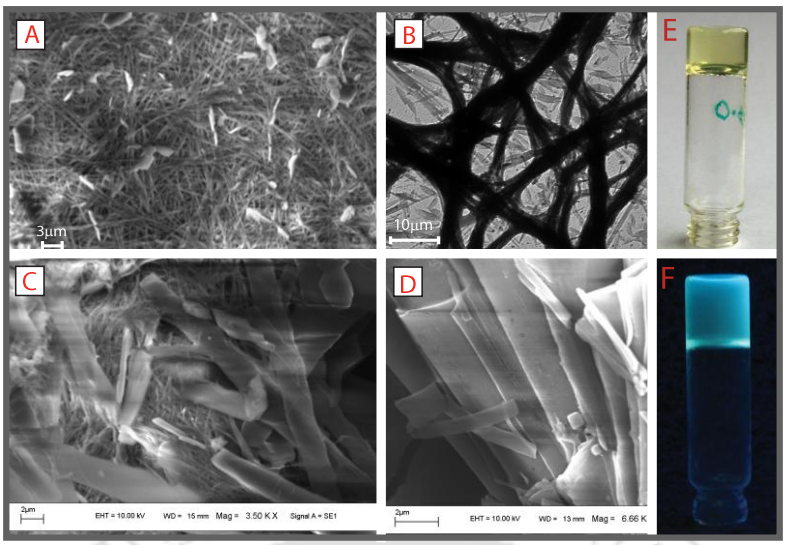

Figure 9. : *Different types of morphology of xerogel, SEM images (**A, C, D**) and TEM image (**B**), gel under naked eye (**E**) and under UV light (**F**).*

Chapter 7. In the previous chapter, we have observed pyrene derived L-leucine and D-leucine gel synthesis, aggregation pattern of hydrogel and organogel as well as their morphology at different conditions. Thus, we felt the necessity to understand the binding mode of Li^+ in hydrogel as well as aggregation pattern of pyrene moiety of those gelators by exploring the coordination chemistry with Cu(II) and Zn(II) metal ion instead of Li^+.

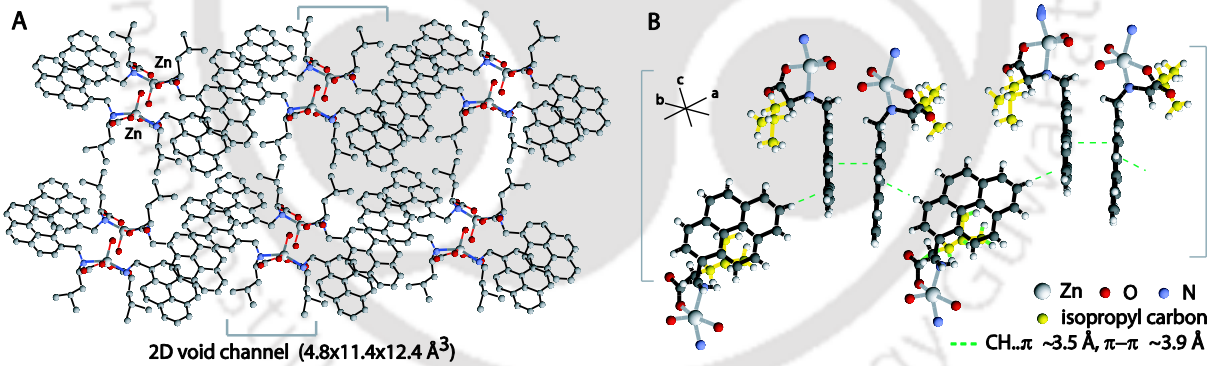

Figure 10. *(A) Pyrene derived L-leucine, Zn(II) Complex forms a two dimensional void channel within the crystal lattice. (B) Dimer formation through π…π stacking and CH…π interaction in the Zn(II) complex.*

In this chapter, we have synthesized, characterized and structurally isolated a set of Cu(II) and Zn(II) complexes. Further, the ligand arrangement around the Cu(II)/Zn(II) are such that hydrophobic pyrene units and the side arms lies on one side of the Cu(II)/Zn(II) coordination plane, while coordinated waters lies on the opposite side (Figure **10**). This resulted in a clear separation of hydrophobic and hydrophilic zones in the molecule. Hydrophobic pyrene units of complexes show π– π and CH– π stacking that resulted in a layered structure in the crystal lattice of the complex (figure **10B**). The solid state

fluorescence of complexes forms exclusively excimer at ~450 nm which also supports the lattice arrangement of pyrene ring as dimer. Isopropyl group of L-leucine forms void channels and we could perform insertion of iodine into the channels of Zn(II) crystals as confirmed by the X-ray structure (Figure **11**). The I_2 content of the crystals was measured using the weight loss in TGA (10% wt loss between temperatures 50–130 ºC against calculated weight loss 1.9% for H_2O and remaining ~8% for I_2/monomer). The I_2 concentration in CCl_4 solution was measured spectrophotometrically and estimated I_2 was found to be 7% (calculated 15% for complex $[Zn(P^{L\text{-}leu})_2(H_2O)]0.58I_2{\cdot}H_2O$).

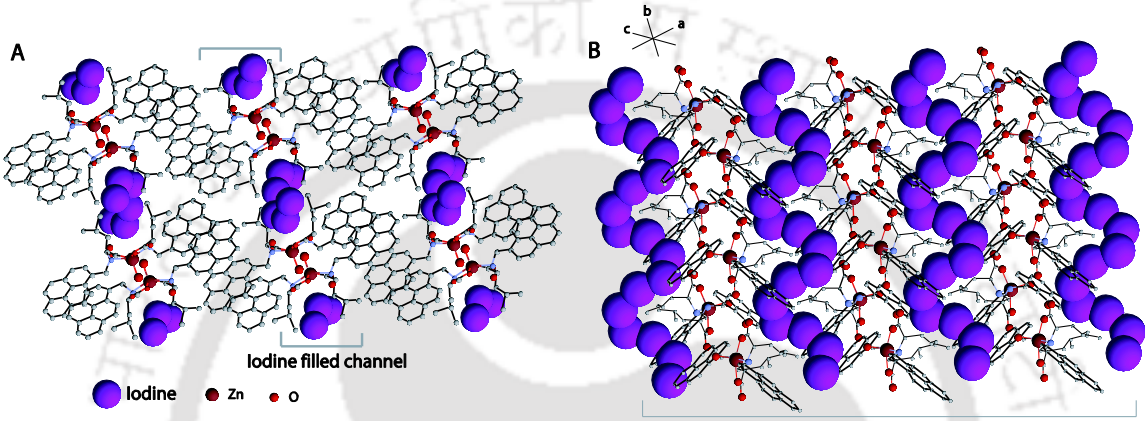

Figure 11. *(A) Iodine filled the two dimensional channel, one disordered I_2 molecule with one asymmetric unit. (B) I_2 molecules inside channel, orients in a helical fashion (Left handed).*

Contents

Chapter 1

Supramolecular chemistry is a branch of chemistry concerned with the coalescence of molecules into noncovalent arrays. Molecular recognition relies upon the complementarity of size, shape, and chemical functionalities **1** (Figure **1.1**). It explores and exploits intermolecular forces, the weak attractions that act over short distances between molecules. These forces hydrogen bonds, aromatic π–stacking, polar and van der Waal's interactions– are the ones that bring molecules together into complexes. Such complexes are temporarily and weakly bound groups of two or more molecules. Molecular recognition is then intimately involved in two separate processes: the binding of one molecule by another and the assembly of multiple molecules into supramolecular structures. There have been many creative contributions to the field of supramolecular chemistry in the construction of receptors, transport agents, enzyme models, and extended arrays. A multi volume series covering supramolecular chemistry far more comprehensively than is possible here has recently been published.[1]

The self-assembling capsules with enclosed cavities are formed by reversible non covalent interaction of two or more, not necessarily identical, subunits. The aggregate so formed should have a well-defined structure in solution and be capable of binding behavior that none of its individual components display alone. This definition naturally places an emphasis on three-dimensional assemblies. It specially excludes indefinite arrays and aggregates that are not designed to act as receptor such as micelles, liquid crystals, mono–layers, metal–ligand structures, and assemblies that exist only in the solid state. As such, self-assembling capsules represent a subset of self-assembling systems.[2] Syntheses of self assembling complexes can be promoted in numerous ways: (1) The strength of the noncovalent interactions that are responsible for maintaining the structural integrity of the complex can be enhanced, (2) The supramolecular complex can be selectively sequestered from solution in order to prevent dissociation of the complex back to its component parts, (3) Finally, a large excess of one of the components can be employed to drive the self-assembly process to completion.[3] This objective can also be achieved by firstly understanding the principles behind the self-organization, self-assembly, and self synthesis processes exhibited by biological systems such as tobacco mosaic virus structure where self-assembly of 2130 identical subunits, each comprising of 158 amino acids **2** (figure **1.1**), as well as the self-assembly of the DNA double helix from two complementary oligonucleaotides is perhaps the most well-known and intensively studied biological paradigm of strict self assembly **3** (Figure **1.1**).

From the scientific point of view and technological interest the assemblies with confined space are enormously important because of their ability to act as reaction container with catalysis by offering high concentration of reactant inside the confined space, gas storage, molecular recognition and to more advanced technological applications as chemical sensors, electrodes, data imaging and storage materials, and even lasers. For example, Rebek *et al*. showed that the rate of reactivity of Diels–Alder reaction accelerated nearly 200–fold inside the dimeric capsule, based upon glycoluril subunit.[4] Raymond *et al*. reported a highly charged, water-soluble, metal–ligand assembly with a hydrophobic interior cavity that thermodynamically stabilizes protonated substrates and consequently catalyzes the normally acidic hydrolysis of orthoformates in basic solution, with rate accelerations of up to 890-fold.[5] Kim *et al*. prepared a homochiral metal-organic porous material that allows the enantioselective inclusion of metal complexes in its pores and catalyses the trans esterification reaction in an enantioselective manner.[6] Aoyama *et al.* reported selective crystalline–phase guest addition, removal and exchange within the cavity, formed by anthracene-bis(resorcinol) derivatives.[7] Hulliger *et al.* demonstrated organic photorefractive materials which have potential application in the fields of high-density optical storage and image-processing techniques.[8] Schuth *et al.* have aligned and elongated highly polarisable pyridinium perchlorate derivative within the parallel channels of molecular sieve $AlPO_4$-5 which demonstrated laser action upon exciting the frequency.[9] Stang *et al.* developed organic square molecule including chiral square as well as their application to catalysis, porous sensing and filtering materials.[10] Thus synthesizing assemblies with confined space of different shape like cages, squares and capsule are challenging to a chemist.

1.1 Non-Covalent or Hydrogen-Bonded Assemblies:

Hydrogen bonding is the favourite intermolecular force in self-assembling systems by virtue of its directionality, specificity, and biological relevance.[11] The molecule designed and synthesized by Zimmerman presents a pattern of hydrogen-bond donors and acceptors on one edge that is complementary to the pattern on the other functioning edge **4** (Figure **1.1**).[12] Another report by Zimmerman published on a three-dimensional self assembling system where self-assembly is controlled by dendrimer substituents.[13] Lehn and co-workers characterized $(melamine)_3.(barbiturate)_3$ rosettes by appending crown ethers from melamine subunits **5** (Figure **1.1**). Rosettes so functionalized can complex alkali metal cations, potassium in particular, and are detectable by ESI-MS.[14] Zhao and Luong have studied a simple self assembling receptor based on the association of (hydropropyl)-*β*-cyclodextrin and

porphyrin tetra carboxylic acid through hydrogen bonding between the acids on porphine ring and the hydroxyls on the upper rim of the cyclodextrins **6** (Figure **1.1**).[15a] This porphyrin-cyclodextrin aggregate was used as an aqueous sensor for pentachlorophenol, an environment pollutant.[15b]

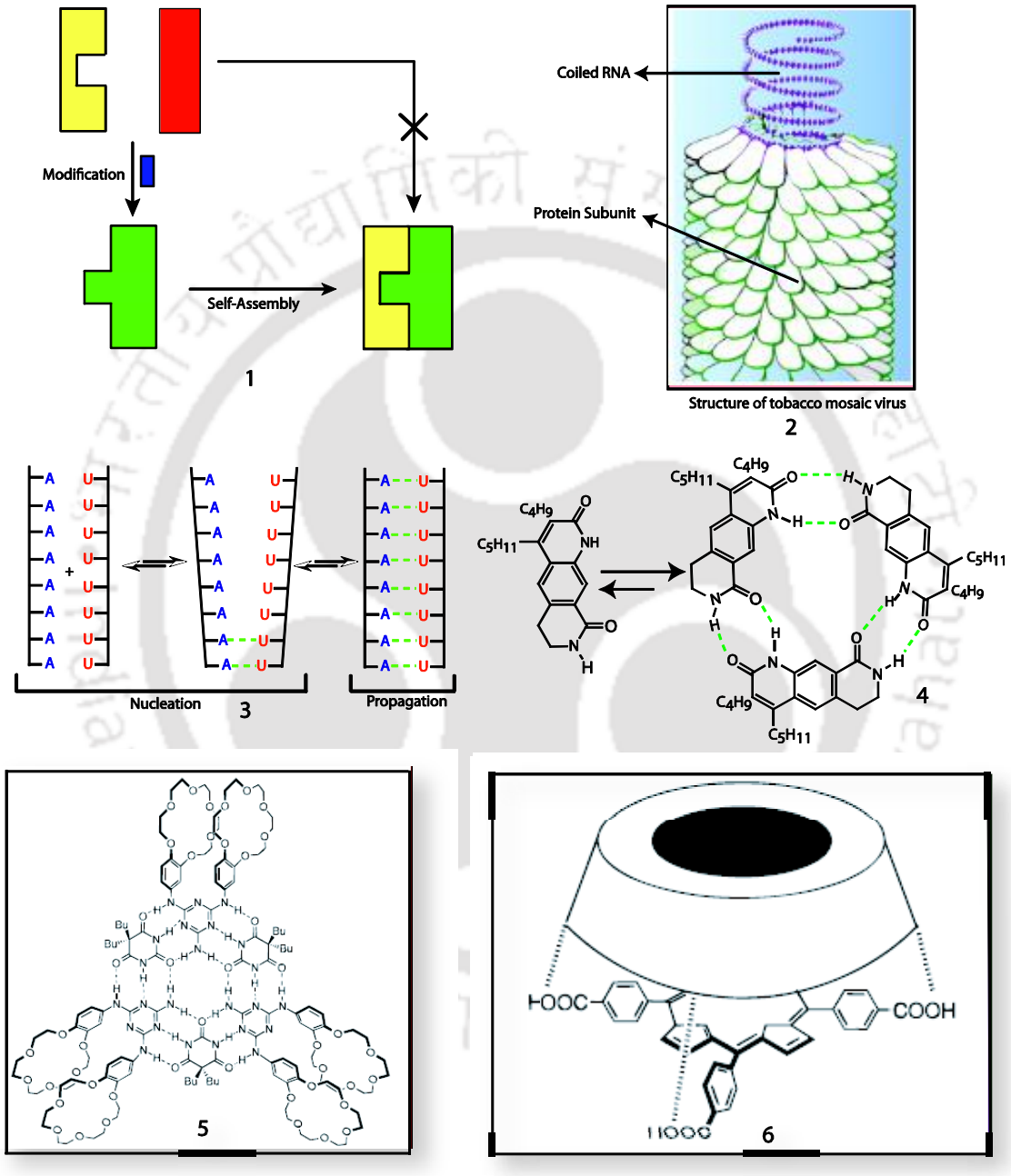

Figure 1.1. *(1) Process of self-assembly via modification. (2) and (3) is the self-assembly in biological systems, (4) – (6) Hydrogen-bonded self assemblies.*

Rebek and co-workers have published an outstanding series of non–covalent dimeric capsules based upon the dimerization of glycoluril derivatives **7** (Figure **1.2**) through its

intrinsic curvature and multiple hydrogen- bonding groups some of which are known as 'tennis balls' or 'softballs' **8** (Figure **1.2**). By variation of the spacer in the glycoluril units Rebek *et al.* controlled the volume of the cavity and encapsulated large guest molecules **9** (Figure **1.2**).[4,16] Recently they demonstrated the broad series of elegant solution phase studies outline the behavior of encapsulated species within this cylindrical capsules. [17]

Recently, Ananchenko *et al.* has described a series of van der Waals capsular **11** assemblies formed by a series of p-alkanoylcalix[4]arenas **10** (Figure **1.2**).[18] The particular novelty associated with these assemblies is the ability to exchange the encapsulated guest species within a single crystal.[19] They also exhibited phototransformation of *cis* and *trans* stilbene.[20]

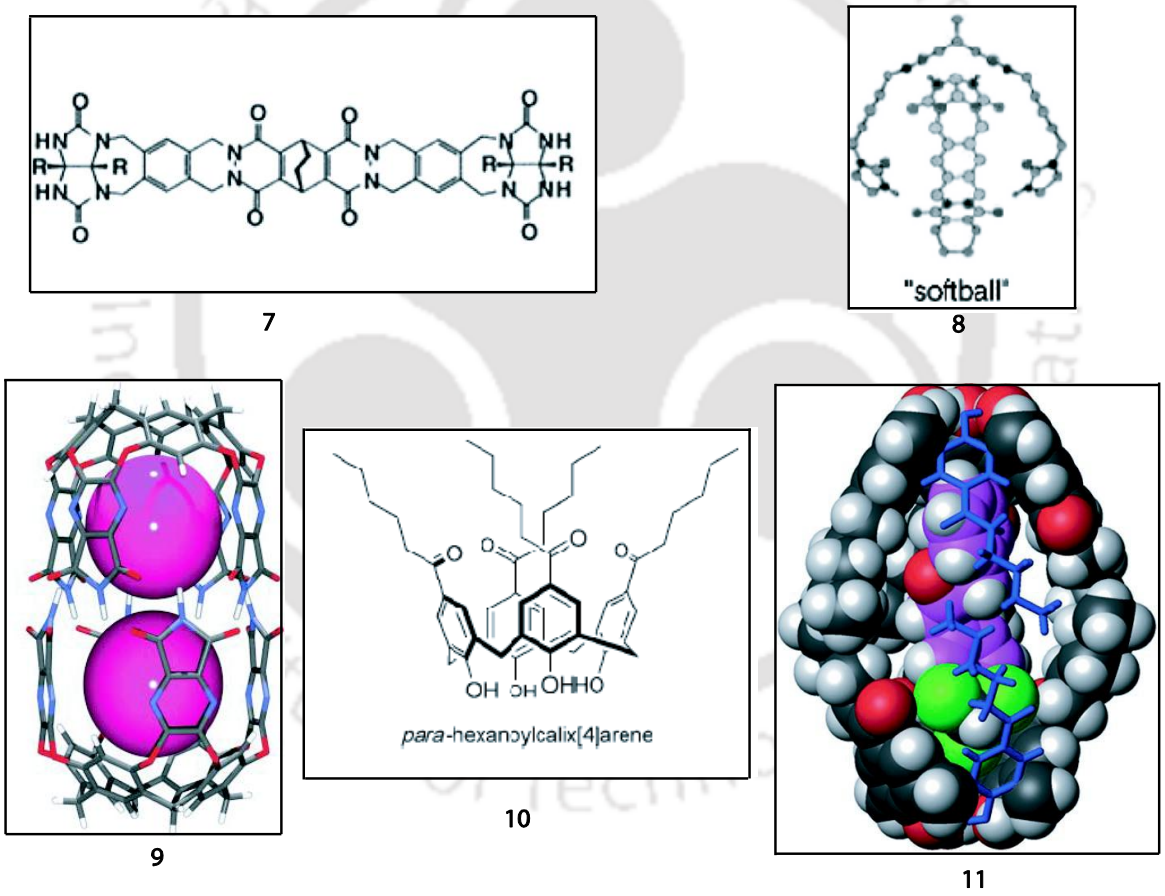

Figure 1.2. *Non-covalent organic assemblies.*

Vittal *et al.* reported centrosymmetric binuclear compound, **12** $[Cu_2(D,L\text{-}Sala)_2(H_2O)].2H_2O$, which is the 1D hydrogen bonded polymers. The two lattice water molecules, two aqua ligands and two carbonyl oxygen atoms also form strong O-H…O bonds to generate a 16-membered ring, creating 2D hydrogen-bonded sheets as displayed in **13** figure **1.3**.[21]

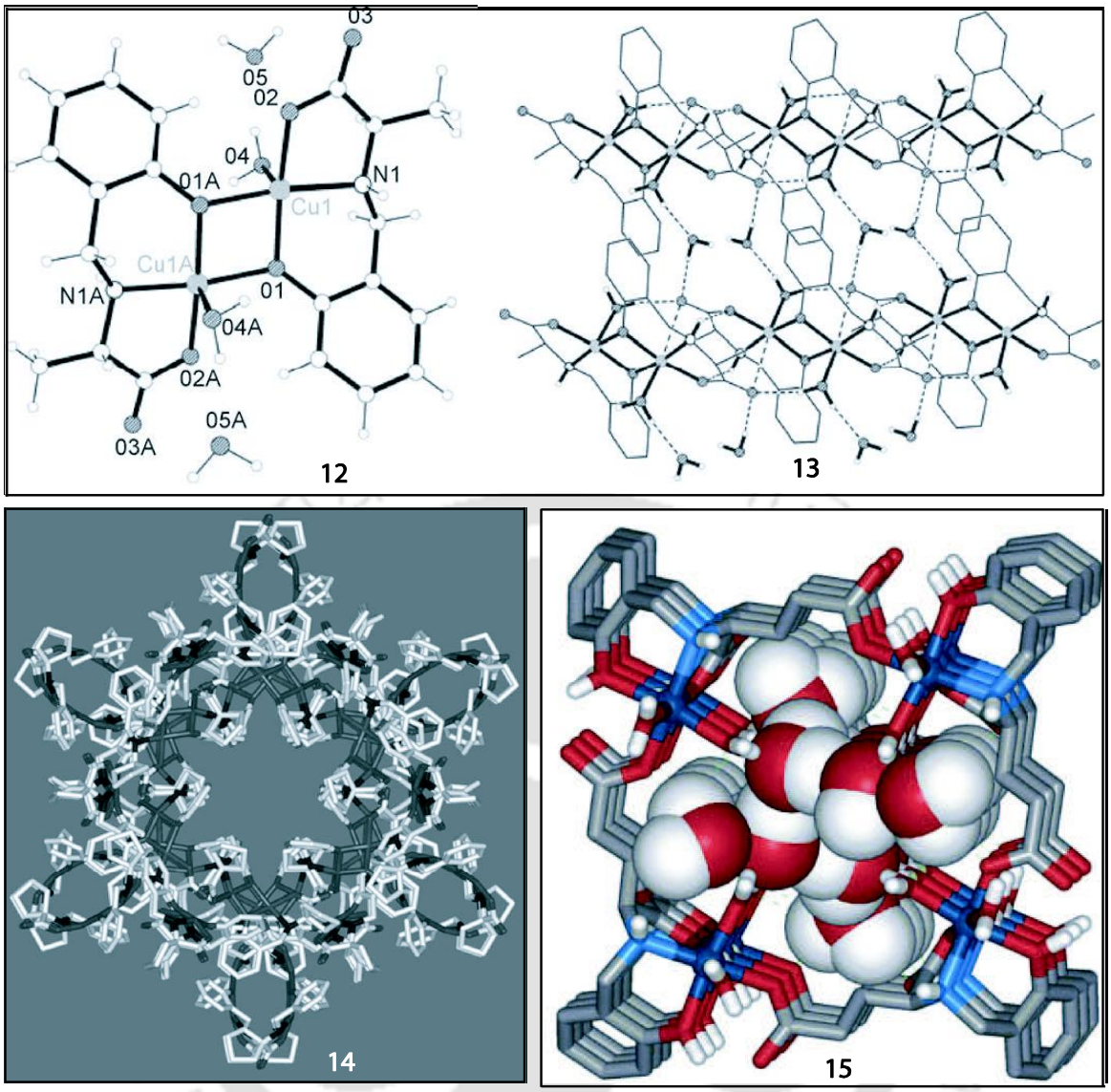

Figure 1.3. *Assemblies stabilized by hydrogen-bond.*

Highlighting the role of single pot crystallization and hydrogen-bonded polymeric structures, the star like channel observed in complex $[Cu_2(Scp11)_2]$ as shown in **14** figure **1.3**, is created by packing of molecules has about 27% empty space in the crystal lattice which is partially occupied by water molecules.[22] Another interesting Ni(II) complex, $[(H_2O)_2\subset\{Ni(HSglu)(H_2O)_2\}]\cdot H_2O$ derived from *N*-(2-hydroxybenzyl)-L-glutamic acid (H_3Sglu) displays a novel helical staircase coordination polymeric structure encapsulating1D helical water chain in the chiral helical channels **15** (Figure **1.3**). The octahedral coordination at the Ni(II) centre is completed by two aqua ligands. Of the six lattice water molecules present in asymmetric unit, two of the four inside the helical pore are hydrogen bonded to produce a 1D helical polymer. Hydrogen bonding is the propagation by the other two water molecules *via* helical water chain and aqua ligands. Dehydration leads to the collapse of the

single crystalline nature as the free standing staircase polymers are not supported by strong covalent interactions.[23]

1.2 Assembly based on Resorcin[4]arene-derivative:

Atwood *et al.* reported self-assembly of hydrogen-bonded nano-capsules based on C-methylresorcin[4]arene or the C-alkylpyrogallol[4]arenes, by changing the upper or lower rim of the corresponding units.[24,25] They have also reported a chiral hexameric capsule in the solid state.[26] Recently, they have focused on quantitative conversion of pyrogallol[4]arene monomers into corresponding hexameric nano-capsules and also the assembly of metal–organic nano-capsules (MONC's) (Cu, Ga) based on preformed capsule as template (Figure **1.4**).[27] The capsule **16** contains total 24 Cu metal centers into all of the theoretical square planar binding sites. This capsule further assemble through coordination of the propanol tails to Cu centres of neighbouring MONC's, the result being an insoluble coordination polymer. They also investigated to encapsulate the probe molecules within these large assemblies with a view to reporting on the interior of this voluminous capsules.[28, 25]

Harrison and co-workers have synthesized a series of resorcin[4]arene-based cavitands **17** (Figure **1.4**) that possess 'upper rim' functionalized with iminodiacetate groups as well as dipyridylimino groups which were useful for metal complexation with copper, iron and cobalt **18** (Figure **1.4**) for example.[29] They also showed a series of elegant structures based on dimeric tetra-metallated capsules that can be pH dependent, and that can reversibly capture organic molecules from water.[30]

Rebek and co-worker recently reported the hydrogen-bonded hexameric capsules where fluorescence resonance energy transfer (FRET) was employed to monitor the dynamics of hydrogen-bonded hexameric assemblies formed from resocin[4]arenes and pyrogallo[4]arenes **19** (Figure **1.4**). Studies were designed to provide future insights into the degree of assembly and stability of these self-assembled capsules at the micro to nanomolar concentration ranges that are not accessible by NMR studies.[31]

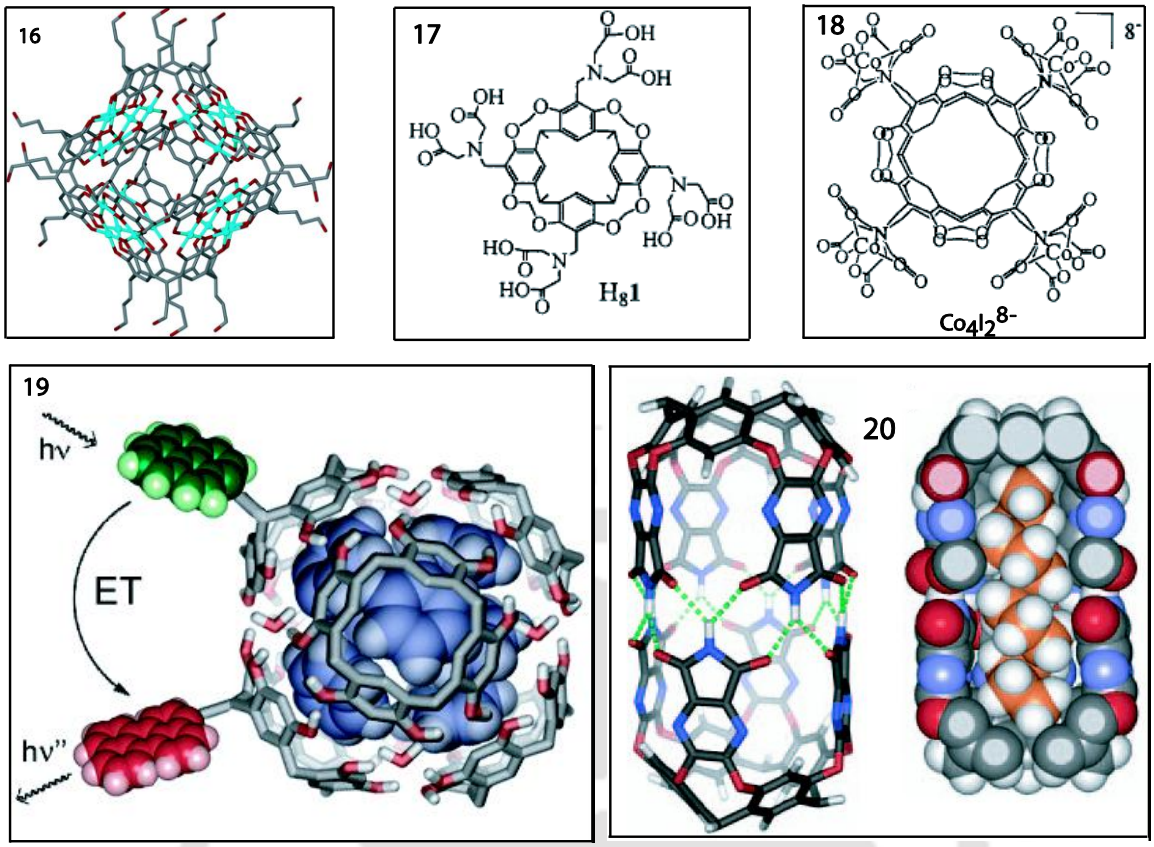

Figure 1.4 *Assemblies based on Resorcin[4]arene-derivative.*

Another report by Rebek, et al., where simple alkanes feature is fully extended conformations as their lowest-energy shapes but can assume coiled, compressed conformations in small spaces **20** (Figure **1.4**). A series of normal alkanes, were encapsulated in self-assembled, hydrogen-bonded complexes. Coiling of the longer alkanes was observed by NMR spectroscopy. The coiling exerts pressure on the interior; the hydrogen bonding seams are loosened, and rotation of the capsule's components occurs on the NMR timescale. The rotation results in interconversion of mirror-image capsule assemblies (racemization). The racemisation rates were determined and shown to increase with the length of the alkane, the longer alkanes exerting more pressure.[32]

1.3 Assemblies based on multi-dentate heterocyclic ligand and metal coordination:

Fujita *et al.* have shown that the combination of the square planer geometry of palladium and platinum with pyridine–based bridging ligand for the construction of highly symmetric supramolecular cages and capsules.[33] The positive charges on the metal centers make the compound highly water soluble; the hydrophobic pocket provided by the ligand is capable of efficient for binding the variety of guest molecule. The triangular tridentate **21** (Figure **1.5**), was assembled into a bowl-like M_6L_4 square –pyramidal cone **22** (Figure **1.5**) in presence of ethylenediamine-protected Pd(II) complex which was further assembled in to a

dimeric capsule **23** (Figure **1.5**) in aqueous media, that accommodates as many as six neutral organic molecules.[34] Almost coplanar triangle hexadentate ligand, **24** (Figure **1.5**) was combined with [(en)Pd(NO_3)$_2$] formed almost fully closed shell molecule **25** but it is unable to allow entry or escape of organic guest molecule during assemble. There is no direct metal-ligand bonding between the supramolecular cages or capsules that comprise the capsule halves. To demonstrate the potential of some of these large metal-organic assemblies, Fujita and co-workers are currently investigating these frameworks for uses that include chirality enrichment through enantiomer recognition.[35] In expectation of tubular structures, a rectangular panel, tetrakis(3,5-pyridine) **26**, was designed.[36] Upon treatment with [(en)Pd(NO_3)$_2$] and with the assistance of a template, a coordination nanotube **27** was formed. The nanotube **27** consists of four molecules of **26** and ten molecules of [(en)Pd(II)]$^{2+}$. A rod like guest such as sodium 4, 4′-biphenylenedicarboxylate is essential in the formation of **27**. At room temperature, the rod like guest stays at a fixed position or only shuttles inside the tube, desymmetrizing the host framework.[37]

Stang and co-workers have also used pyridyl-based ligands **28** (Figure **1.5**) with platinum metal centers to synthesize an impressive series of discrete metallo-supramolecular assemblies. They have used *cis*-Pt(PMe_3)$_2$(OTf)$_2$ as a V-shaped building unit, and react the metal centers with triangular shaped ligands (such as 1,3,5-tris(4-pyridyl-*trans*-ethenyl)benzene) in a 3:2 ratio to build the discrete architectures in near quantitative yield **29** (Figure **1.5**).[38] A series of self-assembled coordination cages of D_{3h} symmetry were also assembled by similar methods using slightly varied platinum subunits and tripodal pyridyl-based ligands.[39]

Raymond and co-workers have used catechol-based ligands **30** (Figure **1.6**) and reacting with iron and gallium centres, the chelating effect and the presence of particular (naphthalene and pyrene) organic spacers between the catechols drives the formation of M_4L_6, **31** (Figure **1.6**) cluster type assemblies (where M= Fe or Ga, and L = catechol-based ligand).[5,40] They have shown that a chiral self-assembled M_4L_6 supramolecular tetrahedron can encapsulate a variety of cationic guests with varying degrees of stereoselectivity. Recently, they encapsulated reactive iridium guests and the C−H bond activation of aldehydes occurs with the host cavity controlling the ability of substrates to interact with the metal center based upon size and shape. In addition, the host container can act as a catalyst itself by restricting reaction space and preorganizing the substrates into reactive conformations.[41]

Saalfrank and co-workers used the tris-bidentate 4-acyl-2-pyrazolin-5-one ligand **32** (Figure **1.6**) with gallium centres to assemble M_6L_6 clusters **33** (Figure **1.6)** that they describe as a 'cylinder'[42] Further modification of the trigonal ligand framework so as to generate tris-malonate-based chelator ligands, followed by combination with iron chloride, resulted in the formation of tetra- and hexa-nuclear metal clusters depending on particular functionalities (O-tBu or O-tolyl, respectively) placed on the ligand framework.[43]

1.4 pH dependent and cation directed assemblies:

Metallacrowns (MCs) with a variety of structural types can also be obtained by self-assembly of metal ions and the reduced Schiff base ligands. In general, MCs are robust in solution and this property can be employed for exchange reactions with metal ions and anions. The selectivity is determined not only by cavity size of the MC but also by the radii of the ions used.[44]

Vittal and co-workers reported the "host-guest" chemistry of Cu(II) compounds containing reduced Schiff base ligands that gives structurally different MC cations in the presence and absence of Li^+ in the cavity as shown in figure **1.7**. The MC cations are very labile in this system with Cu(II) ions and the pH of the solution also found to play an important role. In the 1D coordination polymeric species **34** $[Cu(Hphis)(H_2O)](ClO_4)_2$, the Cu(II) centre is five-coordinated, with the tridendate phis ligand (histidine derivative) bonded in a *mer* fashion (Figure **1.7**).[45] When the potassium salt of phis reacted with Cu(II) salt in a molar ratio, the crystals isolated as **35** $[Cu_3(phis)_3](ClO_4)_3{\cdot}2H_2O$ as shown in figure **1.7**.[45] The compound **36** $[(ClO_4)Li{\subset}Cu_3(phis)_3](ClO_4)_3{\cdot}3H_2O$ has been isolated when a molar equivalent of $LiClO_4$ was added to **35**.[45] The same compound could also be obtained from the lithium salt of phis and $Cu(ClO_4)_2{\cdot}6H_2O$ in a 1:1 molar ratio. It is obvious that the $[Cu_3(phis)_3]^{3+}$ cation, [8-MC-3], has structurally reorganized to accommodate a $LiClO_4$. The pH dependent interconversion of **34**–**36** is summarized in figure **1.7**.

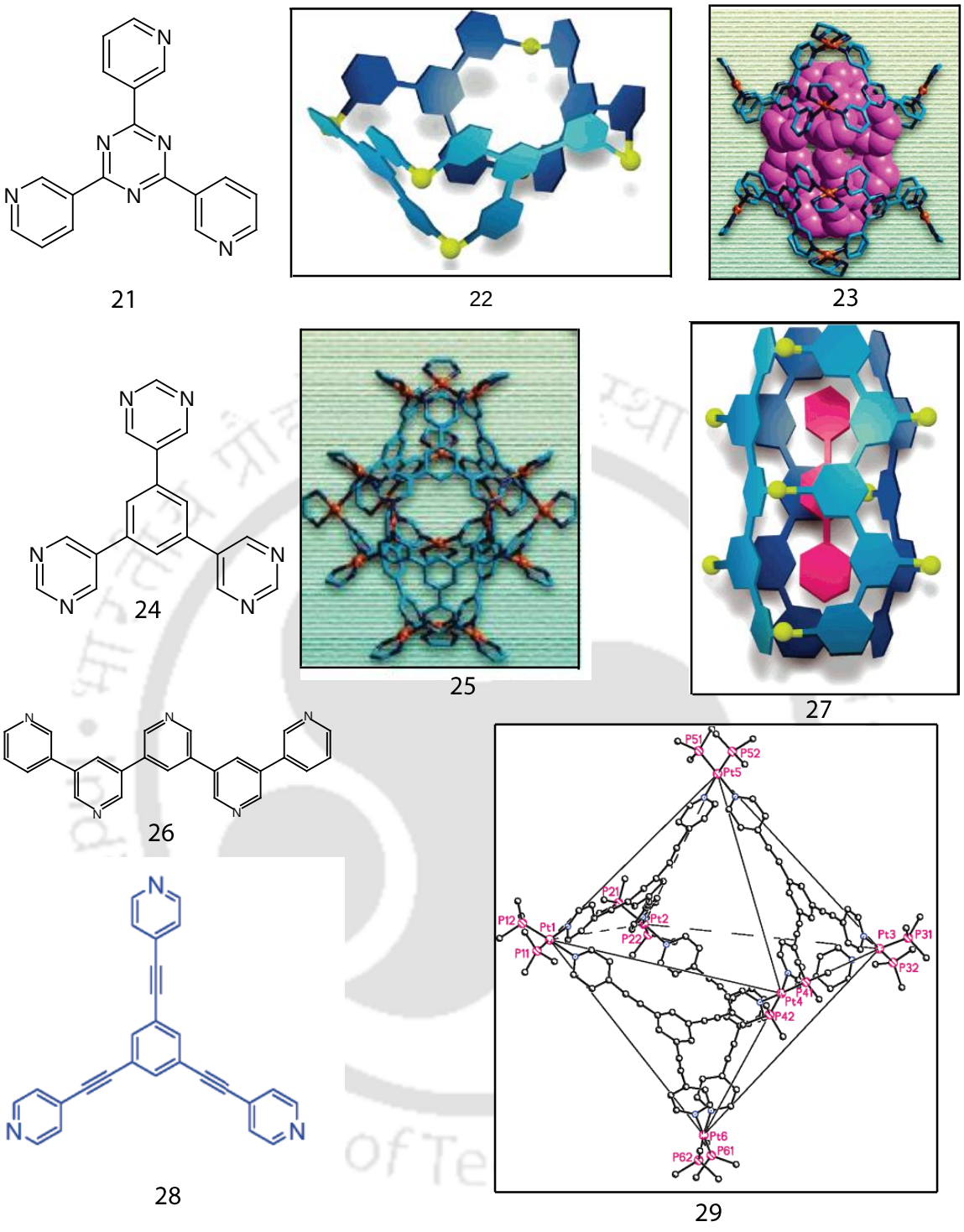

Figure 1.5 *Assemblies (cages or capsules) based on tris(pyridine) based ligand.*

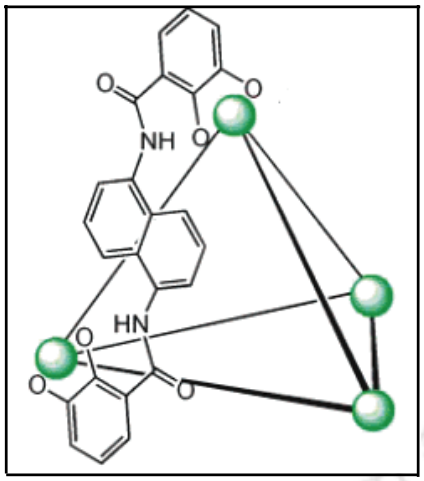

30

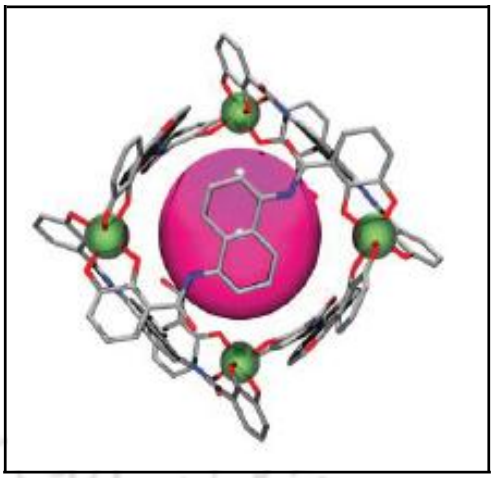

= Fe, Ga

Metal

31

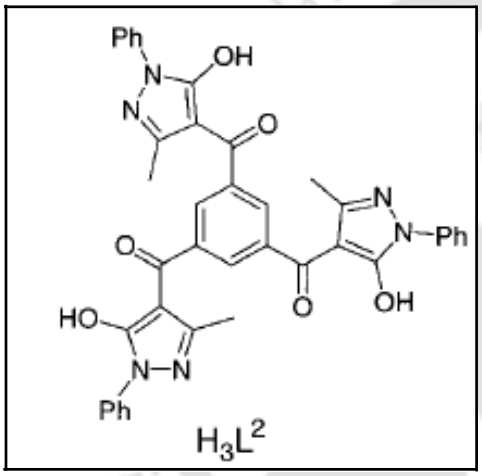

32

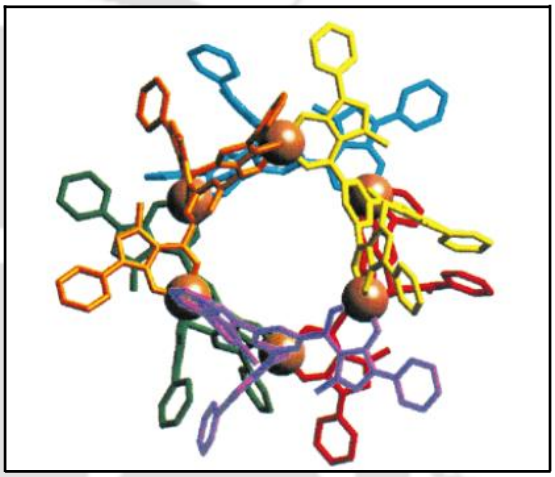

33

Figure 1.6 *Metalo-organic assemblies with multi-dentate heterocyclic ligand.*

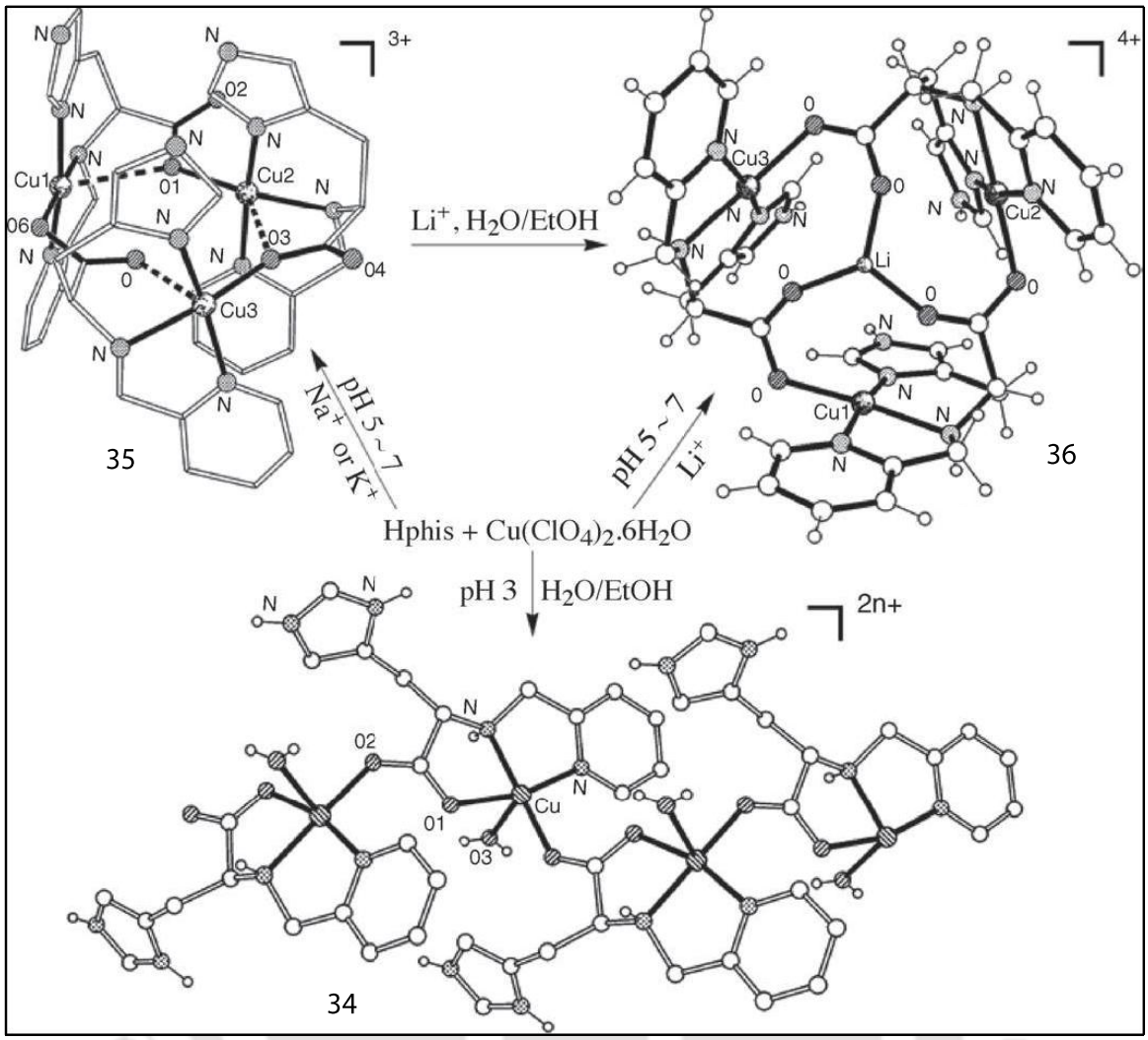

Figure 1.7*pH dependent and cation directed assemblies.*

1.5 Metallasupramolecular structures with amino acid derivative ligands

Earlier our group reported synthesis and characterization of a octanuclear Cu(II) complex **37** with L-histidine derived reduced Schiff base ligand **38** which accommodated four pyridine inside its capsular cavity (Figure **1.8**).[46] It was one of a kind having chirality, H-bonding and labile metal centre within the same molecule. Using the same ligand our group also reported hydroxo bridged one dimensional water removable channel using the Fe(III) metal ion **39** (Figure **1.8**).[47]

The L-histidine derivative **40** used earlier was unique in several ways. Being a non planar tetradentate ligand it promoted formation of multinuclear species unless an external ligand blocked the vacant sites.[46-48] The ambidentate nature of the imidazole arm of L-histidine further increased the difficulty in predicting the final structure.[48]

In this thesis, we had decided to explore the chemistry of the L-leucine derivative. We choose L-leucine over L-histidine to reduce the ligand denticity to three. We expected that this

will allow us synthesizing mononuclear *bis* complexes with Ni(II)/Cu(II) leaving the amino acid arms to control steric crowding in case cavities or channels form because of H-bonding between mononuclear units.

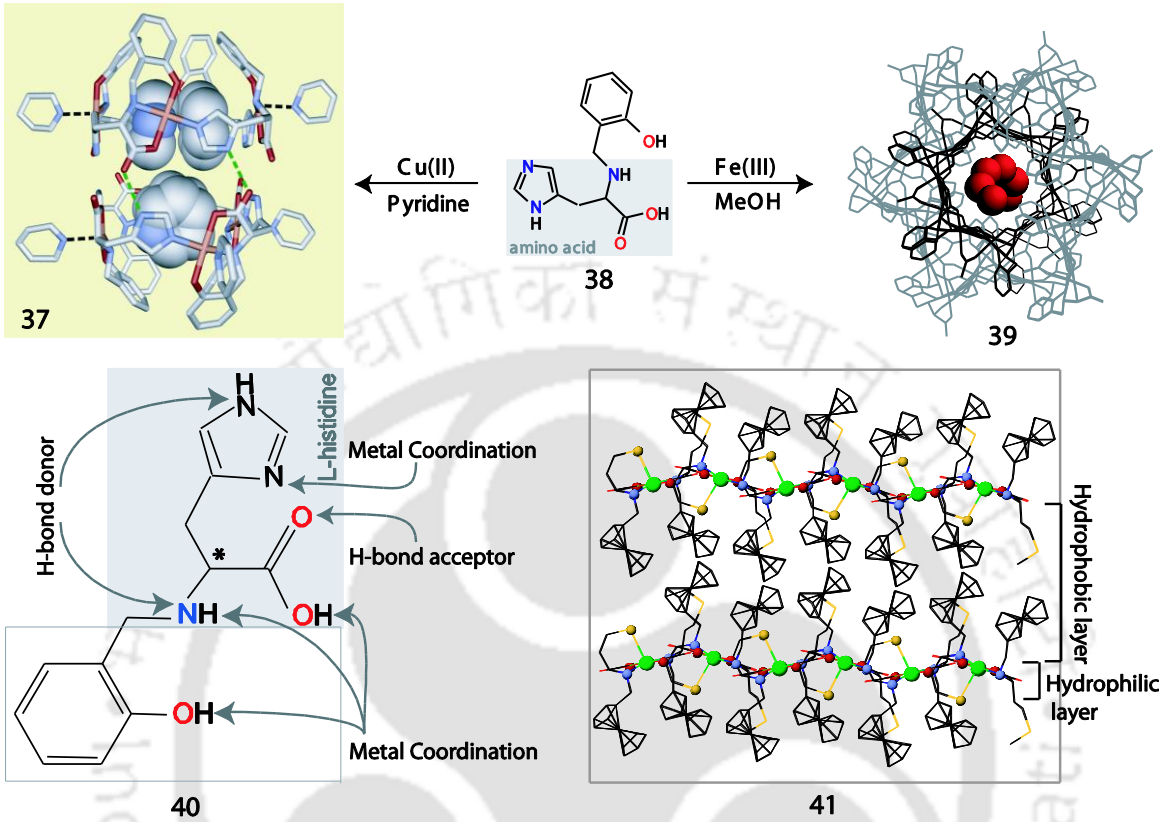

Figure 1.8 *Metallasupramolecular structures derived from amino acid ligands.*

Use of L-leucine allowed us to structurally characterize assemblies those are quite different from earlier observed.[44] We have systematically studied (a) Self assembled multi-nuclear assembly and supramolecular effect (Chapter **2**), (b) step wise assembly or mononuclear to trinuclear conversion (Chapter **3**), (c) Effect of amino acid and cesium cation coordination on the assembly (Chapter **4**), (d) self-assembled hetero-metallic assembly (Chapter **5**). Earlier our group reported, synthesis and characterization of a Cu(II) complex with ferrocenylmethyl L-methionine derived reduced Schiff base ligand where hydrophilic and hydrophobic layers separated within crystal lattice **41**.[49] Based on that observation we have incorporated hydrophobic pyrene instead of ferrocene and studied (e) Assembly of pyrene derivatives as gel and effect of chirality on the formation of gel (Chapter **6**), and (f) Assembly of pyrene derived amino acid complexes forming channels and incorporation of molecular iodine within those channels (Chapter **7**).

References

1. *Comprehensive Supramolecular Chemistry*; Lehn, J.-M., Atwood, J. L., Davies, J. E. D., MacNicol, D. D., Vo¨gtle, F., Ed.; Pergamon: New York, 1996.
2. Conn, M. M.; Rebek, J. Jr. *Chem. Rev.* **1997,** *97*, 1647.
3. Lawrence, D. S.; Jiang,T.; Levett, M. *Chem. Rev.* **1995**, *95,* 2229.
4. (a) Meissner, R.S.; Rebek, J. Jr.; Mendoza, D. J. *Science* **1995**, *270,* 1485. (b) Kang, J.; Rebek, J. Jr. *Nature* **1997**, *385*, 50.
5. Pluth, M. D.; Bergman, R. G.; Raymond, K. N. *Science* **2007**, *316*, 85.
6. Seo, J. S.; Whang, D.; Lee, H.; Jun, S. I.; Oh, J.; Jeon, Y. J.; Kim, K. *Nature* **2000**, *404*, 982.
7. Endo, K.; Kpoke, T.; Sawaki, T.; Hayashida, O.; Masuda, H.; Aoyama, Y. *J. Am. Chem. Soc.* **1997**, *119*, 4117.
8. Langley, P. J.; Hulliger, J. *Chem. Soc. Rev*. **1999**, *28*, 279.
9. Ihlein, G.; Schuth, F.; Krauss, O.; Vietze, U.; Laeri, F. *Adv. Mater*. **1998**, *10*, 1117.
10. Leininger, S.; Olenyuk, B.; Stang, P. J. *Chem. Rev.* **2000**, *100*, 853.
11. Jeffrey, G. A.; Saenger, W. *Hydrogen Bonding in Biological Structures*; Springer-Verlag: Berlin, 1991.
12. Zimmerman, S. C.; Duerr, B. F. *J. Org. Chem.* **1992**, *57*, 2215.
13. Zimmerman, S. C.; Zeng, F.; Reichert, D. E. C.; Kolotuchin, S. V. *Science* **1996**, *271*, 1095.
14. Russell, K. C.; Leize, E.; Van Dorsselaer, A.; Lehn, J. M. *Angew. Chem., Int. Ed. Engl.* **1995**, *34*, 209.
15. (a) Zhao, S.; Luong, J. H. T. *J. Chem. Soc., Chem. Commun.* **1994**, 2307. (b) Zhao, S.; Luong, J. H. T. *J. Chem. Soc., Chem. Commun,* **1995**, 663.
16. Rebek, J. JR. *Acc. Chem. Res*. **1999**, *32*, 278.
17. Biros, S. M.; Rebek, J. Jr. *Chem. Soc. Rev*. **2007**, *36*, 93.
18. Ananchenko, G. S.; Udachin, K. A.; Dubes, A.; Ripmeester, J. A.; Perrier, T.; Coleman, A. W. *Angew. Chem., Int. Ed.* **2006**, *45,* 1585.
19. Ananchenko, G. S.; Udachin, K. A.; Pojarova, M.; Dubes, A.; Ripmeester, J. A.; Jebors, S.; Coleman, A. W. *Cryst. Growth Des*. **2006**, *6*, 2141.
20. Ananchenko, G. S.; Udachin, K. A.; Ripmeester, J. A.; Perrier, T.; Coleman, A. W. *Chem. Eur. J.* **2006**, *12,* 2441.
21. Yang, C.T.; Vetrichelvan, M.; Yang, X.; Moubaraki, B.; Murray, K.S.; Vittal, J. J. *J. Chem. Soc*., *Dalton Trans*. **2004**, 113.
22. Sreenivasulu, B.; Vittal, J. J. *Cryst. Growth Des.* **2003**, *3*, 635.
23. Sreenivasulu, B.; Vittal, J. J. *Angew. Chem., Int. Ed.* **2004**, *43*, 5769.
24. Atwood, J. L.; Barbour, L. J.; Hardie, M. J.; Raston, C. L. *Coord. Chem. Rev.* **2001**, *222*, 3.
25. Dalgarno, S. J.; Power, N. P.; Atwood, J. L. *Coord. Chem. Rev*. **2008**, *252*, 825.

26. MacGillivray, L. R.; Atwood, J. L. *Nature* **1997**, *389*, 469.
27. Dalgarno, S. J.; Power, N. P.; Warrenc, J. E.; Atwood, J. L. *Chem. Commun*. **2008**, 1539.
28. Dalgarno, S. J.; Tucker, S. A.; Bassil, D. B.; Atwood, J. L. *Science* **2005**, *309,* 2037.
29. Fox, O.D.; Dalley, N. K.; Harrison, R. G. *J. Am. Chem. Soc*. **1998**, *120,* 7111.
30. Fox, O. D.; Leung, J. F. Y.; Hunter, J. M.; Dalley, N. K.; Harrison, R. G. *Inorg. Chem.* **2000**, *39*, 783.
31. Barrett, E. S., Dale, T. J., Rebek, J. Jr. *J. Am. Chem. Soc.* **2008**, *130*, 2344.
32. Ajami, D.; Rebek, J. Jr. *Nature Chem*. **2009**, *1*, 87.
33. Fujita, M.; Nagao, S.; Ogura, K. *J. Am. Chem. Soc*. **1995**, *117*, 1649.
34. Fujita, M.; Tominaga, M.; Hori, A.; Therrien, B. *Acc. Chem. Res*. **2005**, *38*, 371.
35. Yoshizawa, M.; Tamura, M.; Fujita, M. *Angew. Chem., Int. Ed.* **2007**, *46*, 3874.
36. Aoyagi, M.; Biradha, K.; Fujita, M. *J. Am. Chem. Soc.* **1999**, *121*, 7457.
37. Tominaga, M.; Tashiro, S.; Aoyagi, M.; Fujita, M. *Chem. Commun*. **2002**, 2038.
38. Schweiger, M.; Yamamoto, T.; Stang, P. J.; Bläser, D.; Boese, R. *J. Org. Chem.* **2005**, *70,* 4861.
39. Kuehl, C. J.; Kryschenko, Y. K.; Radhakrishnan, U.; Seidel, S. R.; Huang, S. D.; Stang, P. J. *Proc. Natl. Acad. Sci. U.S.A*., **2002**, *99*, 4932.
40. (a) Caulder, D. L.; Powers, R. E.; Parac, T. N.; Raymond, K. N. *Angew. Chem., Int. Ed.* **1998**, *37*, 1840. (b) Terpin, A. J.; Ziegler, M.; Johnson, D. W.; . Raymond, K. N. *Angew. Chem., Int. Ed*. **2001**, *40*, 157.
41. (a) Pluth, M. D.; Raymond, K. N. *Chem. Soc. Rev.* **2007**, *36*, 161. (b) Fiedler, D.; Leung, D. H.; Bergman, R. G.; Raymond, K. N. *Acc. Chem. Res*. **2005**, *38*, 351.
42. Johnson, D. W.; Xu, J.; Saalfrank, R. W.; Raymond, K. N. *Angew. Chem., Int. Ed*. **1999**, *38*, 2882.
43. Saalfrank, R. W.; Glaser, H.; Demleitner, B.; Hampel, F.; Chowdhry, M. M.; Schünemann, B.; Trautwein, A. X.; Vaughan, G. B. M.; Yeh, R.; Davis, A. V.; Raymond, K. N. *Chem. Eur. J.* **2002**, *8*, 493.
44. Ganguly, R.; Sreenivasulu, B.; Vittal, J. J. *Coord. Chem. Rev*. **2008**, *252*, 1027.
45. Vittal, J.J.; Xiaobai, W.; Ranford, J.D. *Inorg. Chem*. **2003**, 42, 3390.
46. Alam, M. A.; Nethaji, M.; Ray, M. *Angew. Chem. Int. Ed.* **2003**, *42*, 1940.
47. Alam, M. A.; Nethaji, M.; Ray, M. *Inorg. Chem.* **2005**, *44*, 1302.
48. Alam, M. A.; Koner, R. R.; Das, A.; Nethaji, M.; Ray, M. *Cryst. Growth. Des.* **2007**, *7*, 1818.
49. Sahoo, S. C.; Ray, M. *Dalton Trans*. **2007**, 5148.

Molecules or molecular assemblies with cavities of different sizes and shapes have been synthesized in view of their potential use as selective hosts for anion sensing, catalysis, selective recognition, and separation of guest molecules.[1-3]

Metal complexes of amino acid derived reduced Schiff base ligands generated several interesting architectures including chiral capsule, channels and cavity owing to their flexibility, H-bonding ability, and inherent chirality.[4,5] Earlier, using a L-histidine derivative and Cu(II), our group reported a self-assembled octanuclear assembly accommodating four pyridine molecules inside a cavity.[5a]

The L-histidine derivative used earlier was unique in several ways. Being a non planar tetradentate ligand it promoted formation of multinuclear species unless an external ligand blocked the vacant sites.[5a-c] The ambidentate nature of the imidazole arm of L-histidine further increased the difficulty in predicting the final structure.[5c] We decided to reduce the ligand denticity to three by choosing L-leucine over L-histidine. We expected that this will allow us synthesizing mononuclear bis complexes with Ni(II) leaving the amino acid arms to control steric crowding in case cavities or channels form because of H-bonding between mononuclear units.

In this chapter, using a L-leucine derivative (Scheme **2.1**), we have characterized a set of spontaneously formed multinuclear assemblies binding both cation and anion of a binary salt in the solid state. Considerable amount of works have been reported on the use of metal complexes as a crown ether/cryptand analogue,[6] as well as anion receptor,[7] but few molecular assemblies having both alkali metal ion and an anion binding site exist.[8]

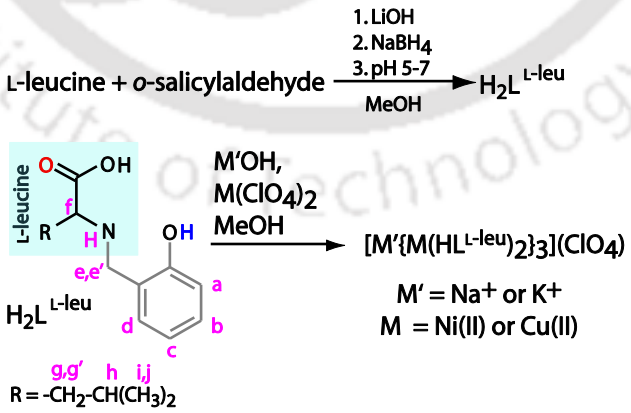

Scheme 2.1. *Synthesis of the ligand and the assemblies along with ^{1}HNMR labeling scheme for the ligand.*

2.1 Experimental section

2.1.1 Materials and Methods

Solvents used were purified prior to use following standard literature procedures. o-Salicylaldehyde and [18]-crown-6 were purchased from Aldrich Chemical Co. L-Leucine was purchased from Sisco Research Laboratories Pvt. Ltd. (SRL), India and used as received.

The IR spectra were recorded on Perkin-Elmer Spectrum One FT-IR spectrophotometer with KBr discs in the range 4000-400 cm^{-1} and electronic spectra on a Perkin-Elmer Lambda 25 and Lambda 750 UV-vis spectrophotometers. The ^{1}H NMR spectrum was recorded using a Varian Mercury plus 400 MHz instrument. Solid-state magnetic susceptibility of the complexes at room temperature was recorded using a Sherwood Scientific Magnetic balance MSB-1. Solution electrical conductivity was measured with Eutech Instruments CON 5/TDS 5 Conductivity Meter. The instrument was calibrated with standard solution. Elemental analyses were performed on a Carlo Erba 1108 and also by using a Perkin-Elmer series II 2400 instrument. Optical rotation of the ligand was measured using a Perkin-Elmer 343 polarimeter. X-Band EPR spectra were recorded with a Jeol JES-FA series spectrometer fitted with a quartz Dewar for measurements at liquid nitrogen temperature. The spectra were calibrated with DPPH (g = 2.0037). Electrospray ionization mass spectra (ESI-MS) were recorded on a Waters (Micromass MS Technologies) Q-Tof Premier mass spectrometer. Na and K ions estimation were done with Flame Photometer-Microprocessor 1381.

Caution! *Perchlorate salts are potentially dangerous as explosives and should only be handled in small quantities, although we have worked with these* ClO_4^- *salts without any incident.*

2.2 Syntheses and characterization

2.2.1 (*S*)-2-(2-Hydroxybenzylamino)-4-methylpentanoic Acid ($H_2L^{L\text{-}leu}$)

A mixture of L-leucine (1.00 g, 7.62 mmol) and $LiOH.H_2O$ (0.323 g, 7.62 mmol) in methanol (25 mL) was stirred for 10 min to dissolve the reactants. A methanolic solution (4 mL MeOH) of *o*-salicylaldehyde (0.930 g, 7.62 mmol) was added drop wise to the above solution. The color of the solution turned yellow. The stirring was continued for 30 min. The solution was then treated with $NaBH_4$ (0.580 g, 15.3 mmol) with constant stirring. The solution became colorless. The solvent was evaporated under reduced pressure and the resulting solid was dissolved in water. The clear solution was then acidified with dil. HCl (pH~5–7). The ligand precipitated as a white solid. The solution was filtered and the residue

was washed thoroughly with water. The solid was dried in vacuum desiccator (yield 1.65 g, 88%). Because of poor solubility, the ^{1}H NMR spectra for the ligand was recorded for lithium salt of the ligand, prepared by adding 2 equiv of $LiOH.H_2O$ in CD_3OD. ^{1}H NMR Li_2L (CD_3OD, 400 MHz. ppm) (Scheme **2.1**): 0.76 (d, 3H, H^j), 0.81 (d, 3H, H^i), 1.36 (m, 1H, H^g), 1.41 (m, 1H, $H^{g'}$), 1.67 (m, 1H, H^h), 3.07 (dd, 1H, H^f), 3.65 (d, 1H, H^e), 3.94 (d, 1H, $H^{e'}$), 6.35 (t, 1H, H^c), 6.45 (d, 1H, H^a), 6.94 (m, 2H, $H^{b,d}$). m/z (ESI-MS, $[LiL]^-$): Calc: 242.22, found 242.02. IR (KBr, cm^{-1}): $\nu(COO)_{asym}$ 1600 (s), 1593 (s); $\nu(COO)_{sym}$ 1393 (m). $[\alpha]_D^{25°} = -15°$ in MeOH, c = 0.2 g/100 mL, in presence of 2 equivalent of $LiOH.H_2O$.

2.2.2 $[K\{Ni(HL^{L\text{-}leu})_2\}_3]ClO_4$ (1)

Ligand $H_2L^{L\text{-}leu}$ (0.200 g, 0.847 mmol) was deprotonated with KOH (0.047 g, 0.703 mmol) in 10 mL MeOH which offered a clear colorless solution. After 20 min a methanolic solution (~ 5 mL) of $Ni(ClO_4)_2.6H_2O$ (0.155 g, 0.424 mmol) was added drop wise to the above solution. The color of the solution changed immediately from green to light blue. The solution was stirred for 2 h and was evaporated to dryness in a rotary evaporator. The resulting crude green solid (0.347 g) was recrystallized by dissolving in minimum volume of MeOH followed by addition of CH_3CN. The diamond shaped purple-blue crystals were obtained after 2 days of slow evaporation. Crystals were dried under vacuum. Yield: 60%. If 2 equiv. of base (relative to ligand) is used then the supernatant solution is green instead of bluish-green but the crystals isolated were identical with those using 1 equiv. of base. Using 2 equiv. base decreases the yield by ~ 20%. Anal. Calcd. for $[K\{Ni(C_{13}H_{18}O_3N)_2\}_3]ClO_4.3H_2O.2CH_3CN$: C, 52.71; H, 6.47; N, 5.99; K, 2.09; found C, 52.62; H, 6.28; N, 5.64; K, 2.10. IR (KBr, cm^{-1}): $\nu(COO)_{asym}$ 1594 (s), $\nu(COO)_{sym}$ 1481 (s), ν(phenolic CO) 1289 (s), $\nu(ClO_4^-)$ 1110, 1043. μ_{eff} (powder, 298K): 2.98 μ_B/Ni. Λ_M (ohm^{-1} cm^2 mol^{-1}): 92 (MeOH), 66 (DMF).

2.2.3 $[Na\{Ni(HL^{L\text{-}leu})_2\}_3]ClO_4$ (2)

This has been prepared following similar procedure described for **1** using NaOH instead of KOH. Diamond shaped purple crystals were obtained within 2–5 min after addition of CH_3CN. Yield: 58%. Anal. Calcd. for $[Na\{Ni(C_{13}H_{18}O_3N)_2\}_3]ClO_4.3H_2O.2CH_3CN.CH_3OH$: C, 52.90; H, 6.63; N, 5.94, Na, 1.21; found C, 52.46; H, 6.22; N, 5.79; Na, 1.30. IR (KBr, cm^{-1}): $\nu(COO)_{asym}$ 1621 (s), $\nu(COO)_{sym}$ 1460 (s), ν(phenolic CO) 1250 (s), $\nu(ClO_4^-)$ 1088. μ_{eff} (powder, 298K): 3.06 μ_B/Ni. Λ_M (ohm^{-1} cm^2 mol^{-1}): 116 (MeOH), 69 (DMF).

2.2.4 $[Na\{Ni(HL^{L\text{-}leu})_2\}_3]CF_3SO_3$ (3)

Ligand $H_2L^{L\text{-}leu}$ (0.100g, 0.423 mmol) was deprotonated with NaOH (0.034g, 0.846 mmol) in 10 mL MeOH which offered a clear colorless solution. A methanolic solution of (~5 mL) $Ni(OTf)_2$ (0.075g, 0.211 mmol) was added drop wise to the above stirring ligand solution. The color of the solution changed from green to light bluish green immediately. The solution was stirred for 2 h and was evaporated to dryness in a rotary evaporator. Diamond shaped purple crystals were obtained within 2–5 min after addition of CH_3CN. Yield: 50%. Anal. calcd for $[Na\{Ni(C_{13}H_{18}O_3N)_2\}_3]CF_3SO_3.10H_2O.CH_3CN$: C, 48.96; H, 6.64; N, 4.93; found C, 48.60; H, 6.70; N, 4.93. IR (KBr, cm^{-1}): $\nu(COO)_{asym}$ 1596 (s), $\nu(COO)_{sym}$ 1462 (s), $\nu(SO_3^-)$ 1272, ν(phenolic CO) 1254 (s). μ_{eff} (powder, 298K): 2.5 μ_B/Ni.[9]

2.2.5 $[K\{Cu(HL^{L\text{-}leu})_2\}_3]ClO_4$ (4)

Ligand $H_2L^{L\text{-}leu}$ (0.200 g, 0.846 mmol) was deprotonated with KOH (0.047 g, 0.703 mmol) in 25 mL MeOH. A solution of $Cu(ClO_4)_2.6H_2O$ (0.156 g, 0.423 mmol) in MeOH (15 mL) was added drop wise to the ligand solution and the stirring was continued for 2 h. The color of the solution at this point is deep green-blue. The solution was concentrated to ~5 mL and 0.5 mL CH_3CN was added. The diamond shaped blue crystals were obtained after two days of slow evaporation. Crystals were dried under vacuum. Yield: 46%. Anal. Calcd. for $[K\{Cu(C_{13}H_{18}O_3N)_2\}_3]ClO_4.3H_2O.CH_3OH$: C, 51.31; H, 6.54; N, 4.54; found C, 51.44; H, 6.47; N, 4.67. IR (KBr, cm^{-1}): ν(OH) 3444 (b), $\nu(COO)_{asym}$ 1633 (s), 1587 (s), $\nu(COO)_{sym}$ 1462 (s), 1386 (m), 1086. μ_{eff} (powder, 298K): 1.78 μ_B/Cu. Λ_M (ohm^{-1} cm^2 mol^{-1}): 114 (MeOH), 70 (DMF). EPR (MeOH, 77 K): $g_\parallel = 2.247$, $g_\perp = 2.051$, $A_\parallel = 180$ G.

2.2.6 $[Na\{Cu(HL^{L\text{-}leu})_2\}_3]ClO_4$ (5)

This has been prepared following similar procedure described for **4** using NaOH instead of KOH. The solution was concentrated to ~5 mL and 0.5 mL CH_3CN was added. The diamond shaped blue crystals were obtained after 2 days of slow evaporation. Crystals were dried under vacuum. Yield: 46%. Anal. Calcd. for $[Na\{Cu(C_{13}H_{18}O_3N)_2\}_3]ClO_4.4H_2O.2CH_3OH.CH_3CN$: C, 51.61; H, 6.71; N, 5.14; found C, 51.72; H, 6.87; N, 5.11. IR (KBr, cm^{-1}): ν(OH) 3445 (b), $\nu(COO)_{asym}$ 1633 (s), 1588 (s), $\nu(COO)_{sym}$ 1462 (s), 1386 (m), 1277 (m), 1087. μ_{eff} (powder, 298K): 1.72 μ_B/Cu. Λ_M (ohm^{-1} cm^2 mol^{-1}): 118 (MeOH), 91 (DMF).

2.2.7 $[K\{Cu(HL^{L\text{-}leu})_2\}_3]NO_3$ (6)

The synthesis and crystallization procedure are identical with that of **4** except $Cu(NO_3)_2.6H_2O$ was used in place of perchlorate salt. Yield: 54%. Anal. Calcd. for $[K\{Cu(C_{13}H_{18}O_3N)_2\}_3]NO_3.6H_2O$: C, 51.54; H, 6.65; N, 5.39; found C, 51.71; H, 6.40; N,

5.40. IR (KBr, cm^{-1}): ν(OH) 3436 (b), $\nu(COO)_{asym}$ 1629 (s), 1588 (s), $\nu(COO)_{sym}$ 1462 (s), 1384 (s), 1277 (m), 1086 (m). μ_{eff} (powder, 298K): 1.69 μ_B/Cu. Λ_M (ohm^{-1} cm^2 mol^{-1}): 118 (MeOH), 77 (DMF).

2.2.8 X-ray Data Collection, Structure Solution and Refinement

Crystals of the complexes obtained during synthesis were used for X-ray analysis. The crystals were mounted on glass fiber. All geometric and intensity data for the crystals were collected at room temperature using a Bruker SMART APEX CCD diffractometer equipped with a fine focus 1.75 kW sealed tube Mo-Ka (λ = 0.71073 Å) X-ray source, with increasing ω (width of 0.3º per frame) at a scan speed of either 3 or 5 s/frame. The SMART software was used for data acquisition and the SAINT software for data extraction. Absorption corrections were done using SADABS only as either kinds of absorption did not help.[10] After the initial solution and refinement with SHELXL, the final refinements were performed on WinGX environment using SHELX97.[11] All non-hydrogen atoms were refined anisotropically. Where ever possible, the hydrogen atoms were located from the difference Fourier maps and were refined isotropically. Thus some of the C–H bond will not be ideal and may vary. Most of the hydrogen atoms attached to the solvent molecules could not be located or fixed, so the molecular weight may not match. Selected crystallographic data have been summarized in Table **2.1.**

2.3 Results and discussion

2.3.1 Synthesis and solid state structures

The diamond shaped crystals of the assemblies $[K\{Ni(HL^{L\text{-}leu})_2\}_3]ClO_4$ **(1)**, $[Na\{Ni(HL^{L\text{-}leu})_2\}_3]ClO_4$ **(2)**, $[Na\{Ni(HL^{L\text{-}leu})_2\}_3]CF_3SO_3$ **(3)**, $[K\{Cu(HL^{L\text{-}leu})_2\}_3]ClO_4$ **(4)**, $[Na\{Cu(HL^{L\text{-}leu})_2\}_3]ClO_4$ **(5)** and $[K\{Cu(HL^{L\text{-}leu})_2\}_3]NO_3$ **(6)** were readily isolated by mixing ligand, metal salt and alkali metal bases in correct proportions (2:2:1) and standing the solution for 2–3 days. If 2 equiv. of base per ligand is used to deprotonate both the phenolic and carboxylic acid proton, the color of the solution become darker and of a different hue (Syntheses and characterization section **2.2**) but eventually yields crystals of **1** to **6** after several days as characterized by comparing FTIR, UV-vis and structural parameters. Use of extra base decreases the yield. We think the use of 2 eqiv. base per ligand initially form the bis complex, $[M^{II}(L^{L\text{-}leu})_2]^{2-}$, where both the ligand protons have been deprotonated (darker solution) which gradually gets partially protonated by hydrolyzing the water present in methanol. Presence of excess base and rate of hydrolysis probably delayed the assembly

formation as well as adversely impacted the yield. Crystallographic characterization of **1-6** shows the assemblies are isostructural (Table **2.1**).

The **1** crystallizes in the space group $C222_1$, where half of the assembly is identical with the other half connected through symmetry (Figure **2.1**). Thus Ni1 is on the crystallographic 2-fold axis and Ni2 is on the general position. Selected bond distances are in table **2.2**. In **1**, K^+ is hexa-coordinated by three $[Ni^{II}(HL^{L\text{-}leu})_2]$ units through six carboxylate oxygens (Figure **2.1a**). In each of the $[Ni^{II}(HL^{L\text{-}leu})_2]$, Ni(II) is hexacoordinated by two facial tridentate ligand where the carboxylate groups from the ligands are *cis* to each other (Figure **2.1b**). The carboxylate oxygens are simultaneously coordinated to Ni(II) and K^+ (Figure **2.1b**). Each of the ligands in **1** has one acidic proton which is H-bonded between phenolic oxygen (O1b) and carboxylate oxygen (O3b) from the neighboring $[Ni^{II}(HL^{L\text{-}leu})_2]$ unit (Figure **2.1b** and **2.2a**). Thus there are six such H-bonds in one molecule of $[K\{Ni(HL^{L\text{-}leu})_2\}_3]^+$. These H-bonds are on the short end of the 2.5–3.0 Å range usual for O..O H-bond distances (Table **2.2**).[12] The aromatic rings of the ligands completely encapsulate the central potassium ion from both sides in a capsular shape with six amino acid residues protruding on the surface (Figure **2.2b**).

While the *cis* orientation of carboxylates allowed the $[Ni^{II}(HL^{L\text{-}leu})_2]$ unit to bind K^+, similar orientation of amines provided a H-bonding site for oxo anions making the capsular assembly, capable of binding both anion and cation of a salt within the same assembly in solid state (Figure **2.2a**).

The conformation at the chiral carbon of the ligand is *S*. In addition to the asymmetric carbon center in the ligand, the coordination of amine N to the Ni(II) gives rise to an asymmetric secondary nitrogen atom which has the *R* configuration. This phenomenon of opposite conformation preference at chiral carbon and amine N has been observed in all the characterized complexes of this ligand.[4,5]

The molecular structures of **2** and **3** showed that overall organization of the assembly is identical with that of **1** differing only by the oxo-anion and central Na^+ ion. Replacement of K^+ with smaller Na^+ reduced the alkali metal to carboxylate length bringing $[Ni^{II}(HL^{L\text{-}leu})_2]$ units closer (Table **2.2**). This in turn shortened the already short inter unit phenol-carboxylate H-bonds (Table **2.2**). The Na-O and K-O lengths are comparable to those found in literature.[13]

Oxo anions form bridges between two neighboring assembly through two H-bonds between amine NH and two different oxygen atoms of the oxo anion creating an extensively

H-bonded three dimensional network. This might be the reason behind poor solubility of the assemblies in common organic solvents. **1** and **2** are soluble in polar DMF and only partially soluble in MeOH and water (< 50 mg in 10 mL MeOH). The presence of additional weak interaction between fluorine and aromatic CH (F1···C18, 3.20 Å) has been observed in **3** which probably reduced the solubility further.[14] Complex **3** is insoluble even in DMF. The lattice also contains acetonitrile and water as solvents of crystallization (Figure **2.3**).

The molecular structures of Cu(II) assemblies, **4**–**6**, have the identical organization with that of Ni(II) assemblies discussed above. What is notable in these structures is the hexacoordination of Cu(II) which otherwise prefers to be pentacoordinated in almost all the complexes reported so far with similar type of ligands.[4,5,6d] The axial bond lengths ($Cu–O_{phenol}$) are much longer than Ni(II) counterparts due to Jahn–Teller distortion (Table **2.2**). In **4**–**6**, the in-plane lengths are slightly shorter and $K/Na–O_{carboxy}$ lengths are longer than corresponding bonds in Ni(II) complexes (Table **2.2**).

Overall, the structural characterization of the six structures (**1**–**6**) showed that six of L-leucine derived tridentate ligand, three Ni(II) or Cu(II) and one K^+ or Na^+ self assemble into rather large (~1 nm) sized assembly having binding site for one alkali metal ion and three sites for oxo anion (Figure **2.2**). The structures also show that substitution of Ni(II) with Cu(II) is possible without destroying the assembly.

Solid state room temperature magnetic moments of **1**–**6** are well within expected range (Syntheses section **2.2**).[9]

Table 2.1. Selected crystallographic data for the complexes

	1	**2**	**3**	**4**	**5**	**6**
empirical formula	$C_{82}H_{108}ClK N_8Ni_3O_{27}$	$C_{84}H_{116}Cl N_8NaNi_3O_{27}$	$C_{87}H_{108}F_3N_{10} NaNi_3O_{22}S$	$C_{84}H_{102}ClCu_3 KN_8O_{27}$	$C_{83}H_{114}ClCu_3 N_8NaO_{27}$	$C_{80}H_{108}Cu_3 KN_7O_{31}$
fw	1888.38	1904.42	1934.01	1920.94	1904.91	1893.45
T(K)	296(2)	296(2)	296(2)	296(2)	296(2)	293(2)
Wavelength(Å)	0.71073	0.71073	0.71073	0.71073	0.71073	0.71073
Crystal system	orthorhombic	orthorhombic	orthorhombic	orthorhombic	orthorhombic	orthorhombic
Space group	$C222_1$	$C222_1$	$C222_1$	$C222_1$	$C222_1$	$C222_1$
a, Å	17.6885(7)	17.7564(8)	17.5336(6)	17.746(2)	17.786(3)	17.8717(16)
b, Å	20.9207(8)	20.9237(10)	21.0148(6)	21.144(3)	21.037(3)	21.262(2)
c, Å	26.7585(10)	26.6820(13)	27.5553(9)	26.968(4)	26.971(4)	26.901(3)
V, $Å^3$	9902.1(7)	9913.2(8)	10153.2(6)	10119(2)	10092(3)	10222.1(17)
z/ρ	4/1.267	4/1.276	4/1.265	4/1.261	4/1.254	4/1.230
μ	0.706	0.669	0.650	0.764	0.729	0.733
coll. reflns	70786	67506	35518	34073	46466	41985
indep reflns	10098	10833	8146	11573	11948	5180
FLACK para.	-0.004(14)	0.002(10)	-0.005(12)	0.009(16)	0.006(12)	0.00(2)
GOF	1.011	1.031	1.044	0.979	1.020	1.053
R1[a]	0.0466	0.0404	0.0383	0.0634	0.0506	0.0546
wR2[a]	0.1287	0.1102	0.0952	0.1327	0.1173	0.1432
R1[b]	0.0653	0.0510	0.0518	0.1308	0.0874	0.0633
wR2[b]	0.1397	0.1152	0.1035	0.1624	0.1173	0.1485

[a] $I>2\sigma$. [b] All data.

1 = $[K\{Ni(HL^{L\text{-}leu})_2\}_3]ClO_4$, **2** = $[Na\{Ni(HL^{L\text{-}leu})_2\}_3]ClO_4$, **3** = $[Na\{Ni(HL^{L\text{-}leu})_2\}_3]CF_3SO_3$, **4** = $[K\{Cu(HL^{L\text{-}leu})_2\}_3]ClO_4$, **5** = $[Na\{Cu(HL^{L\text{-}leu})_2\}_3]ClO_4$ and **6** = $[K\{Cu(HL^{L\text{-}leu})_2\}_3]NO_3$.

Table 2.2. Selected bond distances (Å) of complexes **1-6**

	1			**2**			**3**		
Ni-O_{phenol}	2.162(3)	2.154(3)	2.151(3)	2.147(2)	2.155(2)	2.132(2)	2.150(2)	2.145(3)	2.123(2)
Ni-$O_{carboxy}$	2.021(3)	2.019(3)	2.025(3)	2.015(19)	2.019(19)	2.025(2)	2.012(2)	2.028(2)	2.025(2)
Ni-N_{amine}	2.080(3)	2.085(3)	2.077(2)	2.073(2)	2.087(3)	2.085(3)	2.077(3)	2.079(3)	2.087(3)
K/Na-$O_{carboxy}$	2.675(2)	2.650(2)	2.687(3)	2.642(2)	2.550(18)	2.607(2)	2.627(3)	2.548(2)	2.612(3)
OH...O	2.537	2.591	2.541	2.561	2.517	2.514	2.509	2.561	2.497
	4			**5**			**6**		
Cu-O_{phenol}	2.487	2.465	2.465	2.451	2.476	2.449	2.504	2.461	2.478
Cu-$O_{carboxy}$	1.964(3)	1.956(3)	1.965(4)	1.967(2)	1.960 (2)	1.967(3)	1.957(5)	1.957(4)	1.963(5)
Cu-N_{amine}	2.003(4)	2.020(4)	2.020(5)	2.018(3)	2.013(3)	2.025(3)	2.010(6)	2.015(6)	2.009(6)
K/Na-$O_{carboxy}$	2.743(3)	2.715(3)	2.730(4)	2.598	2.698(3)	2.597(2)	2.666(3)	2.706(4)	2.737(5)
OH...O	2.596	2.621	2.589	2.545	2.545	2.554	2.594	2.644	2.574

1 = $[K\{Ni(HL^{L\text{-}leu})_2\}_3]ClO_4$, **2** = $[Na\{Ni(HL^{L\text{-}leu})_2\}_3]ClO_4$, **3** = $[Na\{Ni(HL^{L\text{-}leu})_2\}_3]CF_3SO_3$, **4** = $[K\{Cu(HL^{L\text{-}leu})_2\}_3]ClO_4$, **5** = $[Na\{Cu(HL^{L\text{-}leu})_2\}_3]ClO_4$ and **6** = $[K\{Cu(HL^{L\text{-}leu})_2\}_3]NO_3$.

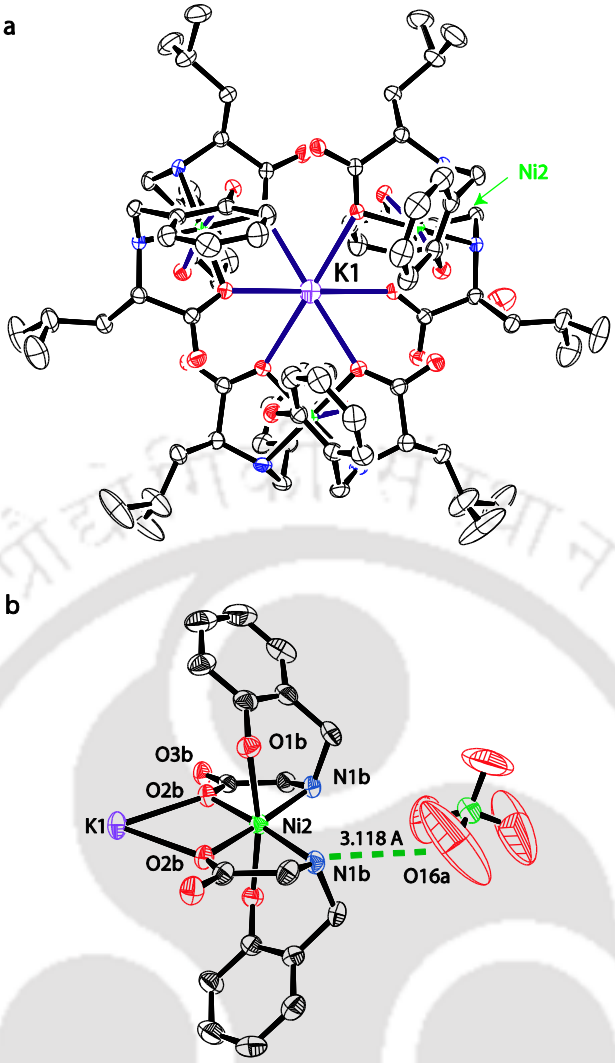

Figure 2.1. *(a) ORTEP diagram of **1** with thermal ellipsoids set to 30% probability level and (b) coordination around one Ni(II) unit showing the cation and anion binding sites.*

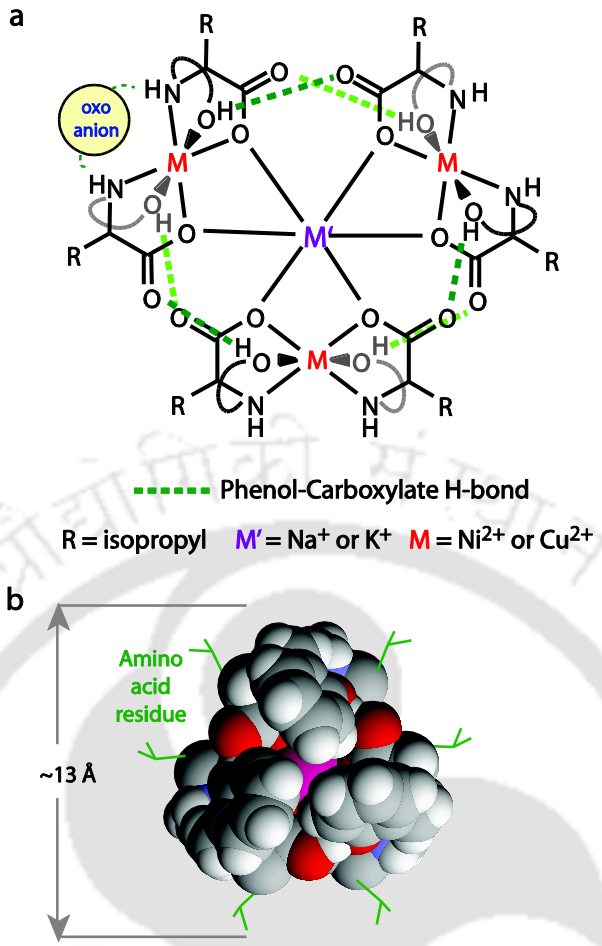

Figure 2.2. *(a) Sketch model of the assembly showing cation as well as anion binding sites and position of the six short hydrogen bonds and (b) space filling model of the assembly with isopropyl groups shown as sticks.*

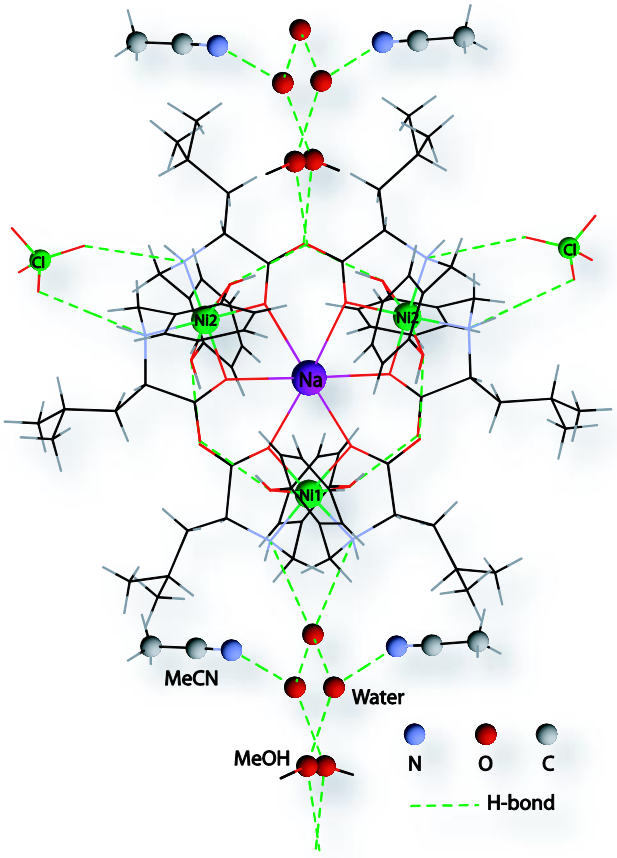

Figure 2.3. *The lattice of **2** also contains acetonitrile and water as solvents of crystallization.*

2.3.2. Solution identity

The solution identities of the assemblies were assessed using solution conductance, ESI-Mass and electron paramagnetic resonance (EPR) spectroscopy. The solution conductance measurement in methanol and DMF showed the complexes as 1:1 electrolyte (Section **2.2**). [9] Thus, the H-bond between the anion and secondary amines are dissociable in H-bond capable solvent. The ESI-Mass spectra of all the complexes show the molecular ion peak with matching isotopic abundance pattern (Figure **2.4**, Table **2.3**) supporting the presence of the assemblies in solution.

One notable difference observed between the mass spectra of **2** and **1** was the weak intensity of molecular ion peak for **2** in MeOH (Figure **2.4a** & **2.5a**). The mass spectrum of **2** shows strong enhancement of the intensity of the molecular ion peak after addition of excess $NaNO_3$ (Figure **2.5b**). Excess Na^+ perhaps reversed the dissociation of the assembly in MeOH, enhancing the molecular ion peak (Scheme **2.2**). This can be due to the partial dissociation, the equilibrium of which shifts toward assembly in presence of excess Na^+ ion causing the enhancement of the molecular ion peak (Scheme **2.2**). This is also supported by

the visible spectroscopic measurements described in the next section. Mass spectra of the Cu(II) containing assemblies also show less intense molecular ion peaks suggestive of partial dissociation (Figure **2.6**). However, higher dissociation of the Cu(II) complexes compared to Ni(II) complexes might be due to higher lability of the Cu(II) complexes. The EPR spectra of the Cu(II) assemblies in methanol at 77 K are all commensurate with their tetragonally distorted structure (Section **2.2**, Figure **2.7**).[15]

Table 2.3. Mass spectral data.[a]

	exp. *m*/Z (relative intensity)[b]	calc. *m*/Z (relative intensity)[b]
1	1629.5(70), 1630.5(65) 1631.5(100),1632.5(85), 1633.5(85), 1634.5(60), 1635.5(40), 1636.5(30)	1629.54(60), 1630.54(54), 1631.54(100), 1632.54(78), 1633.54(78), 1634.54(52), 1635.54(40), 1636.54(23)
2	1613.5(65), 1614.5(60), 1615.5(100), 1616.5((90), 1617.5(80), 1618.5(40), 1619.5(40), 1620.5(20)	1613.56(63), 1614.56(56), 1615.56(100), 1616.56(77), 1617.56(75), 1618.56(49), 1619.56(36), 1620.56(21)
4	1645.0(35), 1646.0(40), 1647.0(100), 1648.0(65), 1649.0(40), 1650.0(30), 1651.0(20), 1652.0(10)	1644.55(54), 1645.55(48), 1646.55(100), 1647.55(76), 1648.55(73), 1649.55(45), 1650.55(26), 1651.55(13)
5	1628.5(55), 1629.5(55), 1630.5(100), 1631.5(75), 1632.5(70), 1633.5(45), 1634.5(20), 1635.5(10)	1628.58(57), 1629.58(50), 1630.58(100), 1631.58(76), 1632.58(68), 1633.58(42), 1634.58(23), 1635.58(10)
6	1644.3(54), 1645.3(50), 1646.3(100), 1647.3(73), 1648.3(73), 1649.3(48), 1650.3(25), 1651.3(15)	1644.55(54), 1645.55(48), 1646.55(100), 1647.55(76), 1648.55(73), 1649.55(45), 1650.55(26), 1651.55(13)

[a] In methanol. [b] isotopic mass distribution of the molecular ion peak with relative intensity values in parenthesis.

1 = $[K\{Ni(HL^{L\text{-}leu})_2\}_3]ClO_4$, **2** = $[Na\{Ni(HL^{L\text{-}leu})_2\}_3]ClO_4$, **4** = $[K\{Cu(HL^{L\text{-}leu})_2\}_3]ClO_4$,

5 = $[Na\{Cu(HL^{L\text{-}leu})_2\}_3]ClO_4$ and **6** = $[K\{Cu(HL^{L\text{-}leu})_2\}_3]NO_3$.

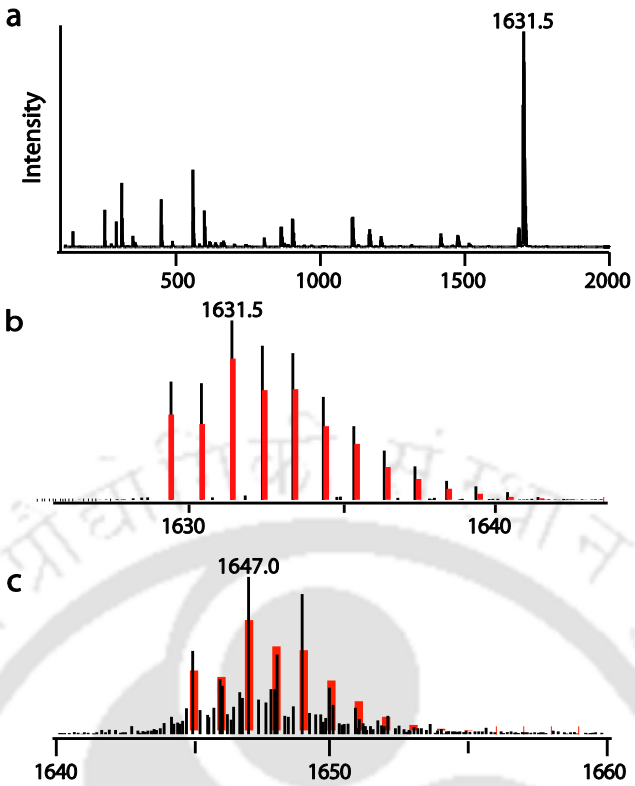

Figure 2.4. *(a) ESI-MS spectrum for **1**, (b) Isotopic abundance pattern calculated (red) and experimental (black) of **1** and (c) is the isotopic abundance pattern of **4**.*

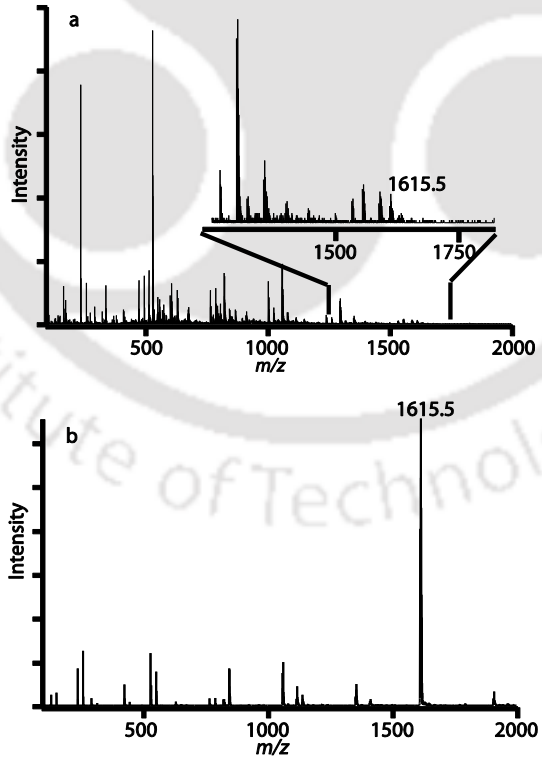

Figure 2.5. *ESI-Mass spectra of **2** in MeOH before (a) and after (b) addition of $NaNO_3$.*

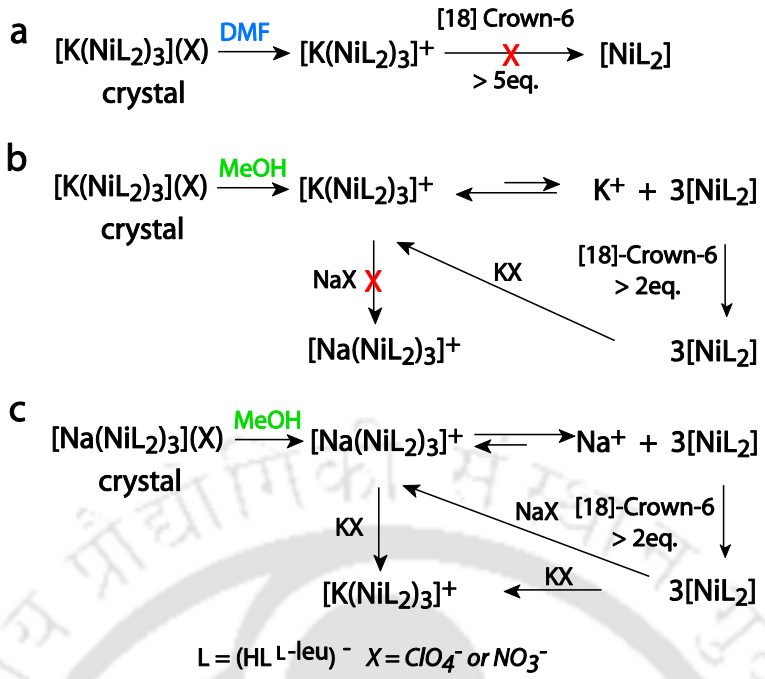

Scheme 2.2. *Schematic representation of the equilibrium presents in solution and inter conversion between the species observed spectrophotometrically.*

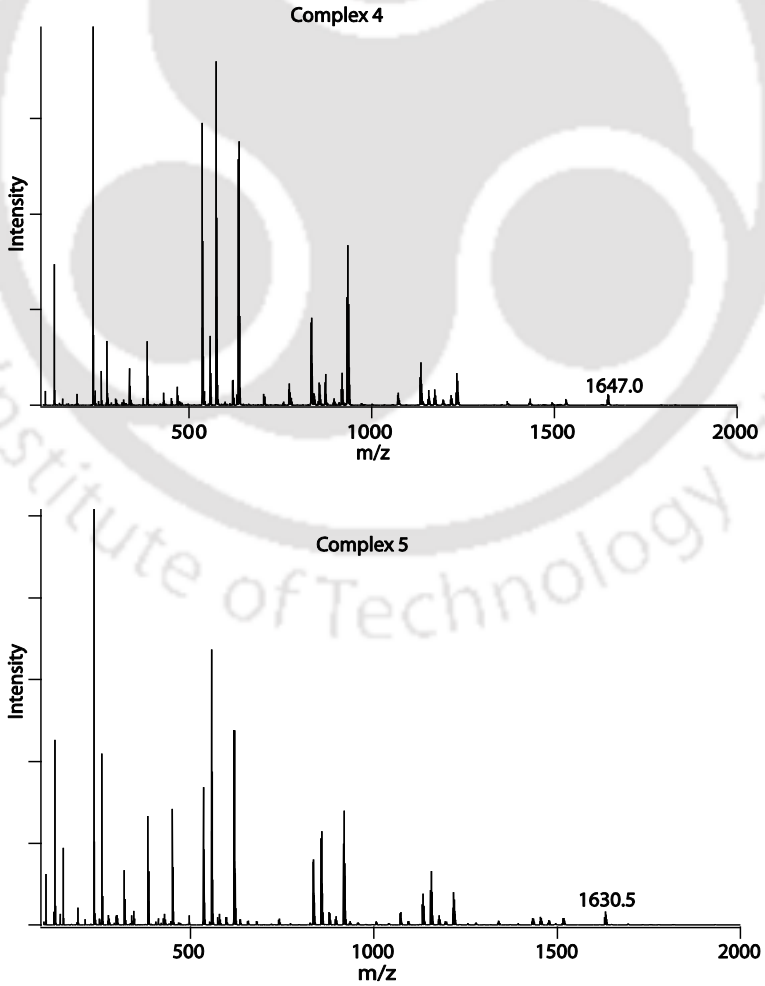

Figure 2.6. *ESI- Mass (+ve) spectra of copper containing assemblies **4** and **5** in MeOH.*

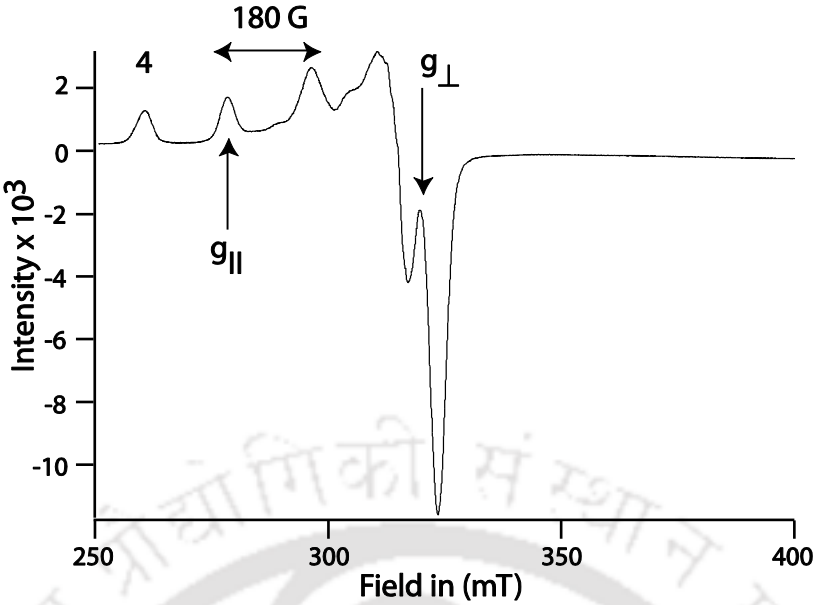

Figure 2.7. *EPR spectra of **4** in MeOH at 77K.*

2.3.3. Absorption spectra in DMF

Octahedral Ni(II) and Cu(II) complexes are known to show d-d transition sensitive to coordination environment.[16] In DMF, both **1** and **2** shows four broad absorption between 300 and 1600 nm (Figure **2.8a**, Table **2.4**). Six coordinate axially elongated Ni(II)'s are known to show multiple overlapped transitions in this region due to lower than octahedral symmetry which lifts the degeneracy of the usual three transitions, $^3T_{1g}(P) \leftarrow {}^3A_{2g}$, $^3T_{1g} \leftarrow {}^3A_{2g}$ and $^3T_{2g} \leftarrow {}^3A_{2g}$ typically observed for octahedral Ni(II) complexes.[15] The small sharp absorption maxima at ~755 nm arising from the forbidden singlet state seen many other six coordinated Ni(II) complexes.[16] The similarity between the spectra of **1** and **2** indicated their structural similarity in DMF (Figure **2.8a**). However, the absorption maxima of **1** at ~ 1200 nm is blue shifted by 70 nm in **2** (Table **2.4** Figure **2.8a**). This peak is usually sensitive ($^3B_{1g} \rightarrow {}^3E_g$ in D_{4h} symmetry) to the relative magnitudes of the axial and equatorial field strengths.[16] The shift does indicate that substitution of Na^+ by K^+ causes minor perturbation in the ligand strengths around the Ni(II). This observation provides an interesting way to distinguish K^+ over Na^+ in the visible region through perturbing a spectroscopically active Ni(II) centre. We think that the difference in charge/radius ratio of the two ions binding with the Ni(II) coordinating carboxylates might have influenced the ligand field strength. The spectra remain unchanged upon addition of excess KNO_3 in solutions of **1** (Figure **2.8a**) and $NaNO_3$ in **2** indicating absence of dissociation (Scheme **2.2**). The complex **3** is insoluble in any common solvents. Diffuse reflectance visible spectra of the complexes in the solid state were too noisy for comparison purpose.

Copper complexes with K^+ as central ion in **4** and **6** show one broad d-d transition in DMF, expected for tetragonally distorted Cu(II) (Table **2.4**, Figure **2.8b**).[16] The spectra of **4** and **6** spectra are identical but appears at lower energy (diff. 30 nm) compared to Na^+ containing complex **5**. Addition of sodium nitrate to **5** or potassium nitrate to **4** is expected to shift this equilibrium towards multinuclear assembly. As expected, addition of alkali metal salts leads to sharper the peak ~640 nm for both (Figure **2.8b** & Figure **2.9**). This shows that unlike Ni(II) counterparts both the Cu(II) assemblies are partially dissociated in DMF. This is also supported by the structural observation that K/Na–$O_{carboxy}$ and OH…O, H-bond lengths in Cu(II) assemblies are slightly longer compared to Ni(II) assemblies thus making them more vulnerable to dissociation.

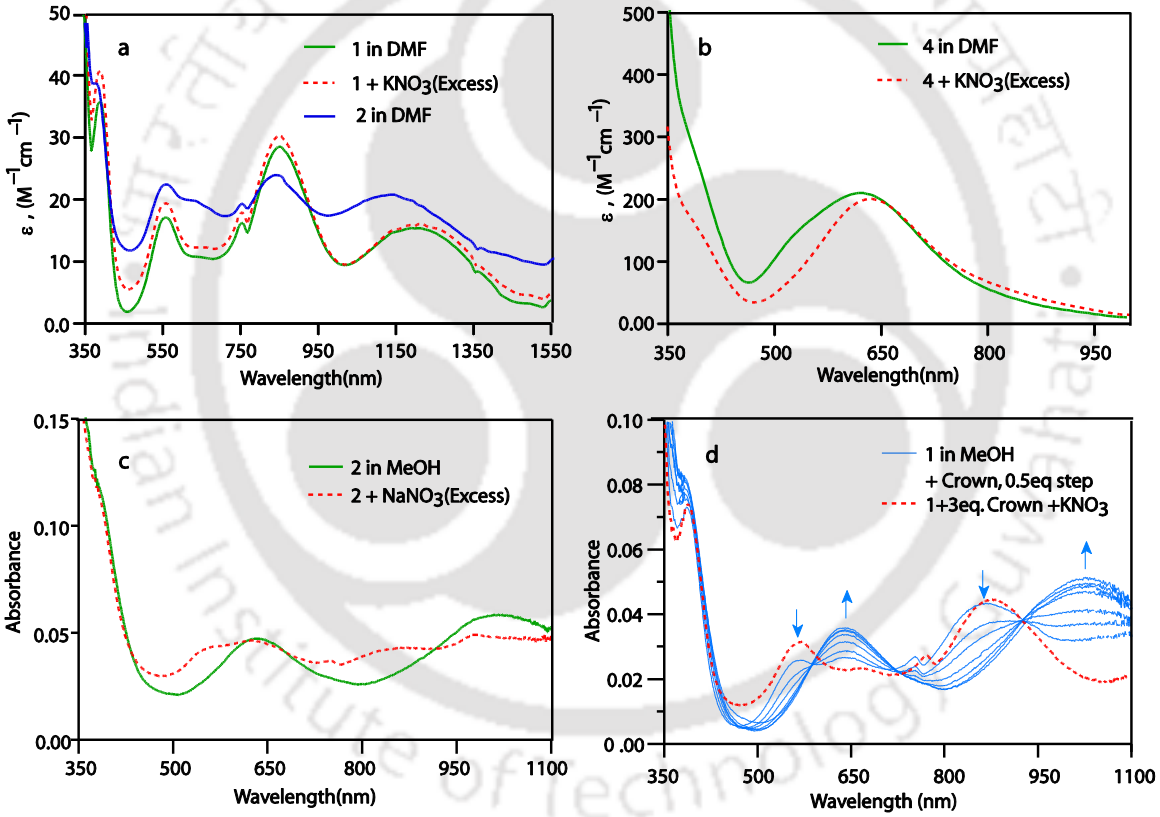

Figure 2.8. *Electronic spectra of the assemblies in different solvents and spectral changes upon addition of salts and [18]-crown-6.*

Table 2.4. Electronic spectral data.[a]

	Solvent	λ_{max}, nm (ε, $M^{-1}cm^{-1}$)
1	DMF	390(35), 565(20), 755(sh), 865(30), 1230(15)
	MeOH[b]	217(32300), 242(sh), 280(12800), 384 (40), 551 (20), 750 sh, 850 (30)
2	DMF	380(40), 565(22), 755(sh), 855(25), 1160(20)
	MeOH[b]	218(33400), 242(sh), 281(13800), 378 (50), 634 (20), 1008 (30)
4	DMF	625(210)
	MeOH[b]	207(52700), 218(sh), 239(sh), 276(24373), 377 (sh), 616(280)
5	DMF	595(220)
	MeOH[b]	207(51000), 218(sh), 239(sh), 275(24100), 376(sh), 615(280)
6	DMF	625(210)
	MeOH[b]	209(52100), 215(sh), 239(sh), 276(23700), 377(sh), 613(275)

[a] Scan range in DMF, 300 – 2000 nm, MeOH, 200 - 1100 nm. [b] ε values were calculated using ~2 mM solution for visible region and 0.01-0.02 mM solution for UV region.

1 = $[K\{Ni(HL^{L\text{-}leu})_2\}_3]ClO_4$, **2** = $[Na\{Ni(HL^{L\text{-}leu})_2\}_3]ClO_4$, **4** = $[K\{Cu(HL^{L\text{-}leu})_2\}_3]ClO_4$, **5** = $[Na\{Cu(HL^{L\text{-}leu})_2\}_3]ClO_4$ and **6** = $[K\{Cu(HL^{L\text{-}leu})_2\}_3]NO_3$.

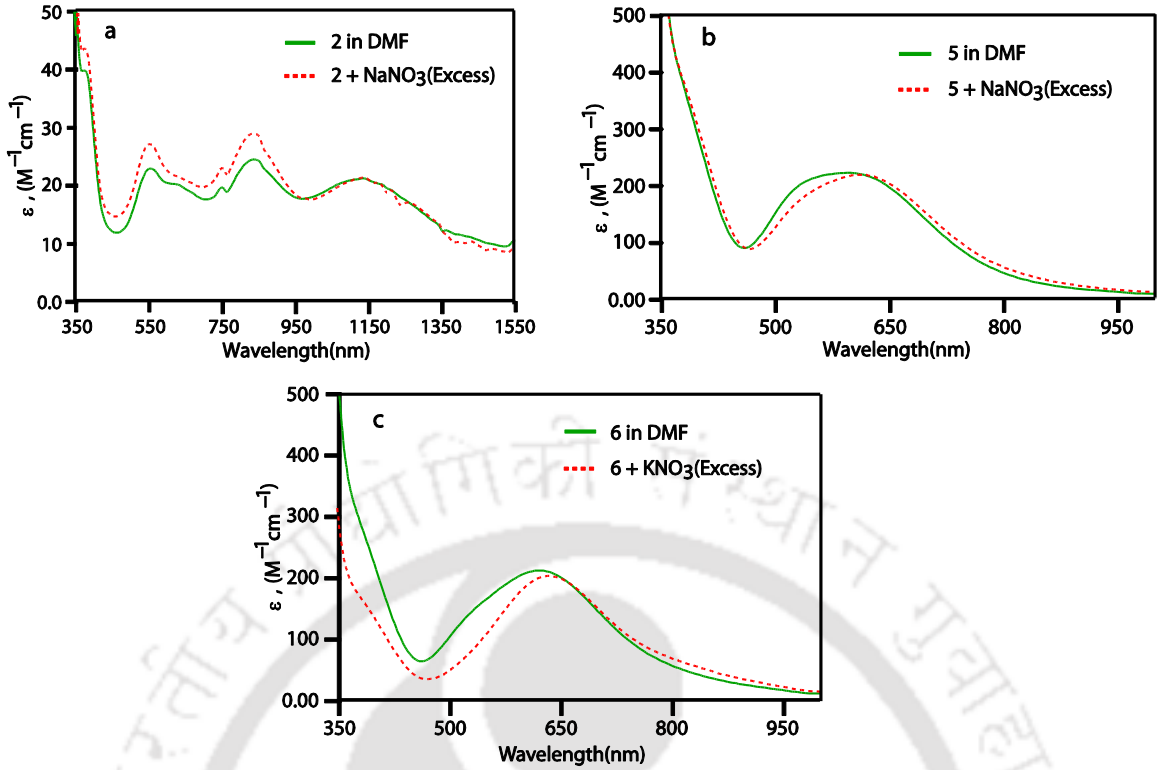

Figure 2.9. *(a) Complex **2** before and after addition of excess solid $NaNO_3$, (b) Complex **5** before and after addition of excess solid $NaNO_3$, (c) Complex **6** before and after addition of excess solid KNO_3.*

2.3.4. Dissociation in MeOH and effect of [18]-crown-6 addition

ESI-Mass spectra of **2** (Figure **2.5**) indicated partial dissociation of the assembly to Na^+ and $[Ni(HL^{L\text{-}leu})_2]$ units in MeOH. To study further, we have recorded the absorption spectra in MeOH (Table **2.4**). Spectra in MeOH were recorded up to 1100 nm due to –OH overtones interference beyond this range.

Out of the three bands ~ 550, 850 and 1200 nm observed in DMF, only first two were visible in MeOH. These two bands were not sensitive to Na^+ or K^+ in DMF. Spectrum of **1** in both the solvent is similar up to 1100 nm range but **2** in MeOH showed substantially different spectrum (Table **2.4**). Suspecting presence of dissociation equilibria, we have recorded spectra after addition of respective salts (Figure **2.8c** & **2.10**). Addition of KNO_3 to **1** enhanced the intensity of the peaks slightly but peak position remains same indicating very little dissociation of **1** in MeOH (Scheme **2.2b**). This is consistent with the ESI-Mass spectral observation (Figure **2.4a**). Complex **2** on the other hand showed pronounced difference in spectra upon addition of $NaNO_3$ indicating appreciable amount of dissociation in solution. Addition of $NaNO_3$ shifts the equilibrium towards multinuclear species and absorption maxima at 560 and 850 nm increases at the expense of peak at 634 and 1008 nm (Figure **2.5**

& **2.8c**). We think the peaks at 634 and 1008 nm were likely of $[Ni(HL^{L\text{-}leu})_2]$ species generated because of dissociation.

When increasing amounts of [18]-crown-6 are added to methanolic solution of **1** and **2**, the intensity of the peaks at 560 and 850 nm decreases while the peaks at 634 and 1008 nm increases (Figure **2.8d**). The sequestering of K^+/Na^+ by [18]-crown-6 generates more of $[Ni(HL^{L\text{-}leu})_2]$ (Scheme **2.2**). This confirms the peaks observed at 634 and 1008 nm in spectrum of **2** are for $[Ni(HL^{L\text{-}leu})_2]$ species. When excess KNO_3 is added to **2**, the spectrum resembles the spectrum of **1** inferring that Na^+ assembly can be converted to K^+ containing assembly. The reverse is not observed (Figure **2.10b**). We conclude that K^+ binds $[Ni(HL^{L\text{-}leu})_2]$ units more strongly compared to Na^+ retaining multinuclear structure in MeOH.

Addition of [18]-crown-6 (>5 eq.) did not show any changes in spectrum of either **1** or **2** in DMF indicating the better stability of the Ni(II) assemblies in DMF (Figure **2.11**). It is likely that MeOH acting both as H-bond donor as well as acceptor interferes with the six H-bonds and facilitates the dissociation of the assembly. On the other hand DMF, which can only act as a H-bond acceptor through the oxygen, is probably unable to dissociate the assembly. These results highlight the role of the six H-bonds in stabilizing the assembly, preventing the sequestration of alkali ion by the [18]-crown-6. Determination of quantitative parameters for these equilibria proved difficult because of low absorbance values along with limited solubility of the complexes.

Copper containing assemblies **4**-**6** in MeOH show single broad absorption ~615 nm (Table **2.4**) not affected by addition of either corresponding salts or [18]-crown-6. The ESI-mass spectra in MeOH show weak molecular ion peaks (Figure **2.6**). Together they indicate greater dissociation of the assembly compared to that of Ni(II) containing assemblies in MeOH.

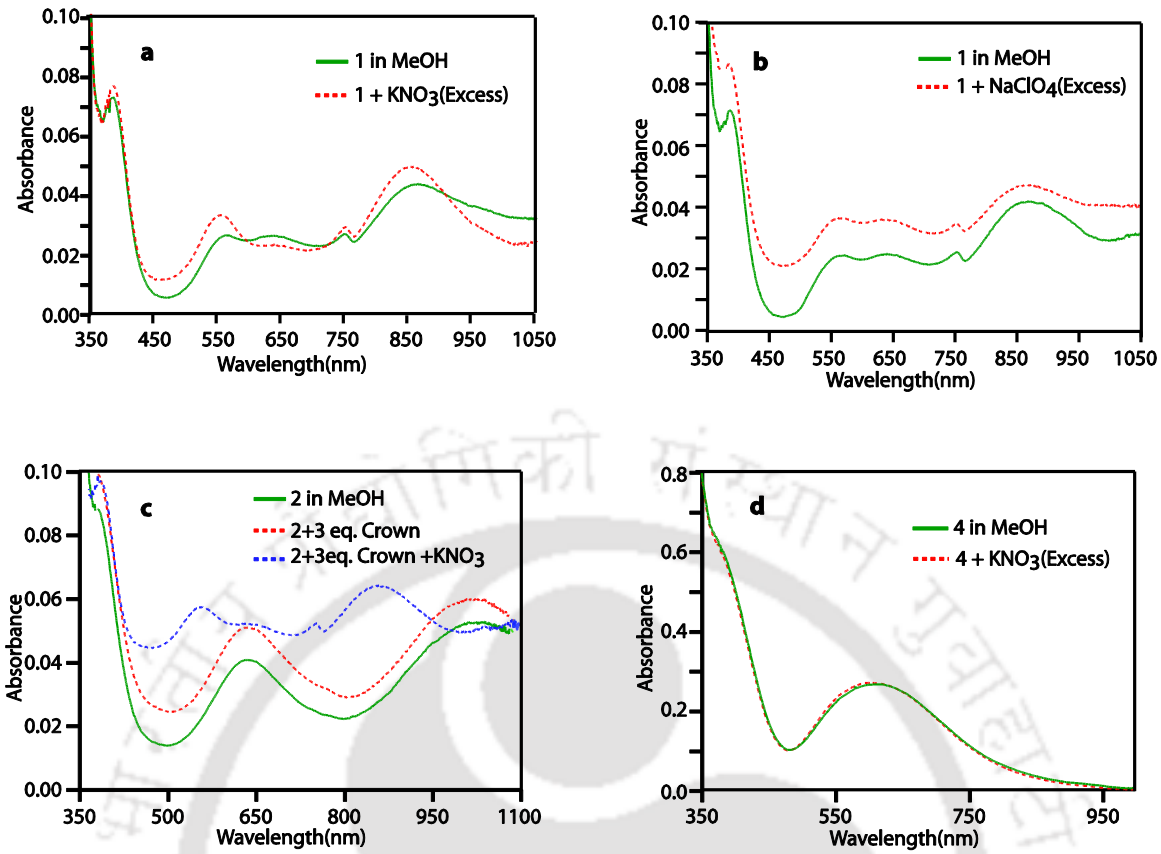

Figure 2.10. *(a) Complex **1** before and after addition of excess solid KNO_3, (b) Complex **1** before and after addition of excess solid $NaClO_4$, (c) Complex **2** before and after addition of 3 equiv. [18]-crown-6 and finally excess solid KNO_3, (d) Complex **4** before and after addition of excess solid KNO_3.*

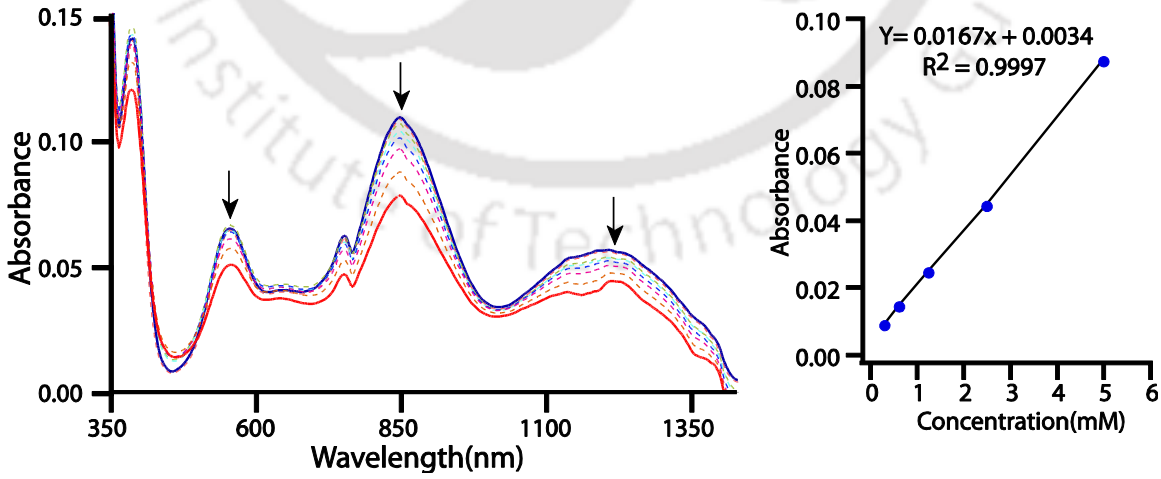

Figure 2.11. *Visible spectra of **1** with stepwise addition of [18]-Crown-6 (0.5 equiv. step) in DMF (Absorbance decreases due to dilution effect were not compensated) and a concentration vs. absorbance plot for **1** in DMF monitored at 565 nm (right).*

Conclusions

In this chapter, we have presented a reaction where an L-leucine derivative, a divalent metal ion and alkali metal ion readily self-assembled into a capsular assembly, having sites for both cation and anion of a binary salt. Identical assembly formation was observed irrespective of alkali metal ion (Na^+ or K^+) or divalent metal ion (Ni(II) or Cu(II)) used. In the assembly, three $[M^{II}(HL^{L\text{-}leu})_2]$ units encapsulate alkali metal ion through six oxygen donors forming a cryptate like adduct.[6] The assembly is homochiral with three potential chiral recognition sites on the surface (three pairs of N–H between the isopropyl groups of L-leucine), two of which are occupied by bridging oxo-anions in the present set of complexes (Figure **2.2**). Solution studies using ESI-Mass and visible spectroscopy revealed retention of the cationic capsular assembly in DMF. However, the better H-bonding capability of MeOH was able to partially dissociate the assemblies in solution.

Interestingly, the visibly silent alkali metal ion within the assembly affects the spectral characteristic of Ni(II) (Figure **2.8a**). We have not come across any report where the shift in visible band of Ni(II) is indirectly influenced by K^+ over Na^+. This perhaps has happened because the bonds and angles in the assembly are interdependent on the bivalent metal ion, alkali ion, and the six strong H-bonds. A change in size of the alkali ion changes the bond lengths and angles in a way that it caused the shift in the d-d transition of the Ni(II) spectra.[19] This overall interdependence and the short H-bonds perhaps forced the Cu(II) to adopt a not so common octahedral geometry. These six short H-bonds stabilize the assembly to such an extent that the assemblies can withstand the sequestration of the alkali metal ion by [18]-crown-6 in weak H-bonding solvent DMF.

While several interesting structural architecture, channels, and capsular motifs have been reported by us and others[4,5] using amino acid derived reduced Schiff base ligands, this work presents formation of a new multifaceted architecture with easily variable sites for two different type of metal ion and anions. The facile formation increases the potential for future exploitation of the architecture for chiral anion recognition.

References

1. Selected reviews on cages and capsules: (a) Stang, P. J.; Olenyuk, B. *Acc. Chem. Res.* **1997**, *30*, 502. (b) Fujita, M. *Chem. Soc. Rev.* **1998**, *27*, 417. (c) Jasat, A.; Sherman, J. C. *Chem. Rev.* **1999**, *99*, 931. (d) Caulder, D. L.; Raymond, K. N. *Acc. Chem. Res.* **1999**, *32*, 975. (e) Olenyuk, B.; Leininger, S.; Stang, P. J. *Chem. Rev.* **2000**, *100*, 853. (f) Seidel, S. R.; Stang, P. J. *Acc. Chem. Res.* **2002**, *35*, 972. (g) Hof, F.; Craig, S. L.; Nuckolls, C.; Rebek, J., Jr. *Angew. Chem., Int. Ed.* **2002**, *114*, 1556. *Angew. Chem., Int. Ed.* **2002**, *41*, 1489. (h) Rebek, J., Jr. *Angew. Chem., Int. Ed.* **2005**, *117*, 2104. (i) Biros, S. M.; Rebek, J., Jr. *Chem. Soc. Rev.* **2007**, *36*, 93. (j) Kawano, M.; Fujita, M. *Coord. Chem. Rev.* **2007**, *151*, 2592. (k) Dalgarno, S. J.; Power, N. P.; Atwood, J. L. *Coord. Chem. Rev.* **2008**, *252*, 825. (l) Ma, L.; Abney, C.; Lin, W. *Chem. Soc. Rev.* **2009**, *38*, 1248.
2. Selected articles on solid with pores and cavities: (a) Davis, M. E. *Nature* **2002**, *417*, 813. (b) Langley, P. J.; Hullinger, J. *Chem. Soc. Rev.* **1999**, *28*, 279. (c) Yaghi, O. M.; Li, H.; Davis, C.; Richardson, D.; Groy, T. L. *Acc. Chem. Res.* **1998**, *31*, 474. (c) Ikegame, M.; Tajima, K.; Aida, T. *Angew. Chem., Int. Ed.* **2003**, *42*, 2154. (d) Kitaura, R.; Kitagawa, S.; Kubota, Y.; Kobayashi, T. C.; Kindo, K.; Mita, Y.; Matsuo, A.; Kobayashi, M.; Chang, H. C.; Ozawa, T. C.; Suzuki, M.; Sakata, M.; Takata, M. *Science* **2002**, *298*, 2358. (e) Kitagawa, S.; Kitaura, R.; Noro, S. *Angew. Chem., Int. Ed.* **2004**, *43*, 2334.
3. (a) MacGillivray, L. R.; Atwood, J. L. *Nature* **1997**, *389*, 469. (b) Mckinlay, R. M.; Thallapally, P. K.; Cave, G.W. V.; Atwood, J. L. *Angew. Chem., Int. Ed.* **2005**, *44*, 5733. (c) Heaven, M. W.; Cave, G. W. V.; Mckinlay, R. M.; Antesberger, J.; Dalgarno, S. J.; Thallapally, P. K.; Atwood, J. L. *Angew. Chem., Int. Ed.* **2006**, *45*, 6221. (d) Dalgarno, S. J.; Power, N. P.; Warrenc, J. E.; Atwood, J. L. *Chem. Commun.* **2008**, 1539. (e) Dalgarno, S. J.; Claudio-Bosque, K. M.; Warren, J. E.; Glass, T. E.; Atwood, J. L. *Chem. Commun.* **2008**, 1410.
4. (a) Ranford, J. D.; Vittal, J. J.; Wu, D. *Angew. Chem., Int. Ed.* **1998**, *37*, 1114. (b) Ranford, J. D.; Vittal, J. J.; Wu, D.; Yang, X. *Angew. Chem., Int. Ed.* **1999**, *38*, 3498. (c) Sreenivasulu, B.; Vittal, J. J. *Angew. Chem., Int. Ed.* **2004**, *43*, 5769. (d) Ganguly, R.; Sreenivasulu, B.; Vittal, J. J. *Coord. Chem. Review* **2008,** *252*, 1027. (e) Sreenivasulu, B.; Vittal, J. J. *Inorg. Chim. Acta* **2009** *362,* 2735. (f) Ma, X. F.; Tian, J. L.; Gu, W.; Gao, S.; Yan, S. P.; Liao, D. Z. *Inorg. Chem. Commun.* **2008**, *11*, 256.

5. (a) Alam, M. A.; Nethaji, M.; Ray, M. *Angew. Chem., Int. Ed.* **2003**, *42*, 1940. (b) Alam, M. A.; Nethaji, M.; Ray, M. *Inorg. Chem.* **2005**, *44*, 1302. (c) Alam, M. A.; Koner, R. R.; Das, A.; Nethaji, M.; Ray, M. *Cryst. Growth. Des.* **2007**, *7*, 1818. (d) Sahoo, S. C.; Ray, M. *Dalton Trans.* **2009**, 3230.
6. (a) Gibney, B. R.; Wang, H.; Kampf, J. W.; V. L. Pecoraro. *Inorg. Chem.* **1996**, *35*, 6184. (b) Saalfrank, R. W.; Maid, H.; Mooren, N.; Hampel, F. *Angew. Chem., Int. Ed.* **2002**, *41*, 304. (c) Vittal, J. J.; Wang, X.; Ranford, J. D. *Inorg. Chem.* **2003**, *42*, 3390. (d) Wang, X.; Vittal, J. J. *Inorg. Chem.* **2003**, *42*, 5135. (e) Nanda, P. K.; Aromi, G.; Ray, D. *Inorg. Chem.* **2006**, *45*, 3143. (f) Mezei, G.; Kampf, J. W.; Pan, S.; Poeppelmeier, K. R.; Watkins, B.; Pecoraro, V. L. *Chem. Commun.* **2007**, 1148. (g) Mezei, G.; Zaleski, C. M.; Pecoraro, V. L. *Chem. Rev.* **2007**, *107*, 4933.
7. (a) Chen, X. M.; Aubin, S. M. J.; Wu, Y. L.; Yang, Y. S.; Mak, T. C. W.; Hendrickson, D. N. *J. Am. Chem. Soc.* **1995**, *117*, 9600. (b) Mizuno, T.; Wei, W. H.; Eller, L. R.; Sessler, J. L. *J. Am. Chem. Soc.* **2002**, *124*, 1134. (c) Lee, C. H.; Na, H. K.; Yoon, D. W.; Won, D. H.; Cho, W. S.; Lynch, V. M.; Shevchuk, S. V.; Sessler, J. L. *J. Am. Chem. Soc.* **2003**, *125*, 7301. (d) Bowman-James, K. *Acc. Chem. Res.* **2005**, *38*, 671. (e) Hay, B. P.; Firman, T. K.; Moyer, B. A. *J. Am. Chem. Soc.* **2005**, *127*, 1810. (f) Kang, S. O.; Powell, D.; Bowman-James, K. *J. Am. Chem. Soc.* **2005**, *127*, 13478.
8. (a) Leharie, M. L.; Scopelliti, R.; Severin, K. *Chem. Commun.* **2002**, 2766. (b) Mahoney, J. M.; Stucker, K. A.; Jiang, H.; Carmichael, I.; Brinkmann, N. R.; Beatty, A. M.; Noll, B. C.; Smith, B. D. *J. Am. Chem. Soc.* **2005**, *127*, 2922. (c) Miyaji, H.; Kim, H.; Sim, E.; Lee, C.; Cho, W.; Sessler, J. L.; Lee, C. *J. Am. Chem. Soc.* **2005**, *127*, 12510.
9. Magnetic moment (B.M.) range for Ni(II): 2.9 - 3.3 and Cu(II) 1.7–2.1. Solid state moment can be lower if weak anti ferromagnetic interaction is present. (a) Figgis, B. N.; Lewis J. *Prog. Inorg. Chem.* **1964**, *6*, 37. (b) O'Connor, C. J. *Prog. Inorg. Chem.* **1982** *29*, 203. (c) Earnshaw, A. *Introduction to Magnetochemistry*, Academic Press, London, 1968. Molar conductance (ohm^{-1} cm^2 mol^{-1}) range for 1:1 electrolyte in DMF: 65-90, MeOH: 80-115. (d) Geary, W. J. *Coord. Chem. Rev.* **1971**, *7*, 81.
10. Blessing, R. *Acta Crystallogr., Sect. A* **1995**, *51*, 33.
11. (a) Sheldrick, G. M. *SHELXL-97: Program for Crystal Structures Refinement*; University of Göttingen: Göttingen, Germany, 1997. (b) Farrugia, L. J. *J. Appl. Crystallogr.* **1999**, *32*, 837-838.

12. O··O range (2.5 to 3.0) Å: (a) Miyake, R.; Tashiro, S.; Shiro, M.; Tanaka, K.; Shionoya, M. *J. Am. Chem. Soc*. **2008**, *130*, 5646. (b) Desiraju, G. R. *Perspective in Supramolecular Chemistry*, Wiley, *Vol 7*. (c) 3b (d) 6d. (e) Yang, C. T.; Moubaraki, B.; Murray, K. S.; Vittal, J. J. *Dalton Trans*. **2003**, 880.
13. K-O distance range (2.6 to 2.9) Å: from Ref 6(a), 6(b) and 6(d) above. A difference of 0.3 Å between K-O and Na-O was observed in two similar crystal where Na^+ or K^+ is bound by DMF. Average Na-O, 2.303, K-O, 2.607Å; (d) Patra, A. K.; Ray, M.; Mukherjee, R. N. *Polyhedron* **2000**, *19*, 1423.
14. Weak CH…F interaction between aromatic C-H and C-F ranging from 2.1 to 3.1 Å has been reported: Teff, D. J.; Huffman, J. C.; Caulton, K. G. *Inorg. Chem.* **1997**, *36*, 4372.
15. (a) Rajendiran, V.; Palaniandavar, M.; Swaminathan, P.; Uma, L. *Inorg. Chem.* **2007**, *46*, 10446. (b) Zurowska, B.; Erxleben, A.; Glinka, L.; Łe˛czycka, M.; Zyner, E.; Ochocki, J. *Inorg. Chim. Acta.* **2009**, *362*, 739.
16. Lever, A. B. P. *Inorganic Electronic Spectroscopy*, 2nd ed.; Elsevier: 1984; p 507.
17. (a) Cotton, F. A.; Daniels, L. M.; Jordan, G. T.; Murillo, C. A. *Chem. Commun.* **1997**, 1673, and references cited therein. (b) Desiraju, G. R. Crystal Engineering. The Design of Organic Solids; Elsevier: Amsterdam, 1989; p 166, and references cited therein. (c) Mazik, M.; Blaser, D.; Boese, R. *Tetrahedron* **1999**, *55*, 7835.
18. The binding of achiral nickel(II) Schiff-base complexes with alkali and alkaline earth metals in solution were reported and in one case, a spectral change upon potassium ion binding has been noted: (a) Carbonaro, L.; Isola, M.; Pegna, P. L.; Senatore, L. *Inorg. Chem*. **1999**, *38*, 5519. (b) Giacomelli, A.; Rotunno, T.; Senatore, L. *Inorg. Chem*. **1985**, *24*, 1303.
19. (a) Gillard, R. D.; Mason, R.; Robertson, G. B. *J. Chem. Soc. A* **1969**, 12, 1864–1871. (b) Moussa, S. M.; Fenton, R. R.; Kennedy, B. J.; Piltz, R. O. *Inorg. Chim. Acta* **1999**, *288*, 29–34. (c) Freeman, H. C.; Snow, M. R.; Nitta, I.; Tomita, K. *Acta Crystallogr.* **1964**, *17*, 1463–1470. (d) Weeks, C. M.; Cooper, A.; Norton, D. A. *Acta Crstallogr., Sect. B* **1969**, *25*, 443–450. (e) Sabolovi, J.; Tautermann, C. S.; Loerting, T.; Liedl, K. R. *Inorg. Chem.* **2003**, *42*, 2268.

In the previous chapter, we have observed spontaneous formation of a multinuclear assembly from the L-leucine derived ligand, bivalent metal ion and alkali metal ions, analogous to cryptate like adduct.[1] In this chapter, we have explored whether the formation is L-leucine specific or not and the formation of assembly occurs in a single or multiple steps. To do that, we have synthesized and characterized a series of monomeric complexes with two different ligands (Scheme **3.1**, **3.2**) and explored their transformation towards multinuclear assembly in presence of alkali metal based binary salts.

Structurally characterized *bis* complexes of Cu(II) with amino acids except L-alanine, L-glycine, and L-isoleucine have *trans* orientation of the two amino acids around Cu(II).[2] Earlier, Vittal and *et al*. reported mononuclear Cu(II) complex using L-serine derived ligand having *cis* orientation.[3] Assemblies in previous chapter had exclusively *cis* orientation of L-leucine around Cu(II)/Ni(II). Thus it would be interesting to know whether the *cis* orientation of two L-leucine derivative originates in the monomeric stage or is a result of assembly formation.

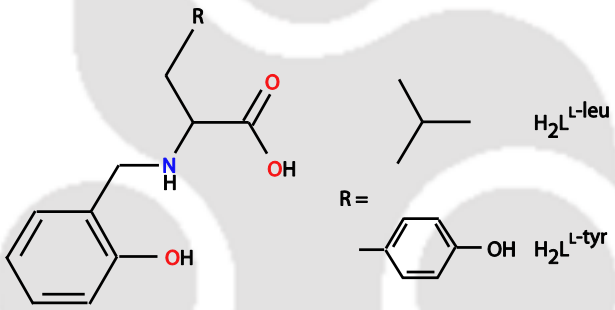

Scheme 3.1. *Ligands used in this chapter.*

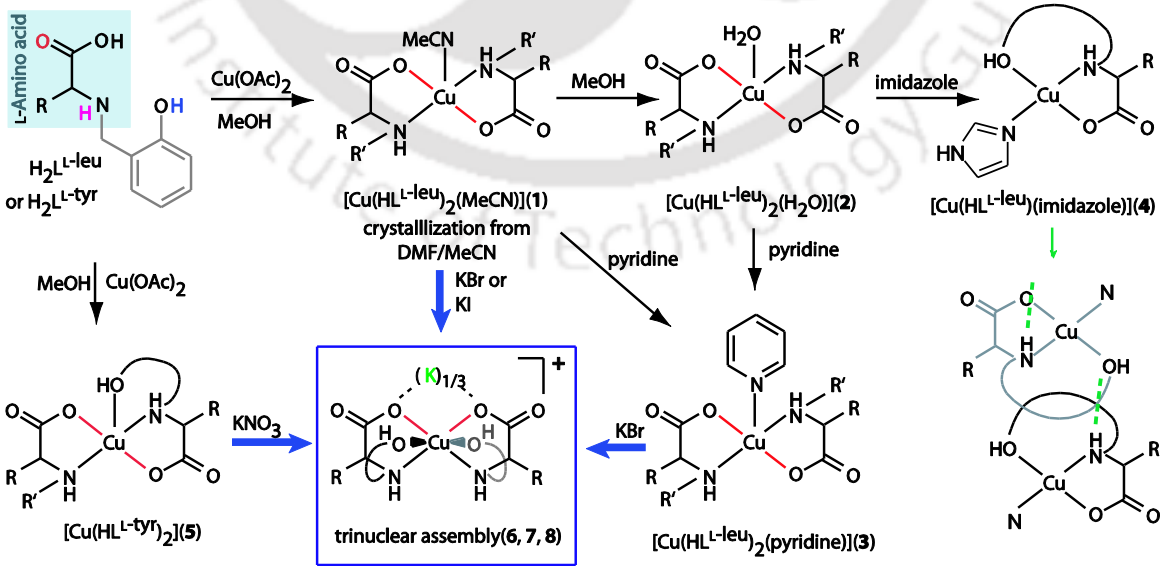

Scheme 3.2. *Synthetic scheme for complexes.*

3.1 Experimental section

3.1.1 Materials and Methods

Solvents used were purified prior to use following standard literature procedure. KBr was purchased from Aldrich Chemical Co. L-tyrosine and KI were purchased from Sisco Research Laboratories Pvt. Ltd. (SRL), India and used as received. The ligand $H_2L^{L\text{-}tyr}$ was synthesized as before.[4]

Details of the instruments used have already been described in Chapter **2**.

3.2 Syntheses

3.2.1 $[Cu(HL^{L\text{-}leu})_2(CH_3CN)]$ (1)

Ligand $H_2L^{L\text{-}leu}$ (0.200 g, 0.846 mmol) was taken in 15 mL MeOH which offered a white undissolved matter. A solution of $Cu(OAc)_2.H_2O$ (0.082 g, 0.421 mmol) in MeOH (10 mL) was added drop wise to the above ligand solution and stirring continued. The color of the solution changed from green-blue to deep blue immediately. The solution was stirred for 1 h and was evaporated to dryness in a rotary evaporator. The resulting crude solid was dissolved in DMF and crystallized by adding equal volume of CH_3CN and left it for slow evaporation for two days. The rod shaped blue crystals were obtained. Isolated crystals were washed with CH_3CN and dried under vacuum desiccator. Yield: 72%. Anal. Calcd. for $[Cu(C_{13}H_{18}O_3N)_2CH_3CN].4CH_3OH$: C, 54.49; H, 7.85; N, 5.95; found C, 54.45; H, 7.77; N, 5.87. IR (KBr, cm^{-1}): ν(OH) 3461 (b), $\nu(COO)_{asym}$ 1626 (s), 1592 (s), 1460 (s), 1382 (s), 1271 (m). μ_{eff} (powder, 298K): 1.64 μ_B. Λ_M (ohm^{-1} cm^2 mol^{-1}): 0.4 (MeOH), 3.0 (DMF).

3.2.2 $[Cu(HL^{L\text{-}leu})_2H_2O]$ (2)

Complex $[Cu(HL^{L\text{-}leu})_2(CH_3CN)]$ (**1**) (0.0500 g, 0.0683 mmol) in MeOH (15 mL) was stirred for 45 min and the solution was left for slow evaporation. The rod like blue crystals obtained within five days. Isolated crystals were dried under vacuum. Yield: 34%. Anal. Calcd. for $[Cu(C_{13}H_{18}O_3N)_2H_2O].2H_2O$: C, 52.95; H, 7.18; N, 4.78; found C, 52.31; H, 6.42; N, 4.62. IR (KBr, cm^{-1}): ν(OH) 3433 (b), 2954 (m), $\nu(COO)_{asym}$ 1625 (s), 1592 (s), 1460 (s), 1384 (s), 1253 (m), 1111, 976, 750 (s), 582. μ_{eff} (powder, 298K): 1.88 μ_B/Cu. Λ_M (ohm^{-1} cm^2 mol^{-1}): 1.3 (MeOH).

3.2.3 [Cu(HL$^{L\text{-}leu}$)$_2$Pyridine] (3)

Complex [Cu(HL$^{L\text{-}leu}$)$_2$(CH_3CN)](**1**) (0.100 g, 0.136 mmol) in MeOH (15 mL) was stirred for 15 min and pyridine (0.019 g, 0.246 mmol) mixed with above stirring solution. The color of solution changed instantly from deep blue to blue-green and solution was kept for crystallization. The rod like blue crystals obtained within three days. Isolated crystals were washed with diethyl ether and dried under vacuum. Yield: 32%. Anal. Calcd. for [Cu($C_{13}H_{18}O_3N$)$_2C_5H_5N$].2H_2O: C, 57.20; H, 6.97; N, 6.46; found C, 56.47; H, 6.37; N, 5.89. IR (KBr, cm^{-1}): ν(OH) 3524 (b), 3294 (m), 2958 (m), ν(COO)$_{asym}$ 1616 (s), 1608 (s), 1461 (s), 1381 (m), 1346 (m), 1273 (m), 1067, 976, 943, 769, 709, 563. μ_{eff} (powder, 298K): 1.92 μ_B/Cu. Λ_M (ohm^{-1} cm^2 mol^{-1}): 0.30 (MeOH).

3.2.4 [Cu(L$^{L\text{-}leu}$)Imidazole] (4)

Complex [Cu(HL$^{L\text{-}leu}$)$_2$(CH_3CN)](**1**) (0.100 g, 0.137 mmol) in MeOH (15 mL) was stirred for 15 min and imidazole (0.0093 g, 0.1370 mmol) was added with above stirring solution. The color of solution changed instantly from deep blue to green and solution was kept for crystallization. The rod like violet-black crystals obtained within three days. Isolated crystals were dried under vacuum. Yield: 31%. Anal. Calcd. for [Cu($C_{16}H_{22}O_4N_3$)]·H_2O: C, 49.85; H, 6.28; N, 10.90; found C, 50.11; H, 6.30; N, 11.02. IR (KBr, cm^{-1}): ν(OH) 3440 (b), 2956 (m), 2921 (s), 2850 (m), ν(COO)$_{asym}$ 1625 (s), 1452 (m), 1384 (m), 1279 (m), 1111 (m), 1071, 752, 532. μ_{eff} (powder, 298K): 1.90 μ_B/Cu. Λ_M (ohm^{-1} cm^2 mol^{-1}): 1.5 (MeOH).

3.2.5 [Cu(HL$^{L\text{-}tyr}$)$_2$] (5)

Ligand $H_2L^{L\text{-}tyr}$ (0.200 g, 0.697 mmol) was taken in 15 mL MeOH which offered a white undissolved matter. A solution of $Cu(OAc)_2 \cdot H_2O$ (0.069g, 0.348 mmol) in MeOH (10 mL) was added drop wise to the above ligand solution and stirring continued. The color of the solution changed from green-blue to deep blue immediately. The solution was stirred for 1 h and then evaporated to dryness in a rotary evaporator. The resulting crude solid was dissolved in DMF and crystallized by adding equal volume of CH_3CN and left it for slow evaporation for two days. The rod shaped blue crystals were obtained. Isolated crystals were washed with CH_3CN and dried under vacuum desiccators. Yield: 68%. Anal. Calcd. for [Cu($C_{16}H_{16}O_4N$)$_2$].2H_2O: C, 57.21; H, 5.40; N, 4.17; found C, 57.13; H, 6.21; N, 4.05. IR (KBr, cm^{-1}): ν(OH) 3434 (b), ν(COO)$_{asym}$ 1623 (s), 1593 (s), 1516 (m), 1462 (m), 1381 (m), 1253 (m), 749. μ_{eff} (powder, 298K): 1.72 μ_B. Λ_M (ohm^{-1} cm^2 mol^{-1}): 0.6 (MeOH).

3.2.6 $[K\{Cu(HL^{L\text{-}tyr})_2\}_3]NO_3$ (6)

Monomer $[Cu(HL^{L\text{-}tyr})_2]$ (**5**) (0.100 g, 0.142 mmol) in MeOH (15 mL) was stirred for 15 min and solid KNO_3 (0.005 g, 0.049 mmol) mixed with above stirring solution. The color of solution changed after 10 min from deep blue to blue-green. The solution was stirred for 4 h and then filtered to remove excess KNO_3, the resulting solution evaporated to dryness in a rotary evaporator. The resulting solid was washed with diethyl ether. The crystalline green-blue compound obtained was dried under vacuum. Yield: 42%. Anal. Calcd. for $[K\{Cu(C_{16}H_{16}O_4N)_2\}_3]NO_3{\cdot}3H_2O$: C, 55.91; H, 4.98; N, 4.75; found C, 56.12; H, 5.06; N, 4.79. IR (KBr, cm^{-1}): ν(OH) 3413 (b), 3247 (m), $\nu(COO)_{asym}$ 1617 (s), 1515 (s), 1460 (m), 1383 (m), 1248, 1086, 814, 758. μ_{eff} (powder, 298K): 1.64 μ_B/Cu. Λ_M (ohm^{-1} cm^2 mol^{-1}): 130 (MeOH), 100 (DMF).

3.2.7 $[K\{Cu(HL^{L\text{-}leu})_2\}_3]Br$ (7)

Complex $[Cu(HL^{L\text{-}leu})_2(CH_3CN)]$ (**1**) (0.0500 g, 0.0683 mmol) in MeOH (15 mL) was stirred for 15 min and solid KBr (0.0027 g, 0.0227 mmol) was added with above stirring solution. The color of solution changed after 10 min from deep blue to blue-green. The solution was stirred for 2 h and then concentrated in a rotary evaporator. The resulting crude solution was recrystallized by adding minimum volume of CH_3CN and left it for slow evaporation. The diamond shaped blue crystals obtained within two days. Isolated crystals were dried under vacuum. Yield: 46%. Anal. Calcd. for $[K\{Cu(C_{13}H_{18}O_3N)_2\}_3]Br{\cdot}7H_2O$: C, 50.60; H, 6.64; N, 4.54; found C, 50.57; H, 6.70; N, 4.66. IR (KBr, cm^{-1}): ν(OH) 3467 (b), 2958 (m), $\nu(COO)_{asym}$ 1633 (s), 1589 (s), 1463 (s), 1389 (m), 1279 (m), 1091, 928, 757, 572. μ_{eff} (powder, 298K): 1.71 μ_B/Cu. Λ_M (ohm^{-1} cm^2 mol^{-1}): 117 (MeOH).

3.2.8 $[K\{Cu(HL^{L\text{-}leu})_2\}_3]I$ (8)

Complex **8** has been prepared following similar procedure as described for **7** using KI instead of KBr. The diamond shaped blue crystals obtained within two days. Isolated crystals were dried under vacuum. Yield: 42%. Anal. Calcd. for $[K\{Cu(C_{13}H_{18}O_3N)_2\}_3]I{\cdot}3CH_3CN{\cdot}5H_2O$: C, 50.79; H, 6.44; N, 6.35; found C, 50.63; H, 6.39; N, 6.01. IR (KBr, cm^{-1}): ν(OH) 3437 (b), 2956 (m), ν(COO)asym 1632 (s), 1586 (s), 1462 (s), 1387 (m), 1278 (m), 1085 (m), 753. μ_{eff} (powder, 298K): 1.74 μ_B/Cu. Λ_M (ohm^{-1} cm^2 mol^{-1}): 98 (MeOH).

3.3 X-ray Data Collection, Structure Solution and Refinement

Crystals of the complexes $[Cu(HL^{L\text{-}leu})_2(CH_3CN)]$ (**1**), $[Cu(HL^{L\text{-}leu})_2H_2O]$ (**2**), $[Cu(HL^{L\text{-}leu})_2Pyridine]$ (**3**), $[Cu(L^{L\text{-}leu})Imidazole]$ (**4**), $[Cu(HL^{L\text{-}tyr})_2]$ (**5**), $[K\{Cu(HL^{L\text{-}leu})_2\}_3]Br$ (**7**), $[K\{Cu(HL^{L\text{-}leu})_2\}_3]I$ (**8**) obtained during synthesis were used for X-ray analysis. The crystals were mounted on glass fiber. The instrumental parameters used for data collections are same as described in the Chapter **2**. Absorption corrections were done using SADABS only as either kinds of absorption did not help.[5] After the initial solution and refinement with SHELXL, the final refinements were performed on WinGX environment using SHELX97.[6] Selected crystallographic data have been summarized in Table **3.1.**

Table 3.1. Selected crystallographic data for the complexes

	1	**2**	**3**	**4**	**5**	**7**
empirical formula	$C_{36}H_{45}CuN_7O_6$	$C_{26}H_{35}CuN_2O_9$	$C_{31}H_{43}CuN_3O_7$	$C_{16}H_{21}CuN_3O_3$	$C_{34}H_{28}CuN_2O_1$	$C_{78}H_{88}BrCu_3KN_6O_{23}$
fw	735.34	582.83	633.25	366.91	704.13	1787.17
T(K)	296(2)	296(2)	296(2)	296(2)	296(2)	296(2)
Wavelength(Å)	0.71073	0.71073	0.71073	0.71073	0.71073	0.71073
Crystal system	monoclinic	monoclinic	monoclinic	orthorhombic	monoclinic	orthorhombic
Space group	*C2*	$P2_1$	*C2*	$P2_12_12_1$	$P2_1$	$C222_1$
a, Å	23.924(2)	12.9260(8)	13.1598(5)	7.1096(3)	12.974(3)	17.675(5)
b, Å	9.7748(9)	8.6269(5)	15.3478(6)	12.0917(4)	10.454(3)	21.173(5)
c, Å	8.7819(8)	13.9941(10)	8.0331(3)	19.7283(7)	14.459(4)	26.561(5)
α, deg	90.00	90.00	90.00	90.00	90.00	90.00
β, deg	92.053	102.650(4)	98.488(2)	90.00	115.029(16)	90.00
γ, deg	90.00	90.00	90.00	90.00	90.00	90.00
V, $Å^3$	2052.3(3)	1522.62(17)	1604.71(11)	1695.99(11)	1776.9(9)	9940(4)
z/ρ	2/1.190	2/1.271	2/1.311	4/1.437	2/1.316	4/1.143
μ	0.580	0.766	0.729	1.305	0.674	0.729
coll. reflns	3578	5885	2680	4751	9575	10757
indep reflns	2926	4787	2257	3669	3912	6697
FLACK para.	0.002(12)	0.011(15)	0.036(13)	0.019(15)	-0.006(19)	-0.002(13)
GOF	0.979	1.034	1.008	0.995	0.813	1.074
R1[a]	0.0374	0.0499	0.0410	0.0390	0.0738	0.0569
wR2[a]	0.0755	0.1275	0.0676	0.0921	0.1639	0.1193
R1[b]	0.0511	0.0654	0.0524	0.0567	0.1680	0.1428
wR2[b]	0.0804	0.1376	0.0710	0.1001	0.1927	0.1549

[a] $I>2\sigma$. [b] All data.

3.4 Results and discussion

3.4.1 Synthesis and selected properties

Complex $[Cu(HL^{L\text{-}leu})_2CH_3CN]$ (**1**) was synthesized using Cu(II) acetate to avoid presence of alkali metal ion which facilitates formation of assembly. The reaction between divalent Cu(II) acetate and ligand $H_2L^{L\text{-}leu}$ in MeOH at 1:2 ratio, resulting solid was crystallized by DMF and MeCN, yielded the rod shaped blue crystals of **1** (Scheme **3.2**). Complex $[Cu(HL^{L\text{-}leu})_2H_2O]$ (**2**) was synthesized by recrystallization of complex **1** in MeOH. Complex $[Cu(HL^{L\text{-}leu})_2$Pyridine] (**3**) was synthesized by addition of pyridine into the methanolic solution of **1** or **2**. Complex $[Cu(L^{L\text{-}leu})$Imidazole] (**4**) was synthesized by stirring complex **1** or **2** and imidazole in MeOH at 1:1 ratio. Complex **5** was synthesized using the Cu(II) acetate and $H_2L^{L\text{-}tyr}$ in MeOH, similar to **1**. However, unlike **1**, **5** did not bind acetonitrile. The rod shaped blue crystals of $[Cu(HL^{L\text{-}tyr})_2]$ (**5**) were isolated within two days in 68% yield (Scheme **3.2**). Complex **6** was synthesized by conversion of monomer $[Cu(HL^{L\text{-}tyr})_2]$ (**5**) to multinuclear assembly $[K\{Cu(HL^{L\text{-}tyr})_2\}_3]NO_3$ (**6**) upon addition of KNO_3 (monomer to KNO_3 ratio 3:1) in MeOH. Though, we could not get single crystal of **6**, the assembly formation was confirmed by ESI-Mass spectroscopic analysis. Complexes $[K\{Cu(HL^{L\text{-}leu})_2\}_3]$Br (**7**) and $[K\{Cu(HL^{L\text{-}leu})_2\}_3]$I (**8**) were synthesized by conversion of monomer **1** to assembly upon addition of KBr and KI respectively in MeOH at the ratio 3:1.

The carboxylate stretches were observed between 1615–1640 and at ~1380 cm^{-1} for ν_{assym} and ν_{sym} respectively.[7] The elemental analyses support the formulation of the complexes. The non-electrolytic nature of the monomers **1**–**5** was confirmed by conductance measurement in MeOH. Conductance of the assemblies **7** and **8** in MeOH falls within the range of 1:1 electrolyte.[8] However, slightly higher value of conductance for the assembly **6** in MeOH as well as in DMF, may be because of traces of KNO_3 as impurity. The room temperature magnetic moment of the complexes are within the range 1.6–1.9 μ_B closer to the spin only value of 1.73 for Cu(II) complexes.[8]

3.4.2 Structural analyses of the monomeric complexes

$[Cu(HL^{L\text{-}leu})_2(CH_3CN)]$ (1). The complex **1** was crystallized in the space group C_2 (Table **3.1**). Half of the molecule of **1** is symmetrical with the other half through C_2 symmetry. The ORTEP diagram of **1** and selected bond lengths have shown in Figure **3.1A**. The square pyramidal geometry around **1** is due to coordination of two $HL^{L\text{-}leu}$ ligands and an acetonitrile coordinated axially (τ = 0.09). The two mono protonated $HL^{L\text{-}leu}$ coordinated in a *trans* N_2O_2

mode and phenols remain uncoordinated to Cu(II). In **1,** conformation at the chiral carbon is *S* as the amino acid used in synthesis was *S* isomer. In addition to the asymmetric carbon center in the ligand, the coordination of amine N to the Cu(II) gives rise to an asymmetric secondary nitrogen atom which has the *R* configuration.

Apart from the coordinated acetonitrile, the crystal contains four acetonitrile molecules. Two of the acetonitrile symmetrically disposed around **1** showing weak CH…N interaction (C15…N3, 3.342 Å).[9] The other two acetonitrile are disordered over four positions with half occupancy. The phenol, carboxylate and amine are H–bonded in a linear three centre two H-bond in a complementary fashion which led to formation of a one-dimensional chain of molecules (Figure **3.1B**). This type of linear three centre two H–bond was never reported in any of the complexes with this type of ligands. The H–bond between phenol and carboxylate at 2.635 Å (O2…O3) is longer than average 2.589 Å observed in previous Cu(II) multinuclear assemblies. Fifth axial coordinated acetonitrile is embedded in the *C2* symmetric cavity (Figure **3.2A**). One notable feature of the lattice is the formation of two dimensional channels within the crystal which accommodates four acetonitrile solvents (Figure **3.2B**). The dimensions of the channels (a cuboid space approximately 5x5.7x9.7 $Å^3$) are larger than those observed earlier by us in a iron(III) complex with L-histidine derived ligand.[10]

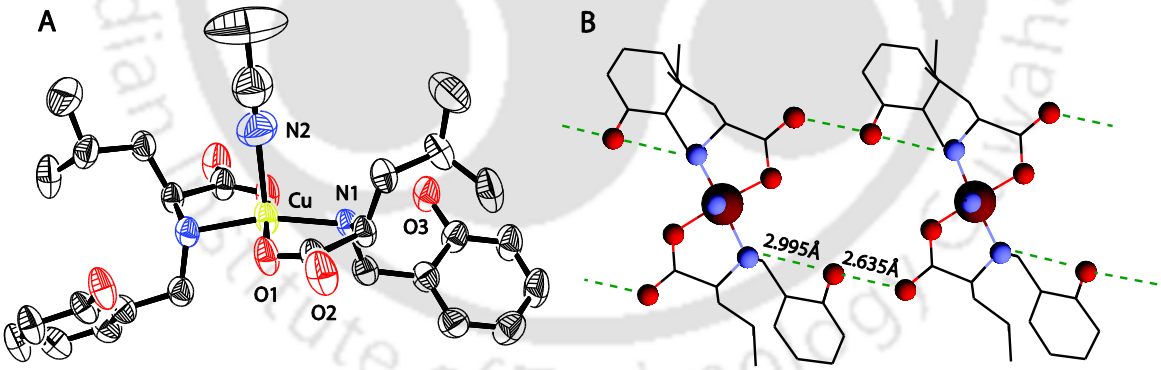

Figure 3.1. *(A) ORTEP diagram of **1** with thermal ellipsoids set to 30% probability level, and (B) Intermolecular and intramolecular hydrogen bonding pattern between two molecular units of **1**.*

*Selected bond distances (A°) and angles (°) for **1**: Cu1–O1 1.9340(16), Cu1–N1 2.008(2), Cu1–N2 2.332(5), N1–Cu1–O1 83.66(7), O1–Cu1–O1 169.95(17), N1–Cu1–N1 164.37(13). H-bonds: N1...O3 2.995(3), O3...O2 2.635(3).*

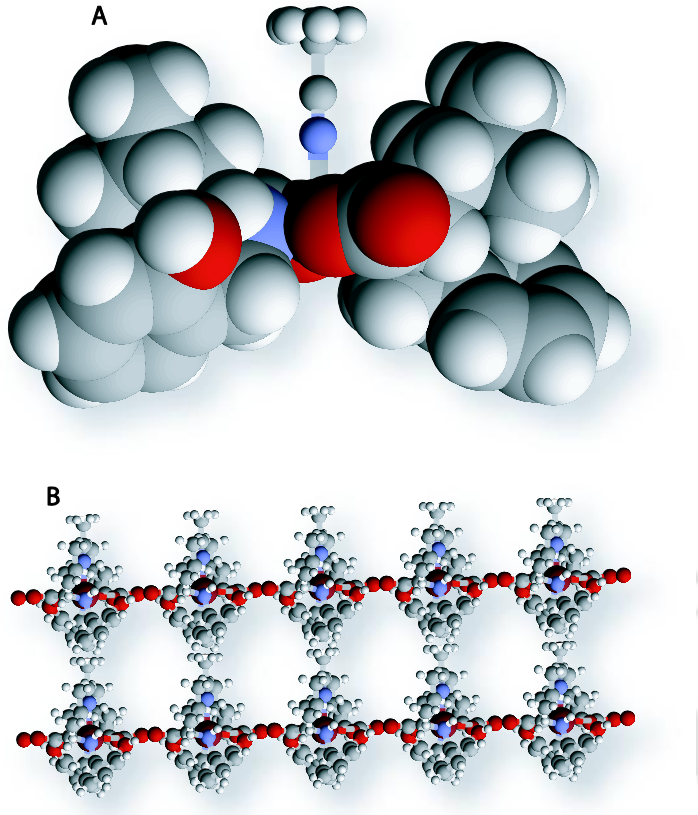

Figure 3.2. *(A) A space filling model of C2 symmetric cavity in **1** and (B) A two dimensional channel within crystal lattice of **1**.*

[Cu(HL$^{L\text{-leu}}$)$_2$H$_2$O] (2). The complex **2** was crystallized in the space group $P2_1$ with two independent mononuclear units in the unit cell (Table **3.1**). The ORTEP figure of one of the mononuclear unit, selected bond lengths and angles for complex is given in Figure **3.3**. The complex is monomeric in nature with regular square pyramidal geometry around the Cu(II) (τ = 0.07).

The in-plane bond lengths for Cu–$O_{carboxylate}$ are within the range 1.92–1.95 Å observed for other amino acid or amino acid derived ligand Cu(II) complexes.[11] The in-plane bond lengths for Cu–N_{amine} are longer at ~2.02 Å compared to corresponding amino acid complexes (1.96–1.98 Å).[11] The axial fifth coordination is provided by a water molecule with short Cu–O distance of 2.248(3) Å for **2** (Figure **3.3**). The axial bond in square-pyramidal Cu(II) is usually long and varies between 2.12 to 2.6 Å for O or N coordination, due to Jahn-Teller distortion.[12] The presence of two isopropyl arm of leucine influenced the coordination of water on the other side and this in turn must have influenced the hydrophobic phenol rings to rotate apart (Cu1–N2–C20 ~113°) compared to structure of **1** (Cu1–N1–C7 ~108°).

Further, the isopropyl groups of leucine in **2** located closer to each other to minimize the hydrophobic effect. Thus, the cavity destroyed because of water coordination (Figure **3.3B**).

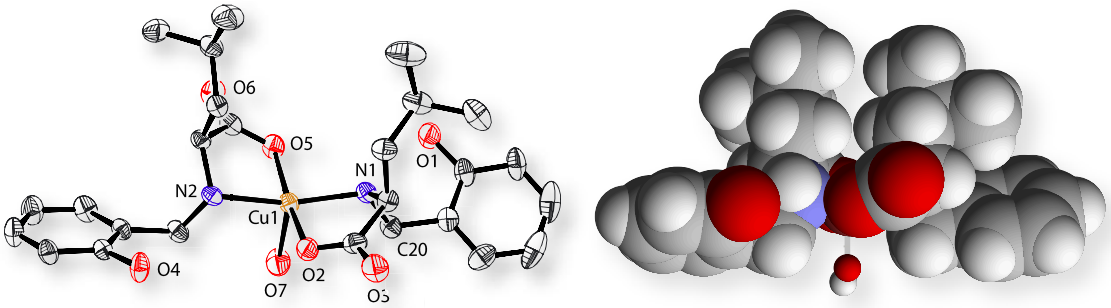

Figure 3.3. *(A) ORTEP diagram of **2** with thermal ellipsoids set to 30% probability level, (B) A space filling model of **2** shows cavity destroyed because of axial water coordination. Selected bond distances (A°) and angles (°) for **2**: Cu1–O2 1.946(3), Cu1–O5 1.948(3), Cu1–O7 2.248(3), Cu1–N1 2.020(3), Cu1–N2 2.044(3), O2–Cu1–O5 167.01(14), O2–Cu1–N1 83.50(14), O5–Cu1–N1 94.22(14), N1–Cu1–N2 162.52(13). H-bonds: N1…O1 2.906, O1…O3 2.630, N2…O4 3.058, O4…O6 2.653, O4…O9 3.014, O9…O7 2.743 A°.*

One prominent feature is the H-bond between axially bound oxygen and water as solvent of crystallization with a O9–O7 bond distance 2.743 Å (Figure **3.4A**, **B**). The usual O…O H-bond distances lies between 2.74 to 3.004 Å.[13] The water molecule as solvent of crystallization, trapped between two monomeric units through H-bond with a O4–O9 distance 3.014 Å and 1.761 Å pulled above the plane, towards axially bound water (O7) of complementary unit (Figure **3.4A**, **B**).

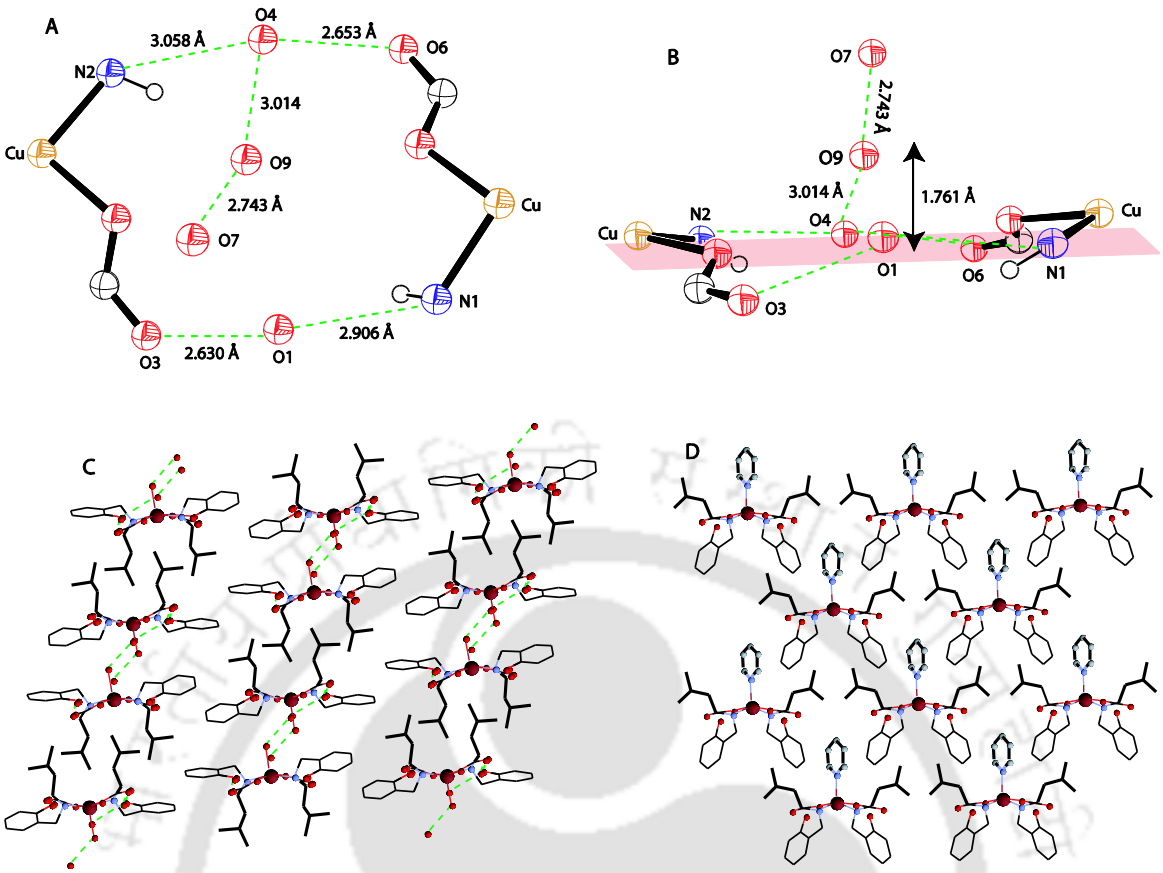

Figure 3.4. *(A) A water molecule trapped within two monomeric units in **2**, (B) Trapped water molecule (O9), pulled above the plane with distance 1.761 Å towards axially bound water O7, (C) Crystal lattice of **2** shows orientation of hydrophobic isopropyl group opposite to axially bound water, and (D) Crystal lattice of **3** shows orientation of hydrophobic isopropyl group towards to axially bound pyridine.*

[Cu(HL$^{L\text{-}leu}$)$_2$Pyridine] (3). The complex **3** was crystallized in the space group C_2 (Table **3.1**). Half of the molecule of **3** is symmetrical with the other half through C_2 symmetry. The ORTEP figure of **3** and selected bond lengths have shown in Figure **3.5A**. The complex is mononuclear with distorted square pyramidal geometry around the Cu(II) (τ = 0.348). The distortion parameter τ was calculated from the structural data where the value of τ should be 0.0 for perfect square-pyramidal geometry and 1.0 for a perfect trigonal bipyramidal (TBP) structure.[14]

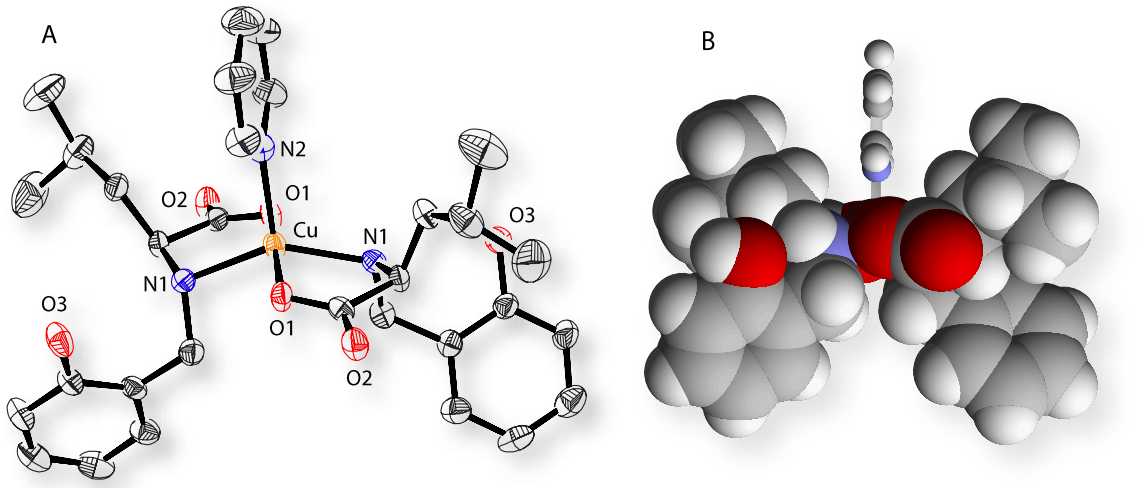

Figure 3.5. *(A) ORTEP diagram of **3** with thermal ellipsoids set to 30% probability level, hydrogen atoms are omitted for clarity and (B) A space filling model of **3** shows that pyridine embedded in C2 symmetric cavity.*

*Selected bond distances (A°) and angles (°) for **3**: Cu–O1 1.9328(19), Cu–N1 2.043(2), Cu–N2 2.185(4), O1–Cu–O1 167.29(16), N1–Cu–N1 146.38(13). H-bonds: N1…O3 2.854, O3…O2 2.659.*

The in-plane bond lengths are comparable with **2**. The axial fifth coordination is provided by a pyridine molecule with Cu–N2 distance of 2.185(4) Å for **3** which is shorter than axially bound acetonitrile Cu(II) distance Cu1–N2 2.332(5) Å for **1** (Figure **3.5** & **3.1**). The axial bond in square-pyramidal Cu(II) is usually long and varies between 2.12 to 2.6 Å for O or N coordination, due to Jahn-Teller distortion.[12] The isopropyl groups of leucine in **3** forms bowl shaped *C2* symmetric cavity, where pyridine is situated (Figure **3.5B**). In **3**, a water molecule as solvent of crystallization trapped between two monomeric units (Figure **3.6** & **3.7C**). The trapped water molecule is 1.167 Å above the plane which is reasonably lower than in **2** (1.761 Å), because of hydrophobic pyridine forced the trapped water molecule to go towards the plane, while in **2** hydrophilic environment on top of the trapped water molecule pulled upward more above the plane (Figure **3.6a**, **b**). Remember relation between plane and trapped water molecule is in opposite direction for **2** and **3**, which is in accordance with axial ligand orientation. Because of hydrophobic axial pyridine in **3**, isopropyl groups of ligand arranged linearly in the lattice, while in **2** hydrophilic axial water and hydrophobic isopropyl arm destroyed the linearity (Figure **3.4C** & **D**).

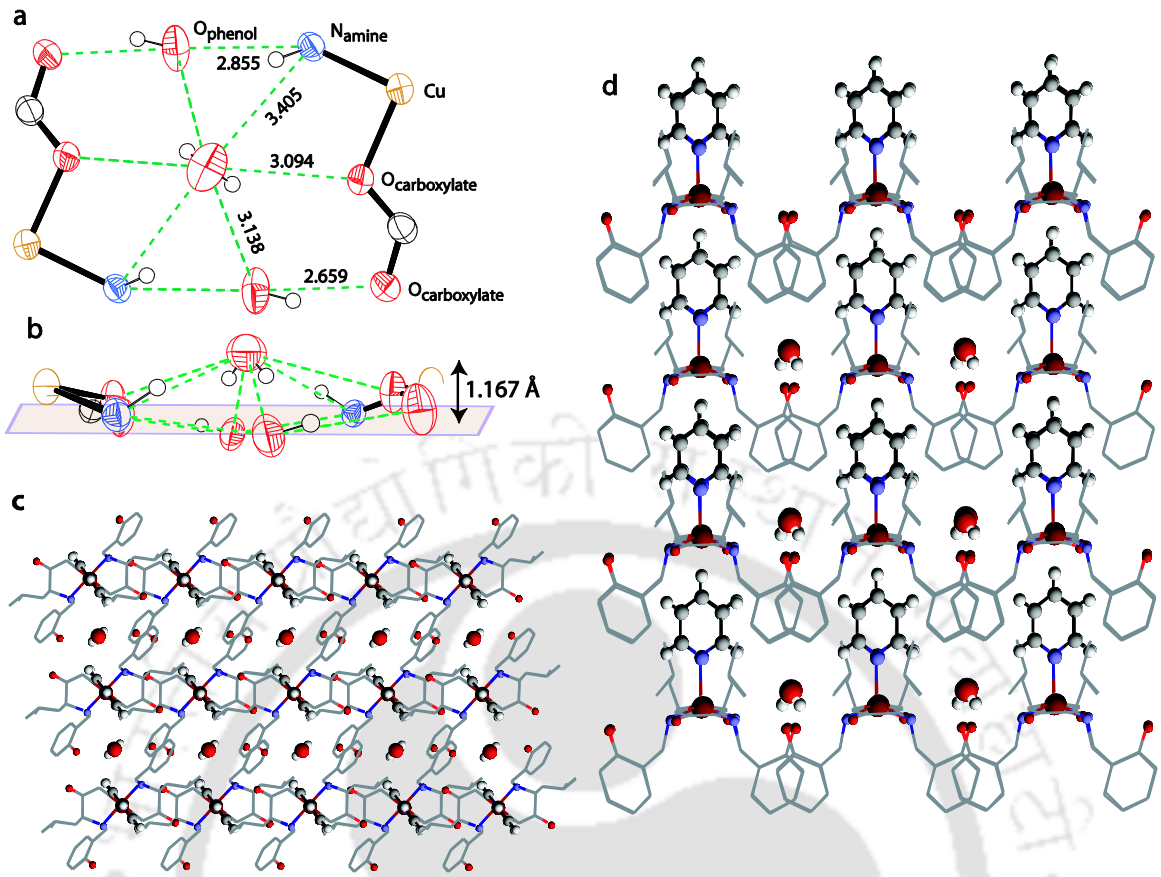

Figure 3.6. *(a) A water molecule trapped within two monomeric units in **3**, (b) Trapped water molecule situated above the plane with distance 1.167 Å (c) Crystal lattice of **3** shows situation of trapped water in the crystal lattice, and (d) Crystal lattice of **3** shows orientation of hydrophobic isopropyl group towards to axially bound pyridine as well as the trapped water molecule situated on the top of the phenol.*

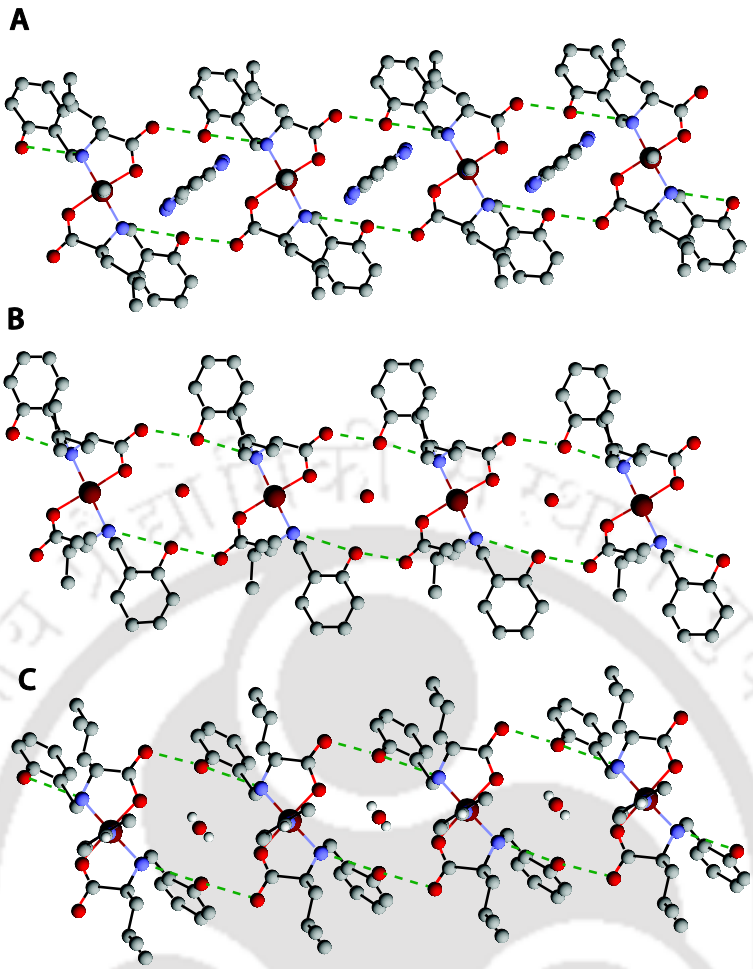

Figure 3.7. *Crystal lattice of **1**, **2** and **3** shows the identical H-bonding pattern where (A) An acetonitrile molecule trapped within lattice of **1**, (B) Trapped water molecule in **2** and (C) Lattice of **3** and position of trapped water molecule.*

Discussion: Structural analysis of **1-3** in the preceding sections can be summarized as follows. Use of starting material free of alkali ion can form the monomeric *bis* complexes where coordination environment around Cu(II) is quite different compared to the assembled multinuclear species. The differences are in the *trans* orientation of the carboxylate groups, non coordination of the phenol are of the ligand and five coordination of the Cu(II) in **1-3** compared to the assemblies. The fifth coordination site of the Cu(II) in **1-3** is amenable to exchange with monodentate ligand without changing the gross structure. The axial binding of pyridine is notable as the transformation of these monomers to assembly would require breaking of the relatively stronger Cu-Pyridine bond along with *trans – cis* reorientation of the ligand arrangement. We will discuss about this aspect in the monomer to assembly transformation results (Section **3.4.5**).

One additional benefit of these structures is the observation of the cavity around the fifth coordination site which is occupied with acetonitrile/pyridine. Potentially these can be removed to form porous material with vacant binding site.

3.4.3 Pyridine vs imidazole in the axial site

Pyridine and imidazole both are strong monodentate ligands and pyridine often substitutes imidazole in the bioinorganic active site model complexes.[15] However, we have previously observed that imidazole preferentially occupies the in-plane coordination sites of Cu(II) even when the option to axial coordination is available.[4] Complexes **1-3** provided us another opportunity to test it one more time. Thus we took the complex **1** and added 1 equiv. imidazole. We isolated complex **4** as crystals. The structural characterization (below) once again[4] showed the strong inherent preference of imidazole to act as an in-plane ligand even if that means to displace one bidentate ligand from the complex.

[Cu($L^{L\text{-}leu}$)Imidazole] (4). The complex **4** was crystallized in the space group $P2_12_12_1$ with four independent mononuclear units in the unit cell. The ORTEP figure of one of the mononuclear unit, selected bond lengths and angles for **4**, are given in figure **3.8**. The geometry of the Cu(II) in complex **4** is square planar with τ value of 0.046, the phenolate, amine and carboxylate donors from the ligand and external imidazole completes the coordination site, where amine and imidazole are *trans* to each other. The lattice diagram shows the 2D honeycomb (Figure **3.9C**) network formed by a complementary H-bonding of uncoordinated carboxylate oxygen and imidazole NH (O2…N3 2.677 Å) and vertical H-bonding of amine and phenolate (N1…O3 2.927 Å) both are within expected range (Figure **3.9A**, **B** and **C**).[16, 10] Interlocking of molecules in lattice through H-bonding like zip as shown in figure **3.9A**.

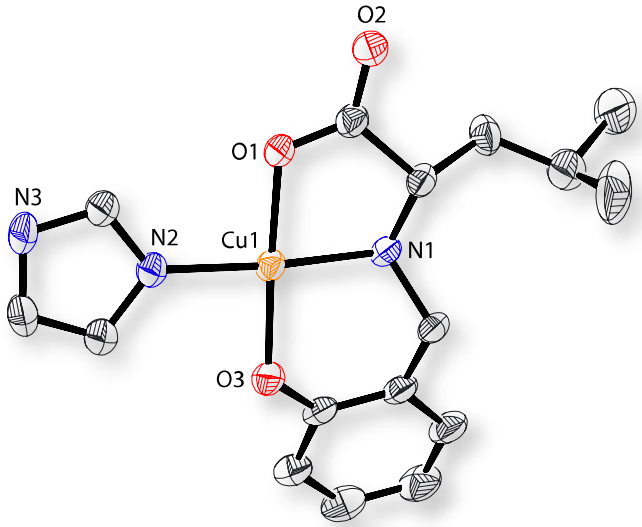

Figure 3.8. *ORTEP diagram of **4** with thermal ellipsoids set to 30% probability level. Selected bond distances (A°) and angles (°) for **4**: Cu1–O1 1.9372(18), Cu1–O3 1.9115(19), Cu1–N1 1.999(2), Cu1–N2 1.965(2), O3–Cu1–O1 175.69(9), O3–Cu1–N2 89.37(9), O1–Cu1–N2 92.87(8), O3–Cu1–N1 94.14(9), O1–Cu1–N1 84.02(9), N2–Cu1–N1 172.93(10). H-bonds: O2…N3 2.677, N1…O3 2.927.*

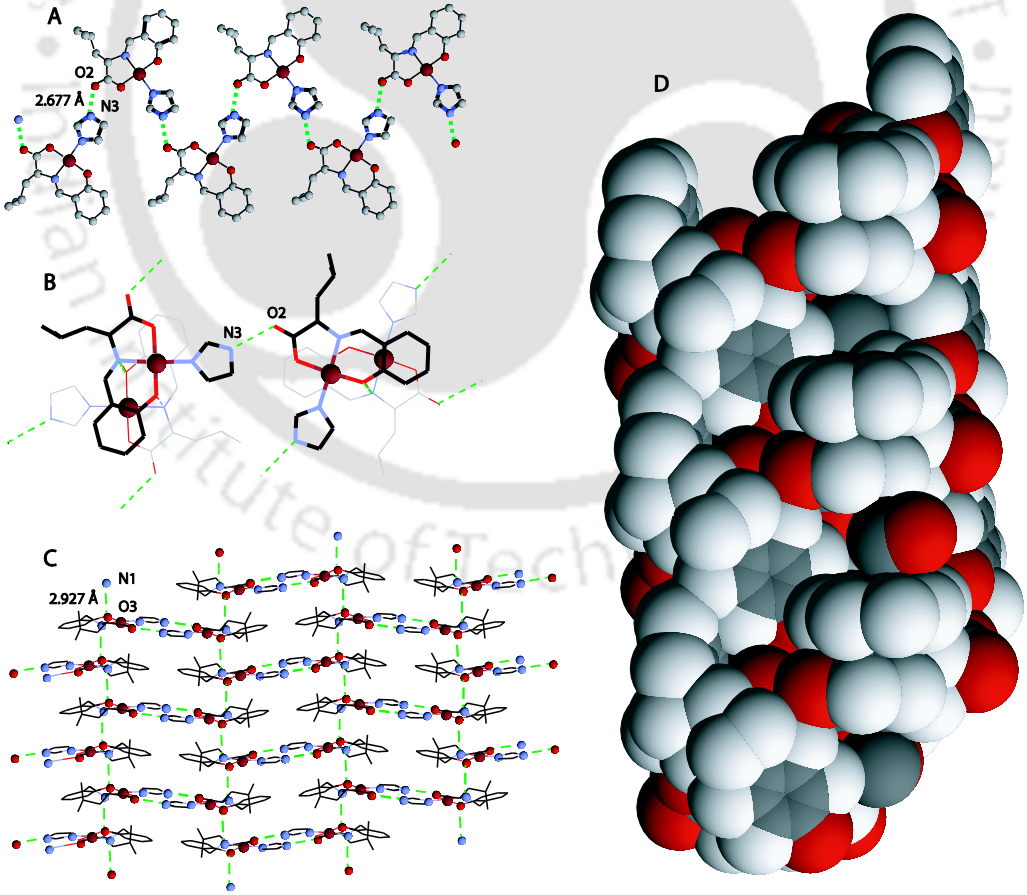

Figure 3.9. *(A), (B), (C) network diagram of **4** and (D) is the spacefill model of the **5** showing columnar structure.*

3.4.4 Mononuclear complex with tyrosine derivative

In complexes **1-3**, the phenolate arm of the ligand remained non-coordinated. We used tyrosine derivative in the similar fashion where we expected to form identical complex with perhaps the formation of a deeper cavity owing to the presence of tyrosine's phenols as we had observed before.[17] However, the structure of the complex (below) showed that unlike in **1-3**, the phenolic arm of the ligand coordinated in the axial position. We are not sure about the reason.

[Cu(HL$^{L\text{-}tyr}$)$_2$] (5). The complex **5** is a mononuclear Cu(II) complex with N_2O_3 coordination environment and crystallized in the space group $P2_1$. The perspective view of the complex **5** has shown as ORTEP diagram in figure **3.10**. The coordination geometry around the copper center in **5** is slightly distorted square pyramidal geometry (τ=0.109) with four of the in-plane coordination from ligand, similar to that in **1, 2, 3**, and rest of the fifth axial coordination filled with phenol from ligand.

The in-plane bond lengths for Cu–$O_{carboxylate}$ are Cu2–O1 1.90845 and Cu2–O5 1.92744, the range 1.92–1.95 Å observed for other amino acid or amino acid derived ligand Cu(II) complexes.[11] The in-plane bond lengths for Cu–N_{amine} are Cu2–N1 1.97920, Cu2–N2 2.02663, longer at ~2.02 Å compared to corresponding amino acid complexes (1.96–1.98 Å).[11] The axial fifth coordination is provided by a phenol from ligand with short Cu2–O3 distance of 2.42086 (Figure **3.10**). The axial bond in square-pyramidal Cu(II) is usually long and varies between 2.12 to 2.6 Å for O or N coordination, due to Jahn-Teller distortion.[12]

Complex **5** displays the interesting feature is the axial binding of phenol instead of acetonitrile unlike previous monomers of L-leucine, while phenol of the tyrosine remain uncoordinated (PKa ~10 for both type of phenol). Crystal also contains two methanol molecules and a water molecule as solvent of crystallization. Crystal packing shows the columnar structure (Figure **3.9D**).

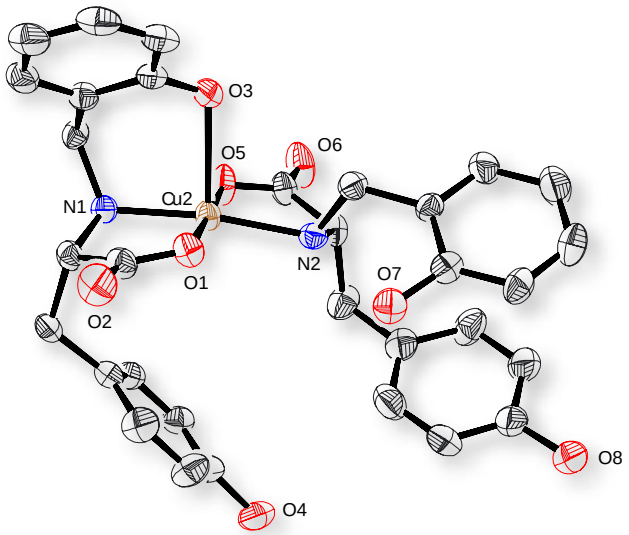

Figure 3.10. *ORTEP diagram of **5** with thermal ellipsoids set to 30% probability level. Selected bond distances (A°) and angles (°) for **5**: Cu2–O1 1.90845, Cu2–O5 1.92744, Cu2–N1 1.97920, Cu2–N2 2.02663, Cu2–O3 2.42086, O1–Cu2–O5 177.53, O1–Cu2–N1 84.85, O5–Cu2–N1 93.32, O1–Cu2–N2 97.20, O5–Cu2–N2 84.36, N1–Cu2–N2 170.95.*

3.4.5 Monomer to assembly formation

The monomer complexes **1**, **2** and **3** were fairly soluble in MeOH. Addition of solid KBr/KI to a methanolic solution of monomers yielded crystals of **7** and **8**, which was confirmed from FTIR, ESI-Mass, visible spectra and X-ray crystallography. However we could not get the single crystals of **6**, but confirmed the monomer **5** to multinuclear assembly formation in presence of KNO_3 from ESI-Mass spectroscopy (Figure **3.13A** and **B**, Table **3.3**). Notable in this transformation is the *trans* orientation of the in-plane ligands in monomers to the *cis* orientation in multinuclear assemblies which is necessary for binding the alkali metal ion (Scheme **3.3**). This result substantiate that carboxylate groups necessary for alkali metal binding were not predisposed in the Cu(II) monomers but was a result of alkali metal ion influenced reorientation (Scheme **3.3**). Further, square pyramidal monomer converted into octahedral after phenol coordination in multinuclear assembly, which was uncoordinated in monomer. On addition of KBr to **1,** a sharp change in d-d transition appears at lower energy (diff. 25 nm) in DMF (Table **3.4**, Figure **3.14A)**. This occurrence also supports the monomer to multinuclear conversion.

In conclusion, despite the different type of fifth axial coordination environment in monomers, they transform into multinuclear assembly in presence of alkali metal salts.

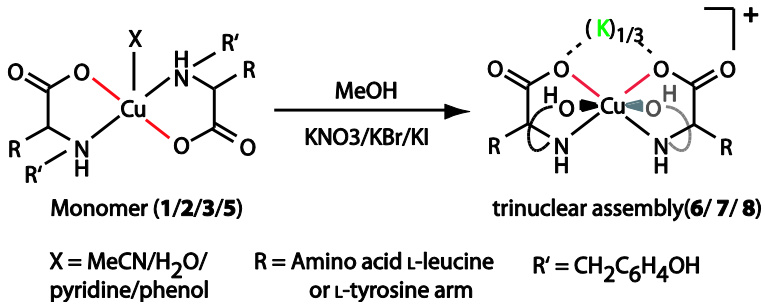

Scheme 3.3. *Monomer (trans) to assembly transformation (cis).*

[K{Cu(HL$^{L\text{-}leu}$)$_2$}$_3$]Br(7) and [K{Cu(HL$^{L\text{-}leu}$)$_2$}$_3$]I(8). The Cu(II) containing assemblies **7** and **8** crystallized in space group *C222$_1$*, where the assemblies are highly symmetrical. The ORTEP view of the complexes [K{Cu(HL$^{L\text{-}leu}$)$_2$}$_3$]Br (**7**) and [K{Cu(HL$^{L\text{-}leu}$)$_2$}$_3$]I (**8**) have shown in figures **3.11** and **3.12**. The selected bond distances are in table **3.2**. Conformation of the six chiral centers on the ligand and six chiral centre generated due to amine coordination are *S* and *R* respectively.

The assemblies consist of three monomeric units of [Cu^{II}(HL$^{L\text{-}leu}$)$_2$], where one monomer is on the crystallographic 2-fold axis and other on general position. Further, three monomeric units hold together by hexacoordinated K^+ through carboxylate oxygens, and six H-bonds between carboxylate oxygen and phenolic proton provide additional strength (Figure **3.11A** and **B**).

The *cis* oriented amines in monomers has two docking sites for Br^- and I^- anions and other monomeric amines used for solvent of crystallization lattice like previous multinuclear assemblies. Bond lengths of the assemblies **7** and **8** are comparable with previous multinuclear assemblies.

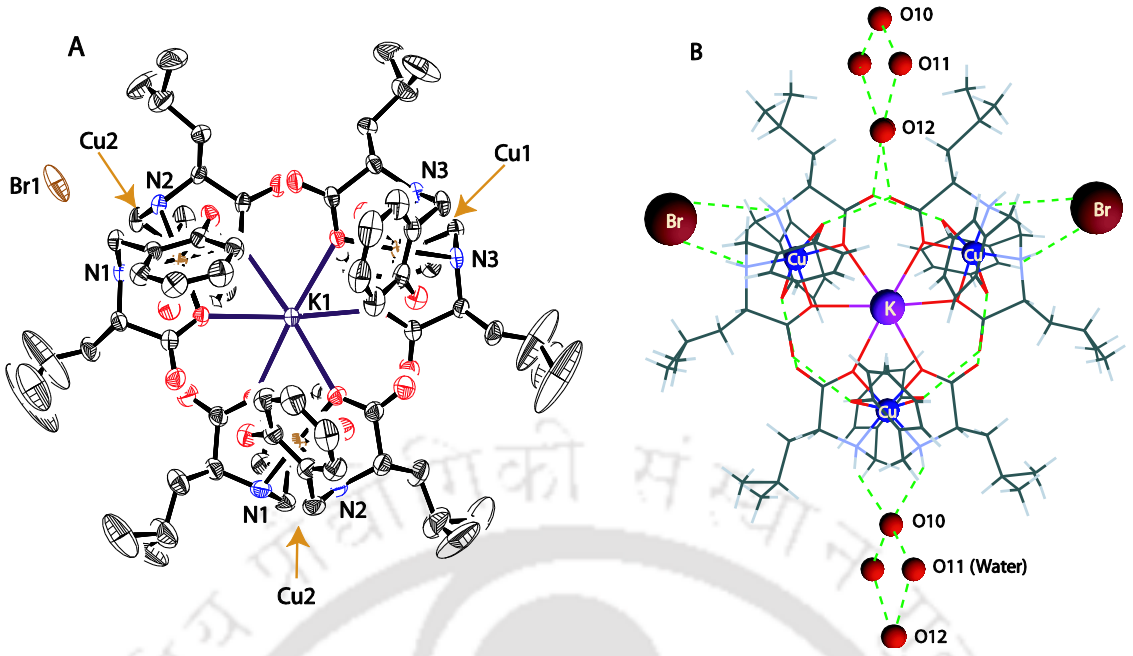

Figure 3.11. *(A) ORTEP diagram of **7** with thermal ellipsoids set to 30% probability level, and (B) The lattice of **7** contains water as solvent of crystallization.*

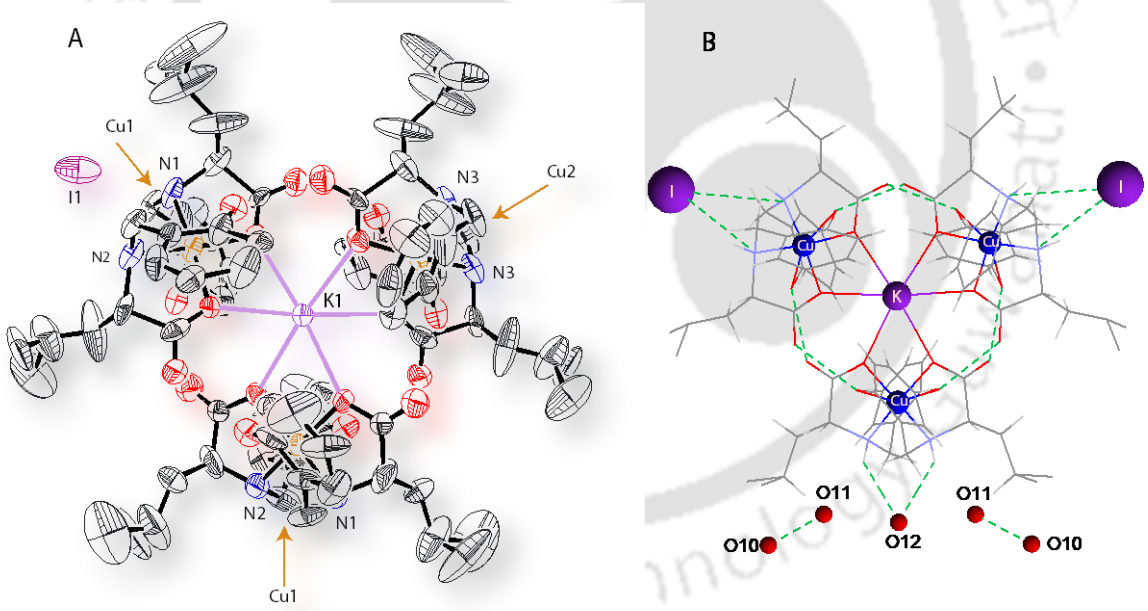

Figure 3.12. *(A) ORTEP diagram of **8** with thermal ellipsoids set to 30% probability level and (B) The lattice of **8** contains water as solvent of crystallization.*

Crystal data for **8**: Empirical Formula $C_{78}H_{64}Cu_3IKN_6O_{25}$, Fw. 1841.97, T(K) 296(2), Crystal system orthorhombic, Space group *C222₁*, a = 18.5555(12)Å, b = 20.9943(13)Å, c = 27.1327(16)Å; β = 90.00º, V = 10569.8(11)Å^3, z = 4, ρcalcd = 1.158 Mg m^{-3}, μ = 0.991mm^{-1}, reflections collected = 9580, independent = 54647, FLACK para. = 0.00, R1 = 0.1161, wR2 = 0.2933 [I > 2σ (I)]; R1 = 0.1548, wR2 = 0.3075 (all data), GOF = 1.258.

Table 3.2 Selected Bond lengths (Å) for the assemblies **7** and **8**.

	7			**8**		
Cu-O_{phenol}	2.473(4)	2.451(4)	2.460(4)	2.477(9)	2.53(1)	2.463(8)
Cu-$O_{carboxy}$	1.965(4)	1.956(4)	1.967(4)	1.925(8)	1.974(8)	1.985(9)
Cu-N_{amine}	2.016(5)	2.020(4)	2.025(5)	2.021(11)	1.995(11)	2.028(12)
K-$O_{carboxy}$	2.737(4)	2.722(3)	2.733(4)	2.756(8)	2.728(9)	2.753(8)
OH...O	2.582	2.603	2.605	2.540	2.609	2.554

Table 3.3 ESI-Mass Data.[a]

	Found *m/z* (Intensity)		Calculated *m/z* (Intensity)	
6	1944.4(52), 1946.4(100), 1948.4(66), 1950.4(25), 1952.4(10),	1945.4(38), 1947.4(88), 1949.4(56), 1951.4(20), 1953.4(2)	1944.42(49), 1946.42(100), 1948.42(81), 1950.42(34), 1952.42(07),	1945.42(53), 1947.42(87), 1949.42(56), 1951.42(17), 1953.42(03)
7	1644.5(58), 1646.5(100), 1648.5(70), 1650.5(28), 1652.5(5),	1645.5(50), 1647.5(78), 1649.5(45), 1651.5(14), 1653.5(2)	1644.55(54), 1646.55(100), 1648.55(72), 1650.55(26), 1652.55(05),	1645.55(48), 1647.55(76), 1649.55(45), 1651.55(12), 1653.55(01)
8	1644.5(56), 1646.5(100), 1648.5(70), 1650.5(21), 1652.5(06),	1645.5(45), 1647.5(72), 1649.5(28), 1651.5(08), 1653.5(05)	1644.55(54), 1646.55(100), 1648.55(72), 1650.55(26), 1652.55(05),	1645.55(48), 1647.55(76), 1649.55(45), 1651.55(12), 1653.55(02)

[a]ESI^+-Mass in methanol. **6** = $K\{Cu(HL^{L\text{-}tyr})_2\}_3]NO_3$; **7** = $K\{Cu(HL^{L\text{-}leu})_2\}_3]Br$; **8** = $K\{Cu(HL^{L\text{-}leu})_2\}_3]I$

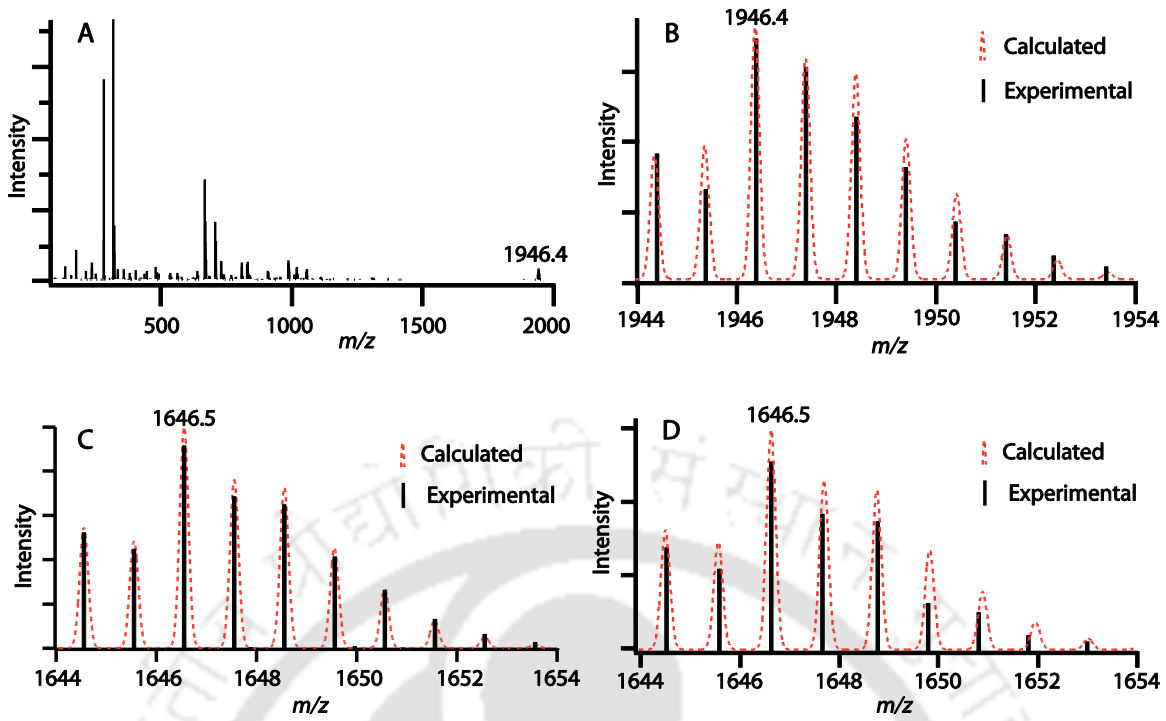

Figure 3.13. *(A) ESI-Mass of complex **6**. Isotopic abundance pattern calculated (red dotted) and experimental (black) (B) complex **6**, (C) complex **7** and (D) complex **8***

3.4.6 Absorption and EPR spectral characteristics of complexes

The UV-visible spectral characteristic data of all the complexes are given in Table **3.4** and the spectra figure of appropriate complexes are shown in figure **3.14**. The absorption maxima between 300 – 400 nm are due to LMCT, origin evident from high ε value (400-800 $M^{-1}cm^{-1}$). The absorption maxima between 600 – 700 nm with ε value ~100 $M^{-1}cm^{-1}$ for monomeric complexes (**1**, **2**, **3** and **5**), ~150 $M^{-1}cm^{-1}$ for complex **4**, and 155 – 275 $M^{-1}cm^{-1}$ for multinuclear assemblies (**6**, **7** and **8**) are of ligand field origin. Several other square-pyramidal Cu(II) complexes with N/O donor environment have similar spectral characteristics.[18,19] The spectral characteristics of monomers are almost identical in DMF and MeOH, except in **3** has ligand field transition 675 nm in DMF, significantly differs with other monomers may be due to more distorted square pyramidal geometry towards trigonal bipyramidal (TBP). The complex **4**, being the only complex with coordination number four has ligand-field transition at 635 nm in MeOH, quite different from the monomers. This suggests retention of square planar geometry in solution. Monomer **5** has ligand field transition at 645 nm in DMF and differs with other monomers may because phenol binding as well as distortion in geometry towards trigonal bipyramidal. Copper complexes with K^+ as

central ion in **6** – **8** show d-d transition in DMF as well as in MeOH, expected for tetragonally distorted Cu(II) (Table **3.4**, Figure **3.14**).[20]

The EPR spectral characteristic of the complexes are shown in figure **3.15** and the data at 77 K are shown in table **3.5**. For coordination geometries corresponding to an elongated octahedron, a square pyramid and square planar, the ground state will be dx^2-y^2. In these cases, the relation $g_{\parallel} > g_{\perp} > 2.0023$ is expected (normal spectrum).[21] The spectral data of the complexes, commensurate the above relation for elongated octahedron assemblies (**6**, **7** and **8**), square pyramidal monomer complexes (**1**, **2**, **3** and **5**) and imidazole bound Cu(II) square planar complex **4**.

Table 3.4 Electronic spectral data.[a]

	Solvent	λ_{max}, nm (ε, $M^{-1}cm^{-1}$)
1	DMF	595 (100)
	MeOH[b]	225(sh), 244(sh), 277 (12000), 356 (sh), 605 (100)
2	DMF	369(sh), 543(sh), 601 (95)
	MeOH[b]	220 (13100), 240(sh), 276 (8000), 380(sh), 617 (95)
3	DMF	372(sh), 543(sh), 619 (100)
	MeOH[b]	280 (9800), 400 (460), 675 (110)
4	DMF	396 (440), 616 (140)
	MeOH[b]	220 (36300), 275 (8000), 400 (800), 635 (170)
5	DMF[b]	362(sh), 554(sh), 645 (72)
	MeOH	235 (11000), 280 (17200), 373(sh), 631 (100)
6	DMF	369(sh), 642 (155)
	MeOH	224 (103300), 278 (34200), 370(sh), 620 (200)
7	DMF	385(sh), 635 (227)
	MeOH	241 (21800), 276 (24300), 620 (275)
8	DMF	372(sh), 538(sh), 621 (200)
	MeOH	240 (16700), 279 (27000), 377(sh), 615 (269)

[a] Scan range in DMF, 300 – 1100 nm, MeOH, 200 – 1100 nm. [b] ε values in the visible region calculated using ~2 mM solution. **1** = $[Cu(HL^{L\text{-}leu})_2MeCN]$; **2** = $[Cu(HL^{L\text{-}leu})_2H_2O]$; **3** = $[Cu(HL^{L\text{-}leu})_2C_5H_5N]$; **4** = $[Cu(HL^{L\text{-}leu})C_3H_4N_2]$; **5** = $[Cu(HL^{L\text{-}tyr})_2]$; **6** = $[K\{Cu(HL^{L\text{-}tyr})_2\}_3]NO_3$; **7** = $[K\{Cu(HL^{L\text{-}leu})_2\}_3]Br$; **8** = $[K\{Cu(HL^{L\text{-}leu})_2\}_3]I$

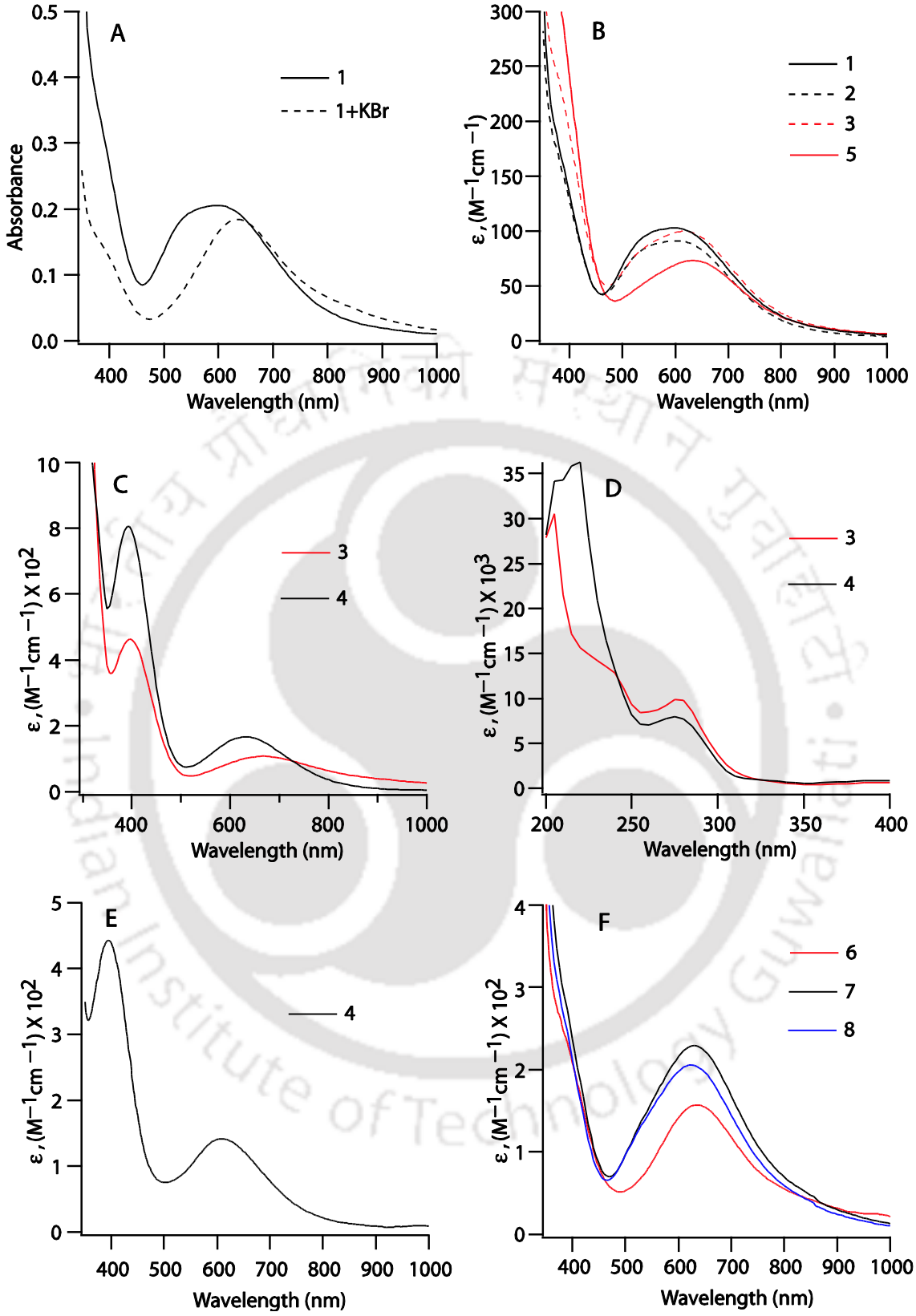

Figure 3.14. *UV-Visible spectra of* (A) *complex **1** before and after addition of KBr in DMF, (B) Monomeric complexes **1, 2, 3** and **5** in DMF,(C) Complexes **3** and **4** in MeOH, (D) complex **3** and **4** in the UV region, (E) Complex **4** in DMF and (F) Complexes **6, 7** and **8** in DMF.*

Table 3.5 EPR data of complexes in MeOH at 77K

Complexes	$g_{\parallel}$	$g_{\perp}$	$A_{\parallel}$/G
(1) $[Cu(HL^{L\text{-}leu})_2MeCN]$	2.235	2.039	183
(4) $[Cu(HL^{L\text{-}leu})C_3H_4N_2]$	2.256	2.051	179
(5) $[Cu(HL^{L\text{-}tyr})_2]$	2.253	2.051	179
(6) $[K\{Cu(HL^{L\text{-}tyr})_2\}_3]NO_3$	2.251	2.049	176
(7) $K\{Cu(HL^{L\text{-}leu})_2\}_3]Br$	2.247	2.047	180

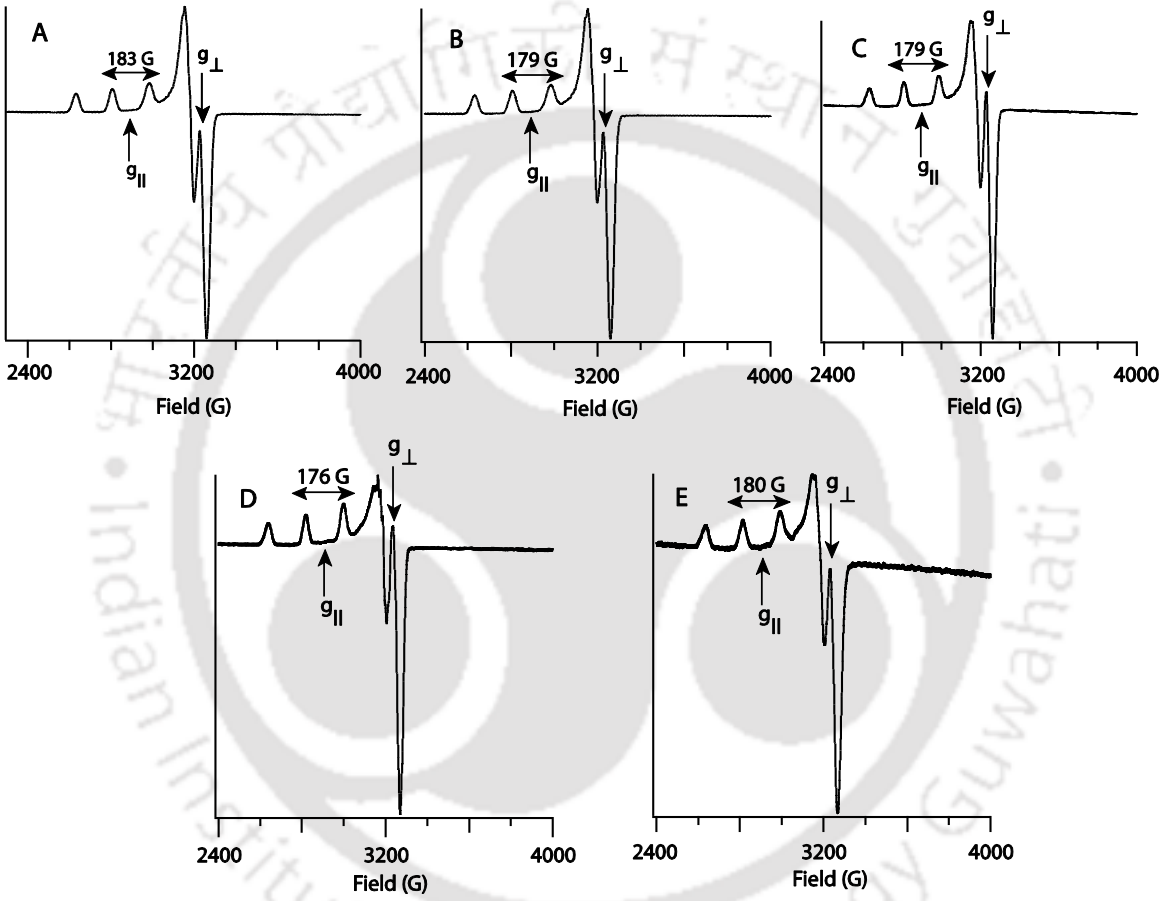

Figure 3.15. *EPR spectra of (A) complex **1**, (B) complex **4**, (C) complex **5**, (D) complex **6** and (E) complex **7** in MeOH at 77K.*

Conclusion

In this chapter, we have discussed the sequential formation of monomers with their different type of axial fifth coordination environment. Despite their different type of stability because of coordination environment, they converge to multinuclear assembly in presence of alkali metal salts. Structural characterization of monomers which showed that without alkali metal ion, Cu(II) adopts a five coordinate geometry with in-plane *trans* N_2O_2 fashion. It is the

alkali metal ion coordination that directs the ligand to adopt *cis* configuration, consequently formation of multinuclear assembly. Overall alkali metal ion and six short H-bonds perhaps forced the Cu(II) to adopt a not so common octahedral geometry, which is proved by characterization of monomers.

Earlier, our group reported monomer to assembly formation using a L-histidine derivative and Ni(II), used for chiral recognition as well as chiral separation.[22] This work presents formation of a new multifaceted monomeric architecture with easy conversion into multinuclear assembly. The conversion increases the potential for future exploitation of the architecture for chiral anion recognition in presence of alkali metal cation-chiral anion salt.

References

1. (a) Gibney, B. R.; Wang, H.; Kampf, J. W.; Pecoraro, V. L. *Inorg. Chem.* **1996**, *35*, 6184. (b) Saalfrank, R. W.; Maid, H.; Mooren, N.; Hampel, F. *Angew. Chem., Int. Ed.* **2002**, *41*, 304. (c) Vittal, J. J.; Wang, X.; Ranford, J. D. *Inorg. Chem.* **2003**, *42*, 3390. (d) Wang, X.; Vittal, J. J. *Inorg. Chem.* **2003**, *42*, 5135. (e) Nanda, P. K.; Aromi, G.; Ray, D. *Inorg. Chem.* **2006**, *45*, 3143. (f) Mezei, G.; Kampf, J. W.; Pan, S.; Poeppelmeier, K. R.; Watkins, B.; Pecoraro, V. L. *Chem. Commun.* **2007**, 1148. (g) Mezei, G.; Zaleski, C. M.; Pecoraro, V. L. *Chem. Rev.* **2007**, *107*, 4933.
2. (a) Gillard, R. D.; Mason, R.; Robertson, G. B. *J. Chem. Soc. A* **1969**, *12*, 1864-1871. (b) Moussa, S. M.; Fenton, R. R.; Kennedy, B. J.; Piltz, R. O. *Inorg. Chim. Acta* **1999**, *288*, 29–34. (c) Freeman, H. C.; Snow, M. R.; Nitta, I.; Tomita, K. *Acta Crystallogr.* **1964**, *17*, 1463–1470. (d) Weeks, C. M.; Cooper, A.; Norton, D. A. *Acta Crstallogr., Sect. B* **1969**, *25*, 443–450. (e) Sabolovi, J.; Tautermann, C. S.; Loerting, T.; Liedl, K. R. *Inorg. Chem.* **2003**, *42*, 2268.
3. Nagarathinam, M.; Saravanan, K.; Leong, W. L.; Balaya, P.; Vittal, J. J. *Cryst. Growth Des.* **2009**, *9*, 4461.
4. Alam, M. A.; Koner, R. R.; Das, A.; Nethaji, M.; Ray, M. *Cryst. Growth. Des.* **2007**, *7*, 1818.
5. Blessing, R. *Acta Crystallogr., Sect. A* **1995**, *51*, 33.
6. (a) Sheldrick, G. M. *SHELXL-97: Program for Crystal Structures Refinement*; University of Göttingen: Göttingen, Germany, 1997. (b) Farrugia, L. J. *J. Appl. Crystallogr.* **1999**, *32*, 837-838.
7. Nakamoto, K. *Infrared and Raman Spectra of Inorganic Compounds*, 5th ed.; Wiley-Interscience: New York, **1997**; Part B.

8. Magnetic moment (B.M.) range for Ni(II): 2.9–3.3 and Cu(II) 1.7–2.1. Solid state moment can be lower if weak anti ferromagnetic interaction is present. (a) Figgis, B. N.; Lewis J. *Prog. Inorg. Chem.* **1964**, *6*, 37. (b) O'Connor, C. J. *Prog. Inorg. Chem.* **1982** *29*, 203. (c) Earnshaw, A. *Introduction to Magnetochemistry*, Academic Press, London, 1968. Molar conductance (ohm^{-1} cm^2 mol^{-1}) range for 1:1 electrolyte in DMF: 65-90, MeOH: 80-115. (d) Geary, W. J. *Coord. Chem. Rev.* **1971**, *7*, 81.
9. (a) Cotton, F. A.; Daniels, L. M.; Jordan, G. T.; Murillo, C. A. *Chem. Commun*. **1997**, 1673, and references cited therein. (b) Desiraju, G. R. *Crystal Engineering. The Design of Organic Solids*; Elsevier: Amsterdam, **1989**; p 166, and references cited therein.(c) Mazik, M.; Blaser, D.; Boese, R. *Tetrahedron* **1999**, *55*, 7835.
10. Alam, M. A.; Nethaji, M.; Ray, M. *Inorg. Chem*. **2005**, *44*, 1302.
11. Structures of Cu(II) complexes with pure amino acids used in this work: (a) McAuliffe, C. A.; Quagliano, J. V.; Vallarino, L. M. *Inorg. Chem*. **1966**, *5,* 1996. (b) Helm, D. V. D.; Franks, W. A. Acta. Crystallogr., *Sect. B* **1969**, *25*, 451. (c) Stephens, F. S.; Vagg R. S.; Willams, P. A. *Acta. Crystallogr., Sect. B*, **1975**, *31*, 841. (d) Ou, C.; Powers, D. A.; Thich, J. A.; Felthouse, T. R.; Hendrickson, D. N.; Potenza, J. A.; Schugar, H. J. *Inorg. Chem*. **1978**, *17*, 34. (e) Hitchman, M. A.; Kwan, L. *J. Chem. Soc., Dalton Trans*. **1987**, 457 (f) Rizzi, A. C.; Piro, O. E.; Castellano, E. E.; Nascimento, O. R.; Brondino, C. D. *Inorg. Chim. Acta* **2000**, *305*, 19.
12. (a) Hathaway, B. J. in *Comprehensive Coordination Chemistry*, ed Wilkinson, G.; Gillard, R. D.; McCleverty, J. A. Pergamon Press, London, **1987**, vol. *5,* p. 533. (b) Addison, A. W.; Sinn, E. *Inorg. Chem*. **1983**, *22*, 1225. (c) Bonamico, M.; Dessy, G.; Mugnoli, A.; Vaeiago, A.; Zambonelli, L. *Acta Crystallogr*. **1965**, *19*, 886. (d) Agus, Y.; Louis, R.; Weiss, R. *J. Am. Chem. Soc*. **1979**, *101*, 3381. (e) Semerci, F.; Yesilel, O. K.; Sahin, E. *J. Inorg. Organomet. Polym.* **2010**, *20*, 334.
13. Holm, R. H.; Kennepohl, P.; Solomon, E. I. *Chem. Rev.* **1996**, 96, 2239.
14. Addision, A. W.; Rao, T. N.; Reedijk, Jr., J.; Rijn, V.; Verschoor, G. C. *J. Chem. Soc.*, *Dalton Trans.* **1984**, 1349.
15. Jr., L. Q. *J. Chem. Soc*., *Dalton Trans*. **1997**, 3933.
16. N(H)…O range: 2.69 to 2.89 Å. (a) Couchman, S. M.; Jeffery, J. C.; Ward, M. D. *Polyhedron* **1999**, *18*, 2633. (b) Kuduva, S. S.; Bläser, D.; Boese, R.; Desiraju, G. R. *J. Org. Chem.* **2001**, *66*, 1621.
17. Sahoo, S. C.; Ray, M. *Dalton Trans.* **2009**, 3230

18. (a)Yang, C. T.; Vetrichelvan, M.; Yang, X; Keith, B. M.; Murray, S.; Vittal, J. J. *J. Chem. Soc., Dalton Trans.* **2004**, 113. (b) Yang, C. T.; Moubaraki, B.; Murray, K. S.; Ranford, J. D.; Vittal, J. J. *Inorg. Chem.* **2001**, *40*, 5934. (c) Xiandong, Y.; Daqing, W.; Ranford, J. D.; Vittal, J. J. *Cryst. Growth Des.* **2005**, *5*, 41. (d) Xiandong, Y.; Ranford, J. D.; Vittal, J. J. *Cryst. Growth Des*. **2004**, *4*, 781. (e) Ranford, J. D.; Vittal, J. J.; Wu, D. *Angew. Chem., Int. Ed.* **1998**, *37*, 1114. (f) So, K. W.; Yang, C T.; Vittal, J. J.; Ranford, J. D. *Inorg. Chim. Acta* **2003**, *349*, 135. (g) Wang, X.; Ding, J.; Vittal, J. J. *Inorg. Chim. Acta* **2006**, *359*, 3481.
19. Admas, H.; Bailey, N. A.; de Barbarin, C. O. R.; Fanton, D. E. *J. Chem. Soc., Dalton Trans.* **1995**, 2323.
20. Lever, A. B. P. *Inorganic Electronic Spectroscopy*, 2nd ed.; Elsevier: Amsterdam, **1984**; p 507.
21. Garribba, E.; Micera, G. *J. Chem. Education* **2006**, *83*, 1229.
22. Sahoo, S. C.; Ray, M. *Chemistry- A European Journal* **2010**, *16*, 5004.

In the previous chapter, we have discussed the various Cu(II) monomers with their different type of axial fifth coordination environment. Despite the differences in axial coordination and ligand orientation, they converge to multinuclear assembly in presence of alkali metal salts. Unfortunately, we were unable to isolate and structurally characterize corresponding Ni(II) monomers. Thus instead of stepwise assembly formation for Ni(II), in this chapter we have followed the direct route (Chapter **2**) and synthesized Ni(II) assemblies with different amino acid derivatives (Scheme **4.1** and **4.2**). Further, we have explored if the assembly can be formed with the alkali ion Cs^+ or not. The results presented in this chapter show that unlike for Na^+ or K^+, counter anion of the salt does affect the assembly formation in case of Cs^+ (Scheme **4.3**).

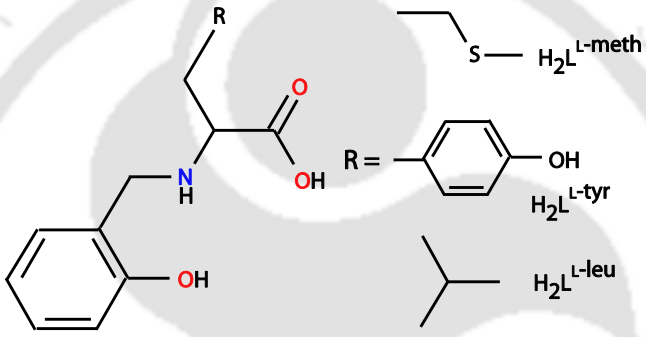

Scheme 4.1. *Ligands used in this chapter*

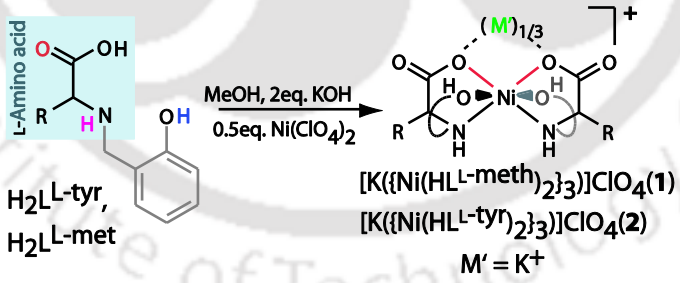

Scheme 4.2. *Synthetic scheme for complexes **1** and **2***

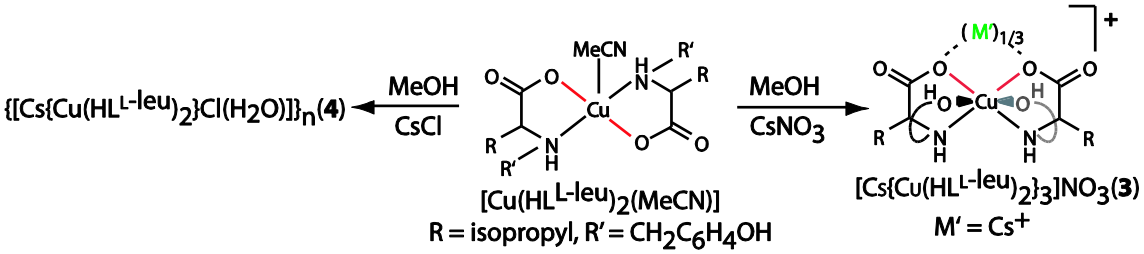

Scheme 4.3. *Synthetic scheme for complexes **3** and **4** .*

4.1 Experimental section

4.1.1 Materials and Methods

Cesium chloride was purchased from Aldrich Chemical Co. L-leucine, L-methionine and L-tyrosine were purchased from Sisco Research Laboratories Pvt. Ltd. (SRL), India and used as received. The ligand $H_2L^{L\text{-meth}}$, $H_2L^{L\text{-tyr}}$, $H_2L^{L\text{-leu}}$ were synthesized as before.[1]

Instrumental descriptions are as described in Chapter **2**.

Caution! *Perchlorate salts are potentially dangerous as explosives and should only be handled in small quantities, although we have worked with these ClO_4^- salts without any incident.*

4.2 Syntheses

4.2.1 $[K\{Ni(HL^{L\text{-met}})_2\}_3]ClO_4$ (1)

Ligand $H_2L^{L\text{-met}}$ (0.500 g, 1.920 mmol) was deprotonated with KOH (0.218 g, 3.26 mmol) in 25 mL MeOH which offered a clear colorless solution. After 20 min, a solution of $Ni(ClO_4)_2.6H_2O$ (0.35 g, 0.97 mmol) in MeOH (15 mL) was added drop wise to the above ligand solution and stirring continued. The color of solution changed immediately from green to light purple-blue. The solution was stirred for 2 h and then evaporated to dryness in a rotary evaporator. The resulting crude solid (0.59 g) was dissolved in pyridine and filtered to remove excess $KClO_4$. Upon evaporation a green colored solid (0.52 g) was obtained. The resulting compound was washed with diethyl ether to remove pyridine. The solid green compound isolated was soluble in dimethyl formamide (DMF) and was recrystallized by diethyl ether diffusion method. The crystals obtained within 3 days was washed with diethyl ether and dried under vacuum. Yield: 52 %. Anal. Calcd. for $[K\{Ni(C_{12}H_{16}O_3NS)_2\}_3]ClO_4.C_2H_6SO$: C, 46.38; H, 5.37; N, 4.38; found C, 46.44; H, 5.25; N, 4.58. IR (KBr, cm^{-1}): ν(OH) 3390 (b), $\nu(COO)_{asym}$ 1593 (s), 1480 (s), 1288 (s), 873 (m), 759 (s). μ_{eff} (powder, 298K): 3.28 μ_B/Ni. Λ_M (ohm^{-1} cm^2 mol^{-1}): 118 (MeOH).

4.2.2 $[K\{Ni(HL^{L\text{-tyr}})_2\}_3]ClO_4$ (2)

Ligand $H_2L^{L\text{-tyr}}$ (0.100 g, 0.363 mmol) was deprotonated with KOH (0.041 g, 0.613 mmol) in 25 mL MeOH which offered a clear colorless solution. After 20 min, a solution of $Ni(ClO_4)_2.6H_2O$ (0.066 g, 0.181 mmol) in MeOH (15 mL) was added drop wise to the above ligand solution and stirring continued. The color of solution changed immediately from green to green-blue. The solution was stirred for 2 h and then evaporated to reduce the volume. The resulting crude solution was recrystallized by adding minimum volume of CH_3CN and left it

for slow evaporation for two days. The diamond shaped purple-green crystals were obtained. Isolated crystals were dried under vacuum. Yield: 56%. Anal. Calcd. for $[K\{Ni(C_{16}H_{16}O_4N)_2\}_3]ClO_4{\cdot}6H_2O{\cdot}CH_3OH$: C, 53.67; H, 5.20; N, 3.87; found C, 52.92; H, 5.25; N, 3.90. IR (KBr, cm^{-1}): ν(OH) 3412 (b), $\nu(COO)_{asym}$ 1613 (s), 1515 (s), 1463 (s), 1246 (m), 814, 759, 539. μ_{eff} (powder, 298K): 3.12 μ_B/Ni. Λ_M (ohm^{-1} cm^2 mol^{-1}): 96 (MeOH).

4.2.3 $[Cs\{Cu(HL^{L\text{-}leu})_2\}_3]NO_3$ (3)

Monomer $[Cu(HL^{L\text{-}leu})_2(CH_3CN)]$ (0.100 g, 0.137 mmol) in MeOH (15 mL) was stirred for 15 min and solid $CsNO_3$ (0.009 g, 0.046 mmol) mixed with above stirring solution. The color of solution changed after 10 min from deep blue to blue-green. The solution was stirred for 2 h and the solution was concentrated by rotary evaporator. The resulting crude solution was recrystallized by adding minimum volume of CH_3CN and leaving it for slow evaporation. The diamond shaped, blue crystals were obtained within five days. Isolated crystals were dried under vacuum. Yield: 39%. Anal. Calcd. for $[Cs\{Cu(C_{13}H_{18}O_3N)_2\}_3]NO_3{\cdot}6H_2O$: C, 49.04; H, 6.33; N, 5.13; found C, 48.83; H, 6.54; N, 5.26. IR (KBr, cm^{-1}): ν(OH) 3437 (b), $\nu(COO)_{asym}$ 1628 (s), 1589 (s), 1461 (m), 1384 (s), 1276 (m), 1086, 754. μ_{eff} (powder, 298K): 1.75 μ_B/Cu. Λ_M (ohm^{-1} cm^2 mol^{-1}): 120 (MeOH), 84 (DMF).

4.2.4 $\{[Cs\{Cu(HL^{L\text{-}leu})_2\}\ Cl\ (H_2O)]\}_n$ (4)

Complex $[Cu(HL^{L\text{-}leu})_2(CH_3CN)]$ (0.050 g, 0.0683 mmol) in MeOH (10 mL) was stirred for 15 min and solid CsCl (0.023 g, 0.1389 mmol) mixed with above stirring solution. The color of solution changed after 10 min from deep blue to blue-green. The solution was stirred for 3 h and left for slow evaporation. The plate like blue crystals obtained within six days. Isolated crystals were dried under vacuum. Yield: 45%. Anal. Calcd. for $[Cs\{Cu(C_{13}H_{18}O_3N)_2\}Cl(H_2O)]{\cdot}2H_2O$: C, 41.21; H, 5.59; N, 3.70; found C, 41.15; H, 5.13; N, 3.93. IR (KBr, cm^{-1}): ν(OH) 3453 (b), $\nu(COO)_{asym}$ 1615 (s), 1604 (s), 1592 (s), 1457 (s), 1384 (m), 1244 (m), 1063, 959, 752 (s), 542. μ_{eff} (powder, 298K): 1.71 μ_B/Cu. Λ_M (ohm^{-1} cm^2 mol^{-1}): 106 (MeOH), 66 (DMF).

4.3 X-ray Data Collection, Structure Solution and Refinement

Crystals of the complexes $[K\{Ni(HL^{L\text{-}met})_2\}_3]ClO_4$ (**1**), $[K\{Ni(HL^{L\text{-}tyr})_2\}_3]ClO_4$ (**2**), $[Cs\{Cu(HL^{L\text{-}leu})_2\}_3]NO_3$ (**3**), $\{[Cs\{Cu(HL^{L\text{-}leu})_2\}Cl(H_2O)]\}_n$ (**4**) obtained during synthesis were used for X-ray analysis. The crystals of **2** and **3** did not diffract well and solution quality for **3** is not as good as the other structures, but the solution provided evidence that it is a trinuclear complex which was further confirmed using ESI-Mass spectrometry (Section **4.4.3**). The structure of **2** could not be solved. The crystals were mounted on glass fiber. X ray data correction and solution procedure are same as described in Chapter **2** unless specified.[2,3] Most of the hydrogen atoms attached to the solvent molecules could not be located or fixed, so the molecular weight may not match. Selected crystallographic data have been summarized in Table **4.1.**

Table 4.1 Selected crystallographic data for the complexes

	1	**4**
empirical formula	$C_{75}H_{66}ClKN_7Ni_3O_{25}S_6$	$C_{26}H_{22}ClCsCuN_2O_7$
fw	1908.38	706.36
T(K)	293(2)	296(2)
Wavelength(Å)	0.71073	0.71073
Crystal system	monoclinic	triclinic
Space group	$P2_1$	$P1$
a, Å	14.5065(19)	5.8930(7)
b, Å	20.224(3)	8.8346(11)
c, Å	17.041(3)	15.801(2)
α, deg	90.00	99.553(6)
β, deg	96.070(9)	99.826(7)
γ, deg	90.00	109.432(6)
V, $Å^3$	4971.4(12)	742.11(16)
z/ρ	2/1.275	1/1.581
μ	0.824	2.078
coll. reflns	54601	6252
indep reflns	8435	3295
FLACK para.	-0.04(2)	0.00
GOF	1.165	1.080
R1[a]	0.0898	0.0582
wR2[a]	0.2089	0.1510
R1[b]	0.1484	0.0660
wR2[b]	0.2458	0.1562

[a] $I>2\sigma$. [b] All data

1 = $[K\{Ni(HL^{L\text{-}met})_2\}_3]ClO_4$, **4** = $\{[Cs\{Cu(HL^{L\text{-}leu})_2\}Cl(H_2O)]\}_n$

4.4 Results and discussion

4.4.1 Synthesis and selected properties

Complex **1** was synthesized by stirring $H_2L^{L\text{-meth}}$, KOH and metal salt $Ni(ClO_4)_2.6H_2O$ together in MeOH at 2:2:1 ratio (Scheme **4.2**), the solution turned purple. Solid of the above reaction washed with pyridine to remove excess $KClO_4$ ($KClO_4$ is insoluble in pyridine) followed by crystallization by diffusing diethyl ether in DMF solution of the complex. The diamond shaped purple crystals were formed within 3-4 days in 52% yield. Complex **2** was synthesized by using same protocol, $H_2L^{L\text{-tyr}}$ taken instead of $H_2L^{L\text{-meth}}$. Upon filtration the precipitate of $KClO_4$ followed by addition of acetonitrile yielded the diamond shaped, purple-green crystals within two days in 56% yield. However, crystals of complex **2** were unstable outside the mother solution so we could not solve the X-ray structure (structural parameters a= 17.99 Å, b= 22.13 Å, c= 26.15 Å, α= 108.12°, β= 90.07°, γ= 90.07°, V= 9894 $Å^3$). Complex **3** was synthesized by monomer $[Cu(HL^{L\text{-leu}})_2(CH_3CN)]$ to multinuclear assembly $[Cs\{Cu(HL^{L\text{-leu}})_2\}_3]NO_3$(**3**) conversion in presence of $CsNO_3$ (monomer to $CsNO_3$ ratio 3:1), crude solution was crystallized with acetonitrile. The diamond shaped, blue crystals of **3** were obtained within five days in 39% yield, because of poor data quality we could not resolve structure (structural parameter a= 18.36 Å, b= 21.09 Å, c= 27.66 Å, α= 90.00°, β= 90.12°, γ= 90.00°, V=10717 $Å^3$). Further, we tried assembly formation with CsCl (CsCl to monomer ratio 2:1) using the synthetic protocol of complex **3**, providentially we got the plate like crystals within one week and resolved the complex **4** as CsCl containing coordination polymer.

IR spectral analysis shows that one broad peak at 1593, 1613, 1628 and 1615 cm^{-1} were identified as asymmetric carboxylate stretches originated from the ligand respectively.[4] The elemental analysis supports the formulation of the complexes as $[Ni(C_{12}H_{16}O_3NS)_2]_3.KClO_4.C_2H_6SO$ (**1**), $[K\{Ni(C_{16}H_{16}O_4N)_2\}_3]ClO_4{\cdot}6H_2O{\cdot}CH_3OH$ (**2**), $[Cs\{Cu(C_{13}H_{18}O_3N)_2\}_3]NO_3{\cdot}6H_2O$ (**3**) and $[Cs\{Cu(C_{13}H_{18}O_3N)_2\}Cl(H_2O)]{\cdot}2H_2O$ (**4**). Conductance of the assemblies in MeOH and DMF falls within the range of 1:1 electrolyte.[5] Solid state room temperature magnetic moment is 3.28 and 3.12 μ_B/metal, which confirms the presence of Ni(II) metal in the assemblies **1** and **2**. Further, assemblies **3** and **4** have solid state room temperature magnetic moment 1.75 and 1.71 μ_B/metal which confirms the presence of Cu(II) metal.[5]

4.4.2 Ni(II) assemblies with different amino acid derivative

Results in Chapter **2** showed that multinuclear assembly can be formed with L-tyrosine derivative in case of Cu(II). Complex **1** and **2** were synthesized to test if the assembly formation occurs with other amino acid derivative and Ni(II) as well. Structural characterization of **1** and ESI-mass spectral evidence (next section) shows that it is possible.

$[K\{Ni(HL^{L\text{-}met})_2\}_3]ClO_4$ (1). The complex **1** crystallizes in space group $P2_1$. The ORTEP[6] view of the complex $[K\{Ni(HL^{L\text{-}met})_2\}_3]ClO_4$(**1**) is shown in figure **4.1**. The selected bond distances and angles are given as foot note of the figure **4.1**. Conformation of the six chiral centers on the ligand and six chiral centres generated due to amine coordination are *S* and *R* respectively.

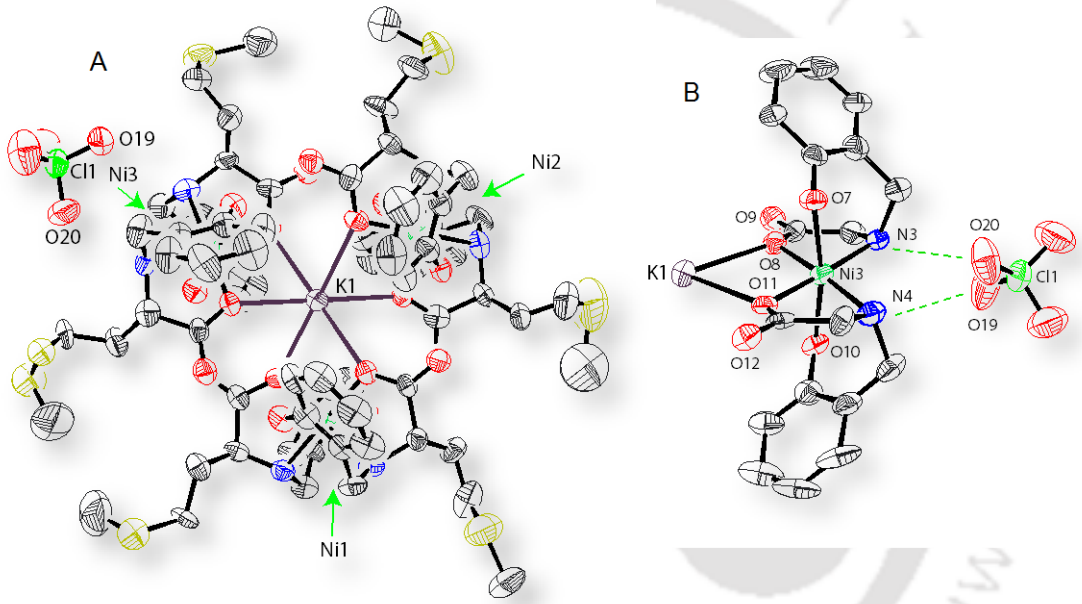

Figure 4.1. *(A) ORTEP diagram of **1** with thermal ellipsoids set to 30% probability level, and (B) coordination around one Ni(II) unit showing the cation and anion binding sites.*

Bond lengths(Å) O8–K1 2.671(8), O11–K1 2.645(9), Ni3–O11 2.017(8), Ni3–O8 2.007(8), Ni3–N3 2.081(10), Ni3–N4 2.063(9), Ni3–O7 2.149(7), Ni3–O10 2.144(8), $O_{phenol}\ldots O_{carboxy}$ ~2.48 Å. Bond angle(°) O8–Ni3–O11 98.7(3), N3–Ni3–N4 100.2(4), N4–Ni3–O11 80.1(4), N3–Ni3–O8 81.2(4), O10–Ni3–O11 87.5(3), O10–Ni–O8 85.9(3).

The assembly consists of three monomeric units of $[Ni^{II}(HL^{L\text{-}meth})_2]$ and these monomeric units hold together by hexacoordinated K^+ through carboxylate oxygens, and six H-bonds between carboxylate oxygen and phenolic proton provide additional strength like other multinuclear assembly in previous chapters. These H-bonds are on the short end of the 2.5–3.0 Å range usual for O…O H-bond distances ($O_{phenol}\ldots O_{carboxy}$ ~2.48 Å).[7] The *cis* orientation of carboxylates allowed the monomeric units to bind K^+, similar orientation of

amines provided a H-bonding site for perchlorate anion making the capsular assembly, capable of binding both anion and cation of a salt within the same assembly in solid state (Figure **4.1**). The in-plane bond distances and angles are more or less same for all the three Ni(II) monomeric units.

Thus, except the change in amino acid arm, the multinuclear assembly is identical with those described in the previous chapters.

4.4.3 Solution identity of $[K\{Ni(HL^{L\text{-}met})_2\}_3]ClO_4$(1) and $[K\{Ni(HL^{L\text{-}tyr})_2\}_3]ClO_4$(2)

The ESI-Mass spectra of the complexes **1** & **2** show the molecular ion peak with matching isotopic abundance pattern (Figure **4.3**, Table **4.2**), supporting the presence of the assemblies in solution. Though, we could not get structure of assembly **2**, the ESI-Mass spectroscopy support the trinuclear formation (Figure **4.2**). The solution identities of the assemblies **1** and **2** were assessed using solution conductance, ESI-Mass and electronic spectroscopy. The solution conductance measurement in methanol and DMF showed the complexes as 1:1 electrolyte (Section **4.2.1**) as observed for similar assemblies .[5]

Electronic spectral characteristic of **1** is similar to L-leucine assembly analogue (Chapter **2**). In DMF, both **1** and **2** shows broad absorptions between 300 and 1500 nm (Figure **4.4**, Table **4.3**). The similarity between the spectra of **1** and corresponding L-leucine analogue (Chapter **2**, Figure **2.8a**) reflected their structural similarity. However, the absorption profile of **2** (Figure **4.4A**) in DMF is somewhat different. We are not sure about the reason but considering the Mass analysis (Figure **4.3**, Table **4.2**) we think it does have the trinuclear core formation. In MeOH, both the assemblies behave like monomeric structure as discussed in Chapter **2**.[1b]

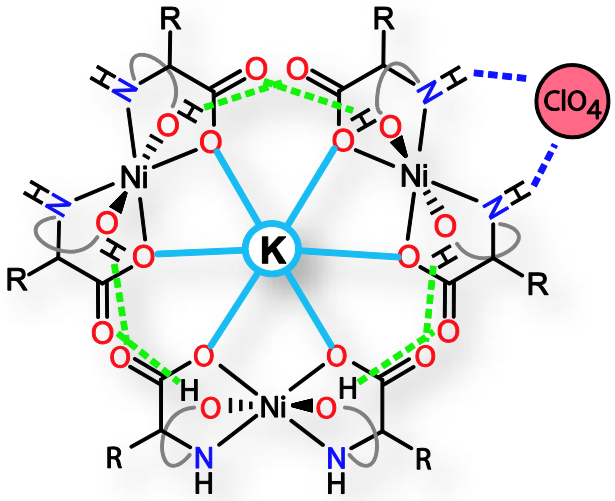

Figure 4.2. *Sketch model for the assembly **2** showing cation as well as anion binding sites and position of the six short hydrogen bonds*

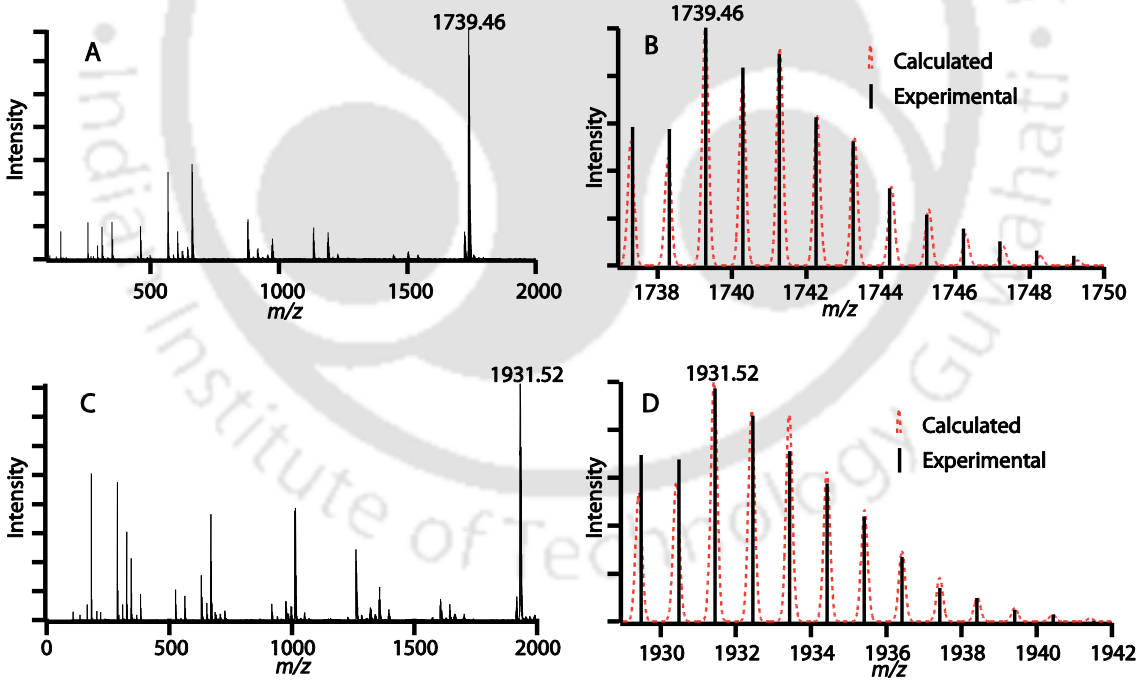

Figure 4.3. *(A) ESI-MS spectrum of **1**, (B) Isotopic abundance pattern calculated (red dotted) and experimental (black) of **1** and (C) ESI-MS spectrum of **2**, (D) Isotopic abundance pattern calculated (red dotted) and experimental (black) of **2**.*

Table 4.2. Mass spectral data.[a]

	Found *m/z* (Intensity)[b]		Calculated *m/z* (Intensity)[b]	
1	1737.4(70), 1739.4(100), 1741.4(93), 1743.4(52), 1745.4(25), 1747.4(11),	1738.4(60), 1740.4(85), 1742.4(65), 1744.4(35), 1746.4(17), 1748.4(08)	1737.28(52), 1739.28(100), 1741.28(91), 1743.28(54), 1745.28(23), 1747.28(08),	1738.28(45), 1740.28(78), 1742.28(63), 1744.28(33), 1746.28(13), 1748.28(04)
2	1929.8(65), 1931.8(100), 1933.8(82), 1935.8(46), 1937.8(13), 1939.8(5),	1930.8(68), 1932.8(86), 1934.8(62), 1936.8(29), 1938.8(09), 1940.8(02)	1929.41(53), 1931.41(100), 1933.41(86), 1935.41(46), 1937.41(18), 1939.41(5),	1930.41(58), 1932.41(88), 1934.41(62), 1936.41(29), 1938.41(10), 1940.41(02)
3	1738.0(65), 1740.0(100), 1742.0(65), 1744(20), 1746.0(3),	1739.0(50), 1741.0(75), 1743.0(40), 1745.0(10), 1747.0(01)	1738.50(56), 1740.50(100), 1742.50(68), 1744.50(22), 1746.50(3),	1739.50(50), 1741.50(75), 1743.50(41), 1745.50(10), 1747.50(01)

[a]ESI^+–Mass in methanol. **1**= $[K\{Ni(HL^{L\text{-}meth})_2\}_3]ClO_4$; **2**= $[K\{Ni(HL^{L\text{-}tyr})_2\}_3]ClO_4$; **3**= $[Cs\{Cu(HL^{L\text{-}leu})_2\}_3]NO_3$. [b] isotopic mass distribution of the molecular ion peak with relative intensity values in parenthesis.

Table 4.3. Electronic spectral data.[a]

	Solvent	λ_{max}, nm (ε, $M^{-1}cm^{-1}$)[b]
1	DMF	385(sh), 550(19), 660(12), 755(sh), 855(27), 1155(14)
	MeOH	238 (27000), 276 (19200), 645 (17), 775(sh), 965 (24)
2	DMF	385(sh), 575(21), 645(24), 755(sh), 855(27), 1065(32)
	MeOH	222(100000), 276 (29300), 634 (28), 1030 (37)
3	DMF	375(sh), 603 (210)
	MeOH	240(sh), 276 (25200), 375(sh), 610 (240)
4	DMF	375(sh), 615 (76)
	MeOH	240(sh), 276 (10800), 375(sh), 623(85)

[a] Scan range in DMF, 300 – 1500 nm, MeOH, 200 – 1100 nm. [b]ε values in the visible region calculated using ~1 mM solution. **1**= $[K\{Ni(HL^{L\text{-}met})_2\}_3]ClO_4$; **2**= $[K\{Ni(HL^{L\text{-}tyr})_2\}_3]ClO_4$; **3**= $[Cs\{Cu(HL^{L\text{-}leu})_2\}_3]NO_3$; **4**= $\{[Cs\{Cu(HL^{L\text{-}leu})_2\}Cl(H_2O)]\}_n$.

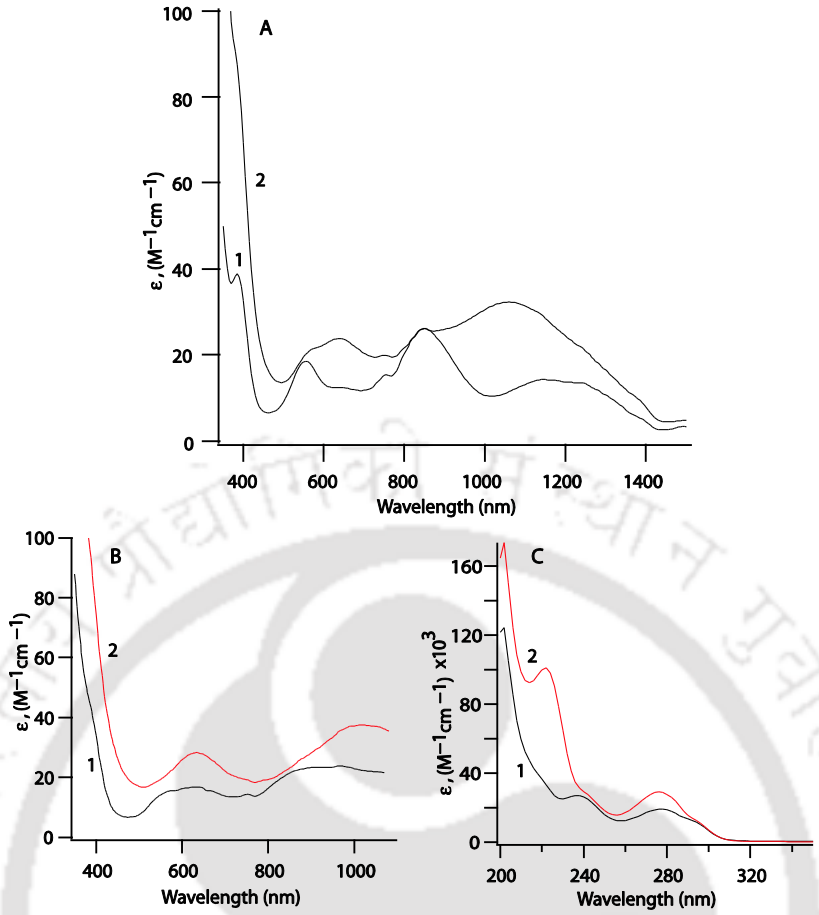

Figure 4.4. *UV-Visible spectra of (A) complexes **1** and **2**, in DMF, (B) and (C) complexes **1** and **2** in MeOH.*

4.4.4 Assembly formation with Cesium salt

In Chapter **2** we had Na^+ (ionic radius 1.02 Å) or K^+ (ionic radius 1.38 Å) as the central metal ion holding the Cu(II) complexes together.[8] We wanted to see how does a larger ion like Cs^+ (ionic radius 1.67 Å) effect the assembly formation. For this we have used the stepwise (addition of salt to monomeric Cu(II) complex) assembly formation shown in Chapter **3**.

Addition of $CsNO_3$ to Cu(II) monomeric complex yielded crystals of **3** which could be solved partially (Figure **4.5**) which showed the formation of trinuclear assembly identical to Na^+ and K^+ analogue (Chapter **2**). ESI-Mass results also support it (Figure **4.10E**). Poor quality of structure prevented comparison of bond length parameters.

Addition of KBr, KI (Chapter **3**) or NaCl (ESI-Mass checked) to Cu(II) monomer results in trinuclear assembly where halide act as an counter ion. Unlike with Na^+, addition of CsCl to Cu(II) monomer resulted in a polymeric species (below) where Cs-Cl bond weakens remains nonetheless.

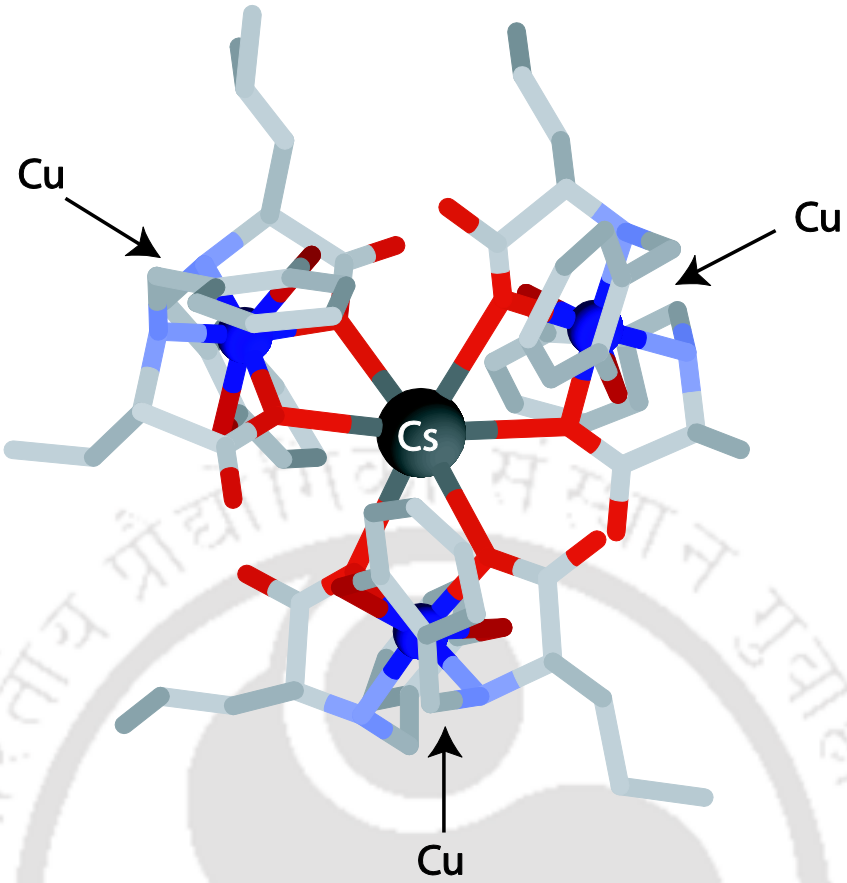

Figure 4.5. *Partially solved structure of [Cs{Cu(HL$^{L\text{-}leu}$)$_2$}$_3$]NO$_3$(**3**).*

{[Cs{Cu(HL$^{L\text{-}leu}$)$_2$}Cl(H$_2$O)]}$_n$ (4). The complex **4** was crystallized in the space group *P1* with one independent asymmetric unit in the unit cell with formula [Cs{Cu(HL$^{L\text{-}leu}$)$_2$}Cl(H$_2$O)]. The ORTEP figure of one of the asymmetric unit, selected bond lengths and angles for complex are given in figure **4.6** and its foot note. Complex is two dimensional coordination polymeric in nature with slightly distorted (τ = 0.176) square pyramidal geometry around the Cu(II) [τ = (β-α)/60, with α and β being the two largest coordination angles]. The amount of distortion parameter τ was calculated from the structural data where the value of τ should be 0.0 for perfect square-pyramidal geometry and 1.0 for perfect trigonal bipyramidal (TBP) structure.[9]

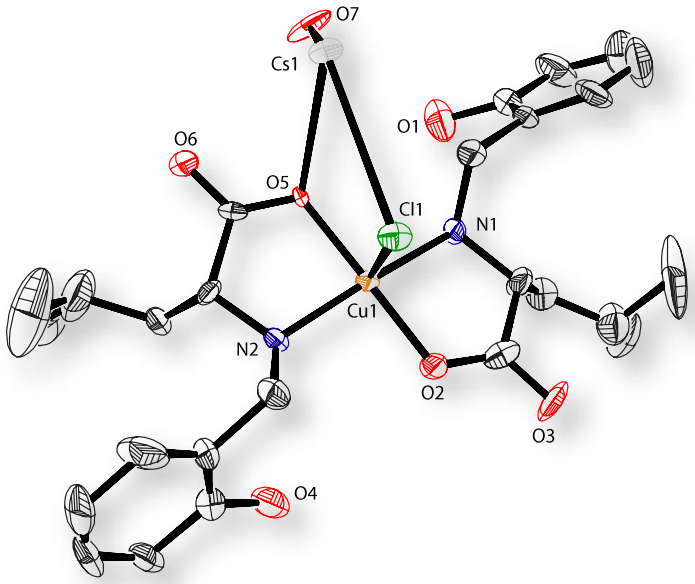

Figure 4.6. *ORTEP diagram of **4** (asymmetric unit) with thermal ellipsoids set to 30% probability level, H atoms are omitted for clarity.*

Bond lengths (Å) for **4**: Cu1–O2 1.933(8), Cu1–O5 1.956(10), Cu1–N1 2.008(10), Cu1–N2 1.961(10), Cu1–Cl1 2.775(4), Cs1–Cl1 3.458(3), Cs1–O1 3.185(12), Cs1–O2 3.206(8), Cs1–O3 3.442(14), Cs1–O4 3.308(14), Cs1–O5 3.399(10), Cs1–O5 3.424(12), Cs1–O7 3.339(14), Cs1–O7 3.341(15). Bond angles (°) for **4**: O2–Cu1–O5 175.9(5), O2–Cu1–N2 94.1(4), O5–Cu1–N2 86.0(4), O2–Cu1–N1 84.8(4), O5–Cu1–N1 94.0(4), N2–Cu1–N1 165.3(5), Cu1–Cl1–Cs1 91.4(1).

The in-plane bond lengths for Cu–$O_{carboxylate}$ are within the range 1.92–1.95 Å observed for other amino acid or amino acid derived Cu(II) complexes.[10] The in-plane bond length for Cu–N_{amine} (Cu1–N1) is longer at ~2.008 Å and another Cu1–N2 shorter at 1.96 Å compared to corresponding amino acid complexes (1.96–1.98 Å).[11] The axial fifth coordination is provided by a chloride ion with Cu–Cl distance of 2.775(4) Å for **4** (Figure **4.6**). The chloro bridging axial bond distance as well as bond angle (Cu1-Cl1–Cs1 91.4°) in square-pyramidal Cu(II) is almost similar to other studies.[11] Further, chloride act as bridging ligand between Cu(II) and alkali metal ion Cs^+ with Cs–Cl bond distance of 3.458 Å (ionic radii of Cs^+ 1.67, Cl^- 1.67Å).[8] Caesium ion bound water bonding distance is Cs1– O7 ~3.339 Å and the water molecule form bridge with other Cs^+. Carboxylate coordinated to Cu(II), also form bridge like water molecule with bonding distance ~3.4 Å (Cs1–O5 3.399 Å, Cs1–O5 3.424 Å). Over all structural features of the **4** is, Cs^+ with coordination number nine, forms two dimensional coordination polymeric structure (Figure **4.7**).

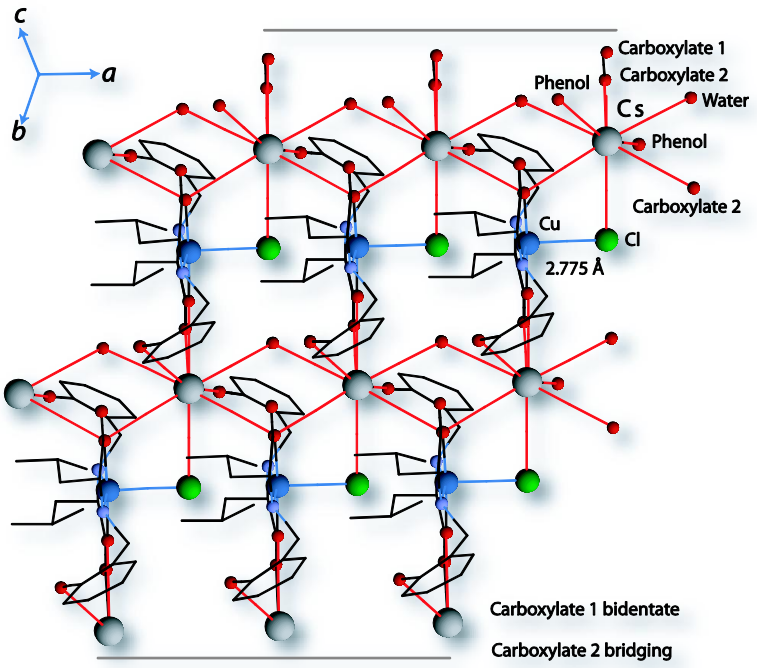

Figure 4.7. *Lattice of complex **4** and coordination around Cs^+.*

The **3** and **4** showed that unlike Na^+ or K^+, assembly formation with Cs^+ depends on the counter anion. What is observed in **4** is that Cs^+ has capacity to bind more than six donors perhaps due to the larger size (Figure **4.7**). This and its ability to retain bonding with chloride resulted in a polymeric network. $CsNO_3$ probably ionizes better which allowed trinuclear formation.

4.4.5 Absorption and EPR spectral characteristics of $[Cs\{Cu(HL^{L\text{-}leu})_2\}_3]NO_3$(3) and $\{[Cs\{Cu(HL^{L\text{-}leu})_2\}Cl(H_2O)]\}_n$(4)

The UV-visible spectral characteristic data of complexes **3** & **4** in DMF and MeOH are given in table **4.3** and the spectra given in figure **4.8**. The absorption maxima between 600–650 nm with ε value ~210 for **3** and 75 dm^3 $mol^{-1}cm^{-1}$ for **4** is of ligand field origin. Several other square-pyramidal Cu(II) complexes with N/O donor environment have similar spectral characteristics.[12,13] The spectral characteristics of **3** and **4** are almost identical in DMF as well as in MeOH. Multinuclear assembly **3** gives a sharper spectrum than the complex **4** with higher epsilon values.

The EPR spectral characteristic of the complexes **3** and **4** are shown in figure **4.9** and the data in methanol at 77 K are shown in table **4.4** The complexes **3** and **4** shows a typical square pyramidal EPR spectra as is evident from their $A_{\parallel}$ values ~179G and g values.[14]

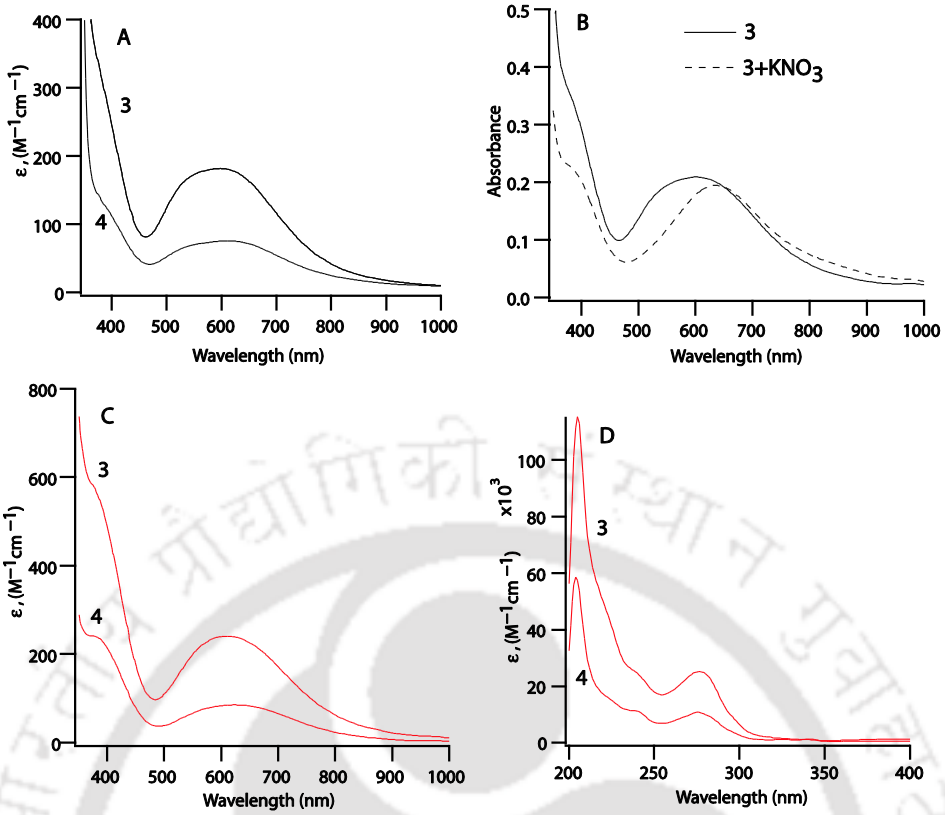

Figure 4.8. *UV-Visible spectra of* (A) *complexes **3** and **4**, in DMF, (B) complex **3** before and after addition of KNO_3 in DMF,(C) Complex **3** and **4** in MeOH and (D) complex **3** and **4** in the UV region.*

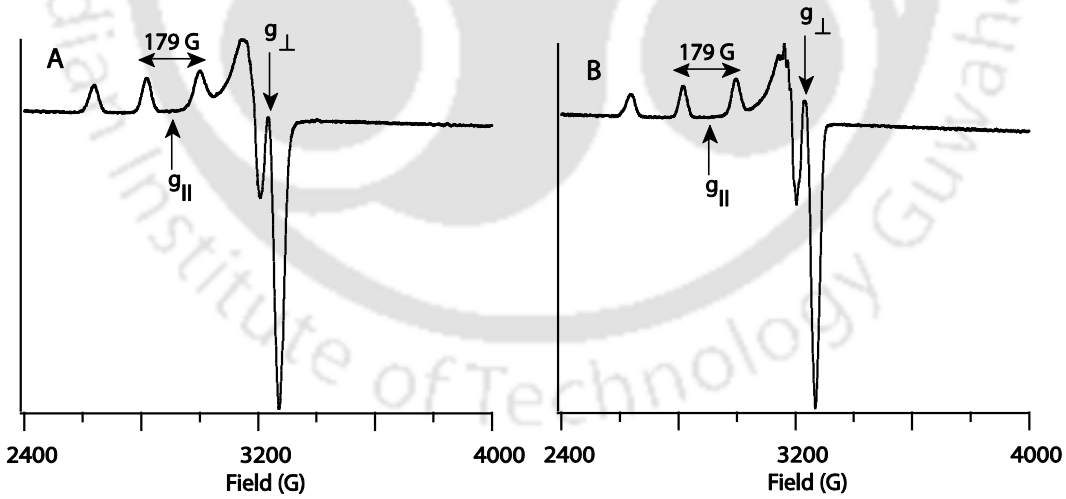

Figure 4.9. *EPR spectra of (A) complex **3** and (B) complex **4** in MeOH at 77K.*

Table 4.4 EPR data of complexes in MeOH at 77K

Complexes	$g_{\parallel}$	$g_{\perp}$	$A_{\parallel}$/G
(3) $[Cs\{Cu(HL^{L\text{-}leu})_2\}_3]NO_3$	2.246	2.021	179
(4) $[Cs\{Cu(HL^{L\text{-}leu})_2\}]Cl$	2.247	2.025	179

4.4.6 Monomer to assembly formation and their relative stability

The complex **4** was soluble in MeOH and after addition of solid $NaClO_4/KNO_3$, it is readily converted into Na^+/K^+ containing multinuclear assembly which was confirmed by FTIR, ESI-Mass, visible spectra and crystal parameter determination. Complex **3** was readily converted into K^+ containing assembly after addition of KNO_3 in DMF which was confirmed by ESI-Mass and visible spectra. These conversions (Figure **4.10**) showed that K^+ containing assembly most stable among all the assemblies.

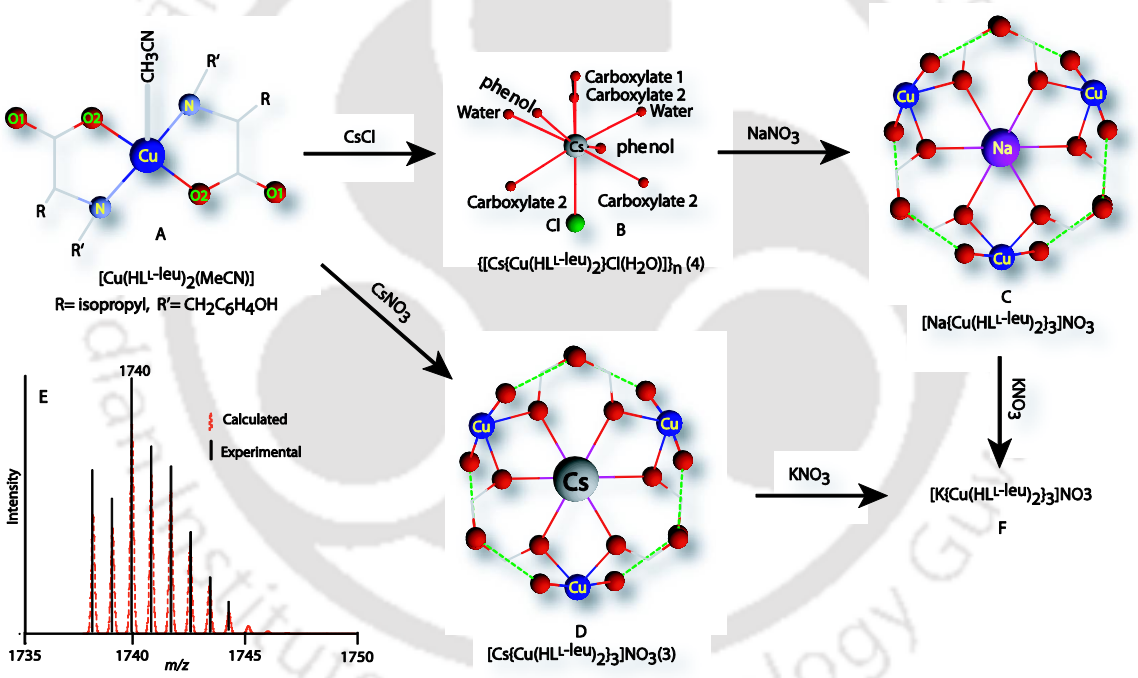

Figure 4.10. *A pictorial representation of coordination around alkali metal ion and sequential conversions of the assemblies where (A) Monomer* $[Cu(HL^{L\text{-}leu})_2(CH_3CN)]$, (B) *Assembly* $\{[Cs\{Cu(HL^{L\text{-}leu})_2\}H_2O]Cl\}_n$, ***(4)*** *(C) Multinuclear assembly* $[Na\{Cu(HL^{L\text{-}leu})_2\}_3]ClO_4$, *(D) Multinuclear assembly* $[K\{Cu(HL^{L\text{-}leu})_2\}_3]NO_3$ *or* $[Cs\{Cu(HL^{L\text{-}leu})_2\}_3]NO_3$ ***(3)*** *and (E) ESI-Mass isotopic abundance pattern of the assembly* $[Cs\{Cu(HL^{L\text{-}leu})_2\}_3]NO_3$ ***(3)*** *red dotted(simulated) black(experimental) in MeOH.*

Conclusion

Results presented in this chapter showed that the assembly formation is independent of amino acid arm as long as these arms do not contain strong donors to interfere with the assembly formation. Further, the reactions with cesium salts showed that indeed the assembly can be formed with Cs^+ as the central metal ion. Compared to Na^+ or K^+, Cs^+ is little different in the sense that it's tendency to bind with Cl^- prevents trinuclear assembly formation. Conversions also showed that K^+ can replace Cs^+ (Figure **4.10**). In Chapter **2** we have observed that K^+ can replace Na^+ as well. These indicate that out of three alkali metal ion K^+ fits best.

References

1. (a) Alam, M. A.; Koner, R. R.; Das, A.; Nethaji, M.; Ray, M. *Cryst. Growth. Des.* **2007**, *7*, 1818. (b) Dubey, M.; Koner, R.R.; Ray, M. *Inorg. Chem.* **2009**, *48*, 9294.
2. Blessing, R. *Acta Crystallogr., Sect. A*, **1995**, *51*, 33.
3. (a) Sheldrick, G. M. *SHELXL-97: Program for Crystal Structures Refinement*; University of Göttingen: Göttingen, Germany, **1997**. (b) Farrugia, L. J. *J. Appl. Cryst.* **1999**, *32*, 837–838.
4. Nakamoto, K. *Infrared and Raman Spectra of Inorganic Compounds*, 5th ed.; Wiley-Interscience: New York, **1997**; Part B.
5. Magnetic moment (B.M.) range for Ni(II): 2.9–3.3 and Cu(II) 1.7–2.1. Solid state moment can be lower if weak anti ferromagnetic interaction is present. (a) Figgis, B. N.; Lewis J. *Prog. Inorg. Chem.* **1964**, *6*, 37. (b) O'Connor, C. J. *Prog. Inorg. Chem.* **1982**, *29*, 203. (c) Earnshaw, A. *Introduction to Magnetochemistry*, Academic Press, London, 1968. Molar conductance (ohm^{-1} cm^2 mol^{-1}) range for 1:1 electrolyte in DMF: 65-90, MeOH: 80-115. (d) Geary, W. J. *Coord. Chem. Rev.* **1971**, *7*, 81.
6. Johnson, C. K. *ORTEP, Report ORNL-3794*; Oak Ridge National Laboratory: Oak Ridge, TN, **1976**.
7. O··O range (2.5 to 3.0) Å: (a) Miyake, R.; Tashiro, S.; Shiro, M.; Tanaka, K.; Shionoya, M. *J. Am. Chem. Soc*. **2008**, *130*, 5646. (b) Desiraju, G. R. *Perspective in Supramolecular Chemistry*, Wiley, *Vol 7*. (c) Yang, C. T.; Moubaraki, B.; Murray, K. S.; Vittal, J. J. *Dalton Trans*. **2003**, 880.
8. Shannon, R. D. *Acta Crystallogr. A* **1976**, *32*, 751.

9. Addision, A.W.; Rao, T. N. Reedijk, J.; Rijn, J. V.; Verschoor, G. C. *J. Chem. Soc., Dalton Trans.* **1984**, 1349.
10. Structures of Cu(II) complexes with pure amino acids used in this work: (a) McAuliffe, C. A.; Quagliano, J. V.; Vallarino, L. M. *Inorg. Chem*. **1966**, *5,* 1996. (b) Helm, D. V. D.; Franks, W. A. *Acta. Crystallogr*., *Sect. B* **1969**, *25*, 451. (c) Stephens, F. S.; Vagg R. S.; Willams, P. A. *Acta. Crystallogr., Sect. B* **1975**, *31*, 841. (d) Ou, C.; Powers, D. A.; Thich, J. A.; Felthouse, T. R.; Hendrickson, D. N.; Potenza, J. A.; Schugar, H. J. *Inorg. Chem*. **1978**, *17*, 34. (e) Hitchman, M. A.; Kwan, L. *J. Chem. Soc. Dalton Trans*. **1987**, 457 (f) Rizzi, A. C.; Piro, O. E.; Castellano, E. E.; Nascimento, O. R.; Brondino, C. D. *Inorg. Chim. Acta* **2000**, *305*, 19.
11. Colacio, E.; Ghazi, M.; Kivekas, R.; Moreno, J. M. *Inorg. Chem.* **2000**, *39,* 2882. (b) Wang, J.; Djukic, B.; Cao, J.; Alberola, A.; Razavi, F. S.; Pilkington, M. *Inorg. Chem*. *46*, **2007**, 8560.
12. (a)Yang, C. T.; Vetrichelvan, M.; Yang, X; Keith, B. M.; Murray, S.; Vittal, J. J. *J. Chem. Soc., Dalton Trans.* **2004**, 113. (b) Yang, C. T.; Moubaraki, B.; Murray, K. S.; Ranford, J. D.; Vittal, J. J. *Inorg. Chem.* **2001**, *40*, 5934. (c) Xiandong, Y.; Daqing, W.; Ranford, J. D.; Vittal, J. J. *Cryst. Growth Des.* **2005**, *5*, 41. (d) Xiandong, Y.; Ranford, J. D.; Vittal, J. J. *Cryst. Growth Des*. **2004**, *4*, 781. (e) Ranford, J. D.; Vittal, J. J.; Wu, D. *Angew. Chem., Int. Ed.* **1998**, *37*, 1114. (f) So, K. W.; Yang, C T.; Vittal, J. J.; Ranford, J. D. *Inorg. Chim. Acta.* **2003**, *349*, 135. (g) Wang, X.; Ding, J.; Vittal, J. J. *Inorg. Chim. Acta* **2006**, *359*, 3481.
13. Admas, H.; Bailey, N. A.; de Barbarin, C. O. R.; Fanton, D. E. *J. Chem. Soc*., *Dalton Trans.* **1995**, 2323.
14. Yokoi, H.; Addison, A. W. *J. Chem. Soc., Dalton Trans*. **1977**, *16*, 1341.

In the previous chapters, we have observed that the trinuclear assemblies are structurally nearly identical irrespective of central alkali ion or divalent metal ions. Even having a different amino acid does not inhibit the assembly formation as long as the amino acid arm is not competing for a coordination site on the divalent metal ion. Comparison of bond length and angles for Ni(II) and Cu(II) containing assemblies with same central alkali metal ion (K^+) did not show any significant difference. As if within a small range of size any one can fit the site where rest of the structure will undergo minor adjustment in bond length and angles to accommodate it. It was specifically observable that even though Cu(II) is expected to have Jahn–Teller distortion which could have disrupted the six coordination required for the assembly, but it did not. The axial lengths were longer (Chapter **2,** Table **2.2**) but not to an extent to disrupt the assembly formation. If the assembly formation is facile and it does not depend on the bivalent metals coordination difference that much as indicated by the results in the previous chapters, is it then possible to mix different metals along with the ligand and the required base to form mixed metal assembly? To test this, we have synthesized and well characterized a mixed metal trinuclear self-assembly of Ni(II) and Cu(II) in the 2:1 ratio using L-leucine derived ligand with metal: ligand ratio 1:2 (Scheme **5.1**).

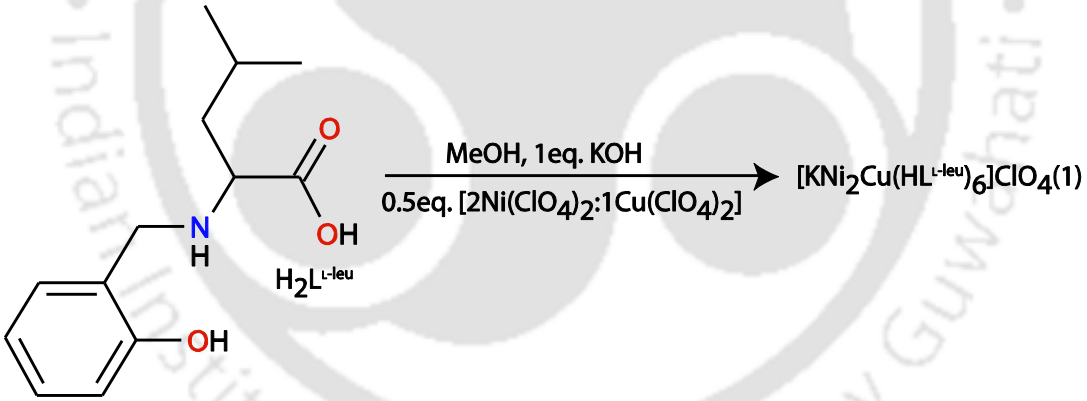

Scheme 5.1. *Ligand used in this chapter as well as schematic representation for complex synthesis.*

5.1 Experimental section

5.1.1 Materials and Methods

Ratio-metric analysis of Ni(II) and Cu(II) was done using Varian spectra 220 FS atomic absorption spectroscopy, AXIOS (PAN analytical) Computerized Sequential X-ray Fluorescence Spectrometer (XRF) and Scanning Electron Microscope, LEO 1430 vp (EDX). Other instruments and material sources have been described in earlier chapters.

Caution! *Perchlorate salts are potentially dangerous as explosives and should only be handled in small quantities, although we have worked with these ClO_4^- salts without any incident.*

5.2 Synthesis

5.2.1 $[KNi_2Cu(HL^{L\text{-}leu})_6]ClO_4$ (1)

Ligand $H_2L^{L\text{-}Leu}$ (0.200g, 0.840 mmol) was deprotonated with KOH (0.047g, 0.837 mmol) in 10 mL MeOH which resulted in a clear colorless solution. A methanolic solution of (~5mL) $Ni(ClO_4)_2{\cdot}6H_2O$ (0.100 g, 0.273 mmol) and $Cu(ClO_4)_2{\cdot}6H_2O$ (0.05 g, 0.135 mmol) was added drop wise to the above stirring ligand solution. Immediately, color change took place from blue-green to deep blue. The solution was stirred for 2 h and was filtered followed by mixing with CH_3CN. A bulk of blue, diamond shaped crystals was obtained within 2 days. Yield: 50%. Anal. Calcd for $[KNi_2Cu(C_{13}H_{18}O_3N)_6]ClO_4{\cdot}12H_2O{\cdot}CH_3OH{\cdot}CH_3CN$: C, 48.05; H, 6.92; N,4.84; found C, 47.96; H, 6.64; N, 4.62. IR (KBr, cm^{-1}): $\nu(COO)_{asym}$ 1622 (s), $\nu(COO)_{sym}$ 1580 (s), 1462(s), 1368(m), 1252, $\nu(ClO_4^-)$ 1084 (m), 756 (m), 572 (m). μ_{eff} (powder, 298K): 2.72 μ_B/metal. Λ_M (ohm^{-1} cm^2 mol^{-1}): 117 (CH_3OH).

5.3 X-ray Data Collection, Structure Solution and Refinement

Crystal of the complex **1** obtained during synthesis was used for X-ray analysis. The crystal was mounted on glass fiber. Detailed structural analysis set up and software used for solving the structure has been described in the earlier chapters. Structure refinement parameters of **1** presented in Table **5.1**.

Table 5.1. Selected crystallographic data for the complex **1**

Empirical formula	$C_{84}H_{102}ClCuKN_8Ni_2O_{27}$	V, Å^3	10009(3)
Fw.	1911.25	z	4
T(K)	296(2)	ρ calcd(Mg m^{-3})	1.268
Wavelength(Å)	0.71073	μ(mm^{-1})	0.724
Crystal system	orthorhombic	coll. reflns	11279
Space group	$C222_1$	indep reflns	5661
a, Å	17.848(3)Å	FLACK para.	0.020(16)
b, Å	20.961(4)Å	GOF	1.016
c, Å	26.754(5)Å	R1[a]	0.0596
α, deg	90.00º	wR2[a]	0.1361
β, deg	90.00º	R1[b]	0.1256
γ, deg	90.00º	wR2[b]	0.1653

[a] I>2σ. [b] All data

5.4 Results and discussion

5.4.1 Synthesis and selected properties

Complex was synthesized by stirring $H_2L^{L\text{-}leu}$, KOH and metal salts ($Ni(ClO_4)_2.6H_2O$ and $Cu(ClO_4)_2.6H_2O$ in 2:1 ratio), together in MeOH at 2:2:1 ratio (Scheme **5.1**), the solution turned blue. Upon filtration the precipitate of $KClO_4$ followed by addition of acetonitrile yielded the diamond shaped blue crystals within two days in 50 % yield. IR spectral analysis shows that one broad peak at 1622 and a peak at 1368 cm^{-1} were identified as asymmetric and symmetric carboxylate stretches originated from the ligand respectively.[1] The complex also showed stretches at 1084 cm^{-1} due to perchlorate anion.[1] The elemental analysis could be matched with the formulation of the complex as $[KNi_2Cu(HL^{L\text{-}leu})_6]ClO_4{\cdot}12H_2O{\cdot}CH_3OH{\cdot}CH_3CN$. Most of these solvent molecules could be identified in the crystal structure (next section). However, we should note that because of the presence of solvents in the crystalline state some of which have tendency to be replaced by water in air make elemental analysis as less of a confirmation of the exact formula in these assemblies. Conductance of the assembly in MeOH falls within the range of 1:1 electrolyte. Solid state room temperature magnetic moment is 2.72 μ_B/metal, which is higher than corresponding all Cu(II) analogue but lower than all Ni(II) analogue.[2] The assembly is highly selective towards Ni(II) and Cu(II) ratio 2:1, because we have tried to make assembly in reverse ratio but selectively, it self-assembles into three copper containing assembly as is confirmed by ESI-Mass spectrometric analysis.

5.4.2 Structure of $[KNi_2Cu(HL^{L\text{-}leu})_6]ClO_4$(1)

The hetero-metallic complex **1** crystallizes in space group $C222_1$, where the assembly is highly symmetrical. The ORTEP[3] view of the complex $[KNi_2Cu(HL^{L\text{-}leu})_6]ClO_4$ (**1**) has shown in figure **5.1**. The selected bond distances and angles are in table **5.2**. The molecular structure including most of the lattice solvent arrangement is identical with those assemblies in the previous chapters. Conformation of the six chiral centers on the ligand and six chiral centre generated due to amine coordination are *S* and *R* respectively.

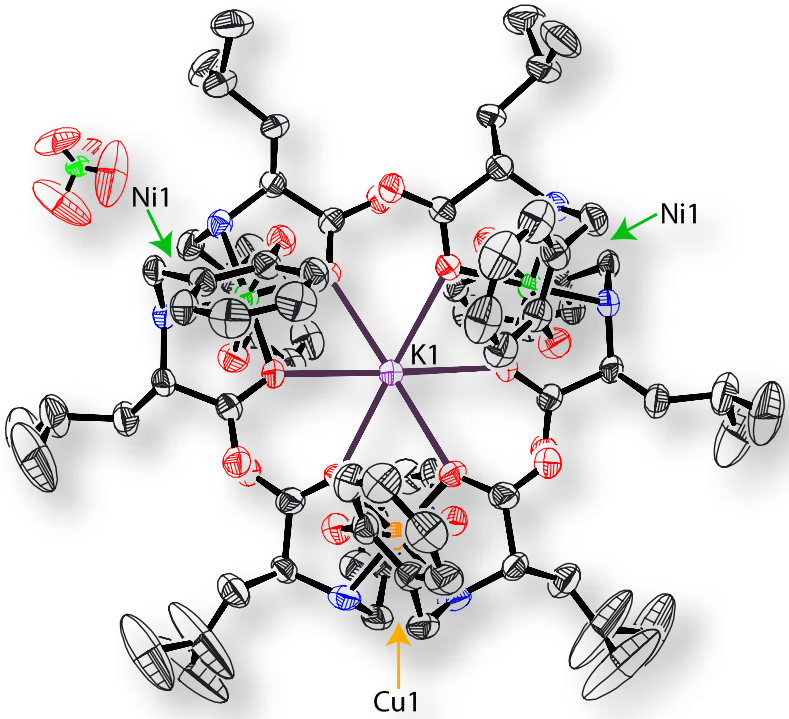

Figure 5.1. *ORTEP diagram of **1** with thermal ellipsoids set to 30% probability level and hydrogen atoms are omitted for clarity.*

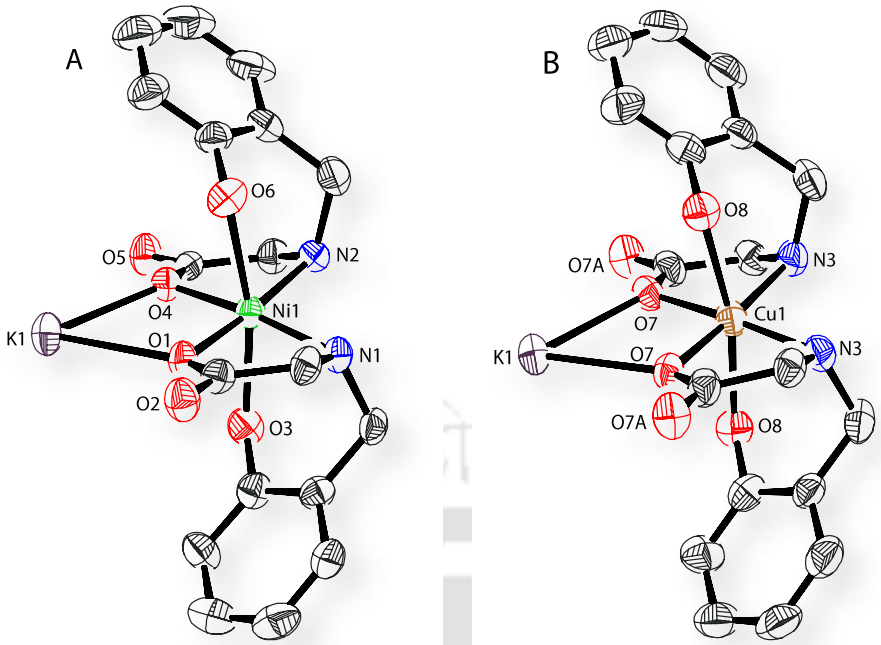

Figure 5.2. *(A) ORTEP diagram as well as labeling scheme of Ni(II) monomer unit and (B) ORTEP diagram for Cu(II) monomer unit.*

The assembly consists of three $[M^{II}(HL^{L\text{-}leu})_2]$ units where one is on the crystallographic 2-fold axis and the other two are on general position. Thus we have two identical $[M^{II}(HL^{L\text{-}leu})_2]$ units and one crystallographically different unit. Further, three monomeric units hold together by hexacoordinated K^+ through carboxylate oxygens, and six H-bonds between carboxylate oxygen and phenolic proton provide additional strength (Figure **5.3**). These H-bonds are on the short end of the 2.5–3.0 Å range usual for O…O H-bond distances (Table **5.2**).[4] The *cis* orientation of carboxylates allowed the monomeric units to bind K^+, similar orientation of amines provided a H-bonding site for perchlorate anion making the assembly, capable of binding both anion and cation of a salt within the same assembly in solid state as before (Figure **5.1**).

As we have two different type $[M^{II}(HL^{L\text{-}leu})_2]$ units in a 2:1 ratio we have assigned them two Ni(II) unit and one Cu(II) unit based on the ESI-Mass, metal ratio analysis, magnetism and UV-visible spectroscopic results (Next sections). As such in a large structure such as this assigning 2Ni: 1Cu or 2Cu: 1Ni does not change the structure solution considerably. The variations of in-plane bond lengths between two different units are similar which does not confirm either of the possibility. The axial bond lengths in assigned ($Cu–O_{phenol}$) are shorter than Ni(II) counterparts which is as such counter intuitive as we

expected longer axial lengths for Cu(II) units due to Jahn-Teller distortion (Table **5.2**). However, the axial lengths for Cu(II) unit is longer than in-plane ligands thus Jahn-Teller distortion is present. To support this assignment we have performed the ESI-Mass analysis on the same batch of crystals (Figure **5.4**, next section).

Table 5.2. Selected bond distances (Å) and angles (°) of complex **1**

Atoms	Bond distances		Atoms	Bond angles
Ni -O_{phenol}	2.269(4)	2.268(4)	O1-Ni1-N1	81.77(15)
Ni -$O_{carboxy}$	1.999(3)	2.007(3)	O4-Ni1-N2	81.23(15)
Ni -N_{amine}	2.044(4)	2.063(4)	O7-Cu1-N3	81.47(16)
K-$O_{carboxy}$	2.709(3)	2.665(3)	O1-Ni1-O4	97.80(13)
OH...O	2.589	2.545	O7-Cu1-O7	98.7(2)
Cu-O_{phenol}	2.203(4)		N1-Ni1-N2	99.76(16)
Cu-$O_{carboxy}$	2.007(4)		N3-Cu1-N3	98.7(3)
Cu-N_{amine}	2.064(5)		N1-Ni1-O3	89.62(16)
K-O7	2.703(4)		N3-Cu1-O8	89.74(16)
O8H...O5	2.548		O4-K1-O1	68.35(10)
			O7-K1-O7	68.57(16)

The *cis* oriented amines in Ni(II) monomers has two docking sites for perchlorate anions (N1…O9 and N2…O10). Additionally six molecules of water, two molecules of Methanol and two molecule of acetonitrile per one trinuclear unit were found within the lattice.

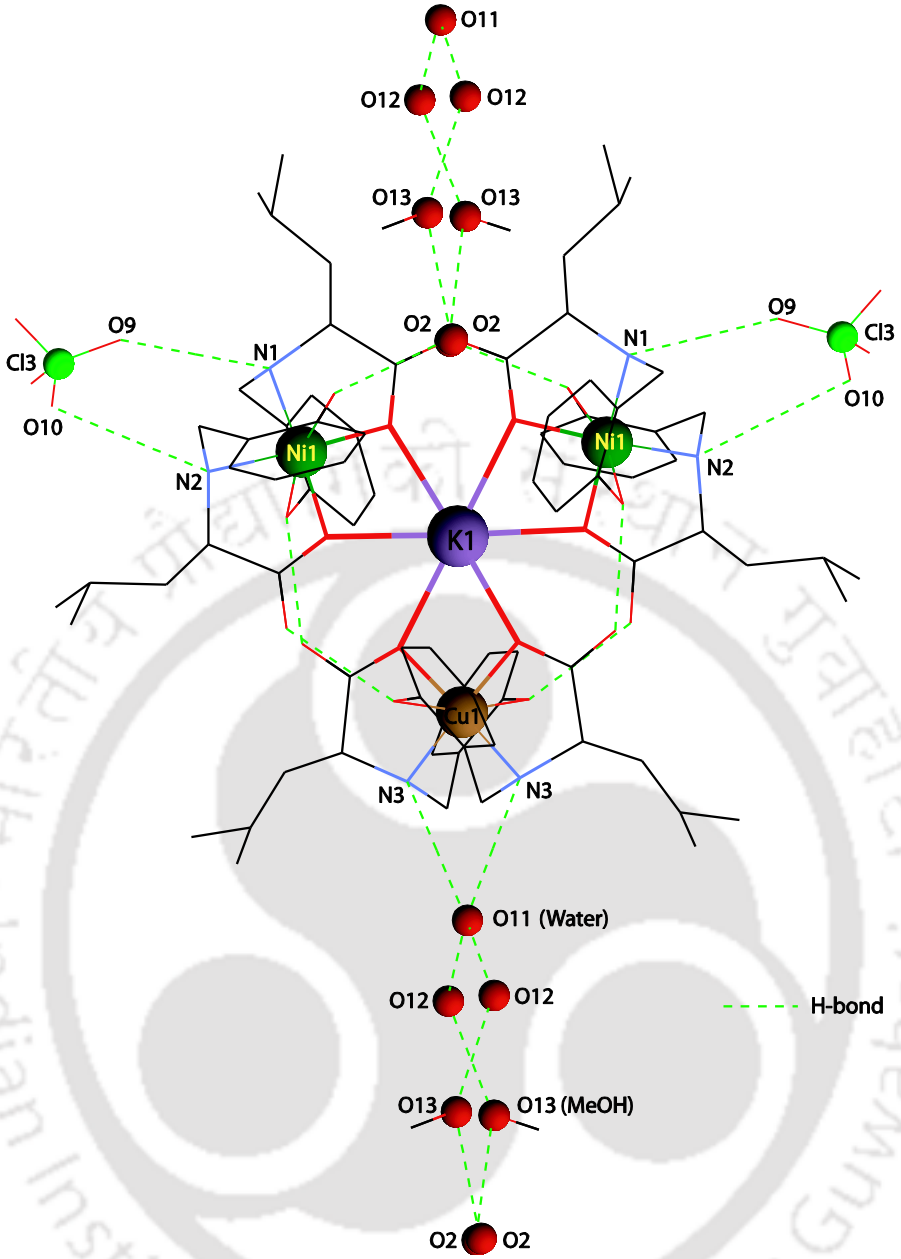

Figure 5.3. *The lattice also contains MeOH and water as solvents of crystallization and two anion binding sites, showing four bridging sites for other molecules in the lattice.*

5.4.3. Mass spectral study

The solution ESI-Mass for complex **1** (same batch of crystals used in X-ray structure) in MeOH consistent with the mixed metal assembly as Ni(II) to Cu(II) ratio is 2:1 (Figure **5.4**, Table **5.3**). The isotopic mass distribution pattern as well as abundance matches quite well with calculated values. The simulated and experimental spectra have been given in figure **5.4A**. The molecular formula of hetero-metallic assembly $[KNi_2Cu(HL^{L\text{-}leu})_6]^+$, ESI +ve *m/z* 1636.7 with 100% intensity within the isotopic abundance pattern indicates that assembly self assemble into Ni(II) to Cu(II) ratio 2:1, as well as stable in solution (Table **5.3**).

The second half of the spectrum (relative intensity) indicate that Ni(II) to Cu(II) ratio 1:2 mixed with Ni(II) to Cu(II) ratio 2:1, may be because of equilibrium exist in solution. Further we should mention that if the Ni(II) and Cu(II) ratio during the synthesis was reversed, the mass shows only $[KCu_3(HL^{L\text{-}leu})_6]^+$. This further suggest that assembly with two Cu(II) and one Ni(II) is not thermodynamically favored. The reason is not very clear at this point.

Table 5.3. Mass spectral data.[a]

	Found *m/z* (Intensity)[b]		Calculated *m/z* (Intensity)[b]	
1	1634.7(80),	1635.7(70),	1634.54(58),	1635.54(51),
	1636.7(100),	1637.7(81),	1636.54(100),	1637.54(77),
	1638.7(75),	1639.7(85),	1638.54(76),	1639.54(49),
	1640.7(68),	1641.7(79),	1640.54(35),	1641.54(19),
	1642.7(51),	1643.7(45),	1642.54(11),	1643.54(05),
	1644.7(30),	1645.7(28)	1644.54(02),	1645.54(01)

[a] In methanol. [b] isotopic mass distribution of the molecular ion peak with relative intensity values in parenthesis.

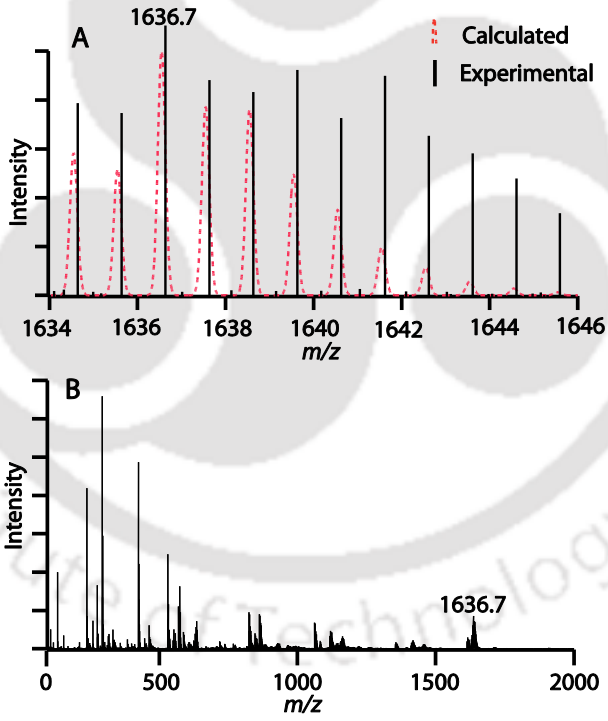

Figure 5.4 *(A) Isotopic abundance pattern calculated (red dotted) and experimental (black) of **1** (B) ESI–MS spectrum for **1**.*

5.4.4. Further analysis on Ni(II) and Cu(II) ratio

The discussions in the preceding section showed the ratio of Ni(II) and Cu(II) is an important factor. To know the ratio of Ni(II) and Cu(II), we performed the X-ray fluorescence (XRF) and energy dispersive X-ray (EDX) analysis of solid crystals on two

different batch of crystals (Batch 1 was used for all the other analysis, EPR, Magnetism reported in this chapter). XRF spectra showed the presence of both Ni(II) and Cu(II) (Figure **5.5**) but due to instrumental software limitation, the ratio could not be determined. Figure **5.6** showed one representative EDX spectra and table **5.4** showed the analysis result. Although there is some discrepancy between batch to batch but ratios are closer to 2:1 (Ni: Cu).

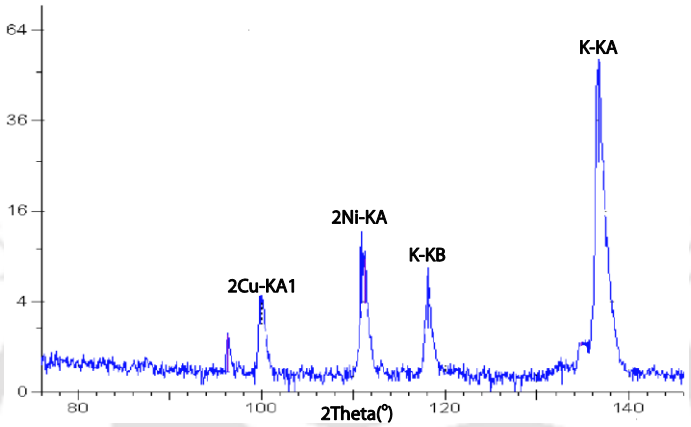

Figure 5.5. *X-ray fluorescence (XRF) graph for mixed metal complex.*

Table 5.4. Energy Dispersive X-ray Analysis data.

	Element	Ni	Cu
Batch 1	Found (%Atomic)	68.51	31.49
	Ratio	2.17	1.00
Batch 2	Found (%Atomic)	64.32	35.68
	Ratio	1.80	1.00

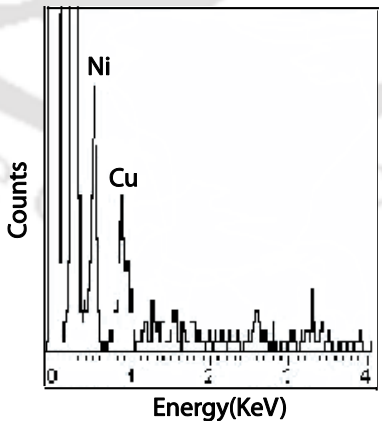

Figure 5.6. *Energy Dispersive X-ray (EDX) graph for mixed metal complex.*

Atomic absorption spectroscopic analyses on solution were performed repeatedly. Though, discrepancy of values was found from batch to batch of samples but Ni(II) is to Cu(II) ratio support 2:1 but not 1:2 (Table **5.5**).

Table 5.5. Atomic Absorption Spectroscopic Analysis data.

Sample	Atom	Calculated (ppm)	Found (ppm)	Ni:Cu[1]
$[KNi_2Cu(HL^{L\text{-}leu})_6]ClO_4$	Ni	10.4	9.85	2.41:1
	Cu	5.64	4.40	
$[KNi_2Cu(HL^{L\text{-}leu})_6]ClO_4$	Ni	5.61	5.66	2.23:1
	Cu	3.04	2.74	
$[KNi_2Cu(HL^{L\text{-}leu})_6]ClO_4$	Ni	10.42	10.23	2.40:1
	Cu	5.64	4.59	
$[K\{Cu(HL^{L\text{-}leu})_2\}_3]Br$	Cu	6.26	6.88	
	Ni	0.00	0.02	
$[K\{Ni(HL^{L\text{-}leu})_2\}_3]ClO_4$	Ni	6.00	5.53	
	Cu	0.00	0.07	

Note: Formula used for calculated value is the same as in analysis. [1]Mol ratio. Three different batches are used for $[KNi_2Cu(HL^{L\text{-}leu})_6]ClO_4$. Compound $[K\{Cu(HL^{L\text{-}leu})_2\}_3]Br$ from chapter **3** (section **3.2.7**).and $[K\{Ni(HL^{L\text{-}leu})_2\}_3]ClO_4$ from chapter **2** (section **2.2.2**).

5.4.5. UV-visible absorption spectra

UV-visible spectrum in DMF (as the assemblies with K^+ are stable in DMF, Chapter **2**, Section **2.3.3**) shows the broad absorption maxima at ~635 nm with ε value 85 dm^3 mol^{-1} cm^{-1} is likely to be of ligand field origin (Figure **5.7**). Several other tetragonally distorted octahedral Cu(II) complexes showed similar spectral characteristics.[5] Six coordinate axially elongated Ni(II)'s are known to show multiple overlapped transitions between 300 and 1500 nm region due to lower than octahedral symmetry which lifts the degeneracy of the usual three transitions, $^3T_{1g}(P) \leftarrow {}^3A_{2g}$, $^3T_{1g} \leftarrow {}^3A_{2g}$ and $^3T_{2g} \leftarrow {}^3A_{2g}$ typically observed for octahedral Ni(II) complexes.[6,7]

As the discussion in preceding section showed the **1** contain both Ni(II) and Cu(II), we have compared the electronic spectra of **1** with assemblies containing all Cu(II) as well as all Ni(II) (Figure **5.7**). The figure **5.7** indicates the spectrum of **1** have the features of both Ni(II) and Cu(II) overlapped together. Further, ε value (85 dm^3 mol^{-1} $cm^{-}1$) at absorption maxima at ~635 nm is 1/3 of Cu(II) containing assembly (230 dm^3 mol^{-1} cm^{-1}). This observation also support that only one Cu(II) monomeric unit is present in the hetero-metallic assembly (Figure **5.7**, Table **5.6**). Like Cu(II), Ni(II) monomeric units of hetero-metallic assembly also gives signature at absorption maxima at ~1220 nm with ε value (12 dm^3 mol^{-1} cm^{-1}) which is reasonably less (close to 2/3) than three Ni(II) containing homo-metallic assembly (ε value ~15 dm^3 mol^{-1} cm^{-1}) represents that less than three Ni(II) monomeric units

present in the hetero-metallic self assembly (Figure **5.7B**, Table **5.6**). Overall features conclude that both Ni(II) and Cu(II) monomeric units are present within the assembly with ratio ~ 2:1.

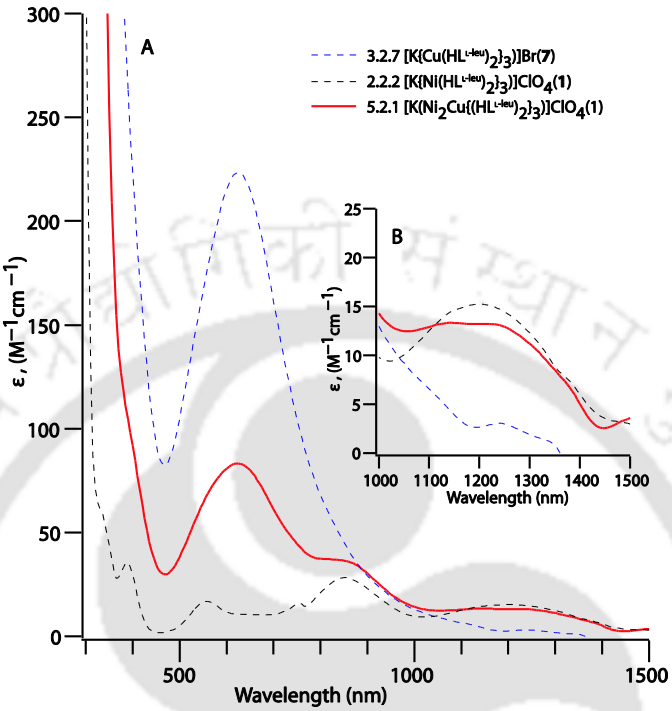

Figure 5.7. (A) *Electronic spectra of the mixed metal assembly **1** (red), copper containing assembly (blue dotted) and nickel containing assembly (black dotted) in DMF and (B) An inset diagram of (A) in the wavelength region 1000-1500 nm.*

Table 5.6. Electronic spectral data.[a]

[b]Complex	λ_{max}, nm (ε, $M^{-1}cm^{-1}$)
(1) $[KNi_2Cu(HL^{L\text{-}leu})_6]ClO_4$	390(sh), 635 (85), 855 (43), 1220 (12)
(2) $[K\{Ni(HL^{L\text{-}leu})_2\}_3]ClO_4$	390(35), 565(20), 755(sh), 860(30), 1230(15)
(3) $[K\{Cu(HL^{L\text{-}leu})_2\}_3]Br$	385(sh), 635 (230)

[a] Scan range in DMF, 300 – 2000 nm, [b] ε Complexes (**2**) $[K\{Ni(HL^{L\text{-}leu})_2\}_3]ClO_4$ from chapter **2** (section **2.2.2)** and (**3**) $[K\{Cu(HL^{L\text{-}leu})_2\}_3]Br$ from chapter **3** (section **3.2.7)**.

5.4.6. EPR spectral study

The solution EPR spectroscopic data for complex **1** at 77K is consistent with the tetragonally distorted octahedral Cu(II) structures of the complexes (Figure **5.8A, B** Table **5.7**).[8] The solution glass spectra of three Cu(II) containing assembly indicates monomeric

structures as expected (Figure **5.8C**).[9] Solid state EPR spectral studies indicates the tetragonally distorted octahedral Cu(II) present in the mixed metal assembly with three resolved hyperfine spectrum ($g_{\|}$=2.256 and $A_{\|}$=181G). While, in the three Cu(II) containing assembly, the hyperfine lines became weak and broadened and thus may be merged within the broad central line, which might be due to all the three Cu(II)'s are spin coupled, with $g_{\perp}$ ~2.107 in the solid state at 77K (Figure **5.8D**, Table **5.7**).[10,11]

Table 5.7 EPR data of complexes[a] at 77K

Complexes[a]	$g_{\|}$	$g_{\perp}$	$A_{\|}$/G
(A) $[KNi_2Cu(HL^{L\text{-}leu})_6]ClO_4$	2.247	2.023	179
(B) $[KNi_2Cu(HL^{L\text{-}leu})_6]ClO_4$	2.256	2.061	181
(C) $[K\{Cu(HL^{L\text{-}leu})_2\}_3]NO_3$	2.246	2.019	179
(D) $[K\{Cu(HL^{L\text{-}leu})_2\}_3]NO_3$		2.107	

[a](A) In MeOH solution, (B) in solid, (C) in MeOH Solution, (D) in solid state at 77K. Complex $[K\{Cu(HL^{L\text{-}leu})_2\}_3]NO_3$ from chapter **2** (section **2.2.7**)

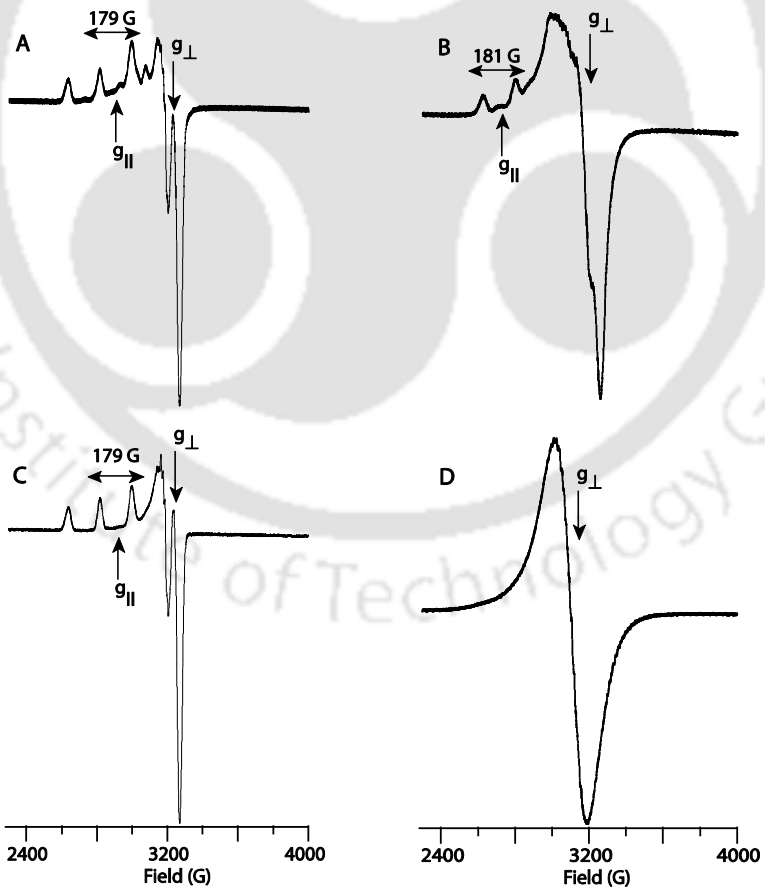

Figure 5.8. *(A) EPR spectra* of $[KNi_2Cu(HL^{L\text{-}leu})_6]ClO_4$ *in MeOH (B) in solid state and (C) EPR spectra of* $[K\{Cu(HL^{L\text{-}leu})_2\}_3]NO_3$ *in MeOH (D) in solid state at 77K.*

Conclusions

In this chapter, we have synthesized and well characterized a hetero-metallic, chiral self assembly with Ni(II) and Cu(II) in the 2:1 ratio. Interestingly, assembly is quite selective towards Ni(II) to Cu(II) 2:1 ratio. The assembly is present in solution which is supported by ESI-Mass spectroscopy. Most importantly the results presented in this chapter showed that the assembly is quite accommodative in terms of bivalent metal ion.

References

1. Nakamoto, K. Infrared and Raman Spectra of Inorganic Compounds, 5th ed.; Wiley-Interscience: New York, 1997; Part B.
2. Earnshaw, A. Introduction to Magnetochemistry; Academic Press: London, 1968. (b) Figgis, B. N.; Lewis, J. P. *Inorg. Chem.* **1964**, *6*, 37.
3. Johnson, C. K. *ORTEP, Report ORNL-3794*; Oak Ridge National Laboratory: Oak Ridge, TN, 1976.
4. O··O range (2.5 to 3.0) Å: (a) Miyake, R.; Tashiro, S.; Shiro, M.; Tanaka, K.; Shionoya, M. *J. Am. Chem. Soc*. **2008**, *130*, 5646. (b) Desiraju, G. R. *Perspective in Supramolecular Chemistry*, Wiley, *Vol 7*. (c) Yang, C. T.; Moubaraki, B.; Murray, K. S.; Vittal, J. J. *Dalton Trans*. **2003**, 880.
5. (b) Ghattas, W.; Giorgi, M.; Gaudin, C.; Rockenbauer, A.; eglier, M. R.; Simaan, A. J. *Bioinorganic Chemistry and Applications* **2007**. (c) Sun, Y.; Wang, Z.; Zhang, H.; Cao, Y.; Zhang, S.; Chen, Y.; Huang, C.; Yu, X. *Inorg. Chim. Acta,* **2007**, *360*, 2565.
6. (a) Rajendiran, V.; Palaniandavar, M.; Swaminathan, P.; Uma, L. *Inorg. Chem.* **2007**, *46*, 10446. (b) Zurowska, B.; Erxleben, A.; Glinka, L.; Łe˛czycka, M.; Zyner, E.; Ochocki, J.; *Inorg. Chim. Acta.* **2009**, *362*, 739.
7. Lever, A. B. P. *Inorganic Electronic Spectroscopy*, 2nd ed.; Elsevier: **1984**; p 507.
8. Yokoi, H.; Addision, A. W. *Inorg. Chem*. **1997**, *16*, 1341.
9. Dubey, M.; Koner, R.R.; Ray, M. *Inorg. Chem.* **2009**, *48*, 9294.
10. Klingele, J.; Prikhod'ko, A. I.; Leibeling, Guido; Demeshko, S.; Dechert S.; Meyer F. *Dalton Trans.*, **2007**, 2003.
11. Spin coupled systems (a) Addison, A.W.; Burke, P. J.; Henrick, K. *Inorg. Chem.* **1982**, *21*, 60. (b) Yang, Fuh-An; Guo, Chih-Wei; Chen, Yao-Jung; Chen, Jyh-Horung; Wang, Shin-Shin; Tung, Jo-Yu; Hwang, Lian-Pin; Elango, S. *Inorg Chem*. **2007**, *46*, 578. (c) Jung, M.; Sharma, A.; Hinderberger, D.; Braun, S.; Schatzschneider, U.;

Rentschler, E. *Inorg. Chem*. **2009**, *48*, 7244. (d) Das S.; Muthukumaragopal, G. P.; Pal, S.; Pal S. *New J. Chem*. **2003**, *27*, 1102.

In the previous chapters, we have synthesized and characterized a set of multinuclear self assemblies and monomers by using salicylaldehyde–amino acid derived ligand as well as observed the effect of cation, anion, and amino acids on assembly formation.

In this chapter, we have redesigned the ligand. Compared to the ligands in the earlier chapters, we have replaced the phenolic part of the ligand by pyrene. This would render the ligand a simple bidentate ligand similar to ferrocene derivatives reported earlier from our group. The absence of phenol would prevent the formation of phenol carboxylate H–bond which played an important role in stabilizing the trinuclear assemblies. On the other hand, whatever the type of assembly it forms (if it does) it would be due to the amino acid. This way the assembly formation observed (if any) might have some relevance to natural system. Pyrene unit here acts as hydrophobic backbone as well as fluorescence probe. One could argue that we could have done such studies directly with amino acids. But results presented earlier from our group[1] showed that a hydrophobic/aromatic substitution at the amine end does produces interesting H–bonded network formation which are simply not possible with unsubstituted amino acids as ligand.

In this chapter, we are presenting results showing that attachment of an aromatic pyrene unit to the amino acid, specifically to leucine, made an easy to synthesize, efficient fluorescent gelator which forms hydrogel exclusively in presence of LiOH. Further, use of other base, different amino acid, variation of chirality showed that gelation is sensitive to amino acid arm, LiOH, solvent and chirality of the amino acids.

Gels find number of important applications in diverse areas.[2] Recently number of reports appeared on gel formation using low molecular weight molecules.[3-5] Majority of such gelators are long chain amphiphiles with amide head groups constituted from amino acids[3] or sugar[4] and few have pyrene[5a-c] or bile acid[5d-f] derivative as gelator. Most of the gelators form hydrogel or organogel alone or along with neutral organic molecule[5b] but fewer[2d] in presence of ionic salt. We have not come across any report where hydrogel formation was observed in presence of LiOH. LiOH, widely used as electrolyte in batteries, used as organogel with polymer gelators.[6]

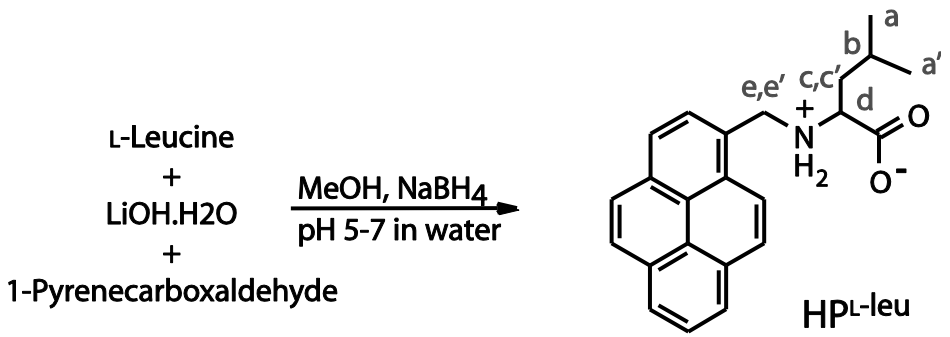

Scheme 6.1. *Synthesis of the gelator as well as ^{1}H NMR labelling scheme*.

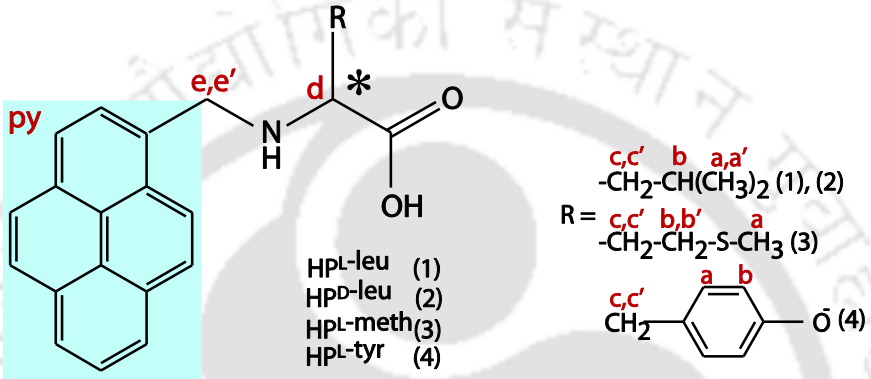

Scheme 6.2. *Gelators used in this chapter as well as ^{1}H NMR labelling scheme*.

6.1 Experimental section

6.1.1 Materials and Methods

Solvents used were purified prior to use following standard literature procedure. 1-pyrene carboxaldehyde was purchased from Aldrich Chemical Co. $NaBH_4$, amino acids and $LiOH.H_2O$ were brought from Merck limited and Sisco Research Laboratories Pvt. Ltd. (SRL), India and used as received.

The IR and UV-vis spectra were recorded on Perkin-Elmer Spectrum One FT-IR spectrophotometer with KBr discs in the range 4000-400 cm^{-1} and electronic spectra on Perkin-Elmer Lambda 25 UV-vis spectrophotometer respectively. The ^{1}H NMR spectra were recorded using Varian Mercury plus 400 MHz instrument. ESI-MS for gelators were recorded using Micromass Quattro II mass spectrometer. Optical rotations were measured using a Perkin-Elmer 343 polarimeter. Fluorescence measurements were carried on a *Cary eclipse* spectrofluorometer using 10 mm path length quartz cuvettes with the slit width of 5 nm at 298 K. Powder X-ray diffraction measurements was done using Bruker D8 Advanced.

Microscopic images were taken using Scanning Electron Microscope, LEO 1430 vp and Transmission Electron Microscope (TEM), JEOL JEM 2100.

6.2 Syntheses

6.2.1 $HP^{L\text{-}leu}$ (1)

L-leucine (0.200 g, 1.52 mmol) and $LiOH{\cdot}H_2O$ (0.064 g, 1.52 mmol) were dissolved in 30 mL dry methanol after stirring for 30 min. A methanolic solution (20 mL) of pyrenecarboxaldehyde (0.351 g, 1.52 mmol) was added drop wise to the amino acid solution. The solution was refluxed for 1 h after which it was treated with sodium borohydride (0.058 g, 1.52 mmol) at room temperature with constant stirring. The color of the solution turned light brown. The solvent was evaporated and the resulting sticky mass was dissolved in water. A cloudy solution was obtained, which was then acidified with dilute HCl and solution pH was maintained between ranges 5-7. The gelator as yellow solid was precipitated out. The solid was filtered, thoroughly washed with water and diethyl ether finally dried under reduced pressure inside a desiccator. Yield: 0.45g (86%). Due to poor solubility of the neutral form, ^{1}H NMR of the gelator was performed by dissolving the solid in methanol in presence of 1 equivalent $LiOH{\cdot}H_2O$. ^{1}H NMR (CD_3OD, ppm) (Scheme **6.2**): H^{Py} (8.003-8.533, m, 9H), $H^{e'}$ (4.576, d, 1H, $J_{ee'}$ = 12.4 Hz), H^{e} (4.225, d, 1H, $J_{ee'}$ = 12.4 Hz), H^{d} (3.349, t, 1H), H^{b} (1.826, m, 1H), $H^{c'}$ (1.555, m, 1H), H^{c} (1.479, m, 1H), $H^{a'}$ (0.982, d, 3H $J_{a'b}$ = 6.8 Hz), H^{a} (0.888, d, 3H J_{ab} = 6.8 Hz). *m/z* (ESI–MS), $[M+H]^+$, 344 (calcd. 344). IR (KBr, cm^{-1}): $\nu(COO)_{asym}$ 1614(s). $[\alpha]_D^{20°}$= –15º in MeOH, c = 0.2 in presence of 1 equivalent $LiOH{\cdot}H_2O$. UV/Vis: λ_{max} [nm] (ε, $M^{-1}cm^{-1}$) in MeOH with 1equiv. of $LiOH{\cdot}H_2O$: 343(48100), 326(36000), 312(sh), 277(38200), 266(sh), 245(29000).

6.2.2 $HP^{D\text{-}Leu}$ (2)

Compound was synthesized by following same procedure as described in $HP^{L\text{-}leu}$, D-leucine taken instead of L-leucine. Yield 0.43g (82%). Due to poor solubility of the neutral form, ^{1}H NMR, UV/Vis measurement was performed by dissolving the solid in methanol in presence of 1 equivalent $LiOH{\cdot}H_2O$. ^{1}H NMR (CD_3OD, ppm) (Scheme **6.2**): H^{Py} (8.457-7.998, m, 9H), $H^{e'}$ (4.519, d, 1H, $J_{ee'}$ = 12.4 Hz), H^{e} (4.185, d, 1H, $J_{ee'}$ = 12.4 Hz), H^{d} (3.286, t, 1H), H^{b} (1.767, m, 1H), $H^{c'}$ (1.498, m, 1H), H^{c} (1.425, m, 1H), $H^{a'}$ (0.930, d, 3H $J_{a'b}$ = 6.8 Hz), H^{a} (0.831, d, 3H J_{ab} = 6.8 Hz). *m/z* (ESI–MS, $[M+H]^+$, 344 (calcd. 344). IR (KBr, cm^{-1}): $\nu(COO)_{asym}$ 1614(s). $[\alpha]_D^{20°}$= +13º in MeOH, c = 0.2 in presence of 1 eqv. $LiOH{\cdot}H_2O$.

UV/Vis: λ_{max} [nm] (ε, $M^{-1}cm^{-1}$) in MeOH with 1equivalent of $LiOH{\cdot}H_2O$: 341(59800), 326(43800), 314(sh), 275(46500), 267(sh), 243(34000).

6.2.3 $HP^{L\text{-}meth}$ (3)

$HP^{L\text{-}meth}$ was prepared following similar procedure as described for $HP^{L\text{-}leu}$ using L-methionine (0.200 g, 1.34 mmol), $LiOH{\cdot}H_2O$ (0.056 g, 1.34 mmol) and pyrenecarboxaldehyde (0.309 g, 1.34 mmol). The solution was refluxed for 1 h before reduction with sodium borohydride (0.051 g, 1.34 mmol) at room temperature. The solid compound was precipitated from water following neutralization between pH 5-7. The solid was washed thoroughly with water and diethyl ether followed by drying under reduced pressure inside a desiccator. Yield 0.43g (88%). Due to poor solubility of the compound in neutral form, ^{1}H NMR, UV/Vis measurements were performed by dissolving the solid in methanol in presence of 1 equivalent $LiOH{\cdot}H_2O$. ^{1}H NMR (CD_3OD, ppm) (Scheme **6.2**): H^{Py} (8.439-7.907, m, 9H), $H^{e'}$ (4.491, d, 1H, $J_{ee'}$ = 12 Hz), H^{e} (4.167, d, 1H, $J_{ee'}$ = 12 Hz), H^{d} (3.328, t, 1H), $H^{bb'}$ (2.567, m, 2H), H^{a} (2.001, s, 3H), $H^{cc'}$ (1.892, m, 2H). *m/z* (ESI-MS, $[M+H]^+$, 362 (calcd. 362). IR (KBr, cm^{-1}): $\nu(COO)_{asym}$ 1605(s). $[\alpha]_D^{20^o}$ = –16º in MeOH, c = 0.2 in presence of 1 equivalent $LiOH{\cdot}H_2O$. UV/Vis: λ_{max} [nm] (ε, $M^{-1}cm^{-1}$) in MeOH with 1equivalent of $LiOH{\cdot}H_2O$: 341(57000), 325(42200), 313(sh), 275(44100), 266(sh), 243(33100).

6.2.4 $HP^{L\text{-}tyr}$ (4)

This was prepared following the method, stirring time and pH range described for $HP^{L\text{-}leu}$ using the following quantities of reagents: L-tyrosine (0.200 g, 1.10 mmol), $LiOH{\cdot}H_2O$ (0.046 g, 1.10 mmol), pyrenecarboxaldehyde (0.254 g, 1.10 mmol) and sodium borohydride (0.042 g, 1.10 mmol). Yield 0.36 g (83%). ^{1}H NMR (CD_3OD, ppm) (Scheme **6.2**): H^{Py} (8.205-7.887, m, 9H), H^{a} (6.948, d, 2H, J_{ab}= 8.4 Hz), H^{b} (6.581, d, 2H, J_{ab}= 8.4 Hz), $H^{e'}$ (4.453, d, 1H $J_{ee'}$ = 12.4 Hz), H^{e} (4.194, d, 1H $J_{ee'}$= 12.4 Hz), H^{d} (3.484, t, 1H), $H^{c'}$ (3.01, d, 1H $J_{cc'}$= 4.8 Hz), H^{c} (2.689, d, 1H $J_{cc'}$= 4.8 Hz). *m/z* (ESI-MS, $[M-H]^-$) 394 (calcd. 394). IR (KBr, cm^{-1}): $\nu(COO)_{asym}$ 1611(s). $[\alpha]_D^{20^o}$= –21º in MeOH, c = 0.2 in presence of 1 equivalent $LiOH{\cdot}H_2O$. UV/Vis: λ_{max} [nm] (ε, $M^{-1}cm^{-1}$) in MeOH with 1eqvuivalent of $LiOH{\cdot}H_2O$: 341(61500), 326(45100), 313(sh), 275(49000), 266(sh), 243(34900).

6.3 Results and discussion

6.3.1 Hydrogel formation and property

Pyrenemethyl-amino acid derivatives were prepared by in situ reduction of the Schiff base formed between 1-pyrenecarboxaldehyde and the corresponding deprotonated amino acids followed by isolation of the neutral form upon acidification (pH ~7) in water (yield 80%, Scheme **6.1**). All the reduced Schiff bases were characterized using ^{1}H NMR spectroscopy and mass spectrometry (Experimental section, Scheme **6.2**). None of the compounds in neutral form are soluble in water, methanol, acetone or chloroform. However, the compounds dissolve in water or methanol in the presence of strong base forming deprotonated anionic form. The $HP^{L\text{-}leu}$ upon addition of LiOH (deprotonation) forms a pale yellow hydrogel within 5 minutes confirmed by inverted vial method (Figure **6.1**). Under identical condition, NaOH forms a gelatinous precipitate while KOH forms clear solution indicating that the size of the cation is important in the gel formation.

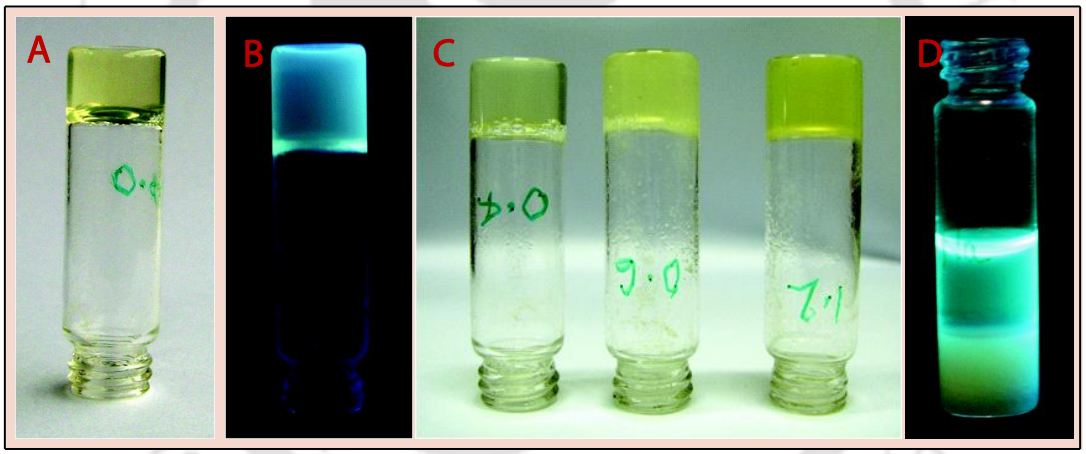

Figure 6.1. *$HP^{L\text{-}leu}$ containing hydrogel in inverted vial (A) under naked eye, (B) under UV light, (C) under naked eye at different concentration (left to right increasing % w/v 0.4, 0.6, 1.2) and (D) NaOH containing gelatinous precipitate under UV light.*

The tightness of the gel and formation time depends upon the quantity of both the gelator as well as the LiOH. Decreasing both the amount of gelator and LiOH increases the gelation time (Table **6.1**). Increasing the quantity of LiOH shortens the gelation time and allowed for fast gel formation with further decrease of gelator (Table **6.1**). At 4% w/v LiOH concentration, gelator requirement (0.1% w/v) is one of the lowest observed among low molecular weight gelators.[3b,4a] Gel formed is thermally stable up to ~90 °C, above which it slowly dried up.

Addition of LiCl in the deprotonated $HP^{L\text{-}leu}$, (LiOH 5 equivalent), does not facilitate gel formation. Addition of excess LiCl does not enhance the tightness of the gel like LiOH.

Table 6.1. Gelation under different conditions.[1]

Gelator	Additive	Gel/Sol	Gelator: LiOH: H_2O	Time (min)
$HP^{L\text{-}leu}$	LiOH	G	1:0.5:0.833	10
		G	1:1.67:0.833	5
		G	1:3.33:0.833	2
		G	1:6.67:1.67	5
		G	1:13.33:3.33	10
		G	1:40:10	15
		G	1:0.5:1.25	60
		G	1:1.25:1.67	240
		G	1:1.67:2.5	600
		G	1:1.67:3.33	600
	KOH	S	1:1.67:0.833	
	NaOH	S	1:1.67:0.833	
$HP^{D\text{-}leu}$	LiOH	G	1: 1.67: 0.833	8
	LiOH	G	1: 6.67: 1.67	5
	LiOH	S	1: 40: 10	
	KOH	S	1: 1.67: 1.67	
	NaOH	S	1: 1.67: 1.67	
$HP^{L\text{-}meth}$	LiOH	S	1: 1.67: 1.67	
$HP^{D\text{-}meth}$	LiOH	S	1: 1.67: 1.67	
$HP^{L\text{-}tyr}$	LiOH	S	1: 1.67: 1.67	

[1] All data at room temperature. Weight percentage of LiOH were calculated using $LiOH{\cdot}H_2O$. Where G = gel, S = sol.

Gel formation is specific to L-leucine derivative as L-methionine and L-tyrosine derivative did not form gel. L-Leucine derivative obtained by replacing pyrenecarboxaldehyde with salicylaldehyde in the synthesis did not form gel as well. These observations highlight *the requirement of aliphatic isopropyl arm and aromatic pyrene moiety on the gelator and presence of LiOH in the gel formation*.

6.3.1a Fluorescence spectroscopy

Presence of pyrene moiety in $HP^{L\text{-}leu}$ imparts fluorescence to the gel as well as provides a way to monitor the gel formation using well known pyrene monomer (λ_{em} 370-400 nm) – excimer (λ_{em} 470 nm) change in fluorescence.[7] Dilute solution of $Li^{+}(P^{L\text{-}leu})^{-}$ in water shows λ_{em} at 376, 395 and 415 nm (λ_{ex} 340 nm) indicative of monomeric form (Figure **6.2**) whereas *the gel emitted at 480 nm indicative of dimer (excimer) form exclusively*. Gradual dilution of the gel in water was monitored at λ_{em} 395 nm and critical aggregation concentration (CAC) was determined to be 0.007 %w/v (Figure **6.2A**).[8] The CAC for D-leucine analogue found to be 0.009 %w/v. These values indicate the aggregation of pyrene units starts at very low concentration. This is comparable to 0.007 %w/v observed for other gelator.[3a] The marginally higher CAC of D-leucine perhaps is the reason behind observed slower rate of gel formation (Table **6.1**). The experiments were repeated and the difference in CAC for two enantiomer was found to be reproducible (CAC for hydrogel of L-isomer 0.007 %w/v and 0.006 %w/v; D-isomer, 0.009 %w/v and 0.008 %w/v from two experiments).

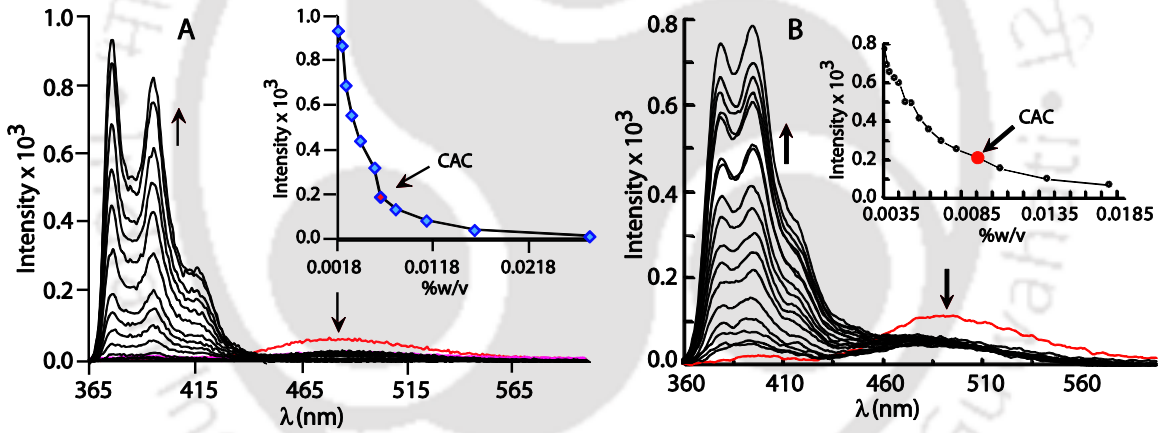

Figure 6.2. *Fluorescence spectra of gradually diluted hydrogel of (A) $HP^{L\text{-}leu}$ and (B) $HP^{D\text{-}leu}$ to determine CAC as shown in inset (λ_{ex} 340 nm, monitored at 395nm).*

6.3.1b Powder diffraction studies

X-ray power diffraction measurements were performed on the dried hydrogel (xerogel) at three different $HP^{L\text{-}leu}$: LiOH ratio (ratios) increasing the LiOH gradually. The powder diffraction pattern of the dried gel at high LiOH concentration showed sharp peaks between 20-45°, almost all of which could be assigned to known diffraction pattern of crystalline LiOH and Lithium carbonate (Figure **6.3**). This confirms the presence of crystalline LiOH and Li_2CO_3 (LiOH absorbing atmospheric CO_2) in the dried gel. Diffraction pattern at lower LiOH concentration shows negligible amount of crystallinity due to LiOH,

but no long range order was observed for the gel. This is not unusual as none of the reported gelators showed any order in the dried state.

Overall, diffraction studies showed some amount of *crystallinity was introduced in the xerogel due to LiOH (and some $LiCO_3$) which is perhaps the result of evaporation induced crystallization*. At low concentration of LiOH, gel does not have long range order.

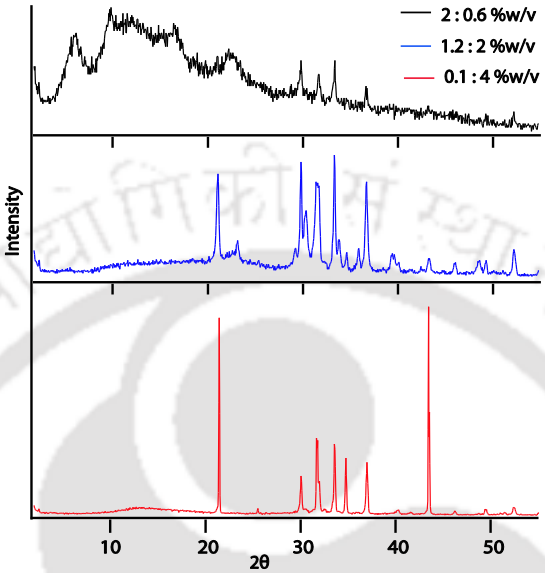

Figure 6.3. *Powder X-ray diffraction pattern of the dried gel at different concentration of gelator: LiOH (black plot 2:0.6 %w/v, blue plot 1.2: 2 %w/v, red plot 0.1:4 %w/v).*

6.3.1c Scanning electron microscopy

The scanning electron microscopic (SEM) image of the dried gel showed stacked layers of thin plates instead of usual firbrous network observed for other reported gels (Figure **6.4A**). SEM image of dried gelatinous precipitate obtained with NaOH showed mixture of thin plates with needles (Figure **6.4B**). Absence of long range plate formation presumably prevents aggregation with NaOH.

Scanning electron microscopy (SEM) of all the known gels shows fiber like formation in the xerogel which form the basis for understanding the mechanism of gel formation.[3] Layered structure of the xerogel revealed through SEM in the present case is usually not observed. One explanation might be that during the slow drying of gel LiOH introduced this crystallinity. X-ray diffraction studies (preceding section) also support that.

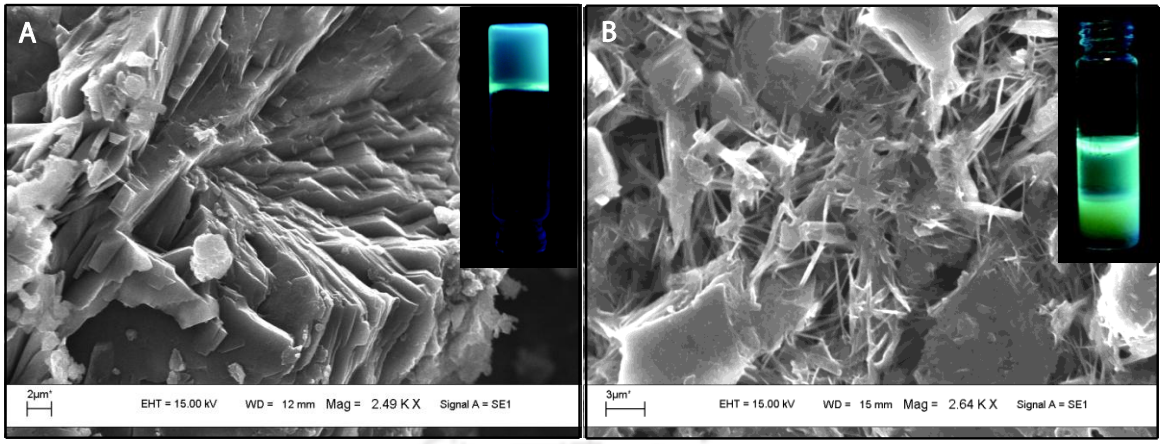

Figure 6.4. *SEM images of (A) xerogel in presence of LiOH (1.2: 2 %w/v) inset shows gel in inverted vial, (B) dried sol in presence of NaOH along with their sol under UV radiation as inset.*

6.3.2 Organogel formation and properties

Both $HP^{D\text{-}leu}$ and $HP^{L\text{-}leu}$ are soluble in dimethyl sulfoxide (DMSO). Interestingly, only $HP^{D\text{-}leu}$ forms organogel in DMSO while $HP^{L\text{-}leu}$ remains in liquid form under the same condition (Table **6.2**). We have tried to make gel with other organic solvent like dimethyl formamide, but the gel formation was only observed in DMSO. When racemic $HP^{\mathbf{DL}\text{-}leu}$ dissolved in DMSO, part of it forms gel and part remained as sol. Organogel formed is thermally stable upto ~80°C, above which it slowly melts and converted into liquid.

Table 6.2. Gelation under different conditions.[1]

Gelator	Solvent	Gel/Sol	%w/v	Time (min)
$HP^{D\text{-}leu}$	DMSO	G	1	45
	DMF	S	1	
$HP^{L\text{-}leu}$	DMSO	S	1	
$HP^{DL\text{-}leu}$	DMSO	G, S	1	45

[1] All data at room temperature. Where G = gel, S = sol.

6.3.2a SEM and TEM images of organogel

Unlike dried hydrogel, SEM and TEM images of xerogel of $HP^{D\text{-}leu}$ reveal three dimensional networks of fibres (Figure **6.5** and **6.6**). SEM of mixture of $HP^{D\text{-}leu}$ and $HP^{L\text{-}leu}$ image reveals separate fibrous network and the ribbon like flat muddled material as shown in figure **6.7**.

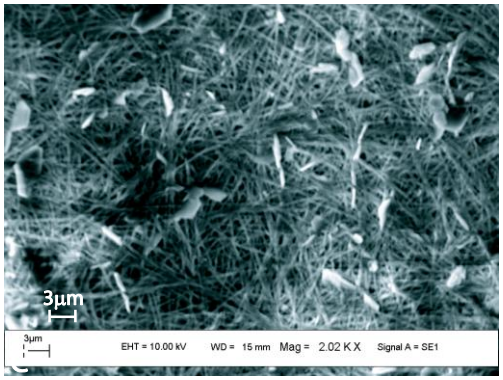

Figure 6.5. *SEM image of dried organogel reveals fibrous network (1 %w/v).*

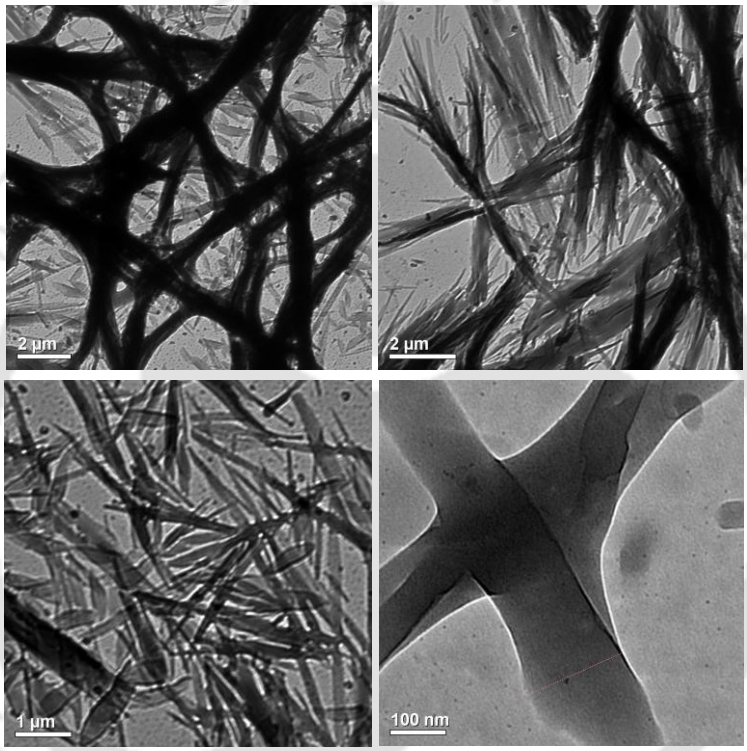

Figure 6.6. *TEM images of the organogel in DMSO quickly dried under vacuum immediately after gel formation at a concentration of 1.2 %w/v. Images at different resolution reveals the fibrous nature.*

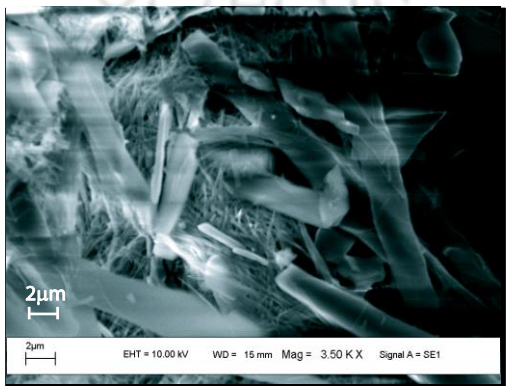

Figure 6.7. *SEM images of dried gel-sol of DL mixture at a concentration of 1 %w/v.*

6.4 Mechanism of formation

Hydrogel formation can be explained by formation of similar bipolar layers at low concentration (CAC values from fluorescent experiment) which are connected through hydroxy bridged chain of hydrated LiOH and H–bonded water which upon drying retains the layer like formation (Scheme **6.3**). The solid state structure of $LiOH.H_2O$ contain lithium ion tetrahedrally coordinated by bridging waters forming three dimensional network.[9] This perhaps was the reason behind enhancement of gel formation in presence of LiOH. Compared to Li^+, Na^+ and K^+ have lower charge radius ratio which perhaps does not allow them to form water/hydroxide bridges as tightly as Li^+ ion.

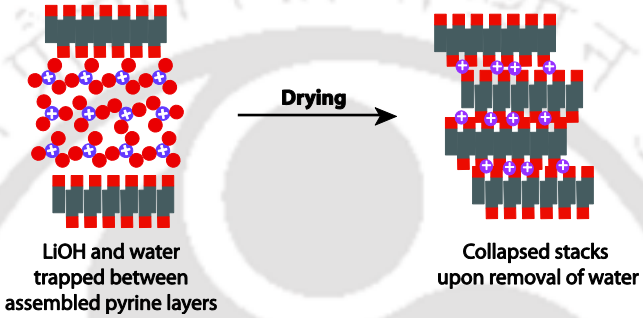

Scheme 6.3. *Proposed scheme for the formation of stacked layers observed in the SEM images.*

Formation of bipolar hydrophobic layers through assembly of amphiphiles has been suggested before[5] but the flat hydrophobic surface of pyrene and its tendency to π stacking and CH..π stacking perhaps allowed it to form relatively long range plates which effectively increased its efficiency to hold ionic salts between the layers. As the gel contains more LiOH than gelator, slow evaporation may have resulted in larger layers.

On the other hand, in case of organogel the fibrous arrangement may be because of the π stacking and CH..π stacking of pyrene as well as the association of the carboxylic acid groups through H-bonds allows long range linear network formation.

Conclusions

In conclusion, replacement of salicylaldehyde unit in the earlier ligand design with pyrene units we encountered a new property of the amino acid derivatives which was not observed before. We have made an observation that ionic LiOH can enhance the gel formation in one of the easiest to synthesize low molecular weight gelator. Our literature survey did not reveal any previous report where a binary salt or hydroxide enhanced gel formation. Considering the importance of LiOH in the battery manufacturing, the observation of high LiOH over gelator ratio (40 times by weight, 36000 times by mol) and a relatively

fast gelation time (15 min), the present work showed a very different route to gel formation compared to polymeric gelators used in batteries.[6]

References

1. Sahoo, S. C.; Ray, M. *Dalton Trans.* **2007**, 5148.
2. (a) Piepenbrock, M. M.; Lloyd, G. O.; Clarke, N.; Steed, J. W. *Chem. Rev.* **2010**, *110*, 1960. (b) Sangeetha, N. M.; Maitra, U. *Chem. Soc. Rev.* **2005**, *34*, 821. (c) Lee, K. Y.; Mooney, D. J. *Chem. Rev.* **2001**, *101*, 1869. (d) Estroff, L. A.; Hamilton, A. D. *Chem. Rev.* **2004**, *104*, 1201. (e) Yang, Z.; Liang, G.; Xu, B. *Acc. Chem. Res.* **2008**, *41*, 315. (d) Lloyd, G. O.; Steed, J. W. *Nature Chem.* **2009**, *1*, 437.
3. (a) Das, D.; Dasgupta, A.; Roy, S.; Mitra, R. N.; Debnath, S.; Das, P. K. *Chem. Eur. Journal* **2006**, *12*, 5068. (b) Khatua, D.; Maiti, R.; Dey, J. *Chem. Commun.* **2006**, 4903. (c) Suzuki, M.; Hanabusa, K. *Chem. Soc. Rev.* **2009**, *38*, 967. (d) Suzuki, M.; Abe, T.; Hanabusa, K. *Journal of Colloid and Interface Science* **2010**, *341*, 69. (d) Leong, W. L.; Batabyal, S. K.; Kasapis, S.; Vittal, J. J. *Chem. Eur. Journal* **2008**, *14*, 8822. (e) Patra, T.; Pal, A.; Dey, J. *Langmuir* **2010**, 26, 7761.
4. (a) Bhuniya, S.; Kim, B. H. *Chem. Commun*. **2006**, 1842. (b) Yan, N.; He, G.; Zhang, H.; Ding, L.; Fang, Y. *Langmuir* **2010**, *26*, 5909.
5. (a) Maitra, U.; Potluri, V. K.; Sangeetha, N. M.; Babu, P.; Raju, A. R. *Tetrahedron: Assymetry* **2001**, *12*, 477. (b) Moffat, J. R.; Smith, D. K. *Chem. Commun.* **2008**, 2248. (c) Hahma, A.; Bhat, S.; Leivo, K.; Linnanto, J.; Lahtinen, M.; Rissanen, K. *New J. Chem*. **2008**, *32*, 1438. (d) Maitra, U.; Kumar, P. V.; Chandra, N.; D'Souza, L. J.; Prasanna, M. D.; Raju, A. R. *Chem. Commun*. **1999**, 595. (e) Babu, P.; Sangeetha, N. M.; Maitra, U. *Macromolecular Symposia* **2006**, *241*, 60. (f) Babu, P.; Sangeetha, N. M.; Vijaykumar, P.; Maitra, U.; Rissanen, K.; Raju, A. R. *Chem. Eur. Journal* **2003**, *9*, 1922.
6. (a) Ogasawara, T.; Débart, A.; Holzapfel, M.; Novák, P.; Bruce, P. G. *J. Am. Chem. Soc.* **2006**, *128*, 1390. (b) Harrup, M. K.; Peterson, E. S.; Stewart, F. F. all of Idaho Falls, Id., U. S. Patent no. 6146787. (c) Shuster, N.; Madison, Ohio, U. S. Patent no. 5427873.
7. (a) Stevens, B. Nature **1961**, *192*, 725. (b) Birks, J. B.; L. Christophorou, G. *spectrochim. acta* **1963**, *19*, 401. (c) Förster, T. *Angew. Chem., Int. Ed.* **1969**, 8333.
8. (a) Kalyanasundaram, K.; Thomas, J. K. *J. Am. Chem. Soc.* **1977**, *99*, 2039. (b) Gouin, S.; Zhu, X. X. *Langmuir* **1998**, *14*, 4025.
9. Alcock, N. W. *Acta Cryst* **1971**, *B27*, 1682.

Replacement of salicylaldehyde with pyrenecarboxaldehyde in the ligand design imparted the gelation property in the ligand itself (Chapter **6**). In this chapter we will focus on the metal complexation properties of those ligands with Cu(II) and Zn(II). The results in this chapter (Scheme **7.1** and **7.2**) will show the formation of empty channels in these complexes, the kind of which was not observed in any of our previous attempts.

Literature citations showed immense interest in development of amino acid bound to pyrene moiety which has been driven in part by the desire to explore photophysical[1a], chemo sensor[1b] and weak non-covalent interactions for the structural stabilization of bioinorganic assemblies[1c] such as π–π stacking,[1d] CH...π interaction.[1e]

Channels is an important structural motifs present in nature. The channels in the membrane bound potassium channels[2a] or water permeation protein aquaporins[2b-d] are formed out of several peptide helices in an approximately C_4 symmetric fashion to form narrow channels (2.8–20 Å dia.) as gateway for K^+ ion or water molecules selectively. The narrow channels in amyloidal fibres (11.8 Å dia.) from extracellular amyloid plaques found in Alzheimer patients,[2e] aquaporin (18 to 2.8 Å dia.) and C_5 symmetric mechanosensitive channels from mycobacterium tuberculosis (18–2 Å dia.)[2f,g] contain chain of water molecules important for their biochemical functions. Apart from the channels present in nature, materials with channels of different pore diameter have been synthesized because of their anticipated use as molecular sieves, sensors, ion exchangers and catalysts.[2h-i] Recently porous channels have been used as template to synthesize nano fibres[2j] and one dimensional array of oxygen molecules.[2k] Thus, several reports appeared on the synthesis of materials with channels, helical structures with chiral or achiral ligand metal complex recently.[2k-y] Despite this, literatures regarding the formation of microporous helical channels with easily removable solvents inside are few[2k,m,o-q] and fewer report on insertion of small molecules[2z] inside the channel.

In the previous chapter, we have observed pyrene derived L-leucine and D-leucine gel synthesis, aggregation pattern of hydrogel and organogel as well as their morphology at different conditions. Thus, we felt the necessity to understand the binding mode as well as aggregation pattern of pyrene moiety of those gelators by exploring the coordination chemistry with Cu(II) and Zn(II) metal ion.

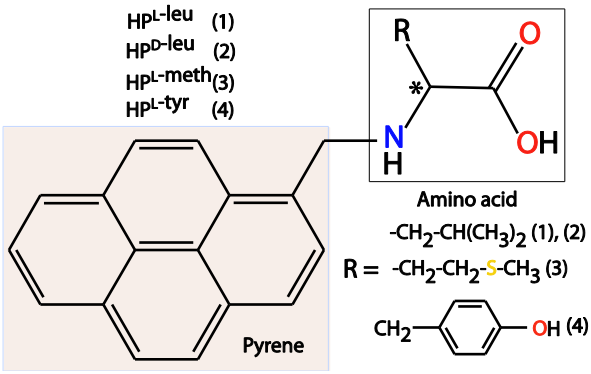

Scheme 7.1. *Ligands used in this chapter.*

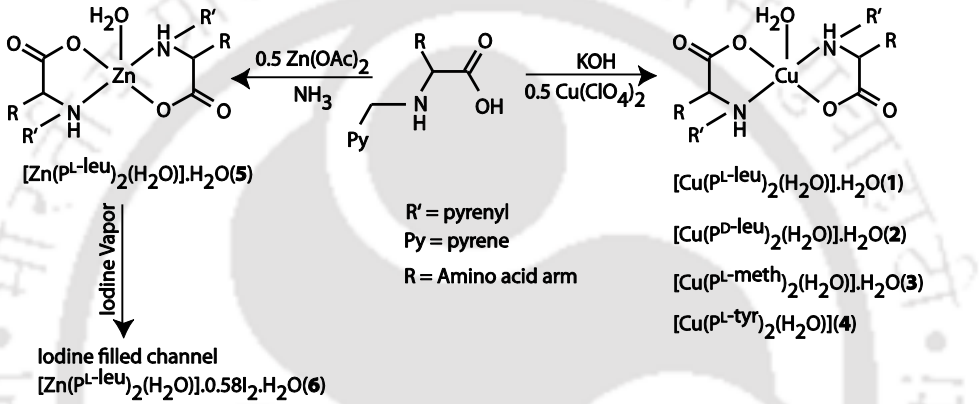

Scheme 7.2. *Synthetic scheme for complex synthesis and iodine filling in the channels.*

7.1 Experimental section

7.1.1 Materials and Methods

Solvents used were purified prior to use following standard literature procedure. $Zn(CH_3COO)_2.2H_2O$, KOH and NH_3 were brought from Merck limited and used as received.

The thermogravimetric analysis (TGA) of the compounds were performed using a Mettler Toledo SDTA 851e TGA thermal analyzer with heating rate of 5 ^oC per min under N_2 atmosphere using 5-10 mg sample per run. Other instruments and material sources have been described in earlier chapters.

Caution! *Perchlorate salts are potentially dangerous as explosives and should only be handled in small quantities, although we have worked with these ClO_4^- salts without any incident.*

7.2 Syntheses

7.2.1 $[Cu(P^{L\text{-}leu})_2(H_2O)].H_2O$ (1)

Ligand ($HP^{L\text{-}leu}$) (0.100g, 0.289 mmol) was deprotonated with KOH (0.016g, 0.285 mmol) in 25 mL MeOH as a result clear light yellow color solution after 30 min. A methanolic solution of $Cu(ClO_4)_2 \cdot 6H_2O$ (0.054g, 0.146 mmol) was added drop wise to the ligand with stirring. The color of the solution changed immediately to blue. The solution was stirred for 2 h and evaporated to dryness in a rotary evaporator. The resulting powder was blue in color and highly soluble in MeOH. Blue crystals were obtained by adding acetonitrile to this methanolic (1:6) solution within 2-3 days. Crystals were filtered and washed with diethyl ether. Yield: 44%. Anal. Calcd for $[Cu(C_{23}H_{22}NO_2)_2.H_2O].H_2O.(CH_3OH)_2$: C, 67.65; H, 6.62; N, 3.28; Found C, 67.28; H 5.91; N, 3.23. IR (KBr, cm^{-1}): $\nu(COO)_{asym}$ 1650(s). μ_{eff} (powder, 298K): 1.88 μ_B. Λ_M (ohm^{-1} cm^2 mol^{-1}): 12.35 (MeOH).

7.2.2 $[Cu(P^{D\text{-}leu})_2(H_2O)].H_2O$ (2)

This has been prepared following similar procedure described for **1** by using $HP^{D\text{-}leu}$ instead of $HP^{L\text{-}leu}$. Blue crystals were obtained by adding acetonitrile to this methanolic solution (1:6) within 4 days. Crystals were filtered and washed with diethyl ether. Yield: 44%. Anal. Calcd for $[Cu(C_{23}H_{22}NO_2)_2.H_2O].H_2O.(CH_3OH)_3$: C, 66.53; H, 6.84; N, 3.17; Found C, 66.64; H, 6.90; N, 3.12. IR (KBr, cm^{-1}): $\nu(COO)_{asym}$ 1652(s). μ_{eff} (powder, 298K): 1.79 μ_B. Λ_M (ohm^{-1} cm^2 mol^{-1}): 8.35 (MeOH).

7.2.3 $[Cu(P^{L\text{-}meth})_2(H_2O)] \cdot H_2O$ (3)

This was prepared by using the method described for **1** with the following quantity of the reagents: ($HP^{L\text{-}meth}$) (0.100g, 0.276 mmol), KOH (0.015g, 0.276 mmol) and $Cu(ClO4)_2 \cdot 6H_2O$ (0.051g, 0.138 mmol). Blue, rod shape crystals of **3** were grown by adding acetonitrile in to the methanolic solution (1:6) within 4 days. Crystals were filtered and washed with diethyl ether. Yield: 62%. Anal. Calcd for $[Cu(C_{22}H_{19}NO_2S)_2.H_2O].H_2O.(CH_3OH)_2$: C, 62.31; H, 5.68; N, 3.16; S, 7.23; Found C, 62.48; H, 5.53; N, 3.05; S, 7.15. IR (KBr, cm^{-1}): $\nu(COO)_{asym}$ 1643(s). μ_{eff} (power, 298K): 1.76 μ_B. Λ_M (ohm^{-1} cm^2 mol^{-1}): 13.57 (MeOH).

7.2.4 $[Cu(P^{L\text{-}Tyr})_2(H_2O)]$ (4)

This was prepared following the method described for **1** with the following quantity of the reagents: $HP^{L\text{-}Tyr}$ (0.100g, 0.253 mmol), KOH (0.014g, 0.253 mmol) and $Cu(ClO_4)_2 \cdot 6H_2O$ (0.053g, 0.144 mmol). Blue colored, tiny crystals were formed within 3 days. Crystals were filtered and washed with diethyl ether. Yield: 54%. Anal. Calcd for $[Cu(C_{26}H_{20}NO_3)_2 \cdot H_2O]CH_3OH$: C, 70.56; H, 5.14; N, 3.11; Found C, 70.14; H, 5.32; N, 3.30. IR (KBr, cm^{-1}): $\nu(COO)_{asym}$ 1646(s). μ_{eff} (powder, 298K): 1.84μ_B. Λ_M (ohm^{-1} cm^2 mol^{-1}): 1.84 (MeOH).

7.2.5 $[Zn(P^{L\text{-}leu})_2(H_2O)] \cdot H_2O$ (5)

Ligand $HP^{L\text{-}leu}$ (0.100 g, 0.289 mmol) was mixed with $Zn(CH_3COO)_2.2H_2O$ (0.014 g, 0.145 mmol) in 25 mL MeOH, which offered a light yellow color solution with suspension. Ammonia solution was added drop wise to the above solution with stirring, resulting solution became clear immediately. The solution was stirred for 2 h and heated on water bath to remove excess ammonia and after filtering kept it for crystallization. Light yellow crystals were obtained within 2-3 days. Crystals were filtered and washed with diethyl ether. Yield: 54%. Anal. calcd. for $[Zn(C_{23}H_{22}NO_2)_2.H_2O].H_2O$: C, 6.14; H, 70.02; N, 3.55; Found: C, 6.19; H 70.11; N, 3.59. IR (KBr, cm^{-1}): $\upsilon(COO)_{asym}$ 1642(s). Λ_M (ohm^{-1} cm^2 mol^{-1}): 0.4 (MeOH).

7.2.6 $[Zn(P^{L\text{-}leu})_2(H_2O)] \cdot 0.58I_2 \cdot H_2O$ (6)

Crystals of **5** (pale yellow, transparent as well as highly fluorescent) were dried at ~80 ºC under reduced pressure for 2 h, resulting no change in color or fluorescence property after drying. Dried crystals (50mg) in a vial along with solid I_2 in a separate vial were kept inside a round bottom flask (50 mL) containing dry silica gel to minimize moisture content. This setup was evacuated first and then warmed to 40–70º C for few minutes, since, complete removal air (moisture) as much as possible and heating ensured production of enough I_2 vapor to fill the void. The setup was kept in this way for five days to saturate the crystals with iodine and the resultant crystals became violet colored as well as non fluorescent and sealed in a glass capillary for X-ray diffraction studies. The I_2 content of the crystals was measured using titration (described below) and tallied with weight loss in TGA (10% wt loss between temperatures 50–130 ºC against calculated weight loss 1.9% for H_2O and remaining ~8% for I_2/monomer) (Figure **7.10**). We arrived at the above procedure after repeating the I_2 doping followed by titration experiments under various conditions. For X-ray diffraction, we did not wash the crystals to ensure that crystals stay saturated with I_2 and loss during X-ray experiment is minimized.

Estimation of I_2 in (6) Single crystals or coarsely ground crystals of **5** (~10-20 mg exactly weighted) were heated in water bath at 70 ºC under reduced pressure for 2 h and then were stored in a closed chamber containing I_2 crystals for 5 days. In this arrangement only iodine vapor can be absorbed in the crystal at room temperature. After 5 days, the samples were washed thoroughly with CCl_4 (three times) at room temperature to remove any I_2 absorbed on the surface of the crystals. The washed crystals were then put into the freshly distilled CCl_4 (~ 6 mL measured) and shaken vigorously. The CCl_4 solution became strongly pink-purple colored due to the released I_2. The I_2 concentration in CCl_4 solution was measured spectrophotometrically. I_2 estimated was found to be 7 % (calculated 15 % for complex $[Zn(P^{L\text{-}leu})_2(H_2O)]0.58I_2{\cdot}H_2O$**(6)**).

Note: *It is difficult to wash the surface only without losing some iodine from the channels as crystal binds iodine loosely. Further, crystals were colored even after release of iodine into CCl_4 for spectrophotometrical analysis indicates that it is not possible to complete recovery for estimation. The structure was done in a sealed tube without washing the crystals.*

7.3 X-ray Data Collection, Structure Solution and Refinement

Crystals of the complexes $[Cu(P^{L\text{-}leu})_2(H_2O)].H_2O$ (**1**), $[Cu(P^{D\text{-}leu})_2(H_2O)].H_2O$ (**2**), $[Cu(P^{L\text{-}meth})_2(H_2O)]{\cdot}H_2O$ (**3**), $[Zn(P^{L\text{-}leu})_2(H_2O)]{\cdot}H_2O$ (**5**), $[Zn(P^{L\text{-}leu})_2(H_2O)]{\cdot}0.58I_2{\cdot}H_2O$ (**6**) obtained during synthesis were used for X-ray analysis. Single crystal of **6** was obtained by filling of iodine into crystals of **5** by iodine vapor diffusion in vacuum desiccator. The crystals were mounted on glass fiber. Crystal **6** was mounted in sealed capillary tube. Details of instrumental setup, data collection and solution were as reported in Chapter **2**. Selected crystallographic data have been summarized in table **7.1**.

Table 7.1 Selected crystallographic data for the complexes

	1	**2**	**3**	**5**	**6**
empirical formula	$C_{46}H_{45}CuN_2O_7$	$C_{46}H_{43}CuN_2O_6$	$C_{44}H_{41}CuN_2O_6S_2$	$C_{46}H_{45}N_2O_6Zn$	$C_{46}H_{45}I_{0.58}N_2O_6Zn$
fw	801.39	783.36	821.45	787.21	850.75
T(K)	296(2)	296(2)	296(2)	296(2)	296(2)
Wavelength(Å)	0.71073	0.71073	0.71073	0.71073	0.71073
Crystal system	monoclinic	monoclinic	monoclinic	monoclinic	monoclinic
Space group	$P2_1$	$P2_1$	$P2_1$	$P2_1$	$P\ 2_1$
a, Å	13.9814(3)	13.9649(5)	14.1689(5)	13.9988(17)	14.1793(12)
b, Å	9.3718(2)	9.3895(3)	9.4920(4)	9.2734(10)	9.3043(7)
c, Å	16.4166(3)	16.2961(6)	15.8906(5)	16.324(2)	16.3431(13)
α, deg	90.00	90.00	90.00	90.00	90.00
β, deg	103.0570(10)	103.398(2)	109.234(2)	103.118(9)	103.332(5)
γ, deg	90.00	90.00	90.00	90.00	90.00
V, Å^3	2095.47(7)	2078.65(13)	2017.85(13)	2063.8(4)	2098.0(3)
z/ρ	2/1.270	2/1.252	2/1.352	2/1.267	2/ 1.347
μ	0.573	0.574	0.695	0.645	1.061
coll. reflns	10003	8322	7280	3880	4709
indep reflns	7515	5917	4412	2569	2755
FLACK para.	-0.013(14)	0.026(12)	0.005(16)	0.00(2)	0.07(3)
GOF	1.001	1.036	1.052	1.070	1.047
R1[a]	0.0574	0.0506	0.0537	0.0413	0.0512
wR2[a]	0.1454	0.1223	0.1136	0.1003	0.1171
R1[b]	0.0786	0.0741	0.1082	0.0496	0.0649
wR2[b]	0.1598	0.1323	0.1334	0.1060	0.1241

[a] $I>2\sigma$. [b] All data

Table 7.2 Selected bond length (Å) and angles (°) for the Cu(II) and Zn(II) complexes

	1	**2**	**3**	**5**	**6**
Cu/Zn-N1	2.036(3)	2.039(3)	2.044(3)	2.082(6)	2.122(6)
Cu/Zn-N2	2.041(3)	2.037(3)	2.030(3)	2.118(6)	2.121(7)
Cu/Zn-O1	1.955(3)	1.962(3)	1.948(4)	2.082(6)	2.091(7)
Cu/Zn-O3	1.935(3)	1.939(3)	1.912(4)	2.030(6)	2.028(7)
Cu/Zn-O5	2.223(3)	2.229(3)	2.244(4)	1.987(6)	1.987(6)
N1-Cu/Zn-O1	82.30(13)	82.76(13)	82.80(2)	79.9(3)	80.1(3)
O1-Cu/Zn-N2	94.65(13)	93.97(13)	95.25(17)	91.9(3)	92.6(3)
N2-Cu/Zn-O3	83.98(13)	84.11(13)	85.18(18)	81.0(3)	81.0(3)
O3-Cu/Zn-N1	95.61(13)	95.68(13)	94.31(18)	95.9(3)	95.0(3)
O5-Cu/Zn-O1	100.44(12)	99.77(11)	99.13(15)	106.4(2)	105.4(3)
O5-Cu/Zn-O3	89.19(13)	89.84(12)	89.36(15)	93.1(2)	94.3(3)
O5-Cu/Zn-N1	100.91(11)	100.99(11)	101.60(14)	107.3(2)	106.8(3)
O5-Cu/Zn-N2	99.77(13)	99.83(12)	95.37(15)	106.4(2)	106.3(3)
O1-Cu/Zn-O3	170.37(14)	170.38(14)	171.40(17)	160.4(2)	160.2(3)
N1-Cu/Zn-N2	159.30(12)	159.17(12)	163.01(15)	146.3(3)	146.9(3)
τ	0.186	0.1863	0.1398	0.2353	0.2216
H-bonding					
O1…O5	2.883	2.880	2.866	2.736	2.769
O2…O6	2.923	2.931	2.946	2.870	2.851
O4…O5	2.686	2.688	2.702	2.633	2.601
O3…O6	2.784	2.790	2.770	2.771	2.783
N2…S2			3.205		
I2…O6					3.359

7.4 Results and discussion

7.4.1 Synthesis and selected properties

The complexes $[Cu(P^{L\text{-}leu})_2(H_2O)].H_2O$ (**1**), $[Cu(P^{D\text{-}leu})_2(H_2O)].H_2O$ (**2**), $[Cu(P^{L\text{-}meth})_2(H_2O)].H_2O$ (**3**), $[Cu(P^{L\text{-}Tyr})_2(H_2O)]$ (**4**) were synthesized using the $HP^{L\text{-}leu}$, $HP^{D\text{-}leu}$, $HP^{L\text{-}meth}$, $HP^{L\text{-}tyr}$ with KOH and $Cu(ClO_4)_2.6H_2O$ in the ratio of 2:2:1 in methanol and recrystallized by adding acetonitrile for **1**, **2**, **3**, **4**. The complex $[Zn(P^{L\text{-}leu})_2(H_2O)]\cdot H_2O$ (**5**) was synthesized by using $HP^{L\text{-}leu}$ and $Zn(CH_3COO)_2.2H_2O$ in the ratio 2:1 in addition to adding few drops of ammonia immediately to complete the deprotonation. The complex $[Zn(P^{L\text{-}leu})_2(H_2O)]\cdot 0.58I_2\cdot H_2O$ (**6**) obtained by iodine vapor diffusion in the desiccator, into the crystals of **5**. The carboxylate stretches were observed at ~ 1640–1650 and at ~1380 cm^{-1} for ν_{assym} and ν_{sym} respectively.[3] The elemental analyses support the formulation of the complexes. The non-electrolytic nature of the complexes was confirmed by conductance measurement in MeOH.[4] The room temperature magnetic moment of the complexes **1**, **2, 3** and **4** are 1.88, 1.79, 1.76 and 1.84 μ_B respectively closer to the spin only value of 1.73 for Cu(II) expected for mononuclear complexes.[5] The presence of water of crystallization in **1** and **5** was confirmed by thermo gravimetric analysis (TGA) (Figure **7.10**). The TGA of **1** and **5** shows loss of 2.3 and 2.5 % weight respectively between 45–80ºC against calculated weight loss of 2.2 % for one H_2O as solvent of crystallization.

7.4.2 X-ray Structural features of $[Cu(P^{L\text{-}leu})_2(H_2O)].H_2O$(1) and $[Cu(P^{D\text{-}leu})_2(H_2O)].H_2O$(2)

The complexes **1** and **2** were crystallized in the space group $P2_1$ with two independent mononuclear units in the unit cell. The ORTEP figure of one of the monomers unit, selected bond lengths and angles for both complexes are given in figure **7.1, 7.2** and table **7.2** respectively. All the complexes are monomeric in nature with slightly distorted (τ 0.1–0.2) square pyramidal geometry around the Cu(II) (Table **7.2**). The amount of distortion parameter τ was calculated from the structural data where the value of τ should be 0.0 for perfect square-pyramidal geometry and 1.0 for perfect trigonal bipyramidal (TBP) structure.[6] In **1**, conformation at the chiral carbon is *S* as the amino acid used in synthesis was *S* isomer. In addition to the asymmetric carbon center in the ligand, the coordination of amine N to the Cu(II) gives rise to an asymmetric secondary nitrogen atom which has the *R* configuration. This phenomenon of opposite conformation preference at chiral carbon and amine N has been observed in all the characterized complexes of this ligand.[7,8] While for **2**, conformation at the

chiral carbon is *R* as the amino acid used in synthesis was *R* isomer and at N is *S* conformation.

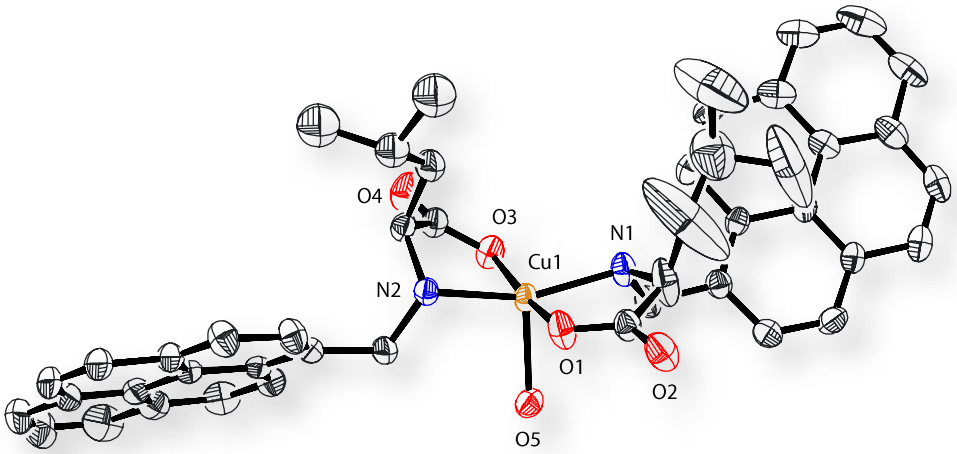

Figure 7.1. *ORTEP diagram for complex **1** with thermal ellipsoids set to 50% probability, solvent molecule and hydrogen atoms are omitted for clarity.*

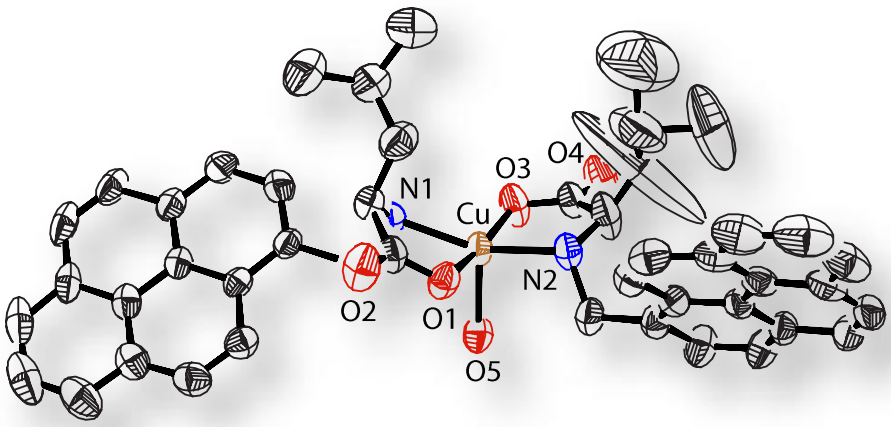

Figure 7.2. *ORTEP diagram for complex **2** with thermal ellipsoids set to 50% probability, solvent molecule and hydrogen atoms are omitted for clarity*.

The in-plane bond lengths for Cu–$O_{carboxylate}$ are within the range 1.92–1.95 Å observed for other amino acid or amino acid derived ligand Cu(II) complexes.[9] The in-plane bond lengths for Cu–N_{amine} are longer at ~2.04 Å compared to corresponding amino acid complexes (1.96–1.98 Å).[9] The axial fifth coordination is provided by a water molecule with short Cu–O distance of 2.223(3) Å and 2.229(3) Å for **1** and **2** respectively (Figure **7.2**, Table

7.2). The axial bond in square-pyramidal Cu(II) is usually long and varies between 2.12 to 2.6 Å for O or N coordination, due to Jahn-Teller distortion.[10]

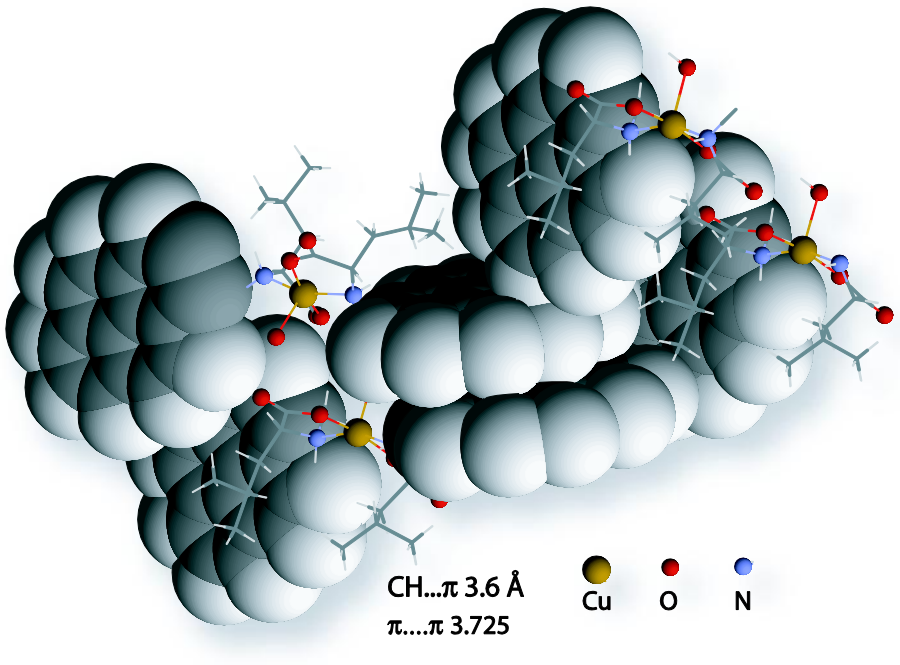

Figure 7.3. *A partial space filling model of complex **1** showing π...π as well as CH...π interactions of pyrene rings within the crystal lattice.*

One prominent feature of structure is the H-bond between axially bound oxygen and another asymmetric unit of leucine carboxylate groups of another monomeric unit with a O5…O4 bond distance of ~2.686 Å and O5...O1 bond distance ~2.880 Å (Figure **7.1**). The usual O…O H-bond distances lies between 2.74 to 3.004 Å.[11] The presence of two isopropyl arm of leucine influenced the coordination of water on the other side and this in turn must have influenced the hydrophobic pyrene moieties to rotate apart. A water molecule as solvent of crystallization was trapped between carboxylate groups of leucine through three centres two H-bond with a bond distances O2…O6 ~2.923 Å and O3…O6 ~2.784 Å. Crystal packing shows pyrene ring –CH to ring π cloud interaction distance ~3.6 Å and C–H...π angle 166.15°, pyrene ring to ring distance of 3.725 Å (Figure 7.3) are within the usual interaction distance range of π....π 3.4–3.8 Å and CH...π range bond length is at the higher values of the accepted distance range (2.5–2.9 Å).[12] Overall, structural feature is a clear separation of hydrophilic and hydrophobic part within the crystal lattice.

7.4.3 X-ray Structural features of $[Cu(P^{L\text{-}meth})_2(H_2O)]\cdot H_2O$ (3)

The complex **3** is a mononuclear Cu(II) complex with N_2O_3 coordination environment and crystallized in the space group $P2_1$. The perspective view of the complex **3** has shown as ORTEP diagram in figure **7.4**. The coordination geometry around the copper center in **3** is slightly distorted square pyramidal geometry (τ = 0.1398) with four of the in-plane, *trans* N_2O_2 coordination from ligand, similar to that in **1** and **2**, and rest of the fifth axial coordination occupied by a water molecule. The crystallographic data, bond lengths and angles are well within expected limits which are summarized in table **7.1** and **7.2**.

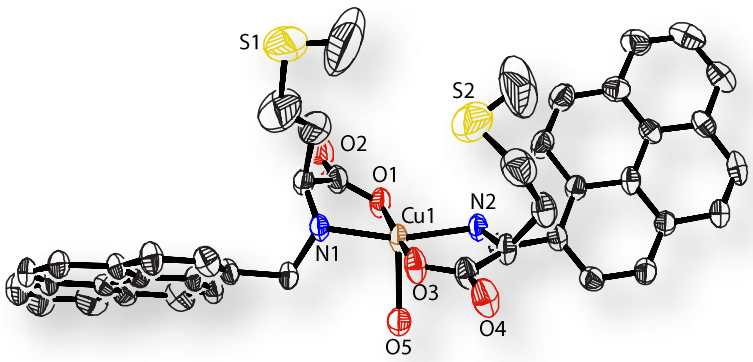

Figure 7.4. *ORTEP diagram for complex **3** with thermal ellipsoids set to 50% probability, solvent molecule and hydrogen atoms are omitted for clarity.*

A recent single X-ray crystallographic study of *Desulfovibrio africanus* ferredoxin I shows N-H···S contacts that conform to Donahue's criteria for hydrogen bonding in which significant N···S distances are confined to range 3.25–3.55 Å, with H-bond angles that deviate by less than 25° from 180°.[13,14]

Complex **3** displays the interesting feature is the additional intra-molecular H-bond between one of the sulfur atom containing methionine arm and the asymmetric secondary nitrogen atom of amine N–H, coordinated to the Cu(II) (Figure **7.5**). The N2···S2 H-bond distance of 3.205 Å, with H-bond angle 129.78° (50.22° deviation from 180°) is shorter than usual N···S H-bond distance range of 3.25–3.55 Å, resulting, methionine arm pulled towards in-plane rather than another arm (4.877 Å).[15,16] Another arm remain gratis from H-bonding, this is the prominent reason of compensation behind slightly less distortion (τ = 0.1398) from square pyramidal geometry than complex **1** and **2** (τ = 0.186, 0.1863). Remaining structural features and hydrogen bonding pattern are similar as complexes **1** and **2**.

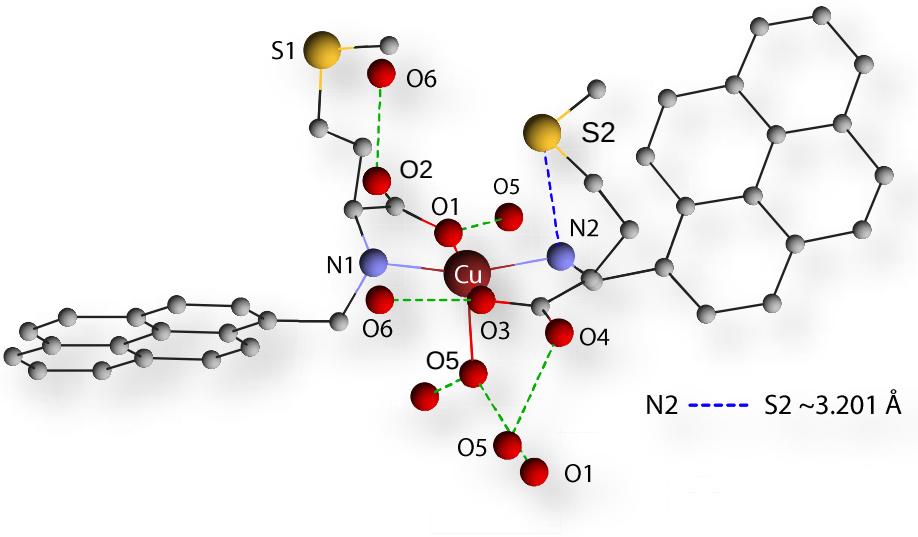

Figure 7.5. *H-bonding pattern of complex **3** with significant N2…S2 H-bonding distance of ~3.2 Å*

7.4.4 X-ray Structural features of $[Zn(P^{L\text{-}leu})_2(H_2O)]\cdot H_2O$ (5) and $[Zn(P^{L\text{-}leu})_2(H_2O)]\cdot 0.58I_2\cdot H_2O$ (6)

The complex **5** was crystallized in the space group of $P2_1$. The ORTEP diagram, selected bond lengths and angles are given in figure **7.6** and table **7.2**. The Zn(II) in **5**, coordinated with four of the in-plane coordination from ligand and the fifth coordination filled with a water molecule. Unlike **1** and **2**, the more distortion towards TBP is significant with a τ value of 0.2353.

The in-plane bond lengths for $Zn–O_{carboxylate}$ are Zn–O1 2.082(6) Å and Zn–O3 2.030(6) Å which has slightly longer bond length than Cu(II) complexes **1**, **2**, **3**. The in-plane bond lengths for $Zn–N_{amine}$ are Zn–N1 2.082(6) Å and Zn–N2 2.118(6) Å. The axial fifth coordination is provided by a water molecule with shorter Zn–O distance of 1.987(6) Å than **1**, **2** and **3** (Table **7.2**). The Zn–O1/N1 bond distances are within comparable range found in square-pyramidal Zn(II) complexes.[10e] The rest of the structural parameters, features are same as **1** and **2** except the shorter H-bond distance between O1...O5 2.736 Å (Table **7.2**).

The complex **6** has iodine in the channel and crystallized in the space group of $P2_1$. The ORTEP diagram, selected bond lengths and angles are given in figure **7.7A** and table **7.2**. Structural parameters, bond lengths and bond angles similar to complex **5**. Like **5** significant distortion with a τ value of 0.2216. One atom (I2) in the iodine molecule is disordered with occupancy 0.58 in the unit cell, and forms H-bond with water (solvent as crystallization), H-bond length I2...O6 3.359 Å (Figure **7.7B**). The high molecular weight iodine is unlikely to

be mistaken with any other atom. The I–I distance matches with that of molecular iodine (2.614 Å).

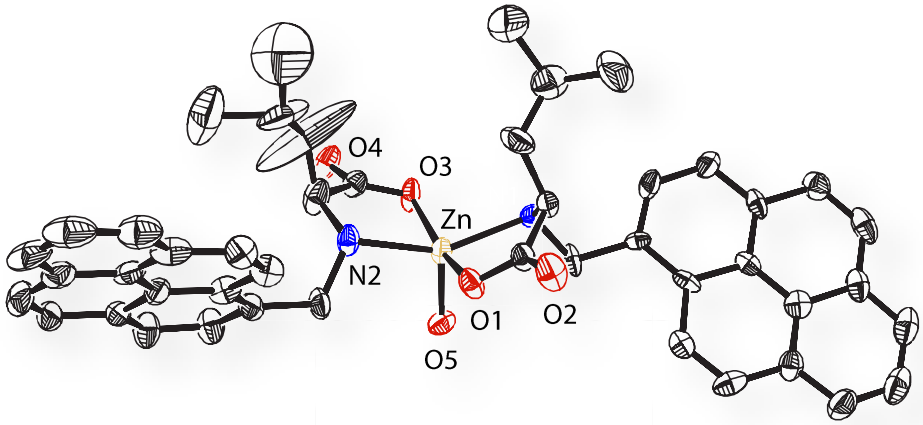

Figure 7.6. *ORTEP diagram for complex **5** with thermal ellipsoids set to 50% probability, solvent molecule and hydrogen atoms are omitted for clarity.*

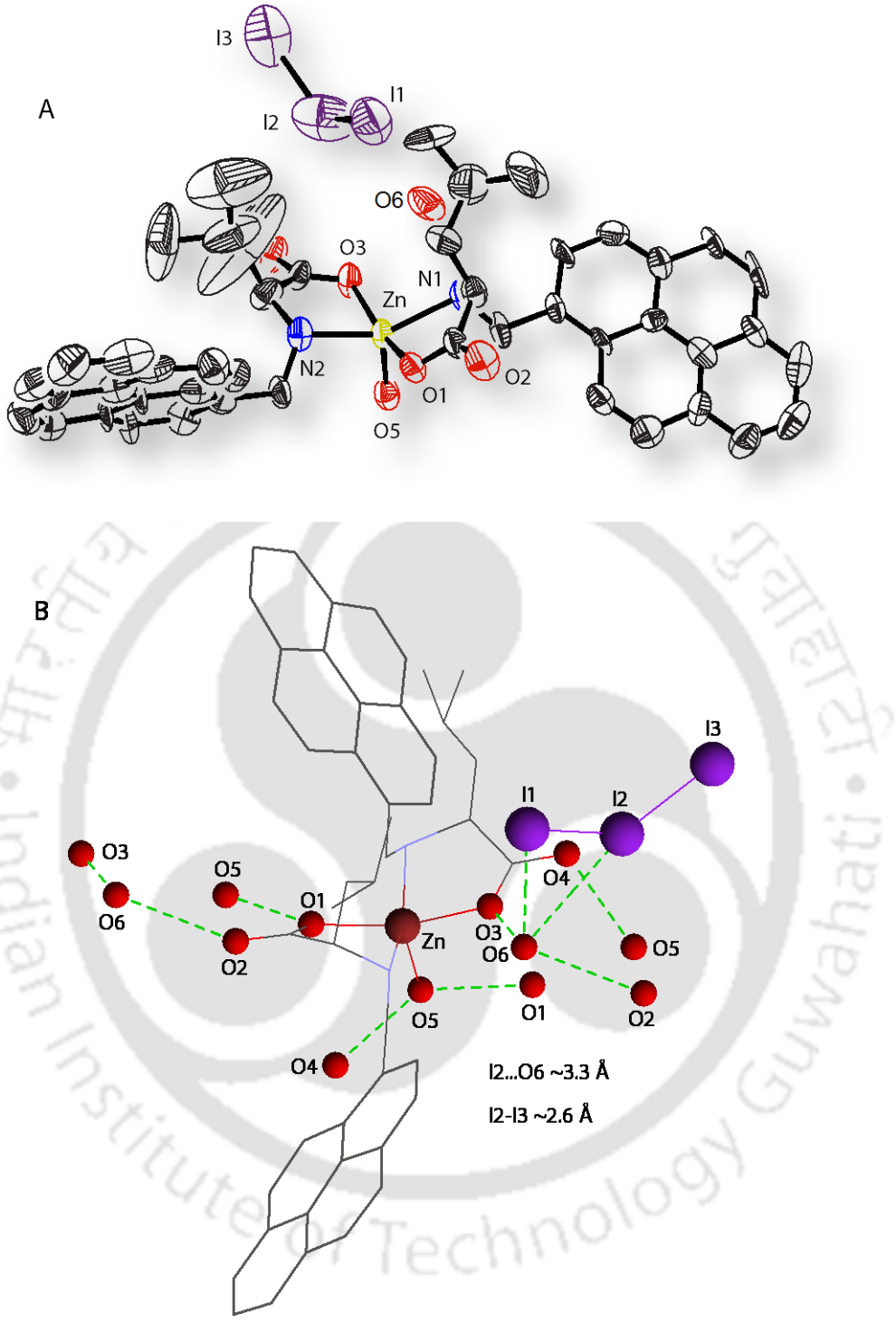

Figure 7.7 *(A) ORTEP diagram for complex **6** with thermal ellipsoids set to 50% probability, solvent molecule and hydrogen atoms are omitted for clarity, where molecular iodine occupancy 0.58 with one disordered atom I1. (B) Hydrogen bonding pattern in complex **6**, where one of the atom (I2) of molecular iodine H-bonded (I2…O6 ~3.3 Å) to water molecule as well as iodine bond length within the range (I2–I3 ~2.6 Å).*

7.5 Formation of Channel and refilling with iodine

All the pyrene derived amino acid complexes form a two dimensional void channel within the crystal lattice (Figure **7.8A**). The dimensions of the channels (a cuboid space approximately 4.8x11.4x12.4 $Å^3$) are larger than those observed earlier by us in a iron(III) complex with L-histidine derived ligand.[7b] Thus, we decided to choose complex **5** for the filling with molecular iodine, because crystals of **5** were transparent, light yellow colored as well as highly fluorescent blue color under UV lamp.

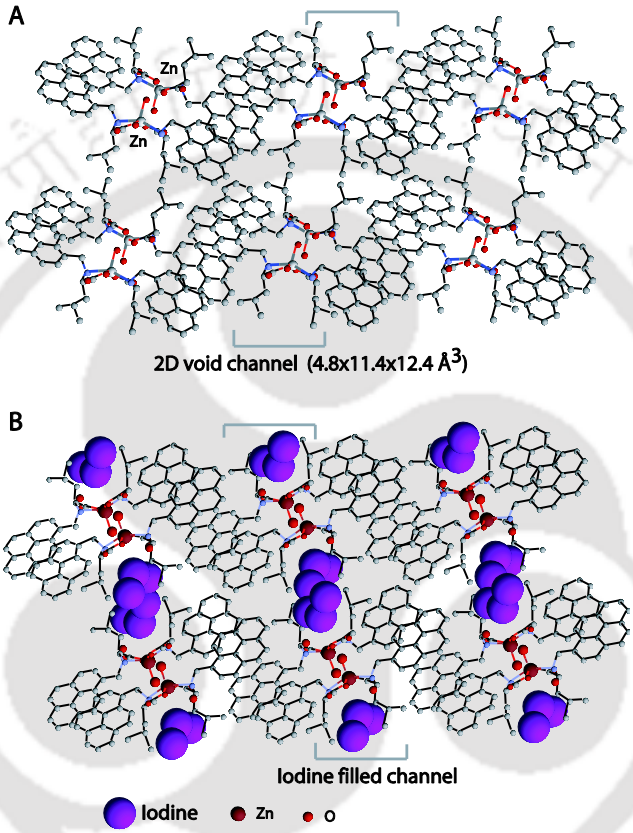

Figure 7.8. *(A) Complex **5** form a two dimensional void channel within the crystal lattice. (B) Iodine filled the two dimensional channel, one I_2 molecule with one asymmetric unit.*

To check, if small molecules can be inserted in the channel, we exposed the crystals of **5** to I_2 vapours in a closed container for 5 days and structurally characterized **6**. The structural parameters of **6** are almost identical with that of **5** (Table **7.2**). The structure of **6** shows that one atom of I_2 molecule (disordered) per mononuclear complex has been incorporated into the channel (Figure **7.8B**). The iodine to solvent of crystallization water oxygen distances (I2–O6 3.359 Å) shows that one end of the I_2 is within weak interaction distances of solvent of crystallization (O6) of one molecule (Figure **7.7B**). Weak polar

interaction of one end of iodine with water inside a crystal have been observed previously[17,18] and only one example of iodine with both side interactions.[7b] I_2 molecules inside a channel orients in a helical fashion (Figure **7.9A**).

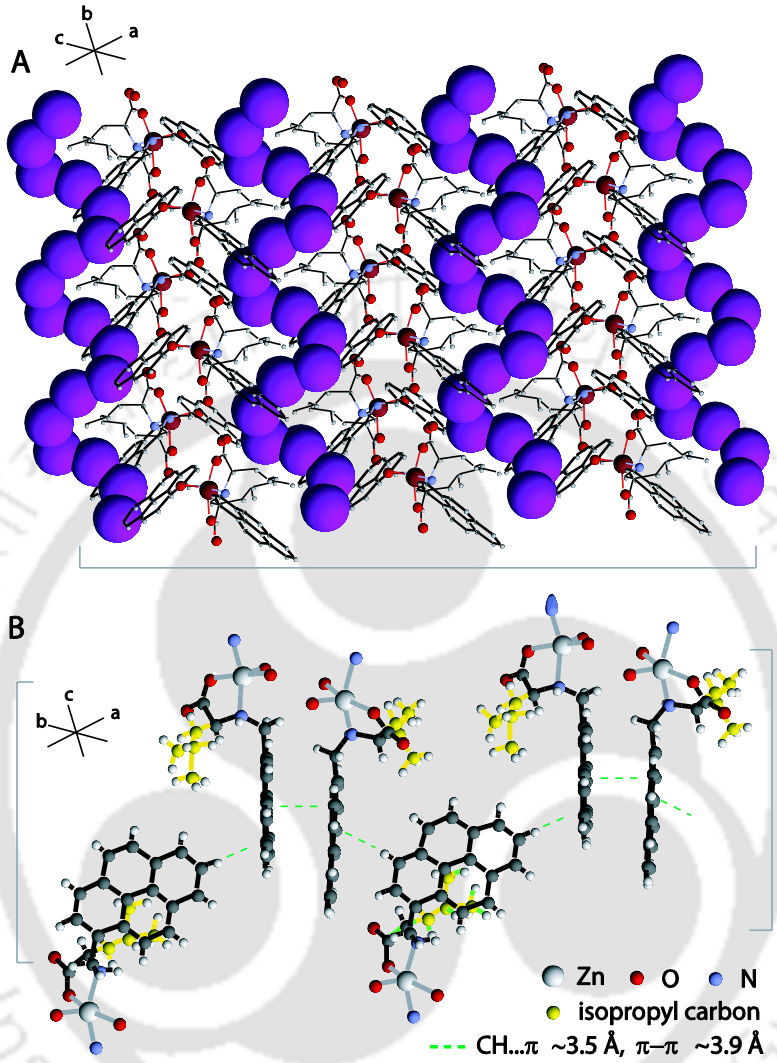

Figure 7.9. *(A) I_2 molecules inside channel of **6** orients in a helical fashion (Left handed). (B) Dimer formation through π...π stacking and CH...π interaction in the complex **5**.*

All the complexes have well defined intermolecular weak interactions of pyrene π-cloud as shown in figure **7.9B**. The solid state fluorescence of complex **5** forms exclusively excimer at ~450 nm which also supports the lattice arrangement of pyrene ring as dimer (Figure **7.9B)**.

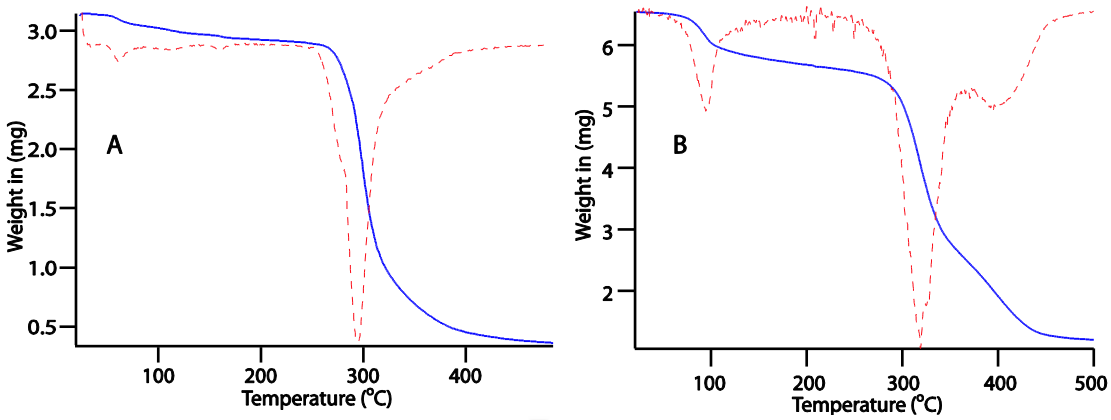

Figure 7.10. *TGA plot (blue line) with respective derivative (DTA) plot (red dotted lines) (A) for the complex **5** and (B) for complex **6**.*

The intactness of I_2 in crystals of **6** were confirmed from their visible spectra in CCl_4.[19] The I_2 content of **6** estimated to be (syntheses section **7.2**) 7% as opposed to calculated value of 15% for $[Zn(P^{L\text{-}leu})_2(H_2O)]\cdot 0.58I_2\cdot H_2O$ (**6**). Considering the fact that I_2 molecules are weakly bound and repeated washings might wash away some of the I_2 molecules from the channel, we assume that the channels have around half of the iodine sites filled with I_2. As the crystals were colored after washings and extraction thus, it is not possible to complete release of iodine from channel. These experiments also confirm that the I_2 incorporated in the channel retains its chemical identity.

7.6 Absorption Spectra and EPR spectral characteristics

The UV-visible and EPR spectral characteristic data of appropriate complexes in MeOH are given in table **7.3** and the spectra figure of **1, 2, 3** and **4** are shown in figure **7.11** & **7.12**. The absorption maxima between 580–590 nm with ε value ~140–185 $dm^3\ mol^{-1}cm^{-1}$ is of ligand field origin. Several other square-pyramidal Cu(II) complexes with N/O donor environment have similar spectral characteristics.[20,21] The spectral characteristics of **1**, **2**, **3** and **4** are almost identical. The absorption maxima between 350–235 nm is the characteristics of pyrene derived ligand.

The EPR spectral characteristic of the complexes **1**, **2**, **3** and **4** are shown in figure **7.12** and the data in methanol at 77 K are shown in table **7.3**. The complexes **1**, **2**, **3** and **4** shows a typical square pyramidal EPR spectra as is evident from their $A_{\parallel}$ values ~178G and g values.[22]

Table 7.3 UV-Visible and EPR data of complexes in MeOH at 77K

Complex	λ[nm] (ε, $M^{-1}cm^{-1}$)	EPR, $g_{\parallel}$, $g_{\perp}$	$A_{\parallel}$/G
1	590(182), 343(119300), 327(91500), 315(sh), 276(148300), 266(90200), 257(sh), 242(226000), 236(sh)	2.249, 2.049	179
2	588(175), 343(78700), 327(60200), 315(sh), 276(98300), 266(59800), 257(sh), 242(151800), 236(sh)	2.247, 2.037	178
3	585(147), 344(98100), 328(75200), 315(sh), 277(11800), 266(73800), 258(sh), 243(182700), 236(sh)	2.246, 2.059	181
4	590(159), 344(56600), 329(42200), 316(sh), 277(72500), 266(45400), 258(sh), 243(103000), 235(sh)	2.255, 2.051	178

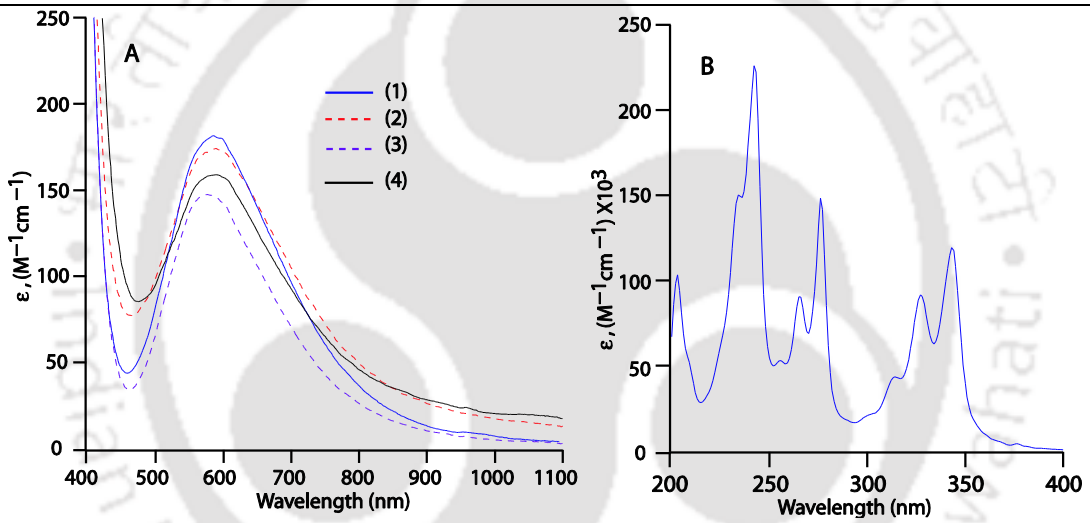

Figure 7.11. *(A) UV-Visible spectra of complexes **1**, **2**, **3**, **4** and (B) UV-Visible spectra of complex **1** in MeOH.*

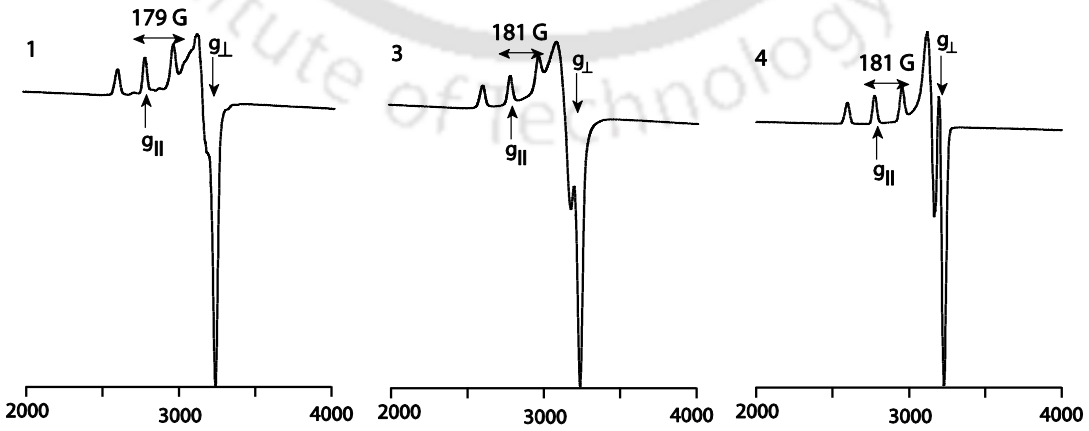

Figure 7.12. *EPR spectra of the complexes 1, 3, 4 in methanol at 77K.*

Conclusions

In conclusion, we have synthesized a reusable enantiopure solid with two dimensional helical void channel (11–12 $Å^3$ diameters). The presence of complementary H-bond donor (amine) and acceptor (carboxylato) in the same ligand as well as π–π stacking and CH–π interaction contributed to the robustness of the crystal. Also helical arrangement of weak interaction capable group (carboxylato, water) inside a channel strongly influences the guest organization, a concept behind the use of channels for chiral separation[23] or template[23].

References

1. Pyrene sensor and importance of complexes. (a) Winnik, F. M. *Chem. Rev*. **1993**, *93*, 587. (b) Krämer R. *Angew. Chem., Int. Ed.* **1998**, *37*, 772. (c) Yamauchi, O.; Odani, A.; Takani, M. *J. Chem. Soc., Dalton Trans.* **2002**, 3411. (d) Janiak, C. *J. Chem. Soc., Dalton Trans*. **2000**, 3385. (e) Suezawa, H.; Yoshida, T.; Umezawa, Y.; Tsuboyama S.; Nishio, M. *Eur. J. Inorg. Chem.* **2002**, 3148. (f) (i) Poulos, T. L.; Finzel, B. C.; Howard, A. J. *J. Mol. Biol.* **1987**, *195*, 687. (ii) Crane, B. R.; Arvai, A. S.; Gachhui, R.; Wu, C.; Ghosh, D. K.; Getzoff, E. D.; Stuehr, D. J.; Tainer, J. A. *Science* **1997**, *278*, 425. (iii) Sellmann, D.; Soglowek, W.; Knoch, F.; Moll, M. *Angew. Chem., Int. Ed. Engl.* **1989**, *28*, 1271. (iv) Carter, C. W. Jr. *J. Biol. Chem.* **1977**, *252*, 7802. (v) Novoa, J. J.; Rovira, M. C.; Rovira, C.; Veciana, J.; Tarre´s, J. *Adv. Mater*. **1995**, *7*, 233.

2. Amino acid Zn complexes, porous channels importance (a) Doyle, D. A.; Cabral, J. M.; Pfuetzner, R. A.; Kuo, A.; Gulbis, J. M.; Cohen, S. L.; Chait, B. T. MacKinnon, R. *Science* **1998**, *280*, 69. (b) de Groot, B. L.; Engel, A.; Grubmüller, H. *J. Mol. Biol.* **2003**, *325*, 485. (c) de Groot, B. L.; Grubmüller, H. *Science* **2001**, *294*, 2353. (d) Sui, H.; Han, B. G.; Lee, J. K.; Walian, P.; Jap, B. K. *Nature* **2001**, *414*, 872. (e) Perutz, M. F.; Finch, J. T.; Berriman, J.; Lesk, A. *Proc. Natl. Acad. Sci. USA* **2002**, *99*, 5591. (f) Chang, G.; Spencer, R. H.; Lee, A. T.; Barclay, M. T.; Rees, D. C. *Science* **1998**, *282*, 2220. (g) Fu, D.; Libson, A.; Miercke, L. J. W.; Weitzman, C.; Nollert, P.; krucinski, J.; Stroud, R. M. *Science* **2000**, *290*, 481. (h) Davis, M. E. *Nature* **2002**, *417*, 813. (i) Ikkala, O.; ten Brinke, G. *Science* **2002**, *295*, 2407. (j) Ikegame, M.; Tajima, K.; Aida, T. *Angew. Chem., Int. Ed.* **2003**, *42*, 2154. (k) Kitaura, R.; Kitagawa, S.; Kubota, Y.; Kobayashi, T. C.; Kindo, K.; Mita, Y.; Matsuo, A.; Kobayashi, M.; Chang, H. C.; Ozawa, T. C.; Suzuki, M.; Sakata, M.; Takata, M. *Science* **2002**, *298*, 2358. (l) Abrahams, B. F.; Moylan, M.; Orchard, S. D.; Robson, R. *Angew. Chem., Int. Ed.*

2003, *42*, 1848. (m) Herges, R.; Deichmann, M.; Wakita, T.; Okamoto, Y. *Angew. Chem., Int. Ed.* **2003**, *42*, 1170. (n) Zhao, B.; Cheng, P.; Dai, Y.; Cheng, C.; Liao, D. Z.; Yan, S. P.; Jiang, Z. H.; Wang,G. L. *Angew. Chem., Int. Ed.* **2003**, *42*, 934. (o) Xu, X.; Nieuwenhuyzen, M.; James, S. L. *Angew. Chem., Int. Ed.* **2002**, *41*, 764. (p) Coleman, A. W.; Da Silva, Nouar, E.; F.; Nierlich, M.; Navaza, A. *Chem. Commun.* **2003**, 826. (q) Dalrymple, S. A.; Shimizu, G. K. H. *Chem. Commun.* **2002**, 2224. (r) Kniep, R.; Will, H. G.; Boy, I.; Röhr, C. *Angew. Chem., Int. Ed.* **1997**, *36*, 1013. (s) Noord, A. D. C. V.; Kampf, J. W.; Pecoraro, V. L. *Angew. Chem., Int. Ed.* **2002**, *41*, 4668. (t) Woods, C. R.; Benaglia, M.; Cozzi, F.; Siegel, J. S. *Angew. Chem., Int. Ed.* **1996**, *35*, 1830. (u) Custelcean, R.; Ward, M. D. *Angew. Chem., Int. Ed.* **2002**, *41*, 1724. (v) Wu, C. D.; Lu, C. Z.; Lin, X.; Wu, D. M.; Lu, S. F.; Zhuang, H. H.; Huang, J. S. *Chem. Commun.* **2003**, 1284. (w) Smithson, R. J.; Kilner, C. A.; Brough, A. R.; Halcrow, M. A. *Polyhedron* **2003**, *22*, 725. (x) Hasenknopf, B.; Lehn, J. M.; Kneisel, B. O.; Baum, G.; Fenske, D. *Angew. Chem., Int. Ed.* **1996**, *35*, 1838. (y) Petitjean, A.; Cuccia, L. A.; lehn, J. M.; Nierengarten, H.; Schmutz, M. *Angew. Chem., Int. Ed.* **2002**, *41*, 1195. (z) Hertzsch, T.; Budde, F.; Weber, E.; Hulliger, J. *Angew. Chem., Int. Ed.* **2002**, *41*, 2281.

3. Nakamoto, K. Infrared and Raman Spectra of Inorganic Compounds, 5th ed.; Willey Interscience: New York, 1997; Part B.
4. Geary, W. J. *Coord. Chem., Rev.* **1971**, *7*, 81.
5. (a) Earnshaw, A. Introduction to Magnetochemistry; Academic Press: London, 1968. (b) Figgis, B. N.; Lewis, J. P. *Inorg. Chem*. **1964**, *6*, 37.
6. Addision, A.W.; Rao, T. N. Reedijk, J.; Rijn, J. V.; Verschoor, G. C. *J. Chem. Soc. Dalton Trans*. **1984**, 1349.
7. (a) Alam, M. A.; Nethaji, M.; Ray, M. *Angew. Chem., Int. Ed*. **2003**, *42*, 1940. (b) Alam, M. A.; Nethaji, M.; Ray, M. *Inorg. Chem.* **2005**, *44*, 1302. (c) Alam, M. A.; Koner, R. R.; Das, A.; Nethaji, M.; Ray, M. *Cryst. Growth. Des.* **2007**, *7*, 1818. (d) Sahoo, S. C.; Ray, M. *Dalton Trans.* **2009**, 3230.
8. (a) Ranford, J. D.; Vittal, J. J.; Wu, D. *Angew. Chem., Int. Ed.* **1998**, *37*, 1114. (b) Ranford, J. D.; Vittal, J. J.; Wu, D.; Yang, X. *Angew. Chem., Int. Ed.* **1999**, *38*, 3498. (c) Sreenivasulu, B.; Vittal, J. J. *Angew. Chem., Int. Ed.* **2004**, *43*, 5769. (d) Ganguly, R.; Sreenivasulu, B.; Vittal, J. J. *Coord. Chem. Review* **2008**, *252*, 1027. (e) Sreenivasulu, B.; Vittal, J. J. *Inorg. Chim. Acta* **2009**, *362*, 2735. (f) Ma, X. F.; Tian, J. L.; Gu, W.; Gao, S.; Yan, S. P.; Liao, D. Z. *Inorg. Chem. Commun.* **2008**, *11*, 256.

9. Structures of Cu(II) complexes with pure amino acids used in this work: (a) McAuliffe, C. A.; Quagliano, J. V.; Vallarino, L. M. *Inorg. Chem*. **1966**, *5,* 1996. (b) Helm, D. V. D.; Franks, W. A. Acta. Crystallogr., *Sect. B* **1969**, *25*, 451. (c) Stephens, F. S.; Vagg R. S.; Willams, P. A. *Acta. Crystallogr., Sect. B*, **1975**, *31*, 841. (d) Ou, C.; Powers, D. A.; Thich, J. A.; Felthouse, T. R.; Hendrickson, D. N.; Potenza, J. A.; Schugar, H. J. *Inorg. Chem*. **1978**, *17*, 34. (e) Hitchman, M. A.; Kwan, L. *J. Chem. Soc., Dalton Trans*. **1987**, 457 (f) Rizzi, A. C.; Piro, O. E.; Castellano, E. E.; Nascimento, O. R.; Brondino, C. D. *Inorg. Chim. Acta* **2000**, *305*, 19.
10. (a) Hathaway, B. J. in *Comprehensive Coordination Chemistry*, ed Wilkinson, G.; Gillard, R. D.; McCleverty, J. A. Pergamon Press, London, **1987**, vol. *5,* p. 533. (b) Addison, A. W.; Sinn, E. *Inorg. Chem*. **1983**, *22*, 1225. (c) Bonamico, M.; Dessy, G.; Mugnoli, A.; Vaeiago, A.; Zambonelli, L. *Acta Crystallogr*. **1965**, *19*, 886. (d) Agus, Y.; Louis, R.; Weiss, R. *J. Am. Chem. Soc*. **1979**, *101*, 3381. (e) Semerci, F.; Yesilel, O. K.; Sahin, E. *J. Inorg. Organomet. Polym.* **2010**, *20*, 334.
11. Holm, R. H.; Kennepohl, P.; Solomon, E. I. *Chem. Rev.* **1996**, 96, 2239.
12. (a) Liu, Q. X.; Zhao, X. J.; Wu, X. M.; Yin, L. N.; Guo, J. H.; Wang, X. G.; Feng, J. C. *Inorg. Chim. Acta* **2008**, *361*, 2616. (b) Chen, Y.; Zhao, X. J.; Gan, X.; Fu, W. F. *Inorg. Chim. Acta.* **2008**, *361*, 2335. (c) Zhang, J.; Wang, Y.; Huang, X.; Lin, Y.; Chen, X. *Chem. Eur. J.* **2005**, *11*, 552. (d) Mutasem, O. S.; Edward, V. F.; David, S. C. *J. Am. Chem. Soc*. **2002**, *124*, 10887. (e) Janiak, C. *J. Chem. Soc*., *Dalton Trans*. **2000**, 3885. (f) Nishio, M.; Hirota, M.; Umezawa, Y. *The CH/π Interaction (Evidence, Nature and Consequences)*; Wiley-VCH: New York **1998.** (g) Umezawa, Y.; Tsuboyama, S.; Honda, K.; Uzawa, J.; Nishio, M. *Bull. Chem. Soc. Jpn.* **1998**, *71*, 1207. (h) Janiak, C.; Temizdemir, S.; Dechert, S. *Inorg. Chem. Commun*. **2000**, *3*, 271.
13. Donohue, J. *J. Mol. Bio.* **1969**, 45 (2), 231.
14. Davy, S. L.; Osborne, M. J.; Moore, G. R. *J. Mol. Bio.* **1998**, 277 (3), 683.
15. Penfold, B. R. *Acta Cryst.* **1953**, 6, 707.
16. Dhefter, E.; Mautner, H.G. *J. Am. Chem. Soc.* **1967**, 89, 1249.
17. Lu, J. Y.; Babb, A. M. *Inorg. Chem*. **2002**, *41*, 1339.
18. Lu, J. Y.; Babb, A. M. *Chem. Commun*. **2003**, 1346.
19. Benesi, H. A.; Hildebrand, J. H. *J. Am. Chem. Soc.* **1949**, *71*, 2703.
20. (a)Yang, C. T.; Vetrichelvan, M.; Yang, X; Keith, B. M.; Murray, S.; Vittal, J. J. *J. Chem. Soc., Dalton Trans.* **2004**, 113. (b) Yang, C. T.; Moubaraki, B.; Murray, K. S.;

Ranford, J. D.; Vittal, J. J. *Inorg. Chem.* **2001**, *40*, 5934. (c) Xiandong, Y.; Daqing, W.; Ranford, J. D.; Vittal, J. J. *Cryst. Growth Des.* **2005**, *5*, 41. (d) Xiandong, Y.; Ranford, J. D.; Vittal, J. J. *Cryst. Growth Des*. **2004**, *4*, 781. (e) Ranford, J. D.; Vittal, J. J.; Wu, D. *Angew. Chem., Int. Ed.* **1998**, *37*, 1114. (f) So, K. W.; Yang, C T.; Vittal, J. J.; Ranford, J. D. *Inorg. Chim. Acta.* **2003**, *349*, 135. (g) Wang, X.; Ding, J.; Vittal, J. J. *Inorg. Chim. Acta* **2006**, *359*, 3481.

21. Admas, H.; Bailey, N. A.; de Barbarin, C. O. R.; Fanton, D. E. *J. Chem. Soc*., *Dalton Trans.* **1995**, 2323.
22. Yokoi, H.; Addison, A. W. *J. Chem. Soc., Dalton Trans*. **1977**, *16*, 1341.
23. Seo, J. S.; Whang, D.; Lee, H.; Jun, S. I.; Oh, J.; Jeon, Y. J.; Kim, K. *Nature* **2000**, *404*, 982.

FINDINGS OF THE THESIS

The work presented in this thesis started with a simple idea. Our group have been using amino acid derivative ligands (mainly L-histidine) and transition metal ions for building molecular capsule, cavity and channels for quite some time. The ligand design was centered around the L-histidine derivative's non planar four coordination property which promotes multinuclear large rigid architecture with bivalent Cu(II) or Ni(II) and trivalent Fe(III) metal ions. Because of the non planarity of the ligand, the site(s) on the metal ion remain coordinatively unsaturated which lead to multinuclear bridged species.

In this thesis, we had decided to explore a different approach which is centered on making coordinatively saturated metal complex which if form larger assembled architecture it should be through H-bonding between the molecules. Bridging need not be there. We did this using L-leucine or amino acids which form tridentate ligands. We have used M: L ratio 1:2 to form coordinatively saturated complexes with metal ions which prefer octahedral coordination (Ni(II)). For comparison or sometime if we found necessary we did use Cu(II) and Zn(II) as well.

Results presented in Chapter 2 showed an unexpected formation of an assembly of three coordinatively saturated Ni(II) octahedral complexes assembled around alkali metal ion. The assembly was held together through not only the coordination of alkali ion to coordinated carboxylates of the ligands but also through six H-bonds between phenol and non coordinated carboxylate oxygens. Interestingly, this provided stability to the assembly sufficiently to entice Cu(II) to adopt a hexa-coordination not observed in any of the Cu(II) complexes with amino acid derivatives reported before.

Subsequently, it was observed during successful attempts (Chapter 3) to form assembly stepwise, starting with monomeric complexes that (a) in absence of alkali ion the ligands around metal ion adopts a different *trans* configuration which rearranges to form the *cis* configuration needed to form the assembly, (b) simple addition of alkali metal salt transform the monomeric complexes to assembly capturing both ions of an alkali metal salt.

Taking advantage of this second observation we explored the assembly with caesium ion at the centre. Unlike sodium or potassium, reports on coordination ability of caesium are not so common. Results in the Chapter 4 showed that unlike sodium or potassium, assembly

formation ability of caesium is anion dependent perhaps because of its affinity towards chloride ion.

Results up to chapter 4 indicated that the assembly is quite resilient in adapting to different divalent transition metal ion as well as alkali metal ions. We surmised that because of this resilient nature, the assembly might allow formation of mixed metal assembly directly. The results in Chapter 5 showed indeed it is possible to form mixed Cu/Ni assembly just by mixing ingredients in the right proportion. The analysis of the crystals posed number of hurdle as it was not possible to determine Cu/Ni ratio from the structural data alone and we had resort to number of different analysis procedure to come to a reasonable conclusion.

In Chapter 6 & 7 we used a different ligand system by replacing phenol part of the ligand with pyrene. Replacement of phenol which played important role in stabilizing the assembly resulted in a loss of discrete assembly formation but gave rise to entirely different property to the ligands themselves (gelation) and complexation revealed channel formation which is empty to begin with. Formation of empty channels itself remained a challenge as in most of the cases crystals looses it's crystallinity during removal of solvent from the interior of channels; refilling channels are something that few could do until now. We were fortunate to have empty channels which we were able to fill partially with iodine.

Overall this thesis is a exploratory type where we did not solve any existing problem or synthesized immediately usable technologically important materials but the results presented put new observations on several areas such as (a) self assembly of metal complexes forming larger ensemble through non covalent interactions, (b) behaviour of different alkali metal ions in organizing assembly as well as network, (c) mixed metal assembly and (d) gelation process. Some of these aspects will be continued for further development of useful material from our group.

What is perhaps become clearer with this work is that compared to amino acid complexes (most of which are structurally characterized), the derivitization at the amine can give rise to multitude of interesting architecture depending on the derivative. Even exploring simple *bis* complexes are capable of showing variety of assembly and network formation. The chiral and ubiquitous nature of amino acid as well as the transition/alkali metal ions in the natural system provides further impetus to explore the coordination chemistry of this type amino acid based ligands as some of the observations may provide clues to what is probably already happening in natural systems.

List of publications

1. *"Sodium and Potassium Ion Directed Self-Assembled Multinuclear Assembly of Divalent Nickel or Copper and L-Leucine Derived Ligand"*
   Mrigendra Dubey, Rik Rani Koner and Manabendra Ray, **Inorganic Chemistry 2009**, *48*, 9294.

2. *"Effect of metal coordination and intramolecular H-bond on the acidity of phenolic proton in a set of structurally characterized octahedral Ni(II) complexes of L-histidine derivative."*
   Subash Chandra Sahoo, **Mrigendra Dubey**, Md. Akhtarul Alam and Manabendra Ray**, Inorg. Chem. Acta. 2010,** 363, 3055.

3. *"Fluorescent Gels of Pyrenemethyl Amino Acids and their Dependence on Amino Acid Side Chain, LiOH, Chirality and Solvent"*
   Mrigendra Dubey and Manabendra Ray **(manuscript under preparation)**

4. *"Step wise assembly or mononuclear to multi-nuclear assembly conversion"*
   Mrigendra Dubey and Manabendra Ray **(manuscript under preparation)**

5. "*Effect of the Amino acid and Cs^+ coordination on the assembly formation"*
   Mrigendra Dubey and Manabendra Ray **(manuscript under preparation)**

6. "*Synthesis, characterization of Self-assembled mixed metal assembly and study of magnetic behaviour"*
   Mrigendra Dubey and Manabendra Ray **(manuscript under preparation)**

7. "*Pyrene derived Amino acid, Cu(II) and Zn(II) complexes forming reusable enantiopure channel"*
   Mrigendra Dubey and Manabendra Ray **(manuscript under preparation)**

Conferences and Symposia

1. 11th CRSI National Symposium in Chemistry, 6-8 Feb 2009, NCL Pune, India- **Poster presentation**.
2. MTIC-XII, Dec. 2009, held at Indian Institute of Science, Bangalore- **Poster presentation**.
3. ICMS-Cambridge University Winter School on Chemistry and Physics of Materials, 6-10 Dec, 2010 at JNCASR, Bangalore- **Poster presentation**.
4. Frontiers in Inorganic Chemistry (FIC-2010), 11-13 Dec, 2010, held at IACS, Kolkata- **Poster presentation**.

Additions and corrections

1. p iii closure replaced by closer
2. p 2: Name initials removed for consistency from 'K.N. Raymond' to 'Raymond'
3. p5, line 6: works have replaced by work has
4. p 1, line 11: several-volume series replaced by multi volume series
5. p 5: *Highlighting the single pot crystallization and hydrogen-bonded bonded polymeric structures, and star like channels observed in [Cu_2(Scp11)$_2$]. The star like channel, as shown...* changed to- *Highlighting the role of single pot crystallization and hydrogen-bonded polymeric structures, the star like channel observed in complex [Cu_2(Scp11)$_2$] as shown….*
6. p 7, line 1: Another report by Rebek, et al., where simple alkanes feature is fully extended... 'is' added
7. p 8, para 2, line 3: hyphen added as *cis*-Pt
8. p 8, para 2, line 4: gap removed from formula '1,3,5-tris(4-pyridyl-*trans*-ethenyl)benzene)'
9. p 9: LiClO4 corrected to $LiClO_4$
10. p 17, line 19: Added 'Na and K contents have been measured using Flame Photometer.'
11. p 17: H2O corrected to H_2O
12. p 17, synthesis section, line-7: volume of methanol added- 4 mL
13. p 18, 'super latent' removed by 'supernatant'
14. mmol of KOH (0.847) p 18, line 10; (0.846) p 19, line 11; (3.80) and (0.726) p 70, lines 10/-6: corrected to p 18, 19- KOH (0.047 g, 0.703 mmol), p 70/-6- KOH (0.218 g, 3.26 mmol) and KOH (0.041 g, 0.613 mmol).
15. p 21, line 12; p80, line 2; p 89, line 10; p120, lines 3, 4, 19: A non-breaking hyphen used to avoid splitting the chemical formula
16. p 37, line 1: added 'an' before L-leucine derivative
17. p 43, section 3.2.4; p 45, line 3; p 47, line 9; p 55, section 3.4.3, para 2: Formula [Cu(HL$^{L\text{-}leu}$)Imidazole] corrected as [Cu(L$^{L\text{-}leu}$)Imidazole]
18. p 55, line 5: corrected ligand as ligands...
19. p 55, line 6, 7: corrected as However, we have previously observed...
20. p 55, line 11: added 'an' before in plane ligand...

21. p 58, line 3: spelling of ‘methanolic’ corrected
22. p 71, line 11: left it for... corrected as leaving it for....
23. p 79, line 3: Ang unit added as ‘Å’
24. p 81, line 7 from bottom: ‘studies’ added
25. p 82, line 8: added ...spectra ‘given in’ figure...
26. p 88, line 7: offered replaced by resulted in....
27. p 88, line 7-8: ‘mixture’ removed
28. p 88, line 11: mixed replaced by mixing and CH_3CN volume added as ‘(~5 mL)’
29. p 102: Carry corrected to ‘Cary’
30. p 103, line 6: volume added as ’(20 mL)’
31. p 105, spectroscopy replaced by ‘spectrometry’
32. p 110, Figure 6.5: caption SEM image of organogel in presence (1 %w/v) corrected as- *SEM image of dried organogel reveals fibrous network (1 %w/v)*
33. P 114, Scheme 7.2: Complex 4 formula corrected as ‘$[Cu(P^{L\text{-}tyr})_2H_2O](4)$’
34. p 115, line 6: Sentence ‘The color of the solution was changed to blue immediately.’ Changed to ‘The color of the solution changed immediately to blue’
35. p 116, 7.2.6 line 2: Sentence ’50mg of dried crystals in a vial...’ corrected as ‘Dried crystals (50 mg) in a vial...
36. p 117, line 3: grinded replaced by ‘ground’
37. p 129, ‘temperature’ spelling corrected on scale
38. Thesis findings, p 1: Derives replaced by ‘derivatives’
39. Thesis findings, p 2: derivation replaced by ‘derivatization’